Nanoscale Physics of Surfactant Gene Delivery

by

Robert Douglas Evert Henderson

A thesis
presented to the University of Waterloo
in fulfillment of the
thesis requirement for the degree of
Doctor of Philosophy
in
Physics

Waterloo, Ontario, Canada, 2015

Author's Declaration

I hereby declare that I am the sole author of this thesis. This is a true copy of the thesis, including any required final revisions, as accepted by my examiners.

I understand that my thesis may be made electronically available to the public.

Contributions

Portions of Chapter 1 were submitted by me for credit as a final paper in the reading course PHYS 745: Special Topics in Experimental Physics: Kelvin Probe Force Microscopy.

All of the experiments presented in this thesis were conducted by me, and designed by me with advice from my advisors Prof. Zoya Leonenko and Dr. Shawn Wettig, with specific exceptions noted as follows.

The Introduction in Chapter 1 contains some figures that are reprinted from the published work of others. These are always credited to their source, and are presented here for illustrative purposes.

In Chapter 2, I wish to gratefully acknowledge technical training from Dr. Ravi Gaikwad and Andrey Krayev in the early stages of those experiments.

Chapter 4: The pressure-area isotherms presented in this chapter were performed by Taksim Ahmed as a collaboration between the Leonenko and Wettig Labs. Part of the sample preparation and imaging was performed by undergraduate summer co-op student Melissa Prickaerts, whom I trained, guided and co-supervised throughout the work. All of the experiments were designed by me, and all the data analyses are my own.

The gemini surfactants used throughout this work were synthesised and provided by the Wettig Lab.

Abstract

Medicine has met a revolution in the expansion of possibilities for therapy based upon synthetic gene delivery. Imagine the ability to correct problems of a genetic origin with a simple drug – such science fiction fantasies are becoming future's reality. Still in relative infancy, synthetic gene therapy has such potential for so many medical issues that it is a very high priority area of research on a global level. Equally revolutionary is the growth in the use of nanotechnology, now that instruments have been developed to probe most any physical system on the nanometre scale. The relatively new appearance of these technologies leaves research rife with fruit for the picking, and forming new interdisciplinary connections only multiplies the possibilities.

Nature has developed excellent nanoscale machines – viruses – for gene delivery. Unfortunately for human beings, the end result is often detrimental rather than beneficial. Despite this, in typical human fashion we seek to adapt nature's solutions for our own purposes. Such endeavours are extremely difficult undertakings, but we persist for the benefit of all. So far, researchers have figured out how we can pack DNA with nanoscale carriers rather well using surfactants and lipids of various structures, and that these systems do an 'okay' job of transfecting genes. However, we do not really know at all, let alone for certain, why some lipid or surfactant structures are better transfecting agents than others, or really how these carriers enter living cells and become expressed. The answers to these questions can never, ever be solved by observing these systems from the perspective of a single field of study, for in order to understand *why*, and thus to predict a better *how*, we must use the entire spectrum of science from the most fundamental to the most clinical.

Over the decades of fairly clinical and *in vitro* studies that have characterised gene delivery research, precious little literature exists at the extreme end of fundamental physics. And yet, so much depends on the physical interactions of the gene delivery systems and their targets that an understanding of the physics of gene delivery could lead to more focussed and efficient clinical research. For this reason, the present work aims to bring together clinical research into gene delivery with state-of-the-art nanotechnology, observed through the lens of physics. Our primary instrument in this work is the atomic force microscope, which is a type of scanning probe microscope capable of imaging surfaces on nanometre scales using a micromachined cantilever tip. Our particular instrument is one of

the most advanced that is presently available to implement recent developments in Kelvin Probe Force Microscopy (KPFM), a variant of atomic force microscopy (AFM) that is designed to image electrical surface potentials on the nanoscale. In the present work, we utilise an advanced method of frequency modulation KPFM, which allows surface potential imaging with nanometre resolution.

This thesis begins with some of the most promising building blocks of surfactant gene delivery, gemini surfactants, and explores their nanoscale behaviour and interactions with other critical ingredients: lipids and DNA. Gemini surfactants have shown to achieve superior transfection efficiency, while maintaining a high level of versatility and flexibility yet requiring less material. These surfactants are also fairly inexpensive to manufacture. Such benefits make gemini surfactants an attractive candidate for synthetic gene therapy solutions. Further enhancements to transfection efficiency are made with the addition of 'helper' lipids, an issue which we also explore.

A fundamental aspect of the physics of gene delivery is how the systems interact with their targets: a living cell. By constructing a model monolayer of a cell using lipids commonly found in most cell membranes, we compared the structure of a 'plain' model cell monolayer with one which has been infused with gemini surfactant. We found that the gemini surfactant exhibited strong interactions with the gel-phase lipid present in the model monolayer, and that the resulting domains had a more positive surface potential. Using the unique capabilities of KPFM, we were able to show the presence of cationic surfactant in the monolayer from its electrical signal.

As an extension of the above, we added DNA into our monolayers to explore the effects of DNA binding. This binding behaviour is important to understand for the purposes of gene therapy. Our mixture of two cell membrane phospholipids (DOPC and DPPC), with gemini surfactant, showed three distinct domains, which we deduce to be DOPC, DPPC+gemini surfactant, and gemini surfactant+DNA. The latter region was the highest, exhibiting a network of thread-like domains. Most intriguingly, only the 'middle' region exhibited a positive surface potential signal, a fact which can only be determined with KPFM imaging.

We studied mixtures of gemini surfactants, helper lipid and DNA in monolayer form so that we could explore the nanoscale structures that these molecules create. In this

way, we were able to create controlled environments in which to study the interactions of components of gene tranfection complexes. In addition, we used a Langmuir trough to gather pressure-area curves for our monolayers to draw further conclusions on the roles of the various components. We found that gemini surfactants play a significant role in compacting DNA, and that this compaction is enhanced by the presence of the helper lipid DOPE. Furthermore, the nanoscale structure of these monolayers was affected by factors such as acidity and the ratio of helper lipid to gemini surfactant. Finally, we used AFM and KPFM to probe gemini surfactant gene transfection complexes (nanoparticles), which were directly deposited onto an atomically flat substrate. We found that their size distributions are broad, ranging from a few tens of nanometres to a few hundred nanometres.

This research demonstrates the unique capabilities of AFM and KPFM to probe systems of relevance to gene therapy, and that the nanoscale structure of transfection components is affected by a number of key factors such as the particular surfactant, amount of helper lipid, the presence of DNA, and environmental factors such as acidity. Given that the nature of these interactions is typically electrostatic in origin, it is clear that KPFM has a significant role to play. This thesis provides an introduction to novel methodologies for this purpose, illustrated by applications to gemini surfactant systems.

Acknowledgements

It has been a rewarding time, these years in graduate school. I have learnt so much – not just about research, but about people, management, and how universities tick. Along the way I have had the benefit of exploring far more than what normally constitutes doctoral training. For this, and for being surrounded by fantastic individuals, I am grateful.

Were it not for my patient and accommodating advisors, all this would not have been possible. Thank you, Zoya, for bringing me into your group. Shawn, thanks for your support, for collaborating with us, and providing me with an excuse to bring pharmaceutics into my research. To you both: thanks for supporting me throughout my degree and allowing me the freedom to shape my studies into what has turned out to be a rather unconventional package. Speaking of which, my committee members have played a rather larger role than most do during the course of one's doctoral studies. Prof. Wing-Ki Liu, in addition to offering his time to serve on my committee, has helped me navigate university policy whenever I needed assistance. And I cannot count the hours I have taken from Prof. Hartwig Peemoeller discussing the philosophy of universities and teaching. Thanks, Hart, also for being so very gracious in accommodating my unusual requests when it came to teaching assignments. Many thanks also to Prof. Terry McMaster for not only organising a fantastic conference which led to my first visit to Bristol, UK, but also for making the trip all the way from Bristol to Waterloo and serving as my external examiner.

The Waterloo Institute for Nanotechnology has been very generous to award me three of their Nanofellowships, which have been a great support to my graduate education. In addition, I wish to acknowledge support from the Natural Sciences and Engineering Research Council of Canada and the Ontario Graduate Scholarship program.

I am also, of course, grateful for the hospitality and generosity of those with whom I have worked in our research group. When I first arrived, Ravi Gaikwad spent a lot of time teaching me how to do atomic force microscopy. Thanks, Ravi, for all of your help. Elizabeth Drolle and I have been on similar paths to completion (defending on the same day!), and I have benefitted from her expert training in Langmuir monolayer techniques. Brenda Lee, thanks for keeping me sane, and for always being there to help. Simon Attwood was my partner in physics in the lab; thanks to you for all the helpful

conversations. And of course, thanks to Francis Hane for all the homemade bagels! This document was typeset with ✒LaTeX, and I wish to thank all those out there who have contributed to the development of such a wonderful tool.

I spent a great deal of time out and about the campus in the graduate student public service, and have gotten to know some amazing people. Let me begin by thanking my dear colleagues whom I've met from the Graduate Student Association; in particular Mike Makahnouk, Coleen Even, Hassan Nasir, Mahdi Safa and Rose Vogt, for their friendship and dedication. (By the way, if the university is looking for anyone to blame for my annoying presence on dozens of university committees, it's Mike.)

There are some wonderful university administrators who have been a pleasure to work with during my service on more university committees than I can count. I'd like to mention, especially, Chris Read, Bud Walker, Ian Goulden, Dennis Huber, Sue Horton, Bruce Mitchell, Jim Frank, Beth Jewkes, Mark Haslett and Geoff McBoyle, who have been great mentors and colleagues in helping to improve the graduate student experience at Waterloo. Thanks also to my faculty partners-in-mischief David Porreca and George Freeman.

I wish to say, for all to know, that the Department of Physics & Astronomy at Waterloo takes very good care of its graduate students. Our chair, Prof. Jeff Chen, has shown great leadership for the department, a department which has set an example for all others in the university on best practices for graduate student support. Our Faculty teaching fellow, Rohan Jayasundera, has been personally very supportive of me, and he, having also somehow convinced our chair and associate chair, Prof. Michael Balogh, is the reason I was given the opportunity to teach my very own introductory astronomy class. Finally, thanks to Prof. Terry McMahon for being a wonderful dean. I am very grateful to you all.

I have had the benefit of an extremely supportive family, and many, many thanks are due to them. My parents have been nothing but supportive throughout all of my education, and I owe them a huge debt of gratitude. To all my siblings, aunts, uncles and cousins: perhaps this thesis is not so good an answer to the question 'so when do you finish?', but at least I can say that I have.

And the most thanks of all go to my wife, Carolyn. She has been there for me every day, picked things up when I was most busy, and has kept me moving forward. I count myself as ∞ fortunate.

For Carolyn

And for Her Majesty The Queen.

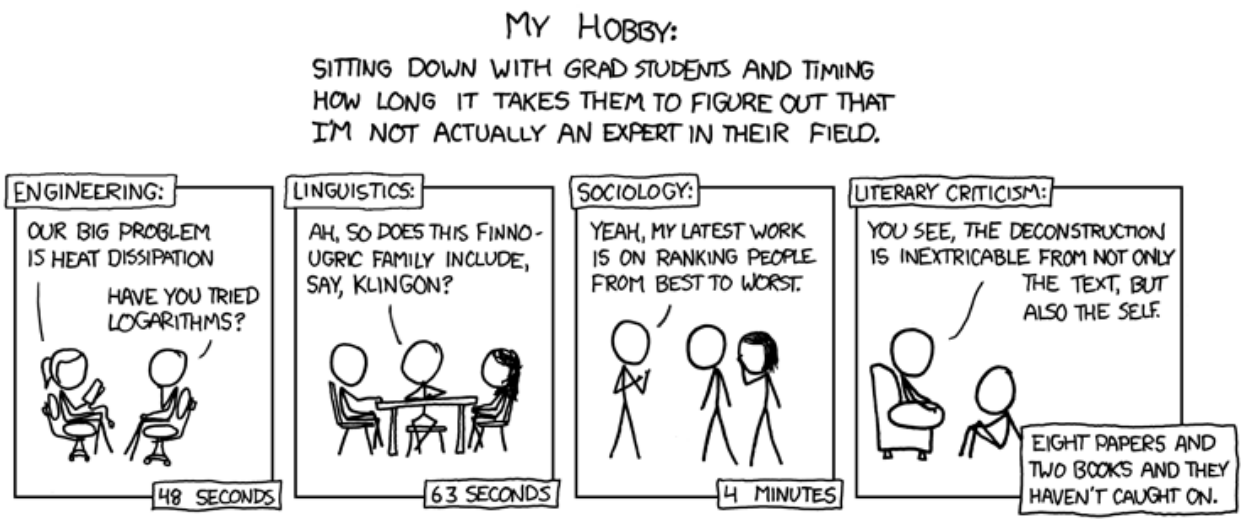

Reprinted from xkcd.com.

There is a theory which states that if ever anybody discovers exactly what the Universe is for and why it is here, it will instantly disappear and be replaced by something even more bizarre and inexplicable. There is another theory which states that this has already happened.

Douglas Adams

Reality must take precedence over public relations, for nature cannot be fooled.

Richard Feynman

rdehende@uwaterloo.ca

University of Waterloo
Department of Physics & Astronomy
200 University Avenue West
Waterloo, ON
N2L 3G1, Canada

uwaterloo.ca/physics-astronomy/
uwaterloo.ca/institute-nanotechnology/

Contents

List of Tables

List of Figures

If we knew what it was we were doing, it would not be called research, would it?

Albert Einstein

Chapter 1

Introduction

1.1 An Overview

At the end of the day, the primary result that this research is driving towards is an improvement in healthcare. Specifically, we would like to have better ways of delivering medicines. By better, we mean of course that medicines (drugs and the like) should be given with maximum benefit and minimal side-effects. Getting there from the fundamental research to which this work contributes is a very large task, but it is important to keep in mind why we are bothering. Delivery of simpler drugs - the ones which are ready to be metabolised immediately upon administration - has been done for centuries (or millennia, depending on what one classifies as a drug). Such therapeutics have been largely figured out. Things get considerably more complicated (and interesting) when we move to the realm of *gene therapy*. In this case, it is possible to manufacture and deliver a piece of DNA coding for a particular protein that is meant to be helpful to the individual receiving such treatment. This DNA fragment must somehow be integrated into the patient's genome or otherwise expressed by their cells, without being damaged or degraded along the complicated and dangerous pathway into the cell nucleus.

Primary methods by which genes may be delivered to cells include the use of viruses (which are very good vehicles for delivering genetic material) and synthetic gene carriers such as lipid-based vesicle systems or surfactants, the latter of which we will discuss in

detail. What we are trying to do here is learn more about how synthetic gene delivery methods work, since they are the most promising for future therapies. The breadth of materials that are available is staggering – there are seemingly endless combinations of functional groups that all yield surfactants capable, at least in some way, of packaging up genes. However, one class of these molecules in particular has risen above the others: gemini surfactants. Superior in terms of aggregation ability – it takes less material to achieve similar results – and transfection efficiency – they do a great job delivering genes – gemini surfactants are the focus of active research.

Studying gene delivery systems such as gemini surfactants combined with genetic material is a difficult task. The spectrum of research stretches broadly, from the most fundamental of physics all the way to clinical application. In between these are *in vitro* transfection and cell viability studies, in which the success of these systems is tested in a laboratory without any human risk. The results of *this* surfactant with *those* genes in *such and such* environments are fairly well understood (or can be made to be understood) by a multitude of studies, but what is not at all understood are the underlying mechanisms and physical interactions and effects which give rise to those results. It would seem that a deeper understanding of the physics, far at the fundamental end of the spectrum, would help drive future research to pinpoint the ultimate gene delivery systems.

It is this last point, the physics of gene delivery, that is the focus of this thesis. DNA molecules (the genes) are *tiny*, and in therapeutic form in fact exist complexed with a carrier system as *nanoparticles* so that they can find, enter, and move about individual cells. Genes, as DNA fragments, are not effectively therapeutic on their own. However, when they are complexed and condensed with other molecules (like lipids and surfactants), their efficiency as transfection agents is boosted significantly. This is why appropriate and efficient gene carrier and delivery systems are so essential for therapy. In order to drill down into the inner workings of these nanoparticles, it is necessary to invoke the use of a few very powerful nanotechnologies. The primary method by which we study physics on the nanoscale in the present work is atomic force microscopy and some of its specialised advanced modes. With this technology, we are able to create images with nanometre resolution to not only visualise gene delivery nanoparticles, but to see how they or their constituent parts interact with their targets (cells). We do this by creating model cellular

environments or gene delivery particles themselves. In addition, the most state-of-the-art techniques allow us to probe the *electrical* properties of these models, and relate them to the topography and other parameters that we have included, such as the relationship of the size or structure of the surfactants to the strength of the interaction with the genes. It turns out, not surprisingly, that imaging in the electrostatic domain is very challenging, and obtaining resolution on the nanometre scale has only become possible in recent years.

Just because we're talking about *nano*technology does not mean that we are absolutely restricted to cutting-edge, modern equipment. For some aspects of the research in this thesis we certainly are, as we have just discussed, but the basic method by which we create the gene delivery environments has been in use for nearly a hundred years. The Langmuir-Blodgett technique is a fairly simple, albeit meticulous and unforgiving, method to create monolayers and deposit them onto substrates for imaging. In addition, the creation of the gene delivery nanoparticles is more straightforward, and has been done on a routine basis in many gene transfection studies. What has never been done, however, is an analysis of their electrostatic properties.

Of course, it is impossible to explore all of the issues in one thesis, but I offer here a few studies which hopefully will open doors and present ideas for more research into the fundamental physics and theory of gene delivery, perhaps leading to more focussed efforts in future clinical research. The basic ideas behind the present work are to show i) the electrostatic properties of simple cell membranes and how the gene carrier molecules interact with them and change these electrostatic properties; ii) how DNA interacts with the systems explored in (i), which would give us some insight into the binding behaviour of DNA; and iii) the details of gene transfection complexes themselves as explored via monolayer techniques and direct imaging of their nanoparticles. These issues are presented within the four 'research' chapters within this thesis. In what follows in the remainder of this introduction are detailed explanations of what gemini surfactants are, the techniques we use to study them, and how this all relates to the gene delivery problem. Examples from the literature are presented for the techniques, to provide the reader with some context on the present state of research and the capabilities of these methods.

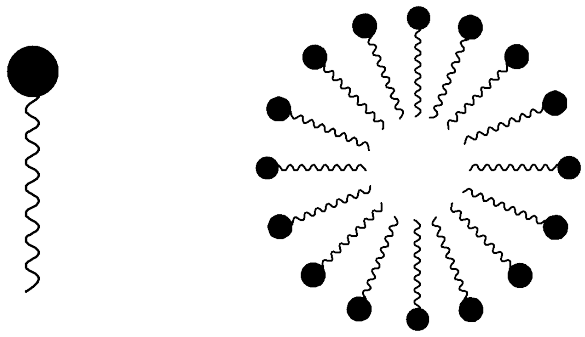

Figure 1.1: Schematic representation of a surfactant molecule (left) with hydrophilic head group and hydrophobic tail, and a group of surfactant molecules (right) in micelle form.

1.2 Gemini Surfactants

Amphiphilic surface active agents (surfactants) are some of the most important structural molecules in biology. One end of the molecule, usually called the head, is hydrophilic (from Ancient Greek, 'water-loving'), while the other end, the tail, is hydrophobic ('water-fearing'). In water, surfactants pack their tails toward each other and form spherical micelle containers (e.g. Israelachvili et al., 1977). By keeping the non-polar hydrophobic parts of the molecules together and away from polar water molecules, the system adopts a conformation that is lower in energy (Israelachvili, 2011). This is illustrated in Fig. 1.1.

This conformation is the principle mechanism by which biological membranes assemble and maintain their structure (to be discussed in greater detail later on in this thesis). Surfactants also have the ability to interact with other molecules and take advantage of their special properties to do other useful things. One very close-to-home example is soap: grease and oil are insoluble in water because they are largely hydrophobic, but they dissolve readily in non-polar substances like the long carbon chains of soap molecule tails. Water dissolves the polar head groups of the soap and carries away the soap, along with the offending dirt.

Another use - and a topic which will come up again as a central issue of this thesis - is to have surfactants carry not dirt, but drug molecules and therapeutic DNA (for gene therapy). In this case, the micelles or other structures could serve as cargo containers that

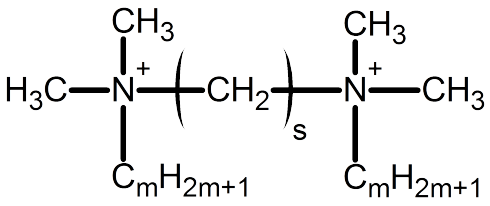

Figure 1.2: General structure of m-s-m gemini surfactants.

package and protect molecules that are to be delivered somewhere in the body. To package DNA, this is especially facilitated if the surfactant happens to have a positive charge to attract itself to the negatively charged backbone of the DNA. We will discuss gene delivery in detail later in § 1.5, but for now it is sufficient to say that surfactants can serve as the containers by which DNA may be delivered to cells for therapeutic purposes, and there are many advantages over other methods (and disadvantages, which serve as some motivation for the present work).

One particular disadvantage which is necessary to point out now is that surfactant delivery of drugs and genes suffers from low cellular uptake compared to other methods like vectors of viral origin (Wettig et al., 2007). However, it has been found that altering the structure of surfactant molecules themselves can have a dramatic impact on the success rate of drug or gene delivery (the so-called 'transfection' rate). This is where 'gemini' surfactants come in.

This special class of surfactants, gemini surfactants (GSs), have two tails and heads, bound by a spacer group (Menger & Littau, 1991, 1993; Bell et al., 2003; Wettig & Verrall, 2001; Kirby et al., 2003; Wettig et al., 2008). The transfection efficiency of these gemini surfactants has been found to be far greater than their single-chain counterparts (e.g. Kirby et al., 2003; Wettig et al., 2007; Wang et al., 2013). Importantly, gemini surfactants carry a 2+ charge, which allows them to strongly interact with DNA electrostatically. With a judicious choice of spacers, heads and tails, these systems can be very versatile with virtually no limit to carrying capacity(Wettig et al., 2008). Gemini surfactants have further advantages of low toxicity, and are relatively inexpensive to manufacture (Menger & Littau, 1991; Wettig et al., 2008). However, their transfection efficiency still does not match that of viral vectors, and it is the subject of current research to find ways of maximising

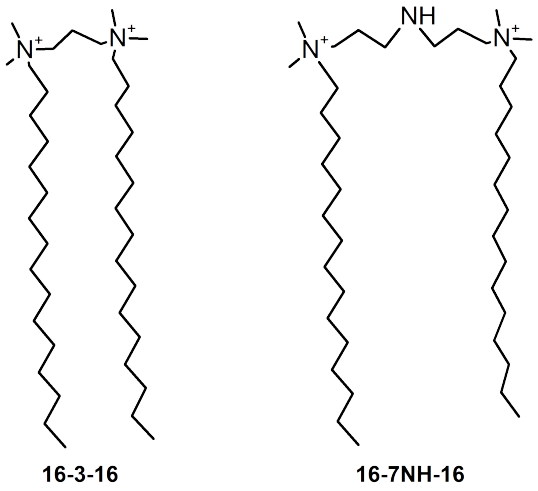

Figure 1.3: Chemical structure of the gemini surfactants 16-3-16 and 16-7NH-16. Note the protonatable amine group in the latter.

their potency to take advantage of their many benefits.

Although they come in many shapes and sizes, in the present work we will be focussing on gemini surfactants which are of the so-called m-s-m type, shown in Fig. 1.2, an example of which is shown in full in Fig. 1.3. In the latter, it is also shown how functional groups can be inserted into, for instance, the spacer chain. Here, for example, we have a protonatable amine group, which carries a positive charge at low pH. Therefore, the surfactants of type m-sNH-m carry different charges depending on the acidity of the surrounding environment. This could be useful, for example, for capture and release of molecules of interest.

1.3 Atomic and Kelvin Probe Force Microscopy

In the last few decades, tools and capabilities for microscopic observations have benefitted from significant advances. Scientists are no longer met with the physical limitations in resolution that are imposed by the use of electromagnetic waves as the medium that

carries information about systems of interest.[1] We have now moved on to the world of the nanometre, and can observe the treasure trove of science that exists at those scales. Instead of using light waves (which cannot probe even tens of nanometres), scientists use nanoengineered cantilever probes to measure minute changes in force while the probe is moved across a surface of interest. By carefully measuring the deflection of this cantilever, surface topography can be determined which leads to a 3D image. Resolutions as high as the atomic scale are achievable with this form of scanning microscopy technique. Of course, this is known as Atomic Force Microscopy (AFM), or more broadly, Scanning Probe Microscopy (SPM) (Allison et al., 2010). In the present work we will be focussing on the basic AFM and the specialised setup of Kelvin probe force microscopy, which images the electrical contact potential difference in sample.

More recent years have led to the development of many different forms of scanning microscopy (Berger et al., 2009). We will discuss a few of them in this review, but our highlight is a technique that can be used to measure the contact potential (or work function) of a sample[2] known as Kelvin Probe Force Microscopy (KPFM). In this case the Kelvin Method that was developed by Lord Kelvin in the 1800s to measure the work function of metals is utilised. When astronomers first peered into new wavelengths, such as radio and X-ray imaging, exciting new discoveries were made; many phenomena are simply not detectable with 'traditional' methods using visible light. By analogy, KPFM allows fundamentally new observations to be made of systems by not only mapping their electrostatic properties, but doing so at nanometre resolution. Under extreme conditions (e.g., low temperature, pressure, isolation), imaging of the surface potential is possible on the sub-molecular level, revealing the charge distribution of single molecules (Mohn et al., 2012).

This review will discuss the history, development and applications of KPFM by building on the fundamental principles of the more general AFM and SPM methods. Specialised

[1] Although the resolution limit from the wavelength of visible light is excellent, it still does not allow us into the world that exists below about 200 nm in scale. However, that didn't really become important until the advent of nanoscience.

[2] More precisely, this technique measures the contact potential difference between the sample and the cantilever probe.

and advanced techniques will also be presented. A survey of applications in both biological and non-biological systems will follow. Finally, there will be some concluding remarks on the future directions and possibilities for research utilising KPFM techniques.

1.3.1 Atomic Force Microscopy

Before we can dive into a discussion on the technicalities of KPFM, we must first understand how a traditional AFM setup works to generate a nanoscale 3D map of a surface of interest. An optical microscope generates an image by using reflected rays of light that are refracted through a series of lenses to magnify an object. However, light has a fundamental limitation that is directly related to its wavelike nature. A resolution limit is imposed simply because it becomes physically impossible to resolve objects that are smaller than the wavelength of the light used to image them ($\sim$200 nm). An electron microscope gets around this by using the wave nature of particles.[3] Electrons have a shorter 'wavelength' than photons, which allows for higher resolution imaging, and can reach nanometre scales.[4] However, electron microscopes suffer from serious limitations despite their excellent resolution. The cost is that the samples must be fixated, dehydrated, stained or coated for imaging via electron scattering or transmission processes (e.g. De Jonge et al., 2009; Hayat, 2012).

Instead of using electrons or electromagnetic waves to image a sample of interest, topography can be measured by 'feeling' (rather than looking), in much the same way as blind individuals can read with the Braille system. AFM instruments generally have the basic setup shown in Fig. 1.4. The probe is a micromachined tip placed at the end of a cantilever. A laser beam shines on the end of the probe and records its deflection as it moves across a surface. The deflection that results is due to the forces of interaction between the tip and the sample. These forces include the primary contact and van der Waals forces, as well as intermolecular bonds, capillary forces (due to liquids and hydrogen bonding), magnetic and electrostatic forces (Kalinin & Gruverman, 2007; Kedrov et al., 2007). As we will see,

[3] This is the so-called 'wave-particle' duality of de Broglie, where all particles can be said to have an associated wavelength that is inversely proportional to their momentum.

[4] Advanced electron microscopes, such as High Resolution Transmission Electron Microscopes (HRTEM), are said to achieve resolutions of up to 0.08 nm!

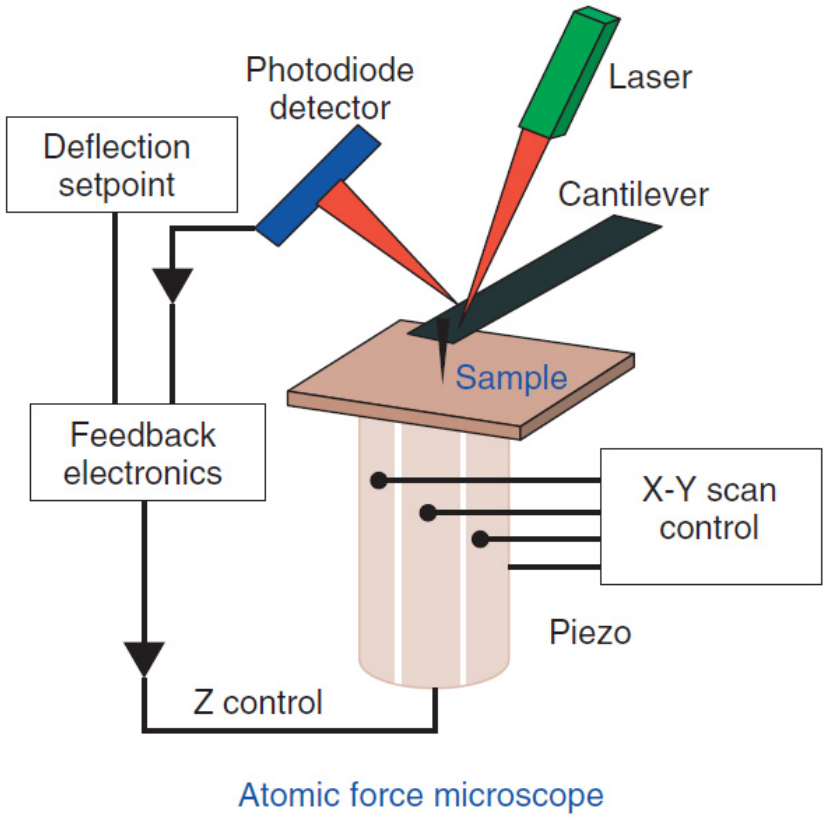

Figure 1.4: The basic AFM setup. Figure reprinted from Allison et al. (2010).

the electrostatic force is of fundamental importance in KPFM. The contact and van der Waals forces can be described in simple terms by the Lennard-Jones potential, which has a very steep wall at close range (r^{-12}) and a long-range tail that decreases as r^{-6},

$$V = \epsilon \left[\left(\frac{r_e}{r} \right)^{12} - 2 \left(\frac{r_e}{r} \right)^{6} \right] \tag{1.1}$$

Here, r_e is the equilibrium distance where the potential is at a minimum, $-\epsilon$. Relative to other forces like electrostatics, the van der Waals force is a short-range interaction.

Imaging Modes of AFM

There are multiple modes available for AFM, each having their applications. In the most basic mode, *contact* mode, the cantilever is dragged along the sample surface, without oscillation, while the reflected laser beam is tracked to indicate the height. This is a very simple mode that does not require any cantilever oscillation, but it suffers from some drawbacks: the dragging forces can damage the sample and the tip, or contaminate the tip, and the resolution is relatively poor.

Non-contact mode offers increased resolution and fewer issues with tip contamination or sample damage. In this mode, the cantilever is oscillated mechanically at close to its fundamental resonance frequency. The tip does not drag along the surface (although in some setups it can briefly touch), but rather the oscillation amplitude itself is kept in a feedback loop with the tip height. As the tip-sample distance (and thus the force of interaction) changes, the cantilever is raised or lowered to maintain the amplitude of oscillation. In this way, the sample topography may be traced. In many studies this is all done in air, but imaging might also be done in liquid (e.g. Putman et al., 1994). For further details and a detailed overview, see Morris et al. (1999).

1.3.2 KPFM Theory

Now that we have introduced the basics of AFM, we will discuss the development and usage of Kelvin probe force microscopy. It is possible to measure the work function of a metallic substance using a simple circuit containing a capacitor. The work function is defined, in simple terms, as the amount of energy that is required to eject a single electron from a metallic surface. Quantum mechanics tells us that electrons are only able to be in states of very specific energies ('energy levels'), and this is of course true for metals as well as individual atoms and molecules. Metallic substances are characterised by heavily overlapping electron distributions, which results in a 'sea' of conduction band electrons free to move around a lattice of atoms. The electrons stay within the vicinity of the nuclei because they are trapped in the internuclear potential energy wells generated by the atoms. It takes energy to free them. Practically speaking, this can be observed as the Photoelectric Effect: one can shine a laser beam of very specific energy at a metallic substance and tune

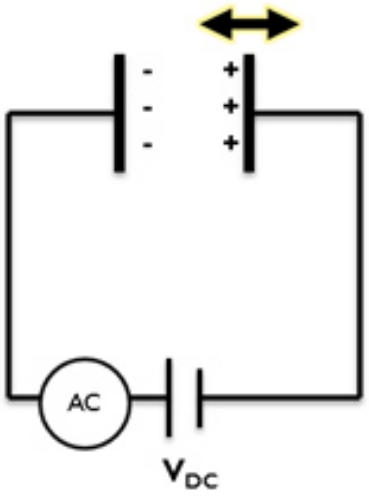

Figure 1.5: An illustration of the original Kelvin probe setup.

the laser to higher energies until electrons are emitted from the surface (and subsequently detected). Below some threshold energy, no electrons are observed. This threshold energy corresponds to the work function. Energy in excess of the work function then goes into the kinetic energy of the electrons as they are emitted from the metallic surface. See Ashcroft & Mermin (1976) for further background on this topic.

Suppose we have a piece of metal and we want to know its work function. Consider the setup of Fig. 1.5, where we have a parallel plate capacitor formed from two different metal plates (with different work functions), connected by a conducting wire. If we do nothing else, as soon as the circuit is completed a current will flow in the wire, driven from an established electric field (which corresponds to an electric potential) between the plates. Essentially, electrons flow to deposit themselves on one of the plates, creating a potential difference between them. This process is driven by the *difference* in the work functions of the metals, since the electrons they contain are sitting at different energy levels.[5]

[5]More precisely, we speak of the highest energy level electrons. When we talk about work functions, we really mean the energy it takes to liberate the electron in the highest occupied energy level (like a valence electron in an atom).

Next, if we mechanically vibrate one of the capacitor plates, the distance between the plates becomes time-varying. This makes the electric field between the plates vary with time, and therefore we get an alternating current (AC) in our wire. Suppose we now apply a compensating voltage to the circuit, which happens to exactly correspond to the difference in the metals' work functions. Then there would be no need for a current to flow, since there is nothing left to balance between the metals. Our AC signal vanishes.

As one can see, the compensating voltage we apply is a direct measure of the difference in the work functions of the metals. Knowledge of the work function of one of the metals allows an absolute determination of the work function of the other. This is known as the Kelvin Method for determining the work functions of metals, and is a key concept in the development of KPFM theory (Nonnenmacher et al., 1991) which we will discuss next.

1.3.3 Historical Overview

KPFM as a microscopy tool was first introduced by Nonnenmacher et al. (1991), which described the first application of Kelvin's method combined with an AFM to produce images of the contact potential difference (CPD) between the tip and a sample surface. In terms of the work functions, the CPD is written

$$v_{\mathrm{CPD}} = \left(\phi_{\mathrm{sample}} - \phi_{\mathrm{tip}}\right)/e \tag{1.2}$$

in which ϕ is the work function and e is the electron charge.

The way in which this is accomplished is by replacing the use of currents in the Kelvin Method with forces, something that AFMs are particularly good at measuring. However, the Kelvin method yields a measurement of the CPD for the entire sample, with no spatial resolution at all. KPFM combines the principles of the Kelvin Method to yield a high resolution CPD measurement system. The basic setup is shown in Fig. 1.6, where we have a conducting cantilever tip that can form a capacitor system with the sample surface. First, as in the Kelvin Method, a capacitor is formed by lifting the tip to a set distance[6] above

[6] Actually, this is set in mV, rather than nm, so really it's a potential setpoint.

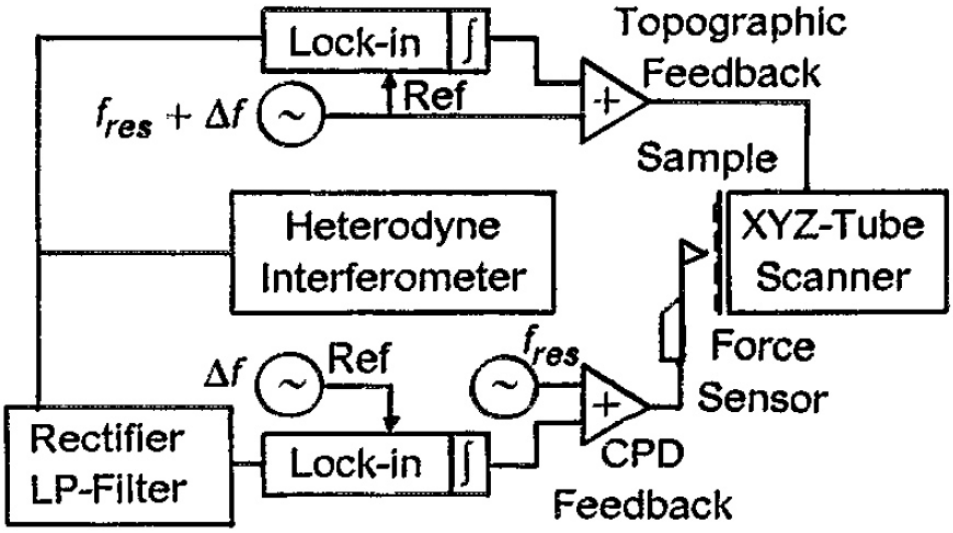

Figure 1.6: Electronics for the basic KPFM setup. Reprinted from Nonnenmacher et al. (1991).

the surface. This is done with the 'trace' step discussed above for AFM. On the retrace, this topographical information is used to maintain a constant height above the sample. This forms the capacitor we discussed previously. Next, as in the Kelvin Method setup, the cantilever is set into oscillation with an AC voltage. As the cantilever probe is sent along the retrace path, a compensating potential difference is applied to minimise the AC-induced oscillations. As before, the oscillations will stop when the compensating voltage cancels out the potential difference, or work function. The results are recorded at each location and used to calculate and map out the contact potential difference. This KPFM operation setup is known also as 'lift mode'. In their first paper, Nonnenmacher et al. (1991) demonstrated this procedure using samples of two different metals and imaged them with KPFM. An example from their work is shown in Fig. 1.7, where surfaces of platinum and gold are imaged together.

A year later, Nonnenmacher et al. (1992) reported a study showing that KPFM could also provide information on the condition of the surfaces that are studied, including crystal structures, contamination and conductivity. The latter was measured by illuminating silicon surfaces and then imaging their surface potentials; electrons would be liberated from

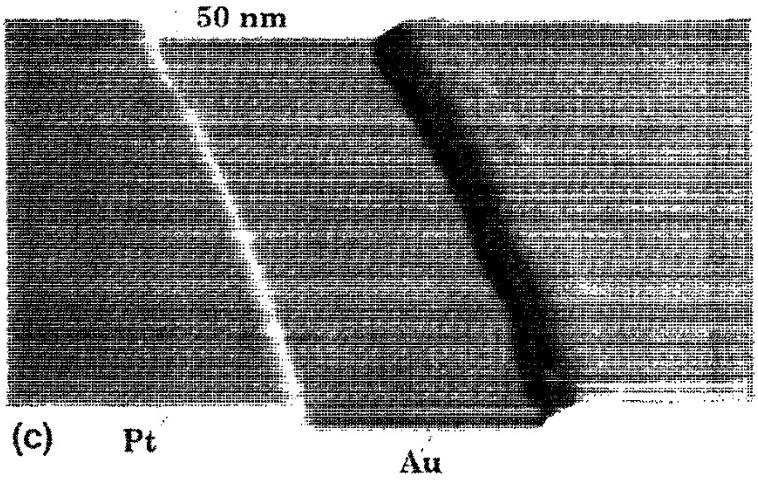

Figure 1.7: One of the first KPFM images of platinum and gold. Reprinted from Nonnenmacher et al. (1991).

the photoelectric effect and then left to conduct along the surface, producing a measurable voltage change. In 1996, Yasutake et al. introduced some improvements to the previous KPFM setup using a frequency modulation technique (see below) with an improved servo mechanism to control the tip separation so that the cantilever never comes into contact with the surface (increasing the potential measurement resolution) and a method to nullify the electrostatic force at the topographical modulation voltage to increase the lateral resolution to 10 nm.

1.3.4 Mathematical Development

It is instructive to put into mathematical form the discussion above, so that we can facilitate a clearer connection with the electronic realisation of KPFM. We can begin by writing down an expression for the force that is experienced by the cantilever tip and the sample, which is dependent upon the electrical potential difference between them and the nature of the capacitor that is formed (see Melitz et al., 2011):

$$F_{\mathrm{ts}}(z) = -\frac{1}{2}\Delta V^2 \frac{dC(z)}{dz} \tag{1.3}$$

Here, the force is dependent on the gradient of the capacitance, C (with respect to the height, z, which is the direction perpendicular to the sample surface), and the difference between the CPD and the voltage that is applied to the tip, ΔV. This voltage difference is simply the CPD plus whatever voltage we apply to the tip. In the case of KPFM, we apply an AC voltage (to oscillate the tip and create the 'vibrating' capacitor) plus a compensating DC voltage. The result can be expressed as (Melitz et al., 2011)

$$\Delta V = V_{\text{tip}} \pm V_{\text{CPD}} = (V_{\text{DC}} \pm V_{\text{CPD}}) + V_{\text{AC}} \sin(\omega t) \tag{1.4}$$

Notice that the V_{AC} component is sinusoidal in time, as alternating currents behave. Putting this expression into our equation for the force detected by the AFM tip, we have

$$F_{\text{ts}}(z,t) = -\frac{1}{2}\left[(V_{\text{DC}} \pm V_{\text{CPD}}) + V_{\text{AC}} \sin(\omega t)\right]^2 \frac{dC(z)}{dz} \tag{1.5}$$

which can be separated into three interesting parts:

$$F_{\text{DC}} = -\frac{dC(z)}{dz}\left[\frac{1}{2}(V_{\text{DC}} \pm V_{\text{CPD}})^2\right] \tag{1.6}$$

$$F_{\omega} = -\frac{dC(z)}{dz}(V_{\text{DC}} \pm V_{\text{CPD}})V_{\text{AC}} \sin(\omega t) \tag{1.7}$$

$$F_{2\omega} = \frac{dC(z)}{dz}\frac{1}{4}V_{\text{AC}}^2\left[\cos(2\omega t) - 1\right] \tag{1.8}$$

Notice that the first, F_{DC}, does not vary with time; it contributes, therefore, to a constant deflection of the tip from the sample surface (that is, a measure of height). The second equation, F_{ω}, vanishes when $V_{\text{DC}} = V_{\text{CPD}}$.[7] Thus, oscillations induced at frequency ω can be monitored and nullified with a judicious choice of V_{DC}, which gives a direct measure of V_{CPD}. Lastly, the third equation, causes oscillations at a different frequency (which typically is not monitored in KPFM) and can be used for capacitance microscopy, which we will not discuss here.

[7] This is a miraculous result. Also, note that the compensating voltage is either equal, or equal and opposite, to the CPD, depending on how the system is set up.

A Note on Electronics

It is useful to present a brief discussion on how the electronics are set up to implement the KPFM system. In the basic form, Nonnenmacher et al. (1991) presented it as follows, with reference to Fig. 1.6. The force-sensing AFM tip is driven at or close to the fundamental resonance frequency, and simultaneously at another frequency that is higher by a small amount. The reason for this will become clearer later on, but the basic idea is to separate the height-measuring signal from the CPD signal. A lock-in amplifier is used to detect changes in the response of the AFM tip oscillation, which will be due to changes in the sample height (for one frequency) or in the CPD (for the other frequency).[8] The signal is then filtered, and an interferometer is used to monitor the tip height. If the signal coming from the lock-in amplifier is non-zero, a feedback loop adjusts the compensating voltage until the lock-in amplifier signal vanishes. The resulting CPD is measured, and the tip moves along the sample.

1.3.5 Advanced Modes: Amplitude and Frequency Modulation KPFM

In recent years, the basic KPFM procedure has been refined with additional techniques and electronics to improve upon the sensitivity, speed and resolution (e.g. Jacobs et al., 1998, 1999; Zerweck et al., 2005; Moores et al., 2010). Here we will discuss two interesting advances in KPFM implementation that have significant advantages over conventional methods. The first is amplitude modulation (AM), and the second is frequency modulation (FM). By analogy with radio frequency transmissions, changes in the amplitude or frequency of the sinusoidal signal coming from the tip are used to carry the information, which in this case is the contact potential difference (or how it is changing) as the tip moves along the surface. The amplitude and frequency changes that are monitored for the KPFM signal are generated by the variation in the forces exerted on the cantilever tip; a

[8] Lock-in amplifiers work by mixing the input signal with a reference frequency, and output a positive signal only of the input signal contains oscillations at the reference frequency. Essentially, a signal is sent from the lock-in amplifier only if the tip is oscillating at or near the reference frequency.

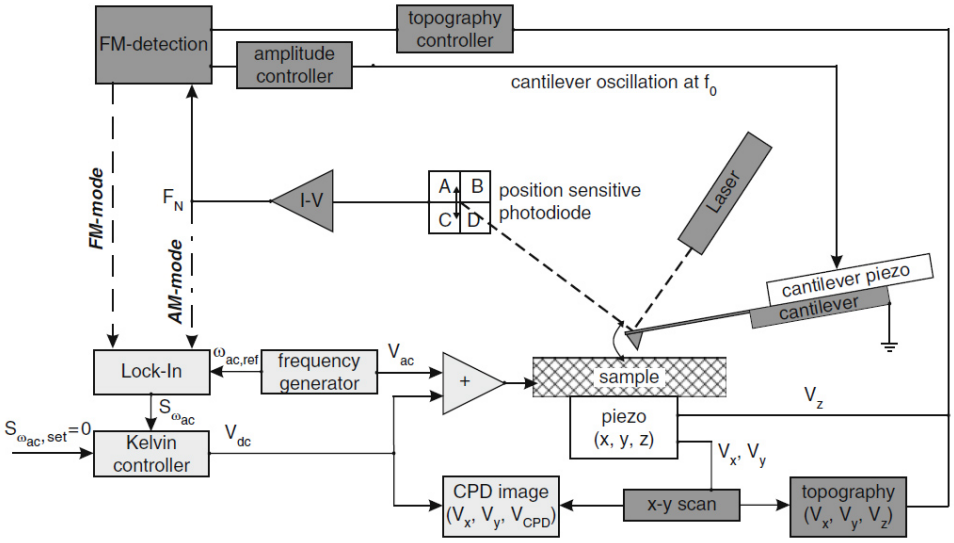

Figure 1.8: A schematic of the KPFM setup with AM and FM modes. Reprinted from Sadewasser & Glatzel (2012, Chap. 2).

change in the force results in a change in the tip oscillation (more on this later). In this way, the feedback signal (essentially the signal that indicates a change in the compensating voltage is necessary) is modulated by the amplitude or frequency of the tip oscillation. As we will see, this modulation scheme creates additional advantages (Zerweck et al., 2005).

One important advantage is the use of frequencies that are not necessarily at the fundamental resonance. Cantilever tips (and other oscillating objects) have more than one resonance frequency, so it is possible to encode multiple signals carried at different resonances. Resonance frequencies above the fundamental mode are called overtones, the first of which is roughly at six times the fundamental frequency. This point is important for the advanced modes discussed below (Zerweck et al., 2005). Fig. 1.8 shows how the setup is expanded for advanced modes, which will be useful as we discuss them.

Amplitude Modulation

In AM mode, changes in the amplitude of the oscillation of the cantilever tip are monitored and the compensating voltage is applied to minimise these changes. Notice from the

equations above that the amplitude of oscillations at frequency ω is non-zero if the CPD is not matched by the compensating voltage. By electrically exciting the AFM tip at, for example, the second resonance frequency (first overtone), the lock-in amplifier can be tuned to that frequency and used in the feedback loop to minimise changes in the amplitude of oscillation at that frequency. Here, the first overtone is used for two reasons. First, the amplitudes of oscillation at harmonic[9] frequencies have very high responses when compared to any random off-resonant frequency, and this helps to achieve an acceptable signal-to-noise ratio. Second, even the softer cantilevers have fundamental frequencies in the range of $\sim 70\,\text{kHz}$, which brings their first overtone to $\sim 440\,\text{kHz}$; anything much higher than that is beyond the capabilities of standard instruments.[10] The fundamental frequency is then left available to mechanically[11] excite the tip so that height measurements can be made simultaneously. Separating the signals in this way mitigates cross-talk between the signals from the CPD and topography (Melitz et al., 2011). Not only does this configuration allow simultaneous measurement of topography and CPD, it allows the tip to scan closer to the sample surface, which increases the spatial resolution. Reducing cross-talk has the effect of increasing the resolution of the CPD measurement (Moores et al., 2010).

Frequency Modulation

An electric field actually changes the fundamental resonance frequency of cantilever tips. Looking at Hooke's law[12], we see that for small oscillations the force between the tip and the sample deflects the cantilever by an amount z, with the spring constant k acting as a

[9] The term 'harmonic' simply means that the frequency is one that sets up resonance in the cantilever, be it the fundamental frequency, first overtone, etc. This need not be limited to the fundamental frequency, since there is an entire spectrum of harmonics.

[10] This means, in effect, that the second overtone is off limits.

[11] As in the traditional AFM, this is done with a piezoelectric crystal rather than an oscillating current.

[12] While this is called a 'law', it actually isn't. This result is only valid for relatively small oscillations. Under such conditions, the frequency of the oscillations is independent of the amplitude (much like all pendulum clocks keep time because their oscillation frequencies are identical). However, as the amplitude increases, the frequency becomes increasingly dependent on it.

constant of proportionality:

$$F = -kz \tag{1.9}$$

Therefore, one can conclude that a force gradient gives us

$$\frac{dF}{dz} = -k \tag{1.10}$$

Furthermore, the fundamental frequency of oscillations for a force-spring system is given by

$$f_0 = \frac{1}{2\pi}\sqrt{\frac{k}{m_{\text{eff}}}} \tag{1.11}$$

in which m_{eff} is the effective mass of the system of interest. Therefore, the presence of a force gradient causes a shift in the 'effective' spring constant, leading to a shift in the fundamental resonance frequency (Giessibl, 1997; Zerweck et al., 2005), which for relatively small force gradients is given by f_0',

$$f_0 \simeq f_0\left(1 - \frac{1}{2k}\frac{dF}{dz}\right). \tag{1.12}$$

This suggests that a shift in the resonant frequency could lead us to a different method of detecting a CPD. In FM mode, the cantilever is oscillated as in AM mode, mechanically at the fundamental resonance frequency and electrically at some other frequency that we call f_{mod}.[13] A feedback loop minimises the electrical oscillations when the compensating voltage nullifies the CPD. However, FM mode takes advantage of the shift in resonance frequency that is experienced in the presence of electrical forces. The system tracks a signal that arises from the oscillation of the electric force gradient that is due to the modulation voltage. Since the fundamental resonance frequency of a cantilever is shifted due to a force gradient, oscillations in the force gradient generate side-band signals. These side-bands are due to frequency mixing arising from the two waveforms (the other being f_{mod}). When two sinusoidal waves are mixed (with frequencies f_0 and f_{mod}), which implies multiplying them

[13] In FM mode, this isn't necessarily the first overtone, since, as we will see, we do not encounter the same difficulties with signal-to-noise as in AM mode. In fact, for reasons that will become clear later, f_{mod} is typically a few kHz.

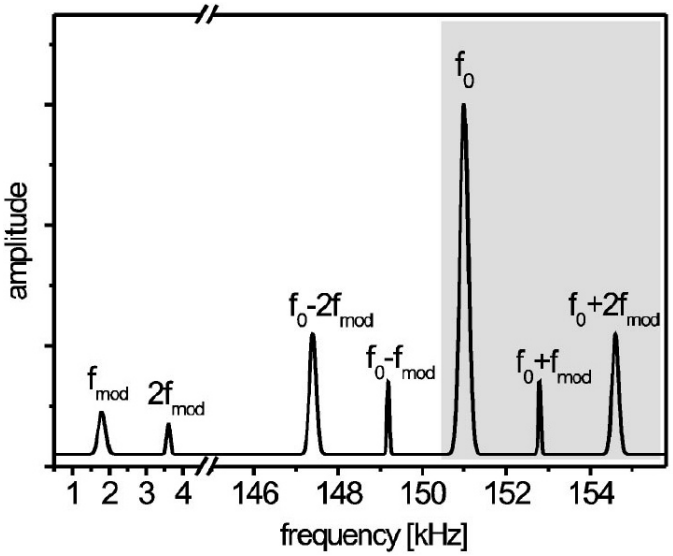

Figure 1.9: A representation of the spectrum of frequencies giving rise to the tip oscillation in FM-KPFM mode. Reprinted from Zerweck et al. (2005).

together, we can see from a standard trigonometric identity that the result is a contribution from two other sinusoids,

$$\cos(2\pi f_0 t)\cos(2\pi f_{\text{mod}} t) = \frac{1}{2}\left\{\cos[2\pi(f_0 - f_{\text{mod}})t] + \cos[2\pi(f_0 + f_{\text{mod}})t]\right\} \tag{1.13}$$

which have frequencies $(f_0 + f_{\text{mod}})$ and $(f_0 - f_{\text{mod}})$. These additional frequencies are known as 'mixing side-bands' and are sensitive to the force gradient (since the force gradient changes the fundamental frequency), instead of just the force, as is the case with the non-mixed frequencies (Zerweck et al., 2005). See Fig. 1.9 for an illustration. Here, the modulation frequency is chosen to be only a few kHz. A KPFM system can track signals at these side-bands in a feedback loop which nullifies them. A null signal at these side-bands indicates a compensated, and thus recorded, CPD. It is important to note that these signals can be nullified *only* because their presence depends upon the quantity $(V_{\text{DC}} - V_{\text{CPD}})$ being nonzero; see Eqns. 1.7 and 1.8.

Since we are not limited to the frequency of the first overtone, soft cantilevers are not required. By using a stiff cantilever, smaller tip-sample separations are possible, which

increase the lateral resolution significantly. Not only is this a nice advantage, it is somewhat of a requirement for this mode to succeed: as we discussed, the FM mode is sensitive to the electrostatic force gradient, a property which is larger nearer to the sample. Very little signal is generated far from the sample. Since the force gradient is large near the sample surface, and not subject to any parasitic influence from the topography, FM-KPFM can achieve the greatest spatial resolution in air (in some cases, on the order of 1 nm). Electric potential resolution down to only a few mV can also be achieved. In contrast, AM-KPFM has much lower spatial resolution, up to a factor of 10 worse than FM-KPFM, which is somewhat dependent on the tip size (Zerweck et al., 2005). Although it has been shown that AM-KPFM can produce greater potential resolution, it gives an inferior signal-to-noise ratio (Zerweck et al., 2005; Moores, 2010).

1.3.6 Applications of KPFM

Potential Differences

In the case of metal samples, as we discussed previously, KPFM measures the difference in the work functions of the tip and sample. Knowledge of the tip's work function allows an absolute measure of the sample's work function. For an insulating material, where there is little or no electrical conduction, we measure simply the electric potential difference between the tip and sample. On a surface, there exists a potential energy surface which we might wish to measure. For membranes, this surface might also be generated from a series of dipoles created from the molecules making up the surface. The dipole fields would be picked up as contributions to the potential difference signal. However, one must take caution in realising that a KPFM signal is most useful when we see contrast in the image. Essentially, we need to see differences between different areas of the sample. If we have a membrane that is composed of two layers and wish to probe its electrostatic properties, for example, we might not be able to detect any significant KPFM signal since the dual layers provide symmetry and result in the same dipole fields, giving rise to no variation in the KPFM image. Therefore, it is often important to look at monolayers in KPFM studies. More on this will be discussed later.

Physics and Materials Science

In most non-biological applications, KPFM is useful in the study of metallic nanostructures and other small-scale processes that might involve charge distributions, work functions or current behaviour. Here we will describe a few brief examples.

Metallic nanostructures are important to understand if we wish to construct technologically useful devices on the nanometre scale. A particularly useful metal is gold, as it has low chemical reactivity and is relatively large. In a study of the deposition of gold nanoparticles onto an InSb surface, Goryl et al. (2005) showed both topographical and KPFM images of the deposition, which is shown in Fig. 1.10. As we can see, the KPFM image reveals interesting features in between the 'usual' rectangular shapes formed by the gold. The researchers suggest that this is due to Indium alloying with the gold atoms, leaving the surfaces between the nanostructures enriched with antimony. Such a conclusion cannot be reached looking at the AFM topography alone.

Given the ability of KPFM to detect surface charges (and thus currents), it seems natural that solar cells would be an interesting application. Indeed, much work has been done on solar cells with KPFM (e.g. Glatzel et al., 2005; Loppacher et al., 2005), and Glatzel et al. (2005) presents an interesting study in which an organic solar cell film was imaged both in the dark and under illumination. The KPFM signal differs markedly for the two conditions, which translates into a difference in the 'photovoltage' of the surfaces before and after illumination.

In addition to metallic nanostructures and solar cells, there are numerous other non-biological applications as well, such as how charges move when metals are used as catalysts in chemical reactions, charge transfer in semiconductors, quantum dots and transistors (see Melitz et al. (2011) for a review).

Biological Applications

Despite the tremendous potential of KPFM to reveal new science in biological systems, only recently has this been practical due to the difficulties that such applications present. For example, there must be sufficient contrast in the CPD signal that can be resolved on

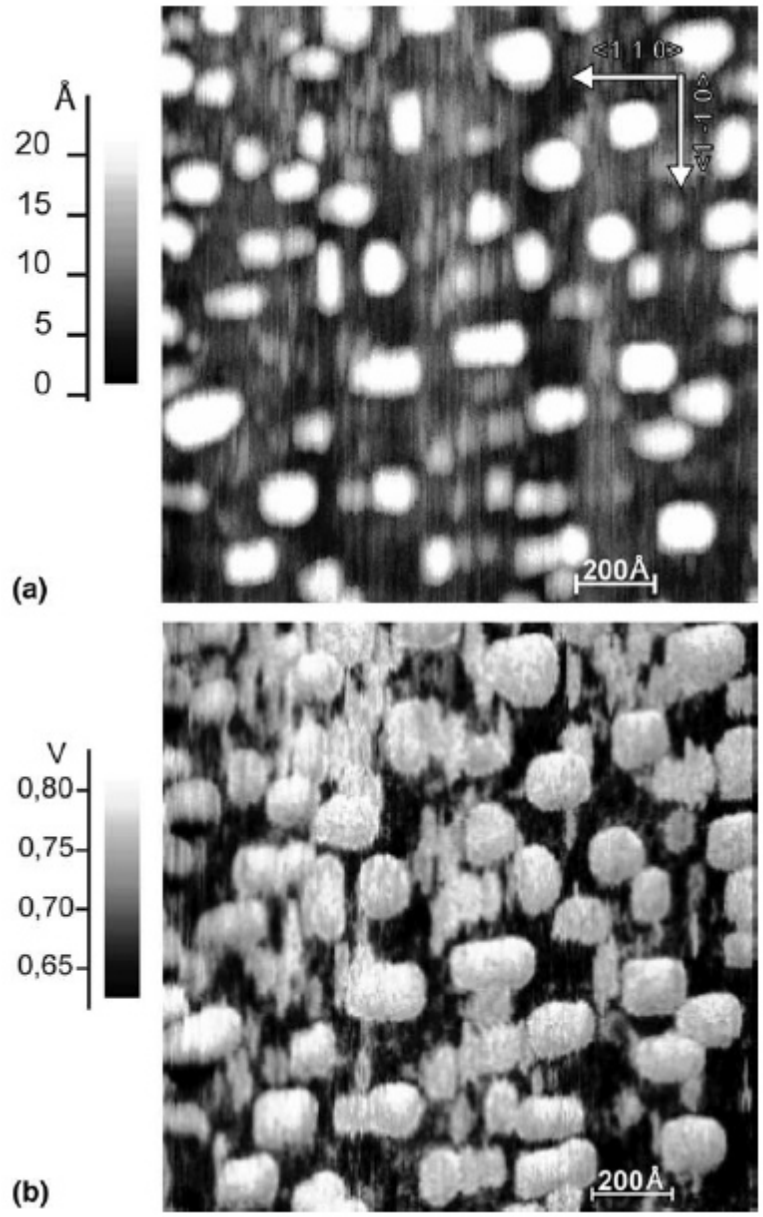

Figure 1.10: Gold deposited onto an InSb surface. (a) AFM image, (b) KPFM image. Features between the gold structures are visible in the KPFM image. Reprinted from Goryl et al. (2005).

the scales at which KPFM functions. If, say, the charge distribution is fairly uniform on the scale of a few tens of nanometres, then the CPD signal will be washed out. Higher resolution KPFM helps to work around this, but development of FM-KPFM is still ongoing.

Nevertheless, there have been a number of promising studies to-date that show the basic capabilities of AFM and KPFM to study biological systems (Kalinin et al., 2007). A large amount of research has been done on cell membranes by imaging lipid monolayers and bilayers, which are relatively straightforward to implement in the lab (see below). Surfactant films are also an important system that can be studied with KPFM, which we will discuss in this section. In a biological context, surfactants are well known to play an important role in lung function; a surfactant essentially reduces surface tension, and allows lungs to expand more freely than if they were coated in water, which has a relatively high surface tension and would resist expansion (e.g. Leonenko et al., 2006). Another interesting application of KPFM is in the study of DNA and proteins. Their structure and functions under various conditions can be studied, this time alongside their electrostatic properties. We will discuss these topics in more detail below.

Lipid Monolayers and Cell Membranes

Thin films, and in particular lipid molecules play a critical role in the function of biological processes. First we will discuss lipids and their role in cell structure and function before discussing recent studies in some detail. A lipid is a type of amphiphilic molecule, which contains a hydrophilic component at one end and two hydrophobic tails at the other. The result is that one end of the molecule is attracted to water, the other end avoiding it. The structures of some common lipids are shown in Fig. 1.11. Cell membranes consist of lipids aligned in two sheets, with the hydrophobic tail ends facing each other, as depicted in Fig. 1.12 below. In this double-sheet format, the structure is known as a lipid bilayer. A single layer of lipid is known as a monolayer. We will talk about the specifics of how monolayers are studied later on. In biological cells, lipid bilayers form the protective barrier that allows them to control what goes in and what doesn't. Proteins present in the membrane form channels which allow the regulation of ion concentrations both within and outside the cell, nutrient intake, expulsion of waste products, and so on (Alberts et al., 2002). Studying membrane structure and composition, and the effects of different building

blocks (lipids) is therefore extremely important.

Also of importance in the study of lipids is their phase, as different lipids can have different structural characteristics at different temperatures. Shown in Fig. 1.12, lipid bilayers of different phases are depicted. The double bond in an unsaturated lipid creates a 'kink' in the chain which disrupts the ordered stacking of the molecules, creating spaces in the bilayer which allows the lipids to move more freely. This is known as a 'liquid' phase, while a fully saturated lipid is generally in a gel-like phase at room temperature.

In the cell membrane, the lipids present are primarily glycerophospholipids (like phosphatidylcholine), sphingolipids, and steroids (like cholesterol) (Alberts et al., 2002). Varying the relative concentration of different lipids in membrane studies helps us to determine their functional role in the cell. For example, a lipid monolayer containing two lipids, one saturated and one unsaturated, would form structures known as lipid 'rafts', where regions of the monolayer are higher than at other places since the two lipids are slightly different in length.

Biological membranes are very difficult to study since their thickness is only on the order of a few to 10 nm. In addition, they are delicate structures that are easily ruptured in a laboratory setting. Ideally, we would like to simply study them directly in their native state, but this is not possible with conventional microscopy. Due to their size, electron microscopy or AFM is required to resolve the nanometre-sized structures present in the membranes. The huge advantage of AFM is that the membrane need not be artificially treated before imaging.

Furthermore, lipids are in general charged structures, and therefore they form an electric potential surface in membrane form. We can use KPFM to study the electrostatic properties of lipid membranes in a biological context. Below, we will discuss a few examples of recent studies.

Examples

Our first example is a study by Leung et al. (2010), where individual DNA molecules were imaged with AFM and KPFM on a mica substrate. The authors experimented with lift-mode KPFM and what they call 'dual frequency mode', which resembles AM-KPFM. They

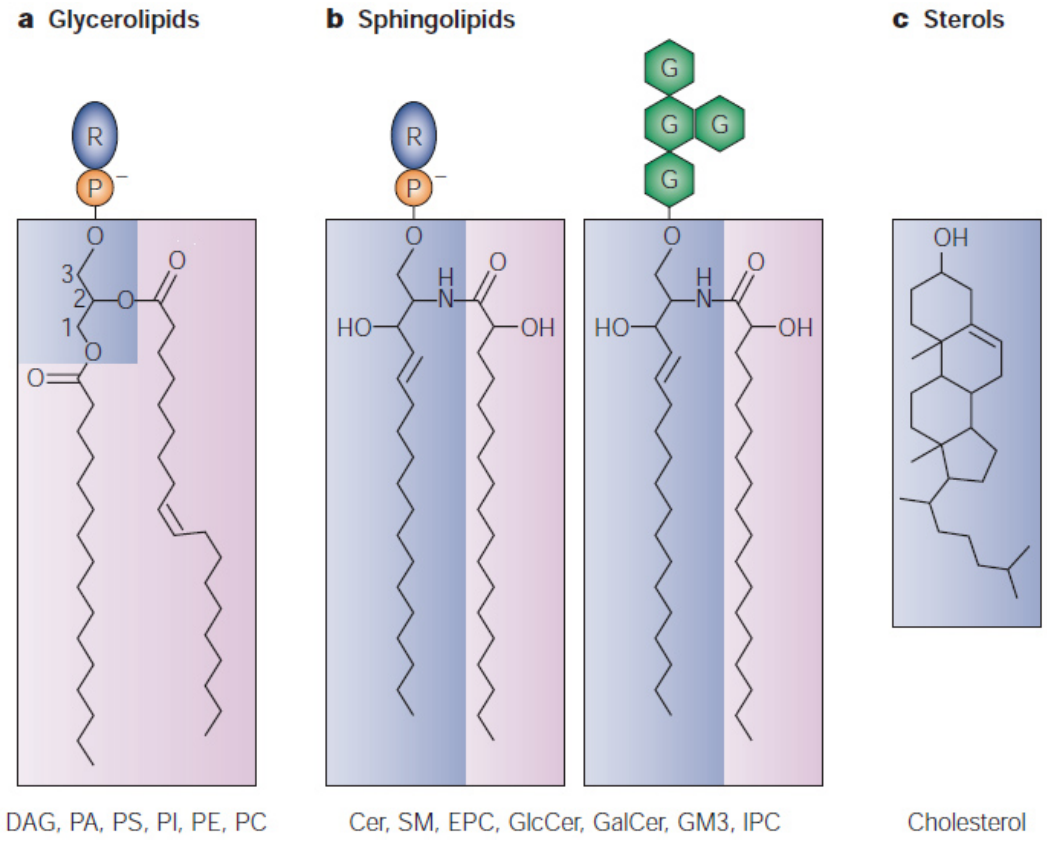

Figure 1.11: Some common membrane lipid structures. The head groups are represented by 'R', and give rise to the different classes; for example: phosphatidylcholine (PC) or phosphatidylethanolamine (PE) in the case of the glycerolipids. Reprinted from Holthuis & Levine (2005); see that paper for further definitions.

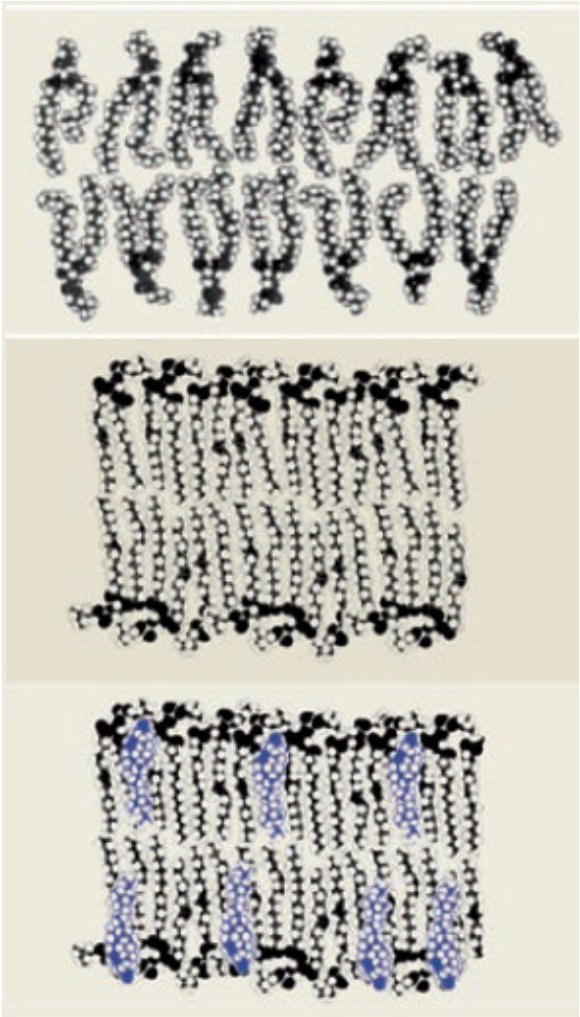

Figure 1.12: An overview of common lipid phases in bilayer structures. Top: liquid crystalline. Middle: solid gel. Bottom: liquid ordered. Reprinted from Van Meer et al. (2008).

found, not surprisingly, that the latter mode resulted in superior resolution. Their image of DNA (both height and CPD relative to mica) is shown in Fig. 1.13. The DNA shows up with a negative CPD when compared to mica, as the DNA is negatively charged. White regions also appear in the image which the authors claim is due to Ni^{2+} ions accumulating on some of the DNA molecules. These Ni^{2+} ions were deposited onto the mica before the DNA in order to provide a 'sticky' surface on which to bind. In an earlier study, the same group imaged DNA and individual biomolecules on a silicon surface (Leung et al., 2009); see Fig. 1.14. In that study, individual avidin (egg protein) molecules were imaged and determined to have a potential difference of about +10 mV each relative to the background. However, the authors point out that silicon is not an ideal substrate to use in biological studies; mica is much more suitable as it is an insulating, polar surface that accepts hydrated samples.

A study on protein binding was done by Sinensky & Belcher (2007), where avidin and neutravidin (a modified avidin) glycoproteins were added to biotin (a B-vitamin) to observe the change in charge distribution with KPFM. They observed that after avidin exposure the surface potential changes dramatically, whereas with neutravidin it does not. Studies such as this pave the way for future experiments to detect charge distributions in protein complexes. It is also important to point out that these studies are done without any dyes, labels or intercalating agents as is necessary in most applications of other methods, like fluorescence microscopy. Such labelling techniques have the potential to alter the sample, which could bias results. KPFM requires no such labelling, which is another significant advantage in biological studies (Thompson et al., 2005).

Another interesting application is imaging actin filaments. Actin filaments play an extremely important role in muscle contraction. When they contract, changes in the distribution of charges can tell us something about their electrostatic functions. Zhang & Cantiello (2009) performed such a study, and imaged actin with both AFM and KPFM. The result is shown in Fig. 1.15 below. Earlier in this review, we discussed three different imaging modes: lift, AM and FM KPFM. In a study on pulmonary surfactant, Moores et al. (2010) demonstrated the practical differences in imaging the surfactant assembly using all three KPFM modes. In this particular study, pulmonary surfactant Bovine Lipid Extract Surfactant (BLES) was combined with 20% cholesterol (by weight) and deposited

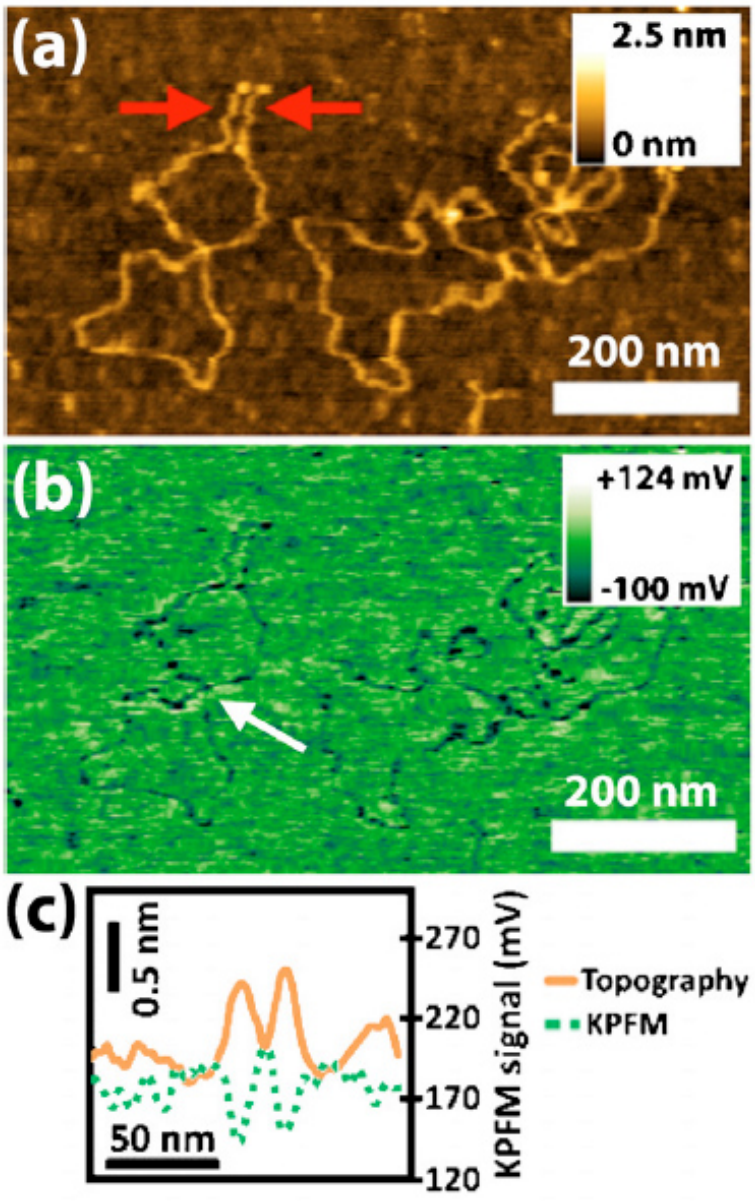

Figure 1.13: KPFM image of DNA molecules on mica. The plots are cross sections showing the presence of the DNA strands as areas of negative surface potential. Reprinted from Leung et al. (2010).

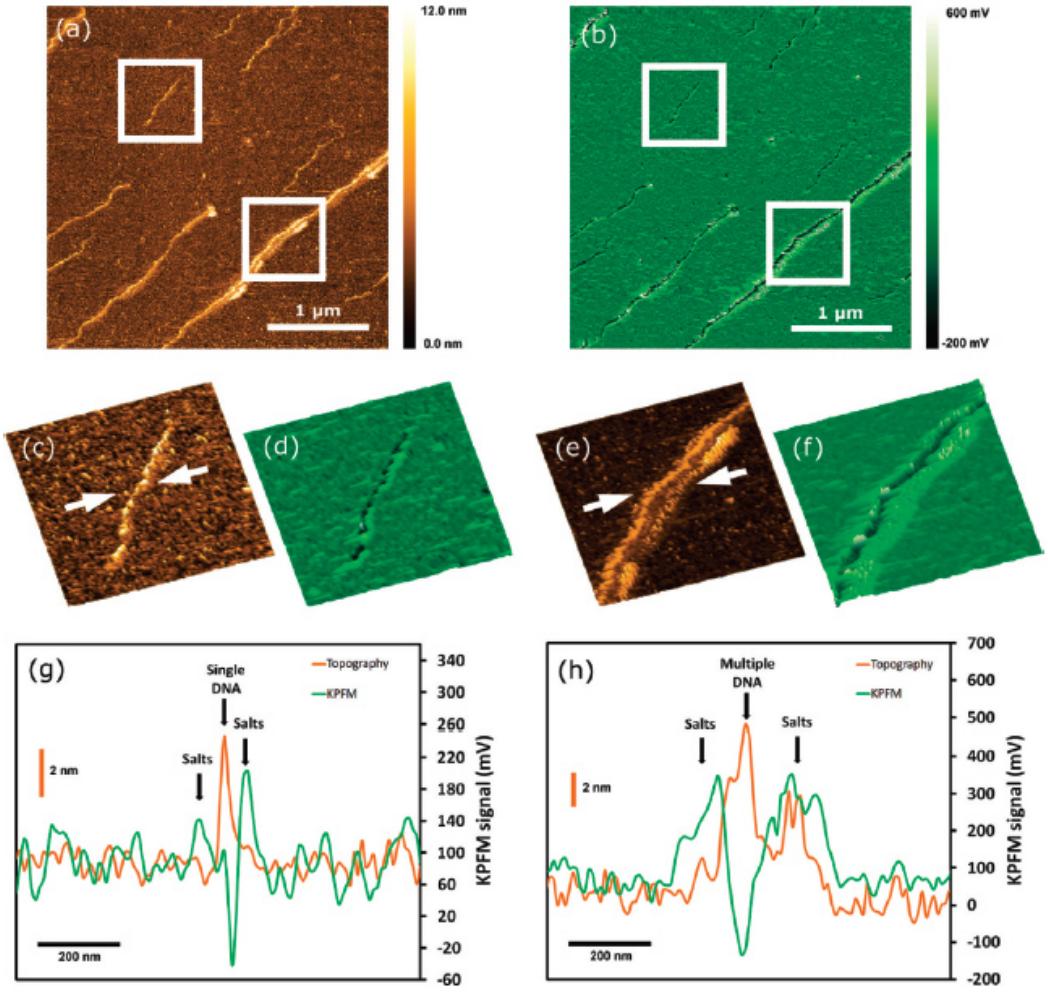

Figure 1.14: Analogous to Fig. 1.13 from the same group, this is an image of DNA on a silicon surface. Images (a) and (b) are AFM and KPFM scans. The white boxes show where the inset images were taken, resolving an individual DNA strand (c,d) and intertwined strands (e,f). The plots (g,h) are cross sections from their respective images above, along the white arrows, showing the presence of the DNA strands as areas of negative surface potential, with some positively charged buffer salts surrounding them. Figure reprinted from Leung et al. (2009).

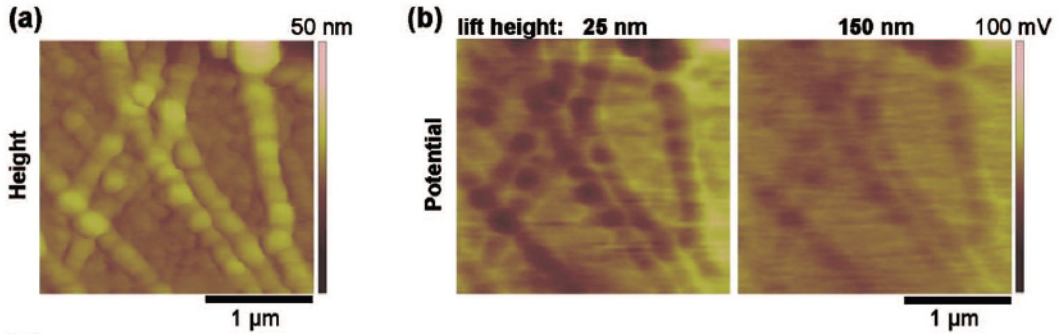

Figure 1.15: AFM (left, a) and surface potential (right, b) images of actin filaments. The surface potential images were taken from two different lift heights in image (b), as shown. Reprinted from Zhang & Cantiello (2009).

onto mica using a Langmuir Blodgett (L-B) trough.

Before we describe the results, it is useful to briefly describe this L-B trough method to deposit a lipid monolayer onto the mica slides for KPFM (and AFM, for that matter) imaging. The trough is a hydrophobic basin into which a liquid (usually water) is poured and purified. A lipid mixture dissolved in an organic solvent is then spread over the top surface of the liquid so that it is only one molecule thick. The hydrophilic head groups will all naturally align themselves with the water, so that the hydrophobic tails point directly upwards out of the tray. Two arms at the end of the basin compress the total surface area, raising the pressure to some desired level and keeping the lipid molecules tightly aligned. A mica slide is usually inserted prior to the lipid deposition, and later raised up out of the solution while the arms keep the pressure constant. As the slide is raised upwards, the lipid monolayer is deposited onto the surface in one thin film. This topic will be discussed in detail later in § 1.4.1.

In Moores et al. (2010), the BLES+cholesterol mixture was imaged in all three KPFM modes, as shown in Fig. 1.16. Clearly, the FM mode achieves superior sensitivity and resolution compared to the other modes, where the signal-to-noise ratio is comparatively low. They observe that cholesterol appears to disrupt the electrostatic potential of pulmonary surfactant, which is a phenomenon that cannot be detected with AFM alone.

In a different study, Hane et al. (2009) studied model surfactant films composed of

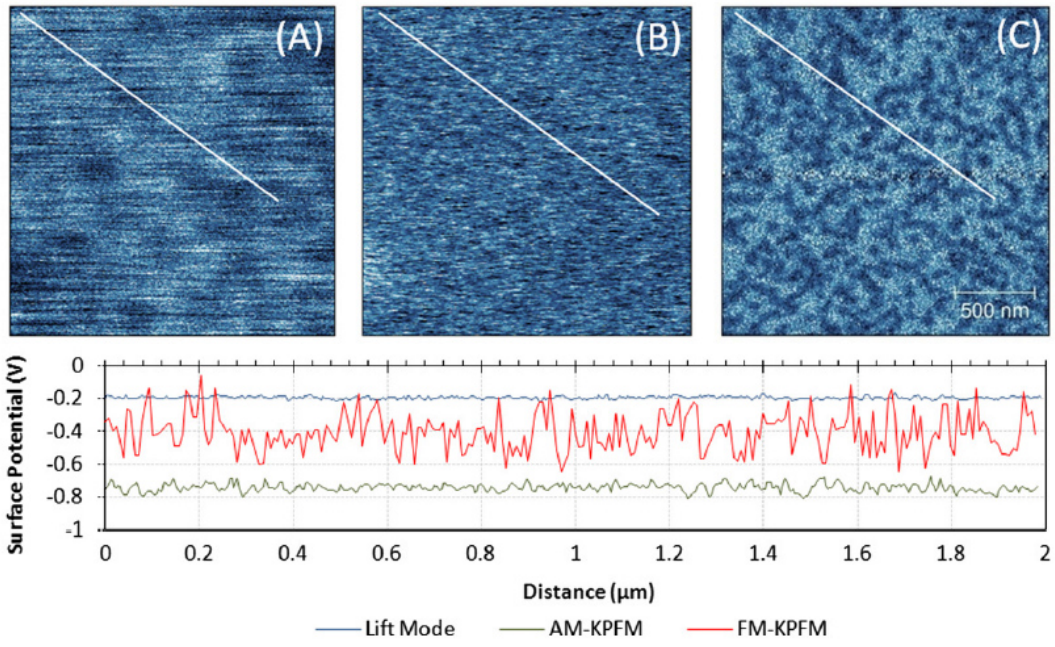

Figure 1.16: Lift mode KPFM (A), AM-KPFM (B) and FM-KPFM (C) images of pulmonary surfactant mixed with 20% cholesterol. In the bottom panel we see cross sections of the surface potentials for each mode. All images are 2 microns on a side. Reprinted from Moores et al. (2010).

DPPC (a large component of the natural BLES surfactant) and eggPC, with and without surfactant protein 'C' (SP-C). Model surfactants are important in that they provide an opportunity to discern the roles of individual components of natural surfactants so that we can determine how they achieve their functions. It turns out that pulmonary surfactant BLES forms multiple layers as part of its function of reducing the surface tension in the lungs. In Hane et al. (2009), AFM and KPFM images are shown (see Fig. 1.17) for the model films, and they showed that the presence of SP-C results in increased KPFM contrast, which is similar to BLES. They conclude that the presence of SP-C in the surfactant film is therefore important. Such contrast is not visible in AFM. To illustrate this point further, Drolle et al. (2012) presented a study in which DPPC monolayers were imaged with AFM and FM-KPFM, with and without cholesterol. The FM-KPFM images revealed nanoscale electrostatic domains which cannot be seen with AFM alone.

KPFM is also useful in detecting binding events of biomolecules (e.g. Gao & Cai, 2009), biomolecules immobilised on surfaces in biocompatibility studies (Cheran et al., 2000), other organic thin films (e.g. Palermo et al., 2006), and the detection of dispersed proteins (Laoudj et al., 2005). In this latter paper, it is pointed out that KPFM could be used to detect proteins that have been dispersed by some method (e.g., electrophoresis), and do so with much higher sensitivity than traditional staining methods. Clearly, the biological applications of KPFM are very promising, with much room for development and new discoveries.

1.3.7 Limitations of KPFM

While KPFM has many excellent features and applications, there are a number of shortcomings to keep in mind. Some of these are resolved in specialised imaging modes, but not all. For example, recall that in lift mode we measure the topography first, then retrace at a constant height above the sample surface to make the KPFM measurement. This has to be done several, if not tens, of nanometres above the surface. The higher the tip is lifted, the more surface the tip 'sees' and thus the result is a blurrier average of nearby space resulting in lower lateral resolution. FM-KPFM does a good job of solving this resolution issue, since it can be performed at closer tip-sample separations.

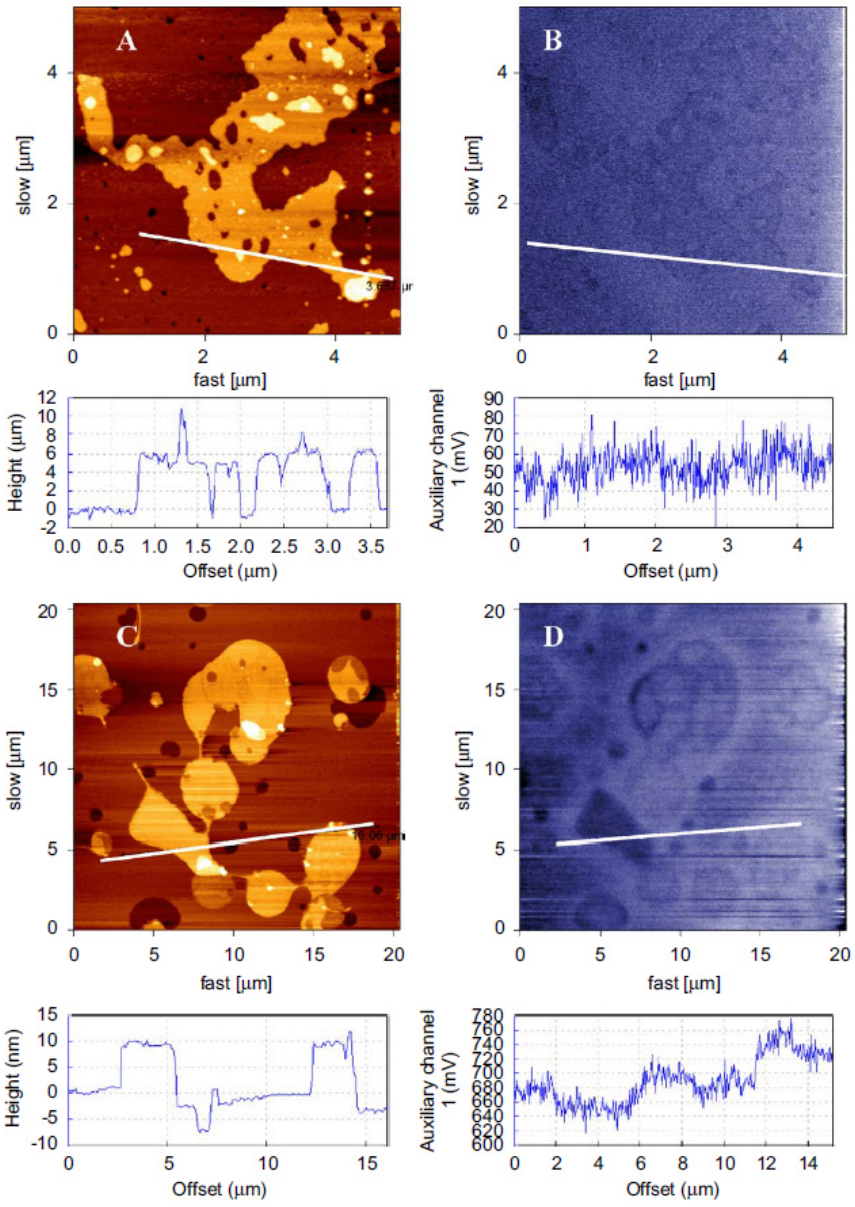

Figure 1.17: AFM (left) and lift-mode KPFM (right) images of a model film of DPPC/eggPG (A-B), and DPPC/eggPG/SP-C (C-D). For each image, cross sections were taken along the white lines shown. Compare the resolution and detail present in the KPFM image here with that of Fig. 1.18. Reprinted from Hane et al. (2009).

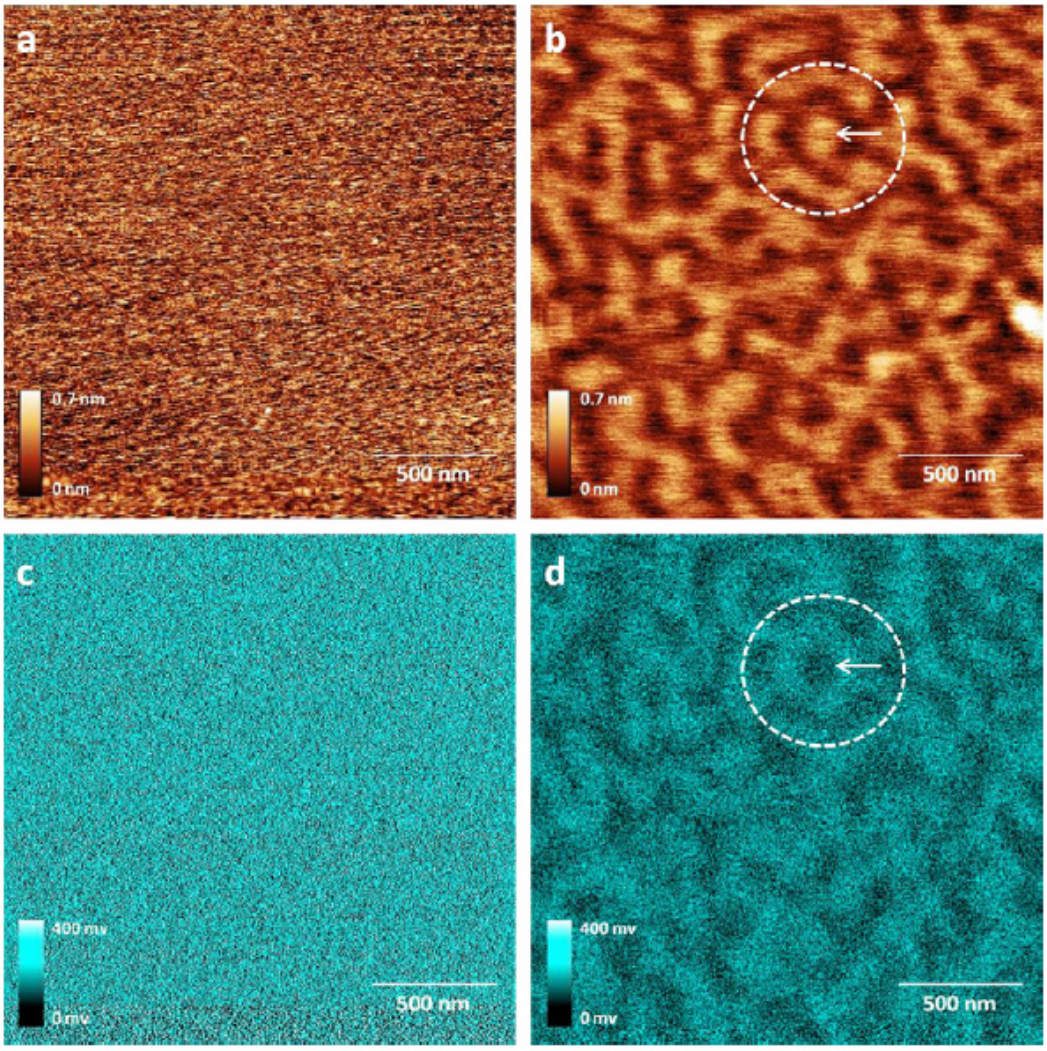

Figure 1.18: Topography (a and b) and FM-KPFM (c and d) of lipid monolayers without cholesterol (left images) and with cholesterol (right images). These images were obtained with the same AIST-NT Smart-SPM that is used in the present work. Reprinted from Drolle et al. (2012).

Oscillating the tip can bring additional problems. It is not the intention to bring the tip into contact with the sample, but sometimes this happens by accident, and charges might flow between them. This either contaminates the tip or alters the surface potential; either way it introduces an undesirable effect.

One of the most significant shortcomings at present is the inability to use KPFM in liquid. To-date, no method has been developed to send a current to the tip without also electrifying the sample, something that is relatively straightforward to implement in air.

Finally, it is worth noting the resolution limits of KPFM. Sub-nanometre resolutions are only achievable with FM-KPFM, which has been a fairly recent development. Resolutions on the order of tens of nanometres are common in lift mode, and so it is useful primarily for systems in which there are significant charges present within large domains that are significantly larger than 10 nm (Zerweck et al., 2005).

1.3.8 Summary and Future Prospects of KPFM

We have discussed the history, theory, development and capabilities of KPFM in this short review. Following an overview of traditional AFM, we discussed the Kelvin Method and how it leads naturally to KPFM via a merger with AFM. We then touched briefly on some historical development and early results, and more recent advanced imaging modes that assisted in solving resolution and sensitivity issues with 'conventional' KPFM in lift mode. Applications of KPFM were discussed, first in a non-biological context and then recent studies of biological systems.

At present, there has been precious little research done using KPFM in biology. This is mainly due to the resolution limits that have only recently been addressed, limits that prevent the CPD imaging of most biological systems. The possibilities are therefore staggering. Virtually any biological system that is charged or possesses an electric field has been relatively unexplored. The next step is to improve upon KPFM methodology and instrumentation to achieve high resolution (< 1 nm) and high sensitivity, and ideally with the capability of implementing this in a liquid environment.

1.4 Monolayers of Amphiphilic Molecules

. . . But recollecting what I had formerly read in Pliny, I resolved to make some experiment of the effect of oil on water, when I should have opportunity. . .

At length being at Clapham where there is, on the common, a large pond, which I observed to be one day very rough with the wind, I fetched out a cruet of oil, and dropt a little of it on the water. I saw it spread itself with surprising swiftness upon the surface; but the effect of smoothing the waves was not produced; for I had applied it first on the leeward side of the pond, where the waves were largest, and the wind drove my oil back upon the shore. I then went to the windward side, where they began to form; and there the oil, though not more than a teaspoonful, produced an instant calm over a space several yards square, which spread amazingly, and extending itself gradually till it reached the leeside, making all that quarter of the pond, perhaps half an acre, as smooth as a looking-glass.

After this, I contrived to take with me, whenever I went into the country, a little oil in the upper hollow joint of my bamboo cane, with which I might repeat the experiment as opportunity should offer; and I found it constantly to succeed. In these experiments, one circumstance struck me with particular surprise. This was the sudden, wide, and forcible spreading of a drop of oil on the face of the water, which I do not know that anybody has hitherto considered. If a drop of oil is put on a polished marble table, or on a looking-glass that lies horizontally; the drop remains in its place spreading very little. But when put on water it spreads instantly many feet round, becoming so thin as to produce the prismatic colours, for a considerable space and beyond them so much thinner as to be invisible, except in its effect of smoothing waves at a much greater distance. . .

–

Benjamin Franklin, 1774
from "Of the stilling of waves by means of oil"

The implications of what Franklin saw go far beyond calming seas. Take his teaspoonful of oil appearing to spread over that half acre. The thickness of such a film, if one does the calculation roughly, must be on the order of 10^{-9} m. A *nanometre*. Franklin, though he did not know it at the time, observed amphiphilic molecules (oil) spread into a monolayer

over the surface of water. That is, the oil spread into a layer only one molecule thick. Furthermore, water has a very high *surface tension*, meaning that it forms a kind of 'skin' at its air-water interface due to its unusually strong polarity. Calming the waves was the result of the surfactant behaviour of oil molecules reducing the surface tension of the water (disrupting the 'skin'). It would not be for over another 150 years that this concept was put to scientific practice by Irving Langmuir and others (e.g. Langmuir, 1934; Blodgett, 1935). For the interested reader, Israelachvili & Ruths (2013) is a nice historical review of this field.

The phenomenon of surface tension arises because there is an *interface*, in this case an interface of air and water. Water has two polar O-H bonds, which, if in an aqueous environment, attract other water molecules so that they all essentially stick together. However, at the interface, there is necessarily an absence of water molecules beyond it. The water molecules are left to interact in a sheet, strongly, which resists breakage (see Fig. 1.19).

If they are introduced to a system like a container of water, amphiphilic molecules don't like to stay in the water; it is energetically more favourable for them to come to the surface (at the interface), so that their hydrophobic tails may be removed from the water. The net effect is a lowering of the surface tension, because the forces between the hydrophobic chains of a surfactant are much less than the attractive forces between water molecules which are able to form hydrogen bonds with each other. As a result, surfactants are, in general, only slightly soluble in water, and beyond a certain concentration form micelles in solution. Gemini surfactants are even less soluble in water than their monomeric analogues. For a detailed reference on this topic the reader is referred to Israelachvili (2011).

In this section, we will discuss in some detail the concepts of monolayer formation, why they are useful, and how they are studied. In this thesis, monolayers are utilised heavily. Combined with nanoscale imaging techniques like AFM and KPFM, we can glean very detailed information about how these molecules behave. It is fortunate that the same properties which give rise to the ability of surfactants to be used as therapeutic agents also facilitates their study.

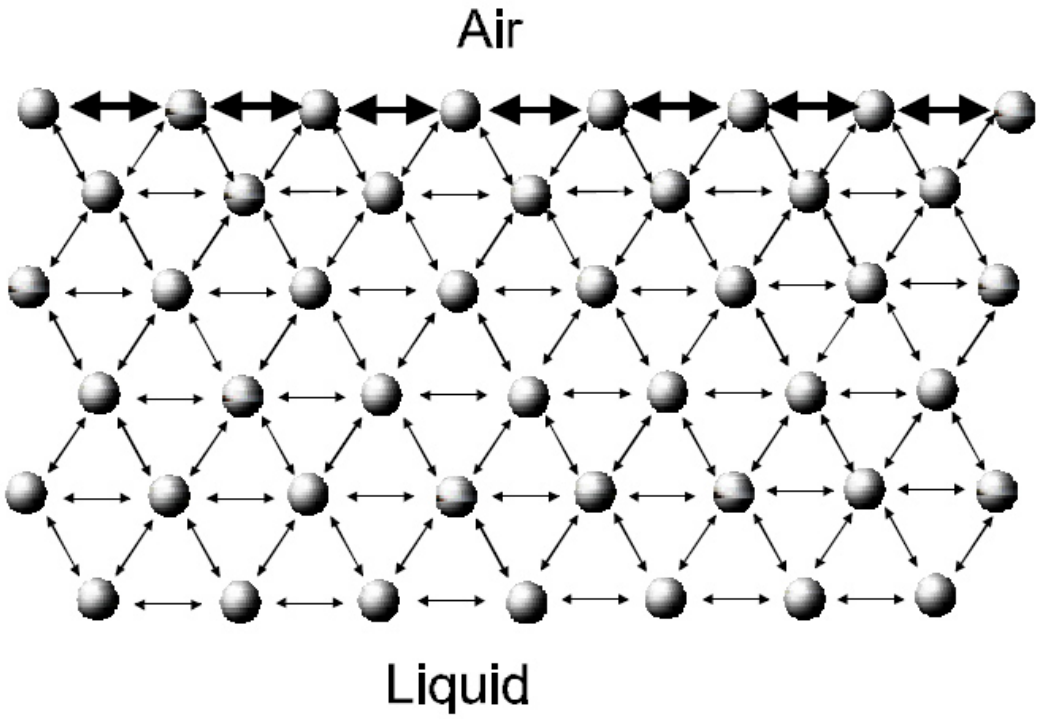

Figure 1.19: Illustration of the two-dimensional arrangement and interactions of molecules in a liquid, particularly at the air-water interface. Reprinted from KSV Nima.

1.4.1 Langmuir Monolayer Techniques

To study monolayers in a controlled environment, Irving Langmuir (Langmuir, 1934) first came up with the instrument design featured in Fig. 1.20. Constructed in this setup, such monolayers are now referred to as 'Langmuir' films. The apparatus, in its most basic form, has a basin to hold a subphase (usually ultra-pure water or buffer), upon which amphiphilic molecules are deposited. In the same way that Franklin's oil experiment worked, the amphiphilic molecules rapidly spread out onto the surface. In general, the molecules are first dissolved in a volatile organic solvent, such as chloroform, which facilitates their deposition and then evaporates away. The trough itself confines the monolayer with movable barriers, which when used to lower the available surface area of the air-water interface serves to increase the surface pressure[14] by lowering the surface tension:[15]

$$\Pi = \gamma_0 - \gamma \tag{1.14}$$

in which γ_0 is the surface tension of the pure subphase, and γ is the surface tension of the subphase with surfactant. In this way, monolayers may be constructed to have various surface pressures depending on the needs of the experimenter.

At approximately the same time as Langmuir's first study, Katherine Blodgett devised a way to construct monolayers on solid surfaces (like glass or mica slides), which also allows multiple layers to be supported (Blodgett, 1935). Thus, monolayers may be created in a Langmuir trough and then fixed on a solid substrate for further study - a method which is called Langmuir-Blodgett deposition, shown in Fig. 1.21. Since those early days of Langmuir and Blodgett, a whole field of research developed which used monolayers to study the behaviour and interactions of amphiphilic molecules (e.g. Goddard & Ackilli, 1963; Swalen et al., 1987; Binks, 1991; McConnell, 1991; Kaganer et al., 1999). In the remainder of this section, we will discuss some of the physics behind these monolayers, and

[14] Note that in this definition, pressure is a one-dimensional quantity, usually expressed in units of $\mathrm{mN\,m^{-1}}$, unlike its two-dimensional counterpart expressed in $\mathrm{N\,m^{-2}}$.

[15] The surface tension is lowered because there are more surfactant molecules per unit area. Recall that surfactant molecules disrupt water molecules from forming a tight 'skin' on the interface; more surfactant molecules means less surface tension.

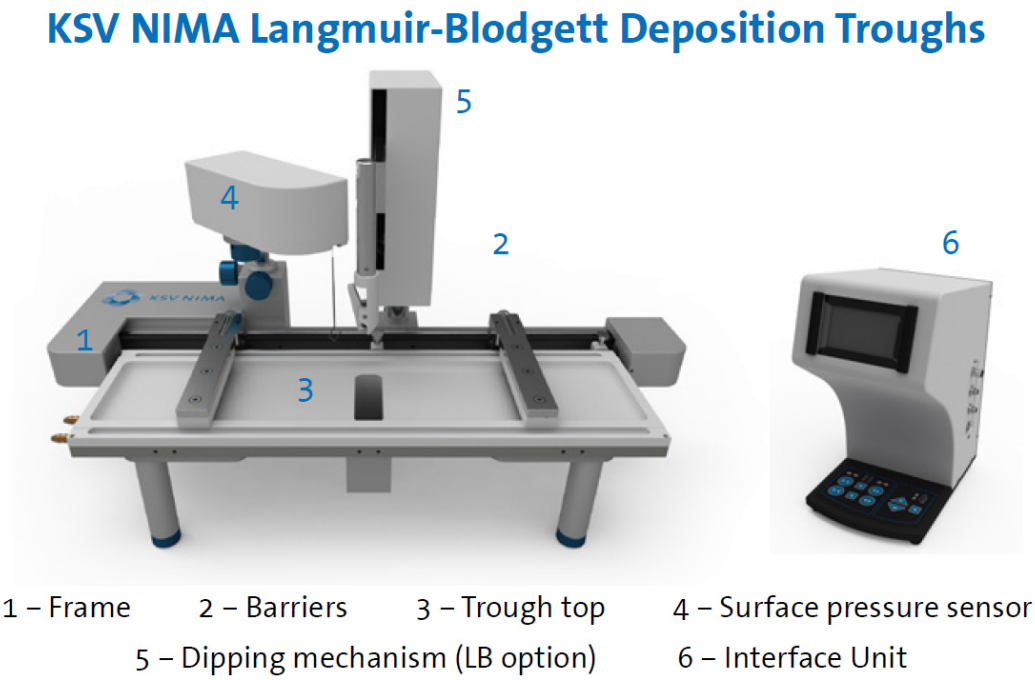

Figure 1.20: A modern Langmuir-Blodgett trough made by KSV Nima. Adapted from a KSV Nima LB Product Brochure.

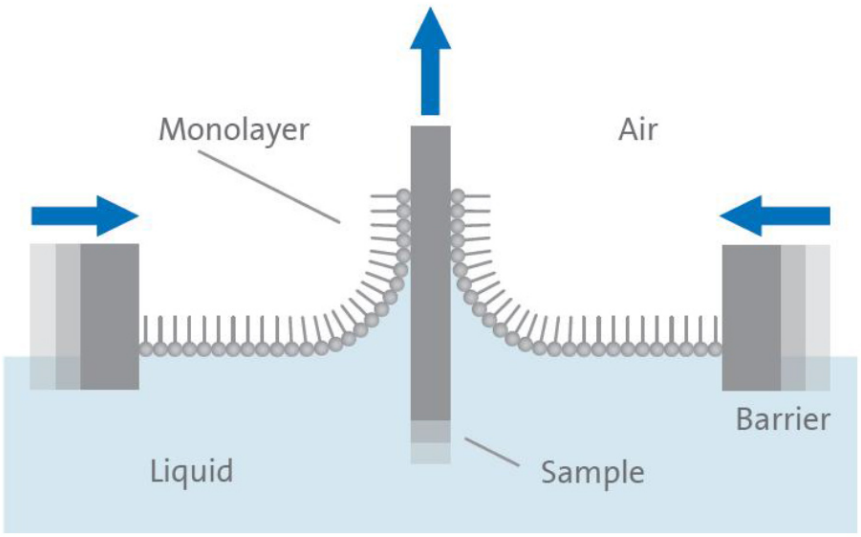

Figure 1.21: Illustration of a monolayer deposition onto a solid substrate. Reprinted from KSV Nima.

how that leads to useful information from the various ways in which these structures are examined.

1.4.2 Physics of Langmuir Films

Surface Pressure Measurement

A critical aspect of the Langmuir technique is to measure the surface pressure accurately. Changes in the surface pressure as a function of the area available per molecule (pressure-area curves, discussed later in § 1.4.3), provide insights into molecular interactions and packing behaviour of the molecules. In order to measure this surface pressure, most Langmuir troughs use a so-called 'Wilhelmy plate', a plate made of either absorbent paper or platinum, partially submerged in the subphase (Fig. 1.22). The plate experiences a number of forces, the sum of which is given by (Gaines Jr, 1966)

$$F = \rho_{\mathrm{p}} g V_{\mathrm{p}} + \gamma 2(t + w)\cos(\theta) - \rho_{\mathrm{l}} g w t d \tag{1.15}$$

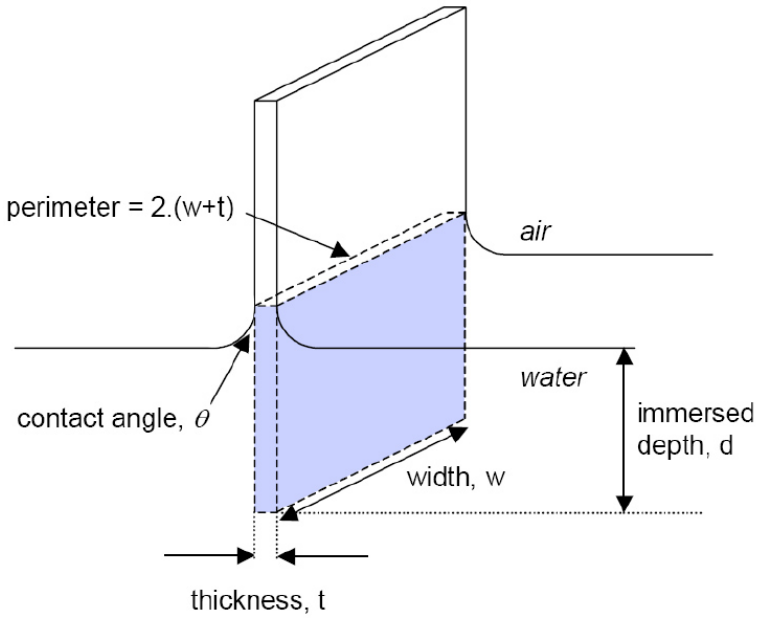

Figure 1.22: Diagram of a wetted plate submerged in a subphase for measuring surface pressure. Reprinted from KSV Nima.

(see Fig. 1.22 for variable definitions, in which V_p is the total volume of the plate). In practice, only changes to the force are monitored as the measurement is zeroed before surfactants are deposited. In the usual setup, the plate is held up by a wire which measures the net downward force. At the start of the experiment, when the plate it initially but barely wetted, the first term of Eqn. 1.15 is negligible, and the change in force is therefore just the surface tension term; this provides (or should provide) a measure of the surface tension of the pure subphase. When the plate is completely wetted, $\theta = 0$, and changes in the surface tension of the interface after surfactant molecules are deposited give the surface pressure:

$$\Delta\gamma = \frac{\Delta F}{2w} \tag{1.16}$$

assuming that the thickness, t, is much smaller than the plate width, w.

Phase Behaviour of Amphiphiles

As a monolayer is compressed, the area available per molecule decreases. Depending on the properties of the molecules themselves, this may result in phase changes. Just as pressure changes can force a phase transition of a gas to a liquid, as monolayer pressures increase, the molecules may behave first as a gas, then a fluid, and then a solid (e.g. McConnell, 1991; Kaganer et al., 1999). The degree of saturation of the hydrocarbon tail of the amphiphiles plays a key role in this phase behaviour. This concept has been introduced already in § 1.3.6, and here we link this to our more detailed discussion on monolayers. For example, observe in Fig. 1.23 the structures of three lipids that are used in the present work, which are commonly found in cell membranes. One of these lipids has tails that are completely saturated (DPPC), while the other two (DOPC and DOPE) have unsaturated tails. In a similar way that unsaturated tails of cooking oil cause it to be liquid at room temperature, while largely saturated fat molecules of butter make it a solid, these lipids have different phase behaviour at room temperature. This will be observed in the studies presented in this thesis, and can also be seen in plots of surface pressure as a function of area available per molecule (see Fig. 1.24 and refer to § 1.4.3).

1.4.3 Studying Lipid Monolayers

While the present work focusses on the use of AFM and KPFM to study monolayers, there are other methods that are useful for our purposes, which do not require depositing the monolayer onto a substrate. As mentioned previously, pressure-area curves are helpful in deducing structural information and molecular interactions. Another method that can be used directly on the Langmuir trough is an imaging technique called Brewster angle microscopy (BAM), which can image monolayers on micrometre scales while it is still at the air-water interface. We discuss some details of these techniques below.

Isothermal Pressure-Area Curves

Pressure-area curves (also known as isotherms, because they are taken at a constant temperature) are widely employed in monolayer research. A standard isotherm is shown

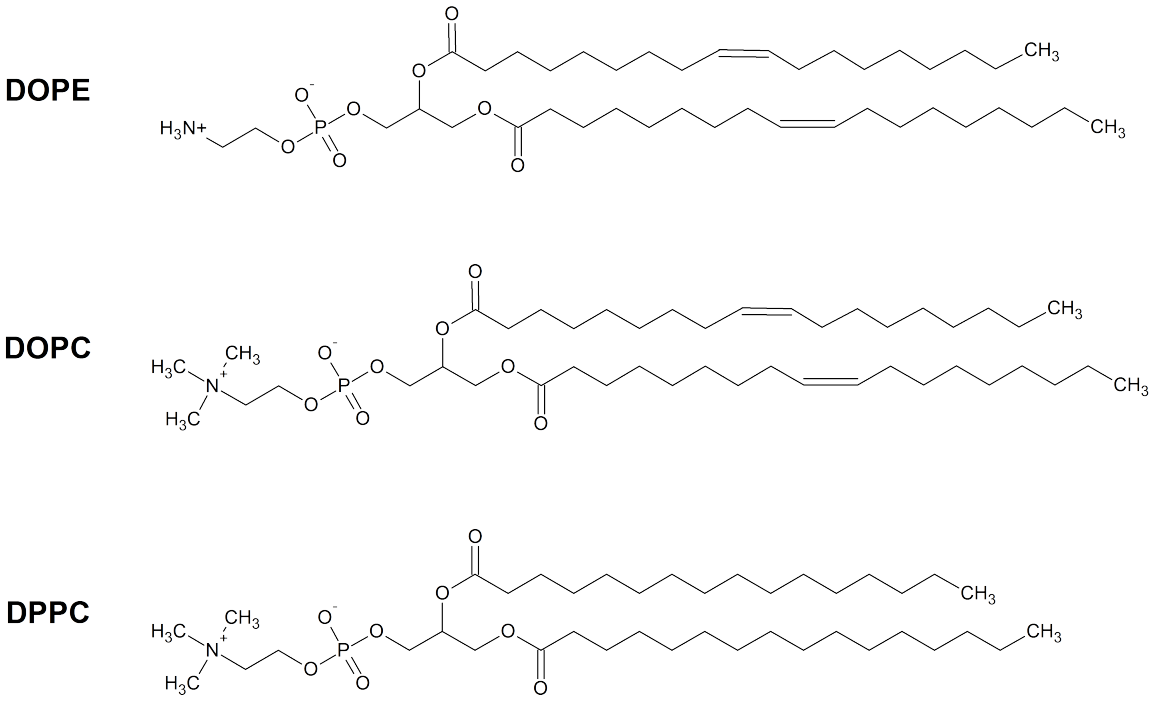

Figure 1.23: Chemical structure of three common phospholipids. These lipids are used throughout this thesis.

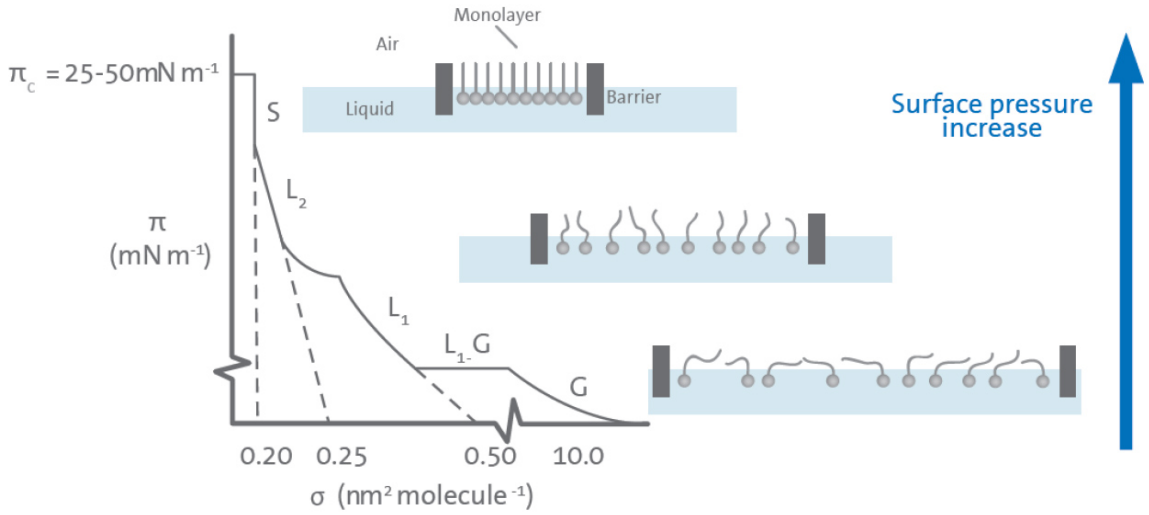

Figure 1.24: Illustration of the behaviour of a Langmuir monolayer in the trough as a function of area, thus producing a pressure-area curve. Reprinted from KSV Nima.

schematically in Fig. 1.24, which also relates the various parts of the curve to what is going on in the trough. At low pressures, the barrier arms are more widely separated, and the amphiphiles are in a gas-like phase. As the pressure is increased, the molecules start packing more closely, some transitioning to a liquid phase, then to all-liquid, a gel-like phase, and finally a solid at very high pressures. The various phase transitions can be identified by the standard features in the graph (McConnell, 1991; Kaganer et al., 1999).

An excellent work by Phillips & Chapman (1968) presents a series of monolayers of DPPC and DPPE, and demonstrates how increasing the tail length of these lipids affects their pressure-area curves: longer carbon chains produce, interestingly, more compact monolayers. This is evidenced by very steep isotherms at low molecular areas. Further, the group's work showed that the ethanolamine counterparts (PE) exhibited more compact monolayers than the phosphocholines (PC), owing to the differences in head group size.

Brewster Angle Microscopy

The Brewster angle microscopy is a useful technique to perform microscopy directly on a Langmuir monolayer (Hénon & Meunier, 1991). While it suffers from the disadvantage of relatively low resolution compared to AFM (on the order of microns), the ability to image without depositing the monolayer onto a solid substrate is helpful for a number of reasons. For example, images may be taken in quick succession to create a 'movie' of the behaviour of monolayers over time, or the very same monolayer may be subjected to changes in the subphase (like the introduction of new material) and the results observed in real time.

The BAM works on the principle of reflectivity at interfaces, where the refractive index changes suddenly. A beam of light normally reflects or refracts at an interface, and the changeover occurs at a special angle (the details are not shown here), called the Brewster angle. Changes in the reflectivity are observed and used to create an image. Areas of the monolayer which have a different refractive index than the others (e.g., denser phases, different materials) show up with contrast (e.g. Hénon & Meunier, 1991). This technique is used in some aspects of the present work to augment the other techniques, for large-scale structure information. Combining BAM with pressure-area isotherms to characterize monolayers is a generally accepted practice (e.g. Kubo et al., 2001; Miñones Jr et al., 2002; Lancelot & Grauby-Heywang, 2007; Prenner et al., 2007).

1.5 The Gene Delivery Problem

Delivering drugs and related therapeutic agents is one of the primary methods of treating almost all unfavourable health conditions. Be it a cream to mitigate a skin condition (topical therapy) or an intravenous chemical solution that is selectively disruptive for cancer therapy, the success of these methods all rely on efficient delivery methods. In principle, an optimal drug delivery system would be: highly versatile - able to carry a variety of therapeutics; efficient - successfully deliver the materials to the body with minimal loss; specific - able to target cell types and areas of the body, as necessary; inert - does not trigger an adverse immune response; and cost-effective - can be manufactured with minimal resources in time, effort and costs. Each of these criteria presents difficult problems that

are the subject of active research.

Of course, nature has already found a highly effective solution for gene delivery: viruses. A virus, in general, contains a DNA or RNA fragment which codes for enough proteins to manufacture new viral particles. The protein coat which surrounds the genetic material protects it from degradation, and is typically constructed with machinery to directly inject the genes into a prospective host cell. This method of gene delivery is highly efficient, having evolved over the entire history of life on Earth. By contrast, synthetic methods of gene delivery have had only a few decades of research and development.

Despite the high efficiency of viral gene delivery, such methods are not optimal for therapies due to their susceptibility to immune responses (Douglas, 2008). In addition, viruses have evolved to carry very specific complements of genetic material, and are not easily modified to deliver synthetic fragments. Fully synthetic methods for gene delivery are thus highly desirable for their customisability and safety, but the cost is decreased efficiency due to their non-viral origin.

1.5.1 The Transfection Pathway

Assuming that we start with, say, a gene that is nicely packaged in a delivery system that manages to arrive at a cell's outer membrane, it must make it into the nucleus where the genome is kept, and then be expressed. This is where real barriers present themselves. It has long been established that the two most likely methods by which entry into the cell may be accomplished are i) endocytosis or ii) membrane fusion (Pedroso de Lima et al., 2001). In the former, the cell membrane inverts and engulfs the gene therapy complex, pinches in on itself, and is carried into the cell with its own membrane coating it. In the membrane fusion scenario, the complex simply fuses directly into the cell membrane and crosses the bilayer into the cell. It appears that endocytosis is likely the dominant effect (Pedroso de Lima et al., 2001; Nakanishi & Noguchi, 2001; Tros de Ilarduya et al., 2010).

Once inside the cell, the complex must then fuse with the endosome's membrane or otherwise disrupt it in order to be released into the cytoplasm (Nakanishi & Noguchi, 2001). Once there, it must travel through the cell to the nuclear envelope, pass into the nucleus, and then be expressed by the cell's transcription machinery. The nuclear

envelope is porous, but ordinarily does not allow the passage of particles large enough to be genetic material (for obvious reasons). All of these passages must be made without any degradation, and each point is an opportunity for enzymes or other cell contents to interact with the therapeutic gene and its delivery system.

1.5.2 Surfactant Gene Delivery

As we introduced in § 1.2, surfactant micelles can serve as rather clever systems for the delivery of genes. The method of action is basically this: the self-assembly of surfactants into micelle 'containers' can package up DNA, which is almost always aided by having the DNA compacted by neutralising its charged backbone, which allows it to condense.[16] This charge neutralisation is important, since the charged nature of DNA can inhibit the strands from associating with themselves simply due to electrostatic repulsion. The most logical way to do this would be to have the positive charges simply located on the surfactant molecules themselves (Pedroso de Lima et al., 2001), although it has also been shown that the presence of metal ions may allow DNA and surfactants to associate (Gromelski & Brezesinski, 2004; Dabkowska et al., 2014). Surfactants with positive charges are simply referred to as cationic surfactants, and all of the gemini surfactants used in the present work are cationic. In fact, gemini surfactants are doubly charged (2+), and it has been shown that multivalent cationic surfactants are in general more efficient at gene transfection (Ahmad et al., 2005). Transfecting agents may also take the form of polymers, peptides, or derivatives of cholesterol (Zhang et al., 2004; Zhou et al., 2013).

One of the landmark papers on the use of cationic surfactants for gene delivery and transfection is Felgner et al. (1987). Even then, the issues surrounding the use of either less synthetic (viral) or more brute force (microinjection) were top of mind. In the decades since, these systems have been studied extensively and many reviews of gene delivery have been published (e.g. Zabner et al., 1995; Noguchi et al., 1998; Pedroso de Lima et al., 2001; Chesnoy & Huang, 2000; Bell et al., 2003; Tros de Ilarduya et al., 2010; Williford et al., 2014), and in more specific studies on cationic surfactants used for this purpose (e.g.

[16] The so-called hydrophobic interaction effects, discussed earlier, are important here.

Lawrence, 1994; Sternberg et al., 1994; Koltover et al., 1998; Zhang et al., 2004; Ahmad et al., 2005; Lv et al., 2006; Ma et al., 2007; He et al., 2011).

The morphology of the complexes formed by cationic surfactants and DNA is a key factor in their transfection behaviour. In a sense, such complexes can be considered nanoparticles, which act as nanopharmaceuticals. Their shapes play a direct role in their interaction with cells. It has been suggested that the surfactants pack the DNA into particles, but that the end result resembles 'beads on a string' (Sternberg et al., 1994), with particles a few hundred nanometres in diameter separated by tubular structures of DNA. Also important is the packing structure of the surfactant molecules. It turns out that lamellar structures are not very efficient at gene transfection, but that a nonlamellar, columnar or, more specifically, a two-dimensional hexagonal structure is more favourable (Koltover et al., 1998; Koynova et al., 2006). Such a structure can actually be induced by the addition of a 'helper lipid' having the appropriate structural characteristics (Wasungu & Hoekstra, 2006).

Helper lipids, as it turns out, are a critical component of successful surfactant (including gemini surfactant) gene delivery systems (e.g. Hui et al., 1996; Camilleri et al., 2000; McGregor et al., 2001; Hirsch-Lerner et al., 2005; Wasungu & Hoekstra, 2006; Dabkowska et al., 2012). A neutral lipid, such as the phosphoethanolamine DOPE, has been found to greatly enhance transfection efficiency (e.g. Hirsch-Lerner et al., 2005). Phosphoethanolamines have tail groups which take up a proportionatey larger volume compared to the head group than, say, the phosphocholines (the latter have extra methyl groups on their heads, attached to the nitrogen atom, which increases the head group volume). Therefore, DOPE tends to pack into structures with negative curvature (such as, say, the *interior* half of cell membranes).[17] Such inverted structure facilitates the disruption of membranes and may therefore promote cell entry (Wasungu & Hoekstra, 2006). In addition, dilution of the cationic surfactant with a neutral lipid allows the mixture to coat and compact DNA with an optimal charge density that is close to the spacing of negative charges on the DNA backbone, particularly as compaction occurs (Dabkowska et al., 2012).

[17] See Israelachvili (2011) for a more detailed quantitative discussion of this topic and the associated 'packing parameter' of surfactant molecules.

1.6 Overview of the Thesis

1.6.1 Research Questions

In subsequent chapters, several research projects are presented which together share a theme of deducing, at least partially, the nanoscale behaviour of molecules that are of interest to drug delivery research. Broadly speaking, the aim of this thesis is to seek answers to the following big questions:

I
How do gemini surfactants interact with lipids commonly found in cell membranes?

II
What does the nanoscale topography look like for monolayers of drug carrying systems, and how does it correlate with its electrical surface potential?

III
What does the electrical surface potential tell us about how gemini surfactants bind to DNA?

IV
How can we use monolayers to determine properties of gene transfection complexes?

V
What are the electrical properties of gene transfection complexes?

VI
Finally, how can we use this research to improve the efficiency of non-viral gene delivery?

1.6.2 Organisation

After the Introduction, this thesis is organised into 5 other chapters. Chapter 2 presents a novel study of KPFM of mixed lipid monolayers that are combined with gemini surfactant.

In Chapter 3, this study is extended to explore the interactions of these monolayers with DNA. With applications to gene therapy, Chapter 4 looks at monolayers of mixtures which are used for gene transfection complexes, and how their topography and KPFM signal compares to the previous chapters' results. The gene transfection complexes themselves are explored in Chapter 5, and comparisons are made with their monolayer analogues. Finally, the entire set of research is summarised in Chapter 6, where broad conclusions are drawn and prospects for future research are indicated. Appendices are included, which present detailed experimental protocols and supplementary data.

Reprinted from xkcd.com.

Observe the light and consider its beauty. Blink your eye and look at it. That which you see was not there at first, and that which was there is there no more.

Leonardo da Vinci

Chapter 2

Characterising Mixed Lipid-Gemini Surfactant Monolayers with Kelvin Probe Force Microscopy

2.1 Introduction

Thus far, in § 1.4, we have discussed what a monolayer is, how it can be constructed in a controlled environment, and how it can be studied (e.g., AFM, pressure-area curves, BAM). Things are relatively straightforward when working with a monolayer composed of a single amphiphilic species. The situation becomes rather more complex as we move into mixtures of two or more amphiphiles. Interpretation of the isothermal pressure-area curves are more difficult, so it becomes necessary to explore a great deal of parameter space (e.g., fraction of each amphiphile present in the monolayer). Attributing certain topographical features in AFM images is similarly difficult. Despite these difficulties, studying such mixtures can yield valuable information on physical interactions at the molecular level.

Mixed monolayers are also extremely important to study from a biological point of view. As we discussed in § 1.3.6, cellular membranes are composed of a bilayer of lipid molecules. One half of this bilayer is simply a monolayer of amphiphilic lipid molecules. Not so simply, the composition of a cell membrane is highly complex, comprised of many

different lipids and embedded protein structures (e.g. Welti & Glaser, 1994). Therefore, an analysis of mixed lipid monolayers can give us information about how cell membranes function.

In one example, cholesterol present in lipid monolayers has been found to induce a 'condensing effect' (e.g. Dynarowicz-Łatka & Hac-Wydro, 2004) which could offer added stability to cell membranes. In the same study, an analysis of the pressure-area curves of mixed monolayers found that the collapse pressure was actually higher for mixtures than either of the pure components, implying that mixed monolayers are more stable than their mono-constituent counterparts (Dynarowicz-Łatka & Hac-Wydro, 2004). This could help to explain the complex nature of cell membranes.

The two common cell membrane lipids DOPC and DPPC have been studied together in monolayer form, along with other members of the phospholipid family, for a long time (e.g. Vie et al., 1998; Kubo et al., 2001; Sanchez & Badia, 2003; Guzmán et al., 2012; Qiao et al., 2013). While domain formation can be seen with a mono-lipid monolayer as the surface pressure is increased (McConlogue & Vanderlick, 1997), interesting structures form with mixtures. Instead of circular patches as in DOPC and DPPC mixtures, DOPC mixed with palmitic acid (a long-chain carboxylic acid) produces domains shaped like winding chains (Hao et al., 2013). Even small differences in amphiphile structure can cause separation in the monolayer, as is seen when similar phospholipids are mixed, differing only in their tail lengths (Kubo et al., 2001). Other factors, such as the degree of saturation and the nature of the head group may be important, as we will see later on.

Domains that contain a condensed phase lipid, such as DPPC at high pressure, tend to cover the monolayer surface more and more as their molar fraction within the monolayer increases, as one might expect (Sanchez & Badia, 2003). However, the fraction of surface coverage is not equal to the molar fraction of the monolayer because the area per molecule of the condensed lipid is smaller, as these lipids are able to pack more closely. Therefore, the relative composition is an important factor to consider when studying these systems.

Monolayers may also be highly sensitive to their environment. For example, in an AFM study, Coban et al. (2007) found that mere exposure to air altered the sizes of domains in monolayers of DOPC and DPPC. In another work, Qiao et al. (2013) showed that exposure to low levels of ozone drastically changed the topography of lipid monolayers. Thus, the

environment plays a significant role in the domain structures of lipid monolayers, which has implications for cellular membranes.

Mixed monolayers can therefore serve as models to study features and interactions of structures that might be present on the complex surfaces of cell membranes. These models can further be useful to obtain information on how other molecules and substances might behave when they encounter a cell, such as in drug delivery. As we discussed in § 1.2, gemini surfactants have been found to be potentially very useful as a novel drug or gene delivery system, and so an understanding of their interactions with cell membranes will be critical. Therefore, the present work aims to characterize model monolayer topography, and how this is affected by the presence of gemini surfactant.

Gemini surfactants in monolayer form have been examined alone (e.g. Qibin et al., 2007), and also in the presence of stearic acid (e.g. Li et al., 2008, 2010). Pure gemini surfactant monolayers do show the formation of tiny domains, suggesting some self assembly (Qibin et al., 2007). In this chapter, we will examine the topography of monolayers containing DOPC and DPPC with gemini surfactant. The mixture of DOPC and DPPC serves as a model for a standard living cell.[1]

In addition to topography, we will be examining the electrical surface potentials of these monolayers with KPFM. The use of KPFM on monolayers in a biological context is very limited to-date, but has been done on, for example, monolayers of pulmonary surfactant (Hane et al., 2009; Moores et al., 2010) and DPPC mixed with phosphatidylglycerol (Hane et al., 2009). The introduction of cholesterol was actually found to induce electrostatic domains in monolayers of DOPC from an analysis of KPFM images (Drolle et al., 2012). As far as we are aware, this is the extent of this kind of KPFM use (although there have been some studies of KPFM on self-assembled monolayers in a non-biological context, such as Sugimura et al. (2002) and Ichii et al. (2004)), and the present work is the first of its kind to combine the KPFM technique with gemini surfactants. Most of the interactions that have been observed with gemini surfactants have been attributed, at least in part, to electrostatics; therefore, it is the aim of this work to unravel some of the electrostatic

[1] While this is a highly simplified and somewhat idealistic model, it allows us to study specific interactions more carefully without the 'trouble' of unknown proteins or other lipids getting in the way.

properties of such interactions.

Monolayers inherently possess a surface potential that arises from the dipole moments of its constituent molecules and any charges that are present (Vogel & Möbius, 1988a,b; Smaby & Brockman, 1990; Mozaffary, 1991; Brockman, 1994). The potential that may be measured by KPFM will also be affected by the properties of the substrate supporting the monolayer, as well as the relative potential of the scanning tip. Despite best efforts, the measurement from KPFM will always be a relative one (Charrier et al., 2008), and so we will primarily be focussing on differences between features.

2.2 Methodology

2.2.1 Lipids and Gemini Surfactants

For the purposes of this study, we require a lipid monolayer composition that provides both topographical contrast (for imaging) and a semblance to cellular membranes. We therefore chose a combination of 1,2-dioleoyl-sn-glycero-3-phosphocholine (DOPC) and 1,2-dipalmitoyl-sn-3-phosphocholine (DPPC). While the DOPC is longer in terms of hydrophobic chain length than DPPC, the unsaturated acyl chains of the DOPC make it somewhat shorter. This difference in height, along with a phase separation upon compression (see below), yields topographical contrast in AFM (Coban et al., 2007). These lipids (phosphatidylcholines) are large constituents of eukaryotic cellular membranes. Lipids were purchased from Avanti Polar Lipids Inc.[2], and dissolved in stock 1 mg/mL solutions of chloroform that were kept in a freezer until needed.

We used gemini surfactants of the type N,N-bis(dimethylalkyl)-α,ω-alkanediammonium dibromide, designated for simplicity as $m-s-m$, in which m is the length of the alkyl tails and s is the length of the spacer group, in carbon atoms. These were synthesized by reflux in acetone of the corresponding α,ω-dibromoalkane and N,N-dimethylalkylamine. After filtering and purifying by recrystallization, the chemical structures and purities were

[2] www.avantilipids.com

confirmed with NMR spectroscopy and surface tensiometry. For full details, see Wettig et al. (2007). The GS in powder form was stored in a desiccator and then dissolved in chloroform (at stock 1 mg/mL) before use.

2.2.2 Langmuir-Blodgett Monolayer Deposition

In preparation for AFM/KPFM imaging, monolayers were created on a Langmuir-Blodgett (LB) trough and deposited onto mica slides as follows. Chloroform solutions of lipid-surfactant mixtures were prepared from stock in appropriate amounts (converted for molar ratios as reported in § 2.3). The LB trough was thoroughly cleaned with chloroform and filled with nanopure water from a Milli-Q system before each experiment. Surface cleanliness was achieved by vacuuming small amounts of water from the basin and confirmed by a pressure test so that compression yielded an increase in pressure of no more than 0.2 mN/m. Freshly-cleaved mica slides were suspended in the dipping well to rest just below the surface. Then, a chosen lipid-surfactant solution was deposited quickly in several drops around the surface to form a monolayer. The monolayer was left to equilibrate (and the chloroform was allowed to evaporate) for 10 minutes before compressing at 12 mm/min to a target pressure of 35 mN/m. This pressure was chosen to roughly correspond to cell membrane specifications (Demel et al., 1975; Seelig, 1987) and to allow phase contrast between the DOPC/DPPC lipids. The monolayer was deposited on the mica by raising the dipping arm slowly at a rate of 2 mm/min while keeping the surface compressed at a constant pressure.

2.2.3 Imaging

Technical Setup for KPFM with Mica Substrates

For KPFM imaging of samples deposited onto mica, it is necessary to prepare the substrate in a manner that allows a bias voltage to be effectively applied. In our experiments, we have determined an optimal setup to be as follows. For square mica slides, we cut a square of aluminum foil several mm larger than the substrate, and adhere this to the bottom of the mica with conductive mesh double-sided tape. The edges are wrapped over onto the

top surface to form a frame. Small pieces of conductive tape are applied to the corners to ensure the foil adheres to the surface. The KPFM electrode (where the bias voltage is applied) is placed onto one of the pieces of conductive tape on the top surface. See Fig. 2.2, and Appendix A for more detail.

AFM and KPFM

Our imaging was performed on two instruments. For contact-mode AFM we used a JPK Nanowizard II[3] and NCH-PPP cantilever tips with a resonant frequency near 150 kHz. High-resolution AM- and FM-KPFM imaging (and associated non-contact mode topography imaging) was performed on an AIST-NT Smart SPM[4], using MikroMasch NSC-14-Cr/Au cantilever tips, which have a resonant frequency near 130 kHz. While the AIST-NT instrument provides superb topography as well as KPFM imaging, its file format is not currently supported by the SPIP software (see below) that we used for surface coverage analysis; therefore, the JPK was used for that component of this study.

In theory, our KPFM setup can produce the topography and surface potential difference images simultaneously, but in practise this does not yield optimal quality for topography. A superior method is to perform, line-by-line, a topography scan followed by a KPFM scan, and this is implemented automatically from the AIST-NT software. Occasionally, edge-effects were found at the point where the scans switched from AFM to KPFM, but this was usually resolved by allowing for a delay of 15 ms between scans. Lateral KPFM resolution was further enhanced by choosing a closer scan height of several nm, and slightly reducing the amplitude of the second scan (for FM mode only).

One can relate the monolayers that are deposited onto mica to their self-assembled form in solution by imagining a section of a micelle being taken away and flattened into a sheet (see Fig. 2.1). Differences in height or phase between the monolayer components can then be measured with an AFM, and their differences in electrical surface potential measured. A schematic of our KPFM setup for imaging of monolayers is shown in Fig. 2.2.

[3] JPK Instruments: www.jpk.com.

[4] Advanced Integrated Scanning Tools for Nanotechnology: www.aist-nt.com.

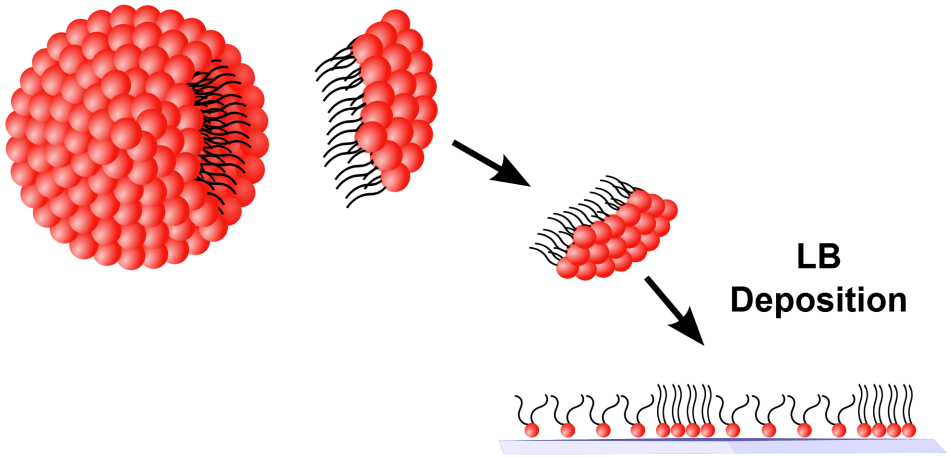

Figure 2.1: Schematic representation relating a monolayer to the lipid-surfactant mixture when in micelle form.

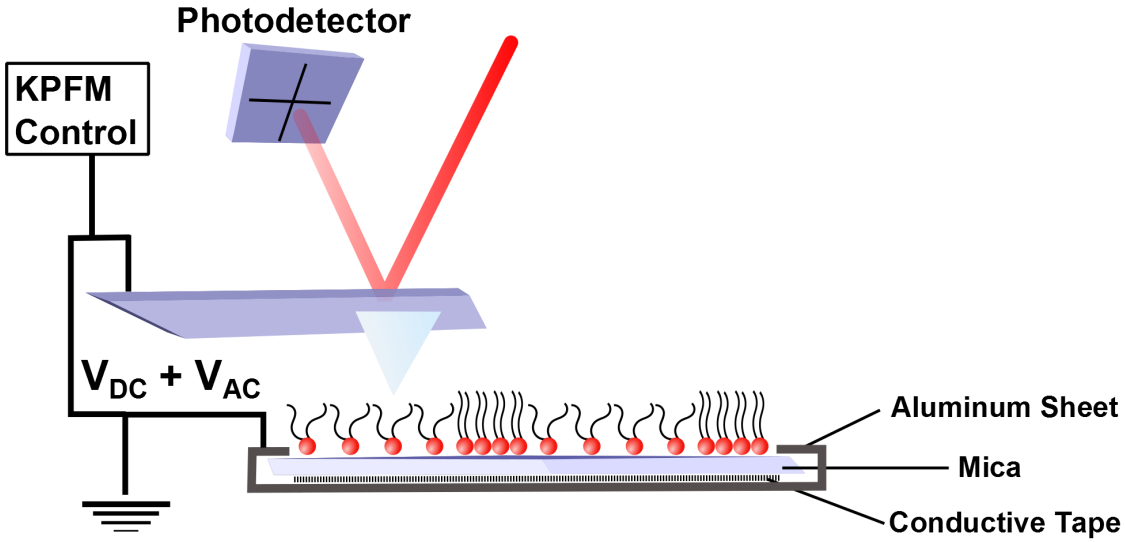

Figure 2.2: Schematic representation of our AFM/KPFM setup for imaging a monolayer.

2.3 Results

2.3.1 Monolayer Composition

A number of previous studies have shown that, when mixed, different phosphatidylcholine lipids (especially those with widely differing phase transition temperatures) form a monolayer composed of domains which exhibit topographical contrast that is clearly shown in AFM images (e.g. Stottrup et al., 2004; Coban et al., 2007). Characterising the effects of gemini surfactant on those monolayers involves two approaches here. First, we consider morphological changes in the domains that form with AFM topographical imaging. Second, we look for changes in the electrostatic properties or the formation of different electrostatic domains.

To identify domains of DOPC and DPPC in our AFM images, we prepare control (no gemini surfactant) monolayers composed of different ratios of DOPC to DPPC. It has been shown that the lipids, in monolayer form, differ in height by approximately 1 nm (Coban et al., 2007), so as the ratio of one lipid increases, we should see a larger amount of area occupied by it. For effects of the gemini surfactant, we add two different GSs to our lipid mixtures: m-s-m = 12-3-12 and 16-3-16, in a DPPC:GS molar ratio of 3:2, which has been found to be an appropriate ratio for effective gene transfection studies when helper lipids are used (Wang et al., 2007).

2.3.2 General Topography

In Fig. 2.3 we show the AFM images of our control samples (no gemini surfactant) containing different ratios of DOPC to DPPC, all performed in contact mode. These lipid mixtures show a characteristic set of domains, where one lipid has formed in a series of circular or polygonal shapes in a matrix of background lipid. We do note that the monolayer topography frequently shows streaks and striations aligned along a particular reference axis. This phenomenon has been reported previously (e.g. Moraille & Badia, 2002; Coban et al., 2007), and is an artefact of the deposition and does not affect our results.

As our goal here is to identify each lipid, we performed a surface analysis on a series of

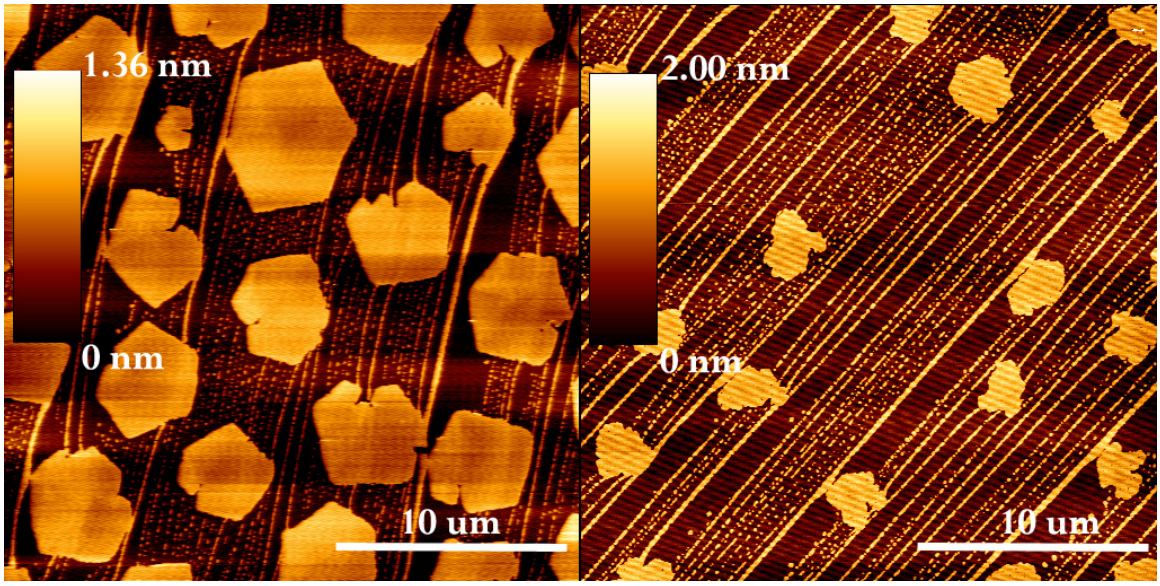

Figure 2.3: AFM images of control monolayers of pure DOPC and DPPC in molar ratios of DOPC:DPPC 3:7 (left) and 1:1 (right), taken with the JPK instrument for analysis in SPIP.

these images from random locations of each of the samples using the program Scanning Probe Image Processing (SPIP). We calculated the fraction of the surface that is covered by the domains (higher, lighter in the images) with two separate methods, and show the results in Table 2.1. The first method uses a histogram of pixel values which takes advantage of the fact that our images are largely composed of pure DOPC and DPPC domains separated by an approximately constant height. This shows up in practise as two peaks in the histogram; the minimum between the two peaks roughly separates the domains and we can then calculate the fraction of the image occupied by the higher-height pixels (which thus calculates the surface covering fraction of the domains). The second method employs an algorithm to identify particles (shapes) in the image, which are then added up to determine their surface coverage.

The results show that the higher domains are DPPC. From the nature of the structure of DPPC, at our deposition pressures it will be in a gel-like phase, while the DOPC will be fluid-like (Schmidt et al., 2009; Giocondi et al., 2010). We can further characterize

Table 2.1: Surface coverage analysis for control samples at two ratios of DOPC:DPPC. The results are shown for both the histogram and particle detection surface coverage analysis, averaged over four experiments, that is described in the text.

DOPC:DPPC (mol)	Domain Coverage (%) (Histogram)	(Particle)	Model Average (%)
1:1	29 ± 3	25 ± 3	27 ± 4
3:7	55.6 ± 0.6	53 ± 4	54 ± 4

these control samples by a cross-section analysis of both the minimally-processed images of Fig. 2.3, and those same images with a small amount of smoothing applied. We find that indeed there is a strong correlation between lipid ratio and the fraction of the surface occupied by the domains. Specifically, at a 1:1 ratio of the lipids (by mol), 27(±4) % of the surface is covered by DPPC, while 57(±4) % is covered at a ratio of 3:7 DOPC:DPPC.

It is also interesting to comment on the effects of adding GSs to the DOPC-DPPC monolayers. We see in Figs. 2.4 and 2.5 (and see below) that the addition of 12-3-12 GS has little or no effect on the DPPC domain structures. However, for 16-3-16 there is increased interaction between the lipid and surfactant leading to intricate domain formation. This is supported by other studies which indicate an antagonistic mixing behaviour of 16-3-16 GS and phospholipid (Akbar et al., 2012). In the case of 12-3-12, possible contributing factors are its higher solubility in water compared to the longer-chain 16-3-16 GS. In the next section, we discuss possible origins and comparisons of the surface potentials for these monolayers, for both the control and the sample containing 16-3-16.

2.3.3 Surface Potential and the Effects of Gemini Surfactant

We present in Figs. 2.4 and 2.5 results of AFM and FM-KPFM imaging, from the AIST-NT instrument, on samples containing the GSs 12-3-12 and 16-3-16, with a control (no GS) sample. In our control sample, we measure a preliminary contact potential difference of 323 ± 32 mV between DOPC and DPPC. This value is an average calculated from multiple scans of separate experiments, with the 'error' as the standard deviation reported from the collection of measurements. Incorporating 12-3-12 GS into the sample gives a surface

potential difference of 338±55 mV, which is consistent with the control. A similar analysis of 16-3-16 images yields a surface potential difference of $\sim 707 \pm 79$ mV between the domains. (See below for a more rigorous determination of these quantities.) As it is confirmed in the topography, 16-3-16 GS interacts very strongly with the DPPC and the increased positive surface potential difference between the domains is consistent with adding cationic molecules to the domains. Therefore, we proceed with consideration only of the 16-3-16 surfactant as compared to the control.

2.3.4 Image Analysis and Domain Properties

Calculating a reliable value for the height and surface potential of the domains in our images requires some careful analysis. The AIST instrument has no software support within SPIP, so more 'hands on' methods are required. In this section, we describe three possible methods by which to analyse these images, but conclude that a direct cross-section analysis provides the most plausible result.

The first method is to use histograms of the pixel values, in much the same way that was done for the surface coverage analysis. In this case, however, instead of using the histograms to calculate a fraction of the total number of pixels, we can use it to determine the difference in the height or surface potential between the domains. Suppose we have, in an ideal situation, a fairly clean background of some height h_b, with Gaussian noise of relatively small standard deviation. Now add domains of height h_d, again with Gaussian-distributed noise with a standard deviation much smaller than $h_d - h_b$. A histogram of these pixel values will show two Gaussian peaks, separated by $h_d - h_b$. We employ this procedure on two high-quality images of each experiment. To mitigate intra-image variation (e.g., flattening effects, artefacts), we draw 5 histograms from each image that were taken from different sub-regions representing good quality domains with background. The result is then averaged for each image (each trial).

A second method is to use the freely available program GWYDDION[5] to extract image statistics. While the algorithms are not as advanced as SPIP, it is straightforward to

[5] gwyddion.net

'paint' a mask onto each image to cover the region of interest, and compute statistical quantities of the masked pixels. An alternative method is to simply threshold an image; that is, to select all pixels above or below a threshold value. In most cases this will suffice to pick out a reasonable amount of background or domains. In most cases, to avoid edge effects, it is necessary to 'shrink' the masks to focus on the central regions of the domains or background. This was done for the same two images as the histogram method above, and the mean and standard deviation of the pixel values were obtained to compute the difference in height and FM-KPFM signal.

Another method is more direct: one may take a series of cross sections within the image and manually select background and domain regions from which to compute height and surface potential differences. While this is more labour intensive and can be subjective if one is not careful, on the whole it is a very reliable method as it allows direct confirmation of the measurements. The AIST-NT image analysis software allows semi-automatic computation of differences within the cross sections by selection of peaks and valleys. For each of our images, 50 measurements were taken in this manner, and their means and standard deviations were obtained. In most cases, a small amount of Gaussian smoothing applied to the images greatly enhanced the quality.

An analysis of the data confirmed that the two trials for each of the histogram and cross section methods, for each experiment, yielded results that were statistically consistent. However, the masking method gave inconsistent values for the means from each trial in all cases. Therefore, we reject the masking method for its unreliability. Summaries of these data are given in Table 2.2. We note that the histogram method produces values that are consistently below those obtained from the direct cross section measurements. This can be explained as follows: the histogram peaks from which we measure the difference gives us the difference between the two most frequent pixel values, assuming a roughly Gaussian distribution for each. The locations of these peaks are sensitive to edge effects of the interfaces between the domains and the background, and to any variation in the calibration (flattening) across the image. It is also true that in our ideal case described above that the histogram method would yield acceptable results, in reality these two issues create problems. The most frequent pixel values are not necessarily those of the top surface of the domains, and this problem is inflated when the domains are not very large

compared to the size of the pixels. For these reasons, the histogram method consistently underestimates the height and FM-KPFM differences. Therefore, we turn to the cross section method from here on.

The use of cross sections to measure differences between the domains and the background is sound for a few reasons. Firstly, the method shows itself to be statistically consistent from image to image. Second, each line is not subject to global variations in the image calibration, since the measurements are taken from a single scan line. And third, many measurements can be obtained on a single image, and the quality of the data confirmed by the experimenter.

Our final result for the height difference between the domains and background (DPPC and DOPC) is 0.331 nm ±0.009 nm, and a contact potential difference of 336 mV ±7 mV. This is somewhat lower than other studies near our deposition pressure (Coban et al., 2007). We should point out that the fluid nature of DOPC at our experimental temperatures likely makes our result somewhat dependent on the surface pressure at deposition (Coban et al., 2007), but this is not critical to our analysis since we use a consistent deposition methodology. With the addition of GS 16-3-16, the height difference increases to 0.574 nm ±0.001 nm, with a contact potential difference of 658 mV ±17 mV.

2.4 Discussion

The maps of electrical surface potential in our samples can be explained by considering the dipole nature of the lipids. A simple uniform monolayer has an electric potential given by Brockman (1994),

$$V = 12\pi\frac{\mu_\perp}{A} \tag{2.1}$$

in which $\mu_\perp$ is the normal component of the dipole moment of each molecule, in MDebye, A is the area per molecule, in Å^2, and V is measured in mV. This is independent of the height of a conductive scanning tip by virtue of the assumption that the sheet of dipoles is infinite in area. However, real monolayers have a finite total area and are possibly made up of domains of different molecules or similar molecules at different orientations or densities, and thus this equation would only be a reasonable approximation for either

Table 2.2: Examples of image analysis results for three methods to compute height and surface potential differences between domains in lipid monolayers: control (DOPC+DPPC 1:1) and with gemini surfactant 16-3-16 (DOPC+DPPC+16-3-16 3:3:2). Values for the histogram method were derived from 5 sectors from each image. For masking, one mask was created for each image of both the domains and background to calculate the difference. Fifty individual measurements were used for each of the cross section values. The cross section method was used to calculate final result for the height and surface potential of the domains relative to the background. See the text for further details.

Method	Height / (nm)				FM-KPFM / (mV)			
	Trial 1		Trial 2		Trial 1		Trial 2	
	$\bar{x}_{1,\mathrm{H}}$[a]	$s_{1,\mathrm{H}}$[b]	$\bar{x}_{2,\mathrm{H}}$	$s_{2,\mathrm{H}}$	$\bar{x}_{1,\mathrm{K}}$	$s_{1,\mathrm{K}}$	$\bar{x}_{2,\mathrm{K}}$	$s_{2,\mathrm{K}}$
	DOPC:DPPC 1:1 (Control) Monolayer							
Histogram	0.274	0.018	0.262	0.017	286.2	31.3	314.0	45.2
Masking	0.276	0.089	0.309	0.085	261.6	64.4	318.8	46.7
Cross Sections	0.328	0.045	0.335	0.043	339.7	40.4	332.6	33.1
	DOPC+DPPC With Gemini Surfactant 16-3-16							
Histogram	0.567	0.026	0.559	0.043	597.8	69.8	567.4	47.1
Masking	0.621	0.104	0.587	0.099	705.0	144.8	632.0	116.5
Cross Sections	0.582	0.047	0.566	0.073	654.3	91.5	660.7	75.0
Combined Cross Section Data[c]								
Control	0.331 ± 0.009 nm				336 ± 7 mV			
With 16-3-16	0.574 ± 0.001 nm				658 ± 17 mV			

[a] Sample mean, $\bar{x}_i$, of trial i, with H (height) or K (FM-KPFM).

[b] Standard deviation of trial.

[c] Margins of error calculated at a 95% confidence level.

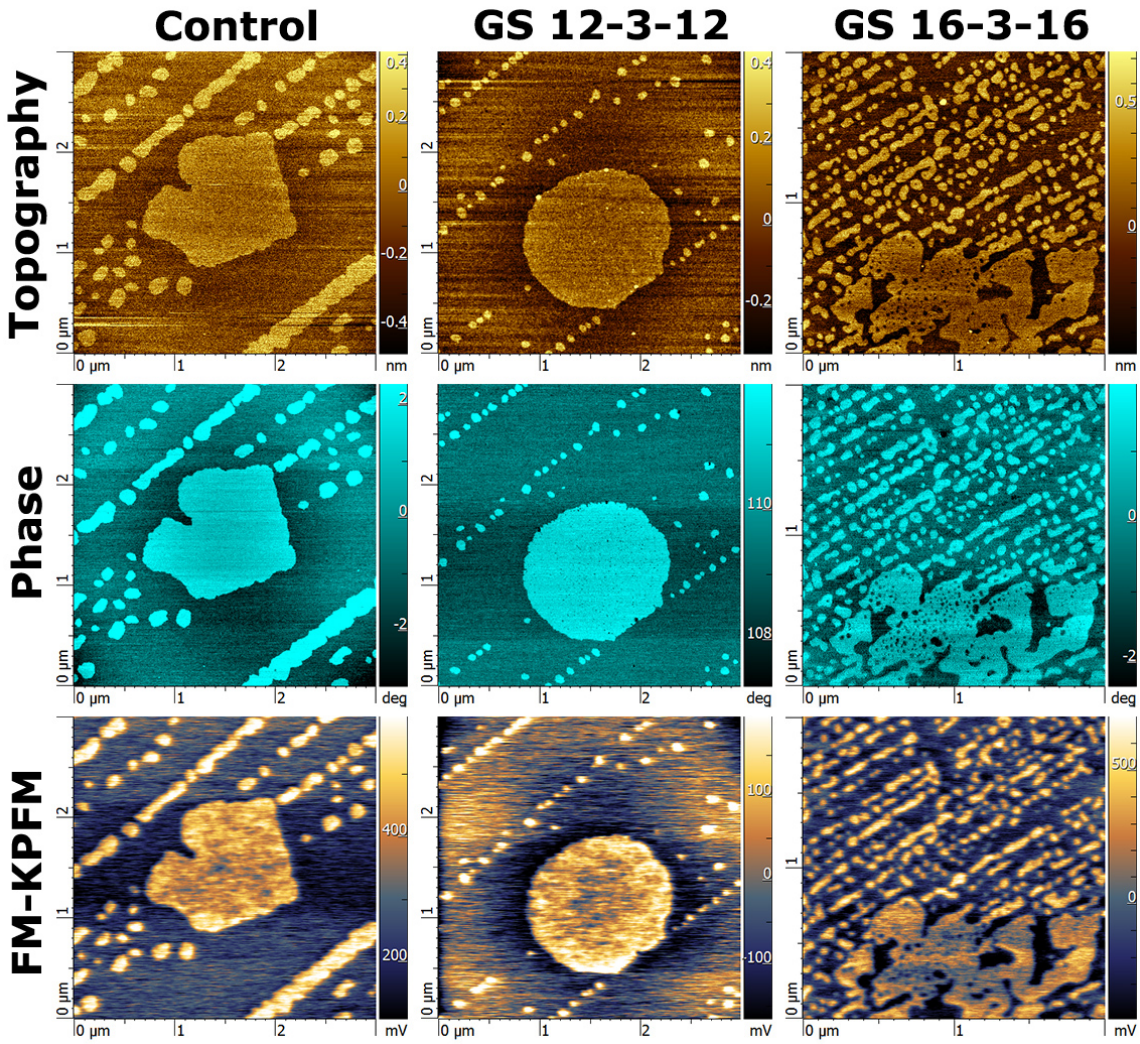

Figure 2.4: AFM and KPFM images of monolayers of DOPC/DPPC with and without GS.

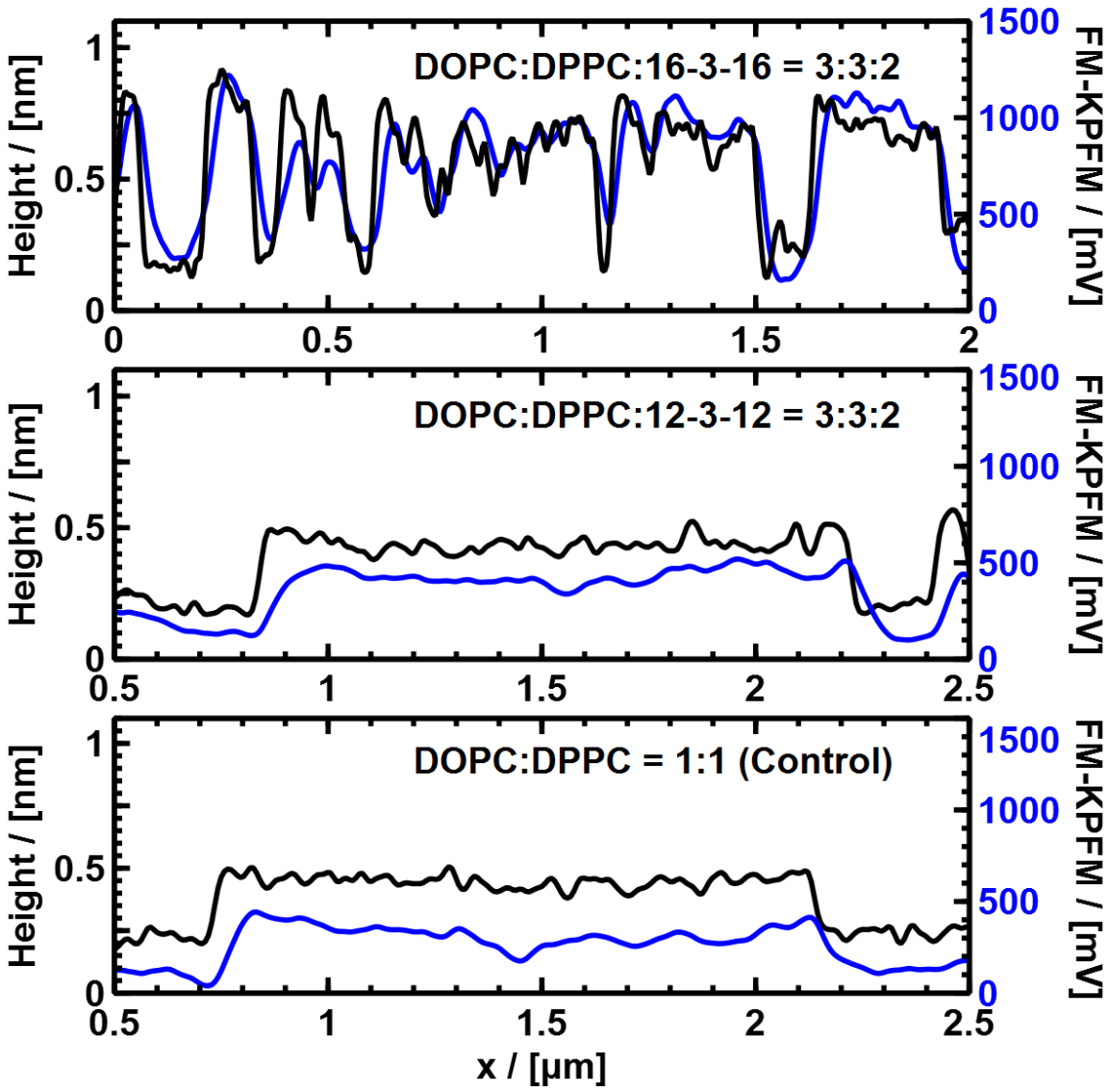

Figure 2.5: AFM (black) and KPFM (blue) image example cross sections of the monolayers in Fig. 2.4.

small scanning heights and/or large domains. Many factors contribute to the resulting dipole moments of the DOPC and DPPC monolayers. For example, how large is the dipole of a single lipid molecule? How densely packed are the lipids in each region? Are they oriented perpendicularly, or at some other angle, to the substrate? What about tip or sample contamination? KPFM analysis can in general only lead to knowledge of relative electrostatic potentials, and a determination of absolute potential can only be done under extreme conditions (Elias et al., 2011) that are beyond the scope of our experiments. Therefore, we must approach the above issues on a relative basis.

There is no straightforward way to address these questions, but it is not necessary to address them all and here we provide a simplified prescription to illustrate the relationship between experiment and theory, guided by Vogel & Möbius (1988a,b); Benvegnu & McConnell (1993); Brockman (1994); Dynarowicz-Łatka et al. (2001); Finot et al. (2010). Given that the hydrophilic mica slides are pulled out of the aqueous sub-phase during the deposition process, the lipid and surfactant molecules will have their head groups oriented toward the substrate, with the hydrophobic tails on the visible surface of the samples. Previous studies have shown that the total dipole moments of phospholipids are positive toward the air (Beitinger et al., 1989; Smaby & Brockman, 1990; Mozaffary, 1991; Brockman, 1994). A review of the literature on this topic shows the dependence of properties such as the dipole moment or surface potential on conditions such as surface pressure, molecular area, and subphase composition for DOPC and DPPC. Table 2.3 presents the results of this review. While the picture is by no means complete, we can glean useful quantities from these data and relate them to our present measurements.

Given our surface analysis results, and the values for the molecular areas Table 2.3, we can say that the molecular density of DPPC is higher than DOPC, and thus DPPC will have a boost to higher values for the surface potential relative to DOPC. This is because the area per molecule is smaller for DPPC. This is in fact what we see for our monolayers in Figs. 2.4 and 2.5. In addition, noting that we measure DPPC to be higher than DOPC, despite DPPC having a shorter carbon chain length, we must conclude that the fluid-like nature of DOPC causes it to be oriented non-perpendicularly to the substrate surface. Therefore, the component of the dipoles of DOPC that is normal to the mica substrate will be smaller than DPPC (at similar density). A combination of these two factors (density and

Table 2.3: Values for dipole moments and surface potential of pure DOPC and DPPC monolayers from the literature.

π (mN/m)	A (Å^2)	ΔV (mV)	$\mu_\perp$ (mD)	Subphase	Reference
			DOPC		
20	78	306	632	H_2O	Beitinger et al. (1989)
30	70	329	610	H_2O	Beitinger et al. (1989)
35	70	–	850	NaCl[a], pH 6	Mozaffary (1991)
45	59	311[e]	486	H_2O	Smaby & Brockman (1990)
45	58	–	463	PBS[b], pH 6.6	Smaby & Brockman (1990)
–[c]	–	384	–	KCl[d]	Luzardo et al. (1998)
			DPPC		
10	69	–	469	PBS[b], pH 6.6	Smaby & Brockman (1990)
20	46	400	488[e]	H_2O	Vogel & Möbius (1988b)
30	44	600	700[e]	H_2O	Vogel & Möbius (1988b)
35	42	700	780[e]	H_2O	Vogel & Möbius (1988b)
35	45	–	700	NaCl[a], pH 6	Mozaffary (1991)
–[c]	–	460	–	KCl[d]	Luzardo et al. (1998)
23	–	640	–	*Simulation*	Lucas et al. (2012)
				Differences in Electrical Surface Potential: $\Delta V = V_{\mathrm{DPPC}} - V_{\mathrm{DOPC}}$	
20	–	94	–	H_2O	(above)
30	–	271	–	H_2O	(above)
35	–	336	–	H_2O[f]	**This work**

[a] Subphase 0.1M NaCl.

[b] Subphase 0.01M phosphate buffer with 0.1M NaCl.

[c] Lipids added until ΔV unchanged. See Luzardo et al. (1998) for details.

[d] Subphase 1mM KCl.

[e] Computed from Eqn. 2.1.

[f] Supported monolayer on mica prepared with LB deposition using a pure water subphase.

orientation) must therefore contribute to the difference in the contact potential between the two lipids. Ultimately, the difference we obtain for the contact potential difference between DOPC and DPPC is in line with the values presented in the studies shown in Table 2.3, in which, for example, at a pressure of 30 mN/m the difference is given to be 271 mV. The trend that we see for the pressure dependence of the potential suggests that the result would be slightly higher for larger pressure (say ours), which is consistent with our results.

Now let us turn to the monolayer containing gemini surfactant 16-3-16. An increase in height is observed upon the addition of this gemini surfactant, which may be due to a more compact and vertical packing of the molecules. The additional contact potential difference that is obtained, compared to the control monolayer, is 328 mV. Given the lack of analogous potential and dipole data for these gemini surfactants compared with the common lipids, for the present purpose, if we make the simplifying assumption that the only *new* contribution to the surface potential is due to the 2+ charges on the surfactant molecules (that is, we assume that the dipole moments of DPPC are the same as the dipole moments of 16-3-16 without the 2+ charge), we can compute a molecular density of gemini surfactant that has integrated into the DPPC domains. Assuming also that the sizes of the domains are much larger than the tip-sample separation during the scan so that we may take the distribution of surfactant molecules to be an infinite sheet of charge, see have

$$V_{\mathrm{e^-\,sheet}} = \frac{z\sigma}{2\epsilon_0} \tag{2.2}$$

in which z is the height of the tip during the measurement and σ is the surface charge density. The density of gemini surfactant molecules is then

$$\sigma_{\mathrm{gemini}} = \frac{\epsilon_0 V_{\mathrm{e^-\,sheet}}}{z} \tag{2.3}$$

since there is a charge of 2+ on each molecule. Making the further assumption that the area per molecule is the same within the DPPC domains infused with gemini surfactant as the DPPC alone (45 Å^2), this calculates to about one gemini surfactant molecule per 4 molecules of DPPC. This is a plausible result (consistent by order of magnitude), given the assumptions and our starting relative concentrations of 3:2 for DPPC:gemini.

2.5 Conclusions

We have explored the effects of GS on lipid-surfactant monolayers using both AFM and KPFM imaging. First, monolayers of pure lipid mixtures containing DOPC and DPPC were used to distinguish between the lipids and visualize the gel-phase domains of DPPC. With an infusion of 12-3-12 GS, little change in the domain morphology was observed, and the electrical surface potential difference is consistent with the control. With the use of 16-3-16, we observe a strong interaction between the gemini surfactant and DPPC, with more intricate domain formation, and a much more positive electrical surface potential difference.

While the morphology of these monolayer mixtures can be determined via AFM, the unique capabilities of KPFM provide valuable information on electrostatic properties. In the present case, this proves to be very useful in confirming the presence of cationic GS.

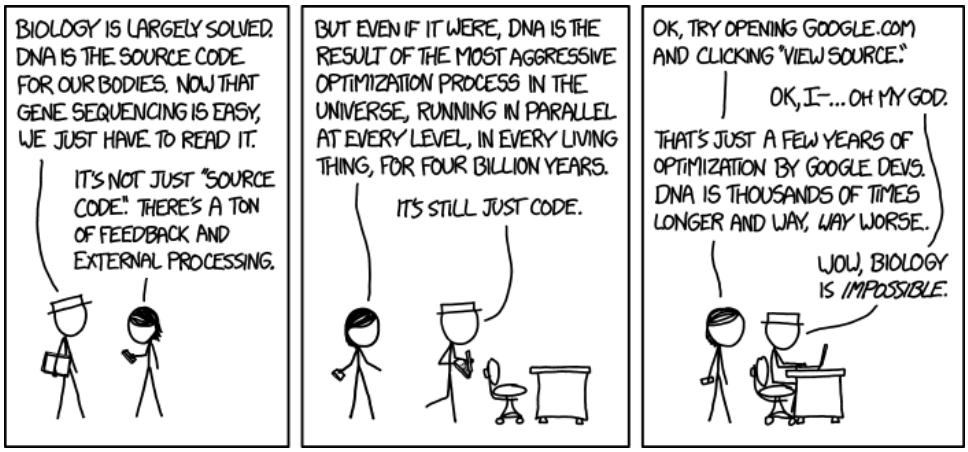

Reprinted from xkcd.com.

Nature uses only the longest threads to weave her patterns, so each small piece of her fabric reveals the organization of the entire tapestry.

Richard Feynman

Chapter 3

The Unique Surface Potentials of DNA-Lipid-Gemini Surfactant Monolayers

3.1 Introduction

In the previous chapter, we investigated the structure and electrical properties of simple mixed monolayer systems that also happen to be biologically relevant. Of course, the ultimate goal is to relate all this to efficient construction of drug and gene delivery vehicles. For gene delivery in particular, the interaction of DNA with these vehicles is crucial. DNA (deoxyribonucleic acid) is the essential blueprint molecule of life, encoding all the necessary information to construct a complete living organism. As we have discussed in § 1.5, the delivery of DNA into cells can be therapeutic, for example to give the cell a necessary set of instructions to construct an otherwise missing or defective protein. Crossing the cell membrane is no trivial task, and therefore an understanding of the interaction of DNA with important membrane lipids and its carrier molecules is necessary.

DNA is a helical, often double-stranded polymer comprised of sub-units called nucleotides, which in turn contain a nitrogenous base, a sugar (deoxyribose) and a negatively-charged phosphate group. The negative charge is critical, because it allows DNA to strongly

interact with other charged molecules. In our case, these other charged molecules are cationic gemini surfactants. The positive charge on the gemini surfactants acts to neutralise negative charge on the DNA, forming a 'complex'.

While it is clear that the nature of the interaction between DNA and cationic surfactants is electrostatic, the details are lacking. Exactly how much surfactant is required to bind with DNA to form a complex? What is its effect on the structure of the DNA molecules in solution, and how do they interact with membrane lipids?

Lipids play an important role in improving the transfection efficiency of these systems (Hui et al., 1996; Chesnoy & Huang, 2000; Hirsch-Lerner et al., 2005). The monolayers that mixtures of these compounds form may be probed by a variety of observational techniques such as fluorescence (e.g. Michanek et al., 2012) and Brewster angle microscopy (e.g. Cárdenas et al., 2005; McLoughlin et al., 2005; Eftaiha & Paige, 2012), and of course a variety of scanning probe microscopy methods (e.g. Hane et al., 2009; Finot et al., 2010).

Investigations of monolayers containing DNA is not altogether a new concept (e.g. Hui et al., 1996; Chesnoy & Huang, 2000; Hirsch-Lerner et al., 2005), although no studies to-date have used KPFM. Pressure-area isotherms (e.g. MacDonald et al., 2006; Erokhina et al., 2007; Pal et al., 2012), BAM (e.g. Cárdenas et al., 2005; McLoughlin et al., 2005; Eftaiha & Paige, 2012; Dabkowska et al., 2014), fluorescence microscopy (e.g. Symietz et al., 2004; Michanek et al., 2012), AFM (e.g. Hansda et al., 2013; Paiva et al., 2013), infrared reflection-absorption spectroscopy (e.g Gromelski & Brezesinski, 2004; Castano et al., 2008) and neutron reflectivity (e.g. Wu et al., 2006) are the methods of choice at present, although overall surface potentials of monolayers have been measured with the Kelvin method (e.g. MacDonald et al., 2006; Paiva et al., 2013). In the latter case, the Kelvin method is applied to the monolayer on a macro scale, giving a surface potential that is averaged over sizes far larger than any domains or structures. Therefore, KPFM has huge promise to investigate the nanoscale electrical properties of these monolayers, and in fact is done so for the first time in the present work. Results from monolayer studies can then be related to their vesicle/liposome form for use in gene therapy applications (Lee & Chang, 2014).

An early example of DNA-lipid interactions was reported in Leonenko et al. (2002), in which AFM was used to investigate DNA binding with lipid bilayers. They found that the

lipid phase was an important factor, as was the type of lipid contained within the bilayer. Specifically, DNA was found to be able to disrupt the bilayer structure more readily if the membrane contained DOPE versus DOPC, and the authors conclude that this is likely due to the smaller head group area of DOPE, which supports a negatively curved structure (like on the interior of cell membranes).

Neutral (or, rather, zwitterionic) lipids, like DPPC, DOPC and DOPE do not readily interact with DNA on their own. Many monolayer studies have shown this (e.g. Gromelski & Brezesinski, 2004; McLoughlin et al., 2005; Cristofolini et al., 2007; Kundu et al., 2008; Mengistu et al., 2009; Campen et al., 2010; Dabkowska et al., 2014; Luque-Caballero et al., 2014), and in order to induce an interaction it is necessary to include divalent cations such as Ca^{2+}, Mg^{2+} or Ba^{2+}. The cations are thought to bind to the negatively-charged phosphate groups on the zwitterionic lipids. This gives the lipid molecules an overall positive charge on the head groups which can then interact with and bind to DNA, forming a monolayer of the complex (Mengistu et al., 2009; Campen et al., 2010). Although neutral lipids require these ions to be present in order to bind DNA, it has curiously been found that DNA will, on its own, form an insoluble monolayer at the air-water interface if it is left for many hours or days to incubate in a Langmuir trough (Dai et al., 2005, 2013). We note that requiring the use of ions to mediate DNA-lipid interactions becomes redundant if one were to employ the use of cationic surfactants in these systems, which is indeed the subject of the present work.

While we are focussed here on the use of DNA, it is noteworthy that the situation becomes rather interesting for RNA. In a study on the interactions of DNA and RNA with DPPC monolayers, Michanek et al. (2012) confirmed the findings of other studies with DNA, that it is unable to associate itself with the zwitterionic lipids, but that single-stranded RNA could. The authors surmise that the hydrophobic nature of single-stranded RNA was enough to allow it to be surface active and associate with the monolayer. When mixed with dioctadecyldimethylammonium bromide (DODAB), the RNA was found to associate with the monolayer far more than electrostatic considerations would lead us to expect, implying that hydrophobic interactions with the lipid and surfactant chains are significant.

In any case, the association of DNA with monolayers causes an overall expansion of

the monolayer. This is clearly seen as higher concentrations of DNA yield larger molecular areas for a given surface pressure (Chen et al., 2002). An interesting study by Rullaud et al. (2014) compared pressure-area isotherms of a cationic calixarene-based surfactant with DNA of different sequences, namely poly-(AT) vs poly-(GC). The additional hydrogen bond of GC makes those strands more tightly bound, and their isotherms are shifted to smaller molecular areas compared with the poly-(AT) DNA. But mere association with DNA is only the beginning. How exactly does the DNA associate, and what is the morphology of such formations? Perhaps the most relevant set of studies to discuss are those from Chen et al. and co-workers (Chen et al., 2002, 2005, 2012). In this series of papers, the interaction of gemini surfactants and DNA was studied by means of pressure-area isotherms complemented by AFM topographical imaging. The 12-s-12 series of gemini surfactants were studied in Chen et al. (2002), while tail length variations were explored in Chen et al. (2005). In the former case, gemini surfactants with spacers of mid-range length (6-10 carbon atoms) had isotherms that were shifted to larger molecular areas compared to very short or very long spacers, suggesting that there is a 'sweet spot' for optimal association. The asymmetric tail lengths (n-s-m surfactants where $n+m=24$) showed increased molecular areas in isotherms of more symmetric surfactants (e.g., $n=m$). Greater association and higher molecular areas could also simply mean less compaction, so we must turn to the morphology on the nanoscale to for more insight into this issue.

Time is also a factor in the extent of association between DNA and cationic surfactants. In a study using octadecylamine, Hansda et al. (2013) showed that DNA gradually associates with the monolayer over the course of several hours, evidenced by increasing surface pressure from the time at which DNA was injected into an aqueous subphase of high pH (11). As the pH was decreased to neutral, the pressure-time curves became less steep, suggesting that DNA interacts more readily with the monolayer at higher pH. In addition, from AFM imaging of these monolayers deposited onto silicon substrates exhibited increased roughness and larger average height values than the monolayers at lower pH. However, it should be noted that this behaviour can very much depend on the type of surfactant that is used. For instance, Dittrich et al. (2011) reported higher molecular areas for lower pH in pressure-area isotherms of cationic diamide lipids with DNA. (As an aside, in the same study, two lipids were used which had identical head groups but different tails, and showed remarkably different transfection efficiency; therefore, the hydrophobic tails

may be a key consideration.) We will explore the influence of pH on DNA monolayers in a later chapter.

While there are many transfection studies which show the promise of DNA-gemini surfactant combinations (e.g. Wettig et al., 2008; Wang et al., 2013), few have focussed directly on the nature of the molecular interactions between the DNA and surfactant (Akbar et al., 2012). While use of AFM and KPFM is widespread on individual systems to map charge distributions in biologically interesting molecules like DNA (Leung et al., 2010), proteins (Lee et al., 2012), or DNA mixed with proteins (Sinensky & Belcher, 2007), no studies to date, of which we are aware, have used the unique capabilities of KPFM to probe the interactions in mixed systems between DNA and drug delivery molecules (i.e., transfection complexes). It is therefore the purpose of this chapter to use a combination of AFM and KPFM imaging to study the interactions of DNA with mixed lipid monolayers containing gemini surfactant. This builds on the previous chapter, in that DNA is added to explore the morphology of the complexes that are formed from its association with the gemini surfactant that has been integrated into the monolayer.

3.2 Methods

3.2.1 DNA-Lipid-Surfactant Monolayer Construction

Sample preparation for AFM and KPFM imaging was performed in a similar method to that which was described in Chapter 2, but briefly: gemini surfactants of the *16-3-16* type were mixed with two lipids: 1,2-dioleoyl-sn-glycero-3-phosphocholine (DOPC) and 1,2-dipalmitoyl-sn-3-phosphocholine (DPPC), both of which were obtained from Avanti Polar Lipids.

Lipids and surfactant were dissolved in chloroform at a concentration of 1 mg/mL and mixed at a molar ratio of 3:3:2 (DOPC:DPPC:GS). Our monolayers were constructed on a clean Nima Langmuir trough (small) filled with approximately 50 mL of nanopure Milli-Q water in which we dissolved single-stranded salmon DNA which was sheared into random lengths by sonication. The final DNA concentration we used was 10 μM in base pairs, comparable to other studies (Chen et al., 2002). Lipid-surfactant mixtures were deposited

on the trough and compressed to a surface pressure of 35 mN/m. Clean mica slides were drawn up through the monolayer at constant pressure to deposit the film, which was dried afterwards with a gentle stream of nitrogen gas and then in a desiccator.

3.2.2 Imaging

Imaging was performed on an AIST-NT Smart SPM using MikroMasch NSC-14-Cr/Au cantilevers of resonant frequency approximately 130 kHz. Details of the methodology are largely described in § 2.2.3, but here we highlight the key parameters of the setup. Topography and surface potential data were obtained in two sweeps per scan line to optimize image quality. For the surface potential scan, we used both AM-KPFM and FM-KPFM (as indicated where appropriate), the latter resulting in higher spacial resolution. For details see Moores et al. (2010). Several scans of each of several samples were obtained to confirm results. Analysis of the images was performed with proprietary AIST-NT image processing software, and GWYDDION for surface roughness measurements. Masks were created manually on the topography images to calculate surface roughness. Cross sections and pixel data were used for other calculations, as described in the text below.

3.3 Results

As a test of the effect of DNA in the subphase, we show in Fig. 3.1 a comparison of topography and AM-KPFM images for the lipid-GS monolayers formed on both pure water and pure water containing DNA. The significance of the structures formed over the pure water subphase was discussed in the previous chapter; in any case, there is clearly strong interaction of the DNA with the monolayer.

Concentrating on the monolayer formed with DNA, we show topography, phase, cantilever oscillation amplitude (Mag), and FM-KPFM images in Fig. 3.2. We note that the FM-KPFM image shows higher resolution than the AM-KPFM image shown earlier in Fig. 3.1. The phase image tracks the phase shift of the cantilever oscillation, in which contrast typically indicates a change that is chemical in nature. We see that there is an intricate web-like network shown in the topography, with three distinct 'levels' of features

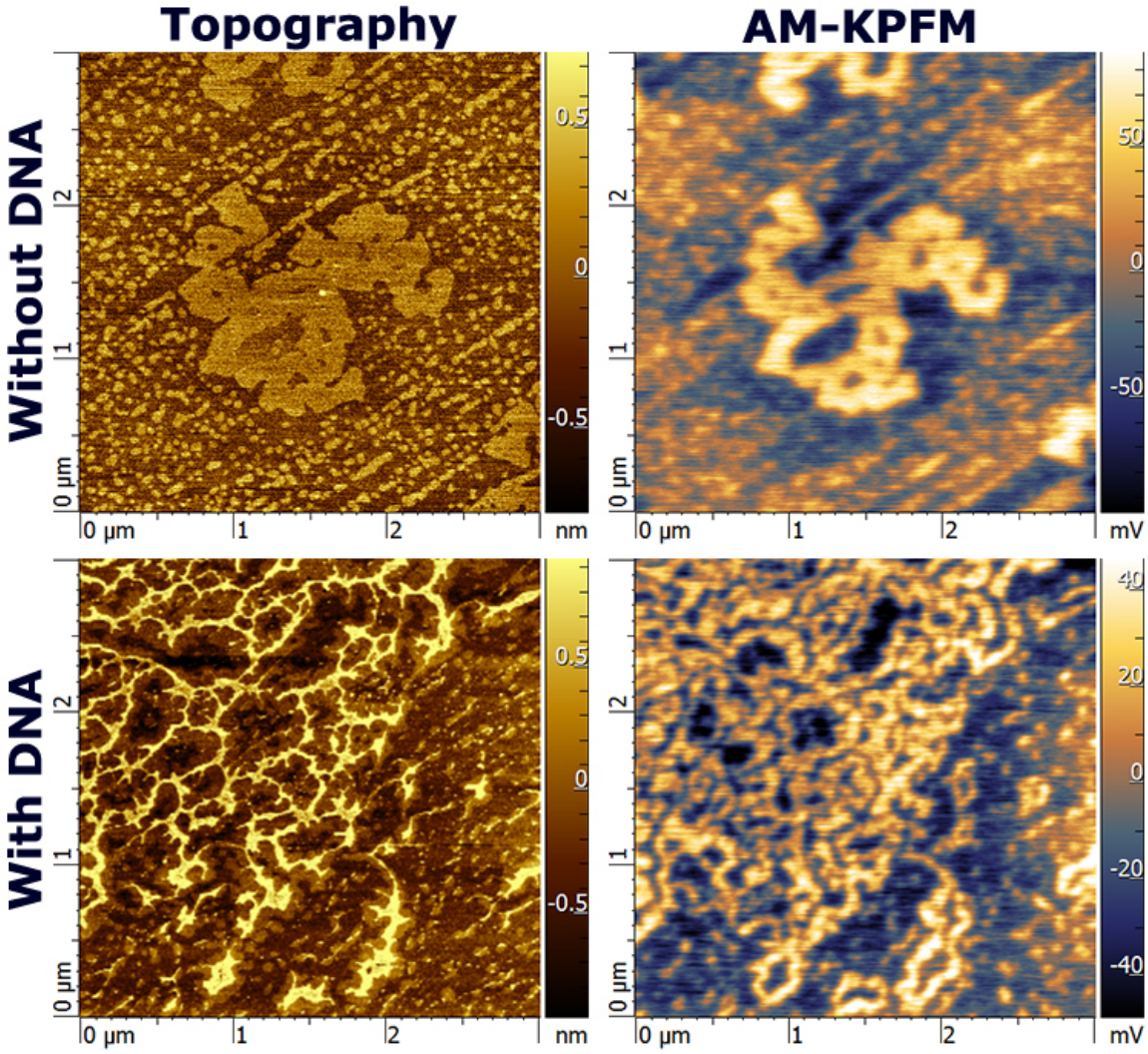

Figure 3.1: AFM topography (top left and bottom left) and AM-KPFM images (top right and bottom right) of DOPC-DPPC-GS monolayers without DNA (top) and with DNA (bottom) present in the subphase at the time of formation and deposition.

in terms of height. The phase and FM-KPFM images correlate with each other and show interesting contrast. Cross-sections of the topography and FM-KPFM images, showing this correlation as well, are presented in Fig. 3.3. Perhaps a more striking demonstration of this result is shown in Fig. 3.4, which shows an overlay of the FM-KPFM signal on top of the topography image of Fig. 3.2, clearly indicating that the FM-KPFM signal arises in the areas directly adjacent to those of the highest height. It is thus clear that there is a positive surface potential difference in the mid-range height regime that surrounds the 'web'. Both the lower and higher height regions appear to have similar and less positive surface potential.

Values for the differences in height between the three regions, and the magnitude of the FM-KPFM signal, were calculated in a manner analogous to that which was used in the previous chapter. While all three image analysis methods were applied to the monolayer images with DNA, the cross-section method was deemed to be superior. Table 3.1 shows the results of these calculations, with uncertainties at computed at a 95% confidence level. The middle domains were found to be 0.446 ± 0.014 nm higher than the background, where the FM-KPFM signal was positive at 561 ± 16 mV. This is a lower height than the control monolayer, and also a slightly lower potential (for possible reasons, see the discussion below). The highest region is 1.197 ± 0.026 nm higher than the middle region (or roughly 1.64 nm higher than the background). We show in Fig. 3.6 a 3D rendering of an illustrative region within the topography image which helps to visualise these three regions of interest.

3.4 Discussion and Conclusions

In an attempt to theorise as to the origin of these structures, we should consider the mechanism of DNA complexing with the gemini surfactant and lipid. Pure DNA in water deposits nothing onto mica; there is simply nothing to drive adhesion. Similarly - and verified by experiment - monolayers composed of pure lipid mixtures (in our case DOPC and DPPC) showed identical topography and KPFM signal with and without DNA present in the water subphase. However, the addition of gemini surfactant results in a strong interaction. This is not a surprise, since the positive charges on the cationic gemini surfactants are attracted electrostatically to negatively charged DNA. It was shown also in Chen et al. (2002) that

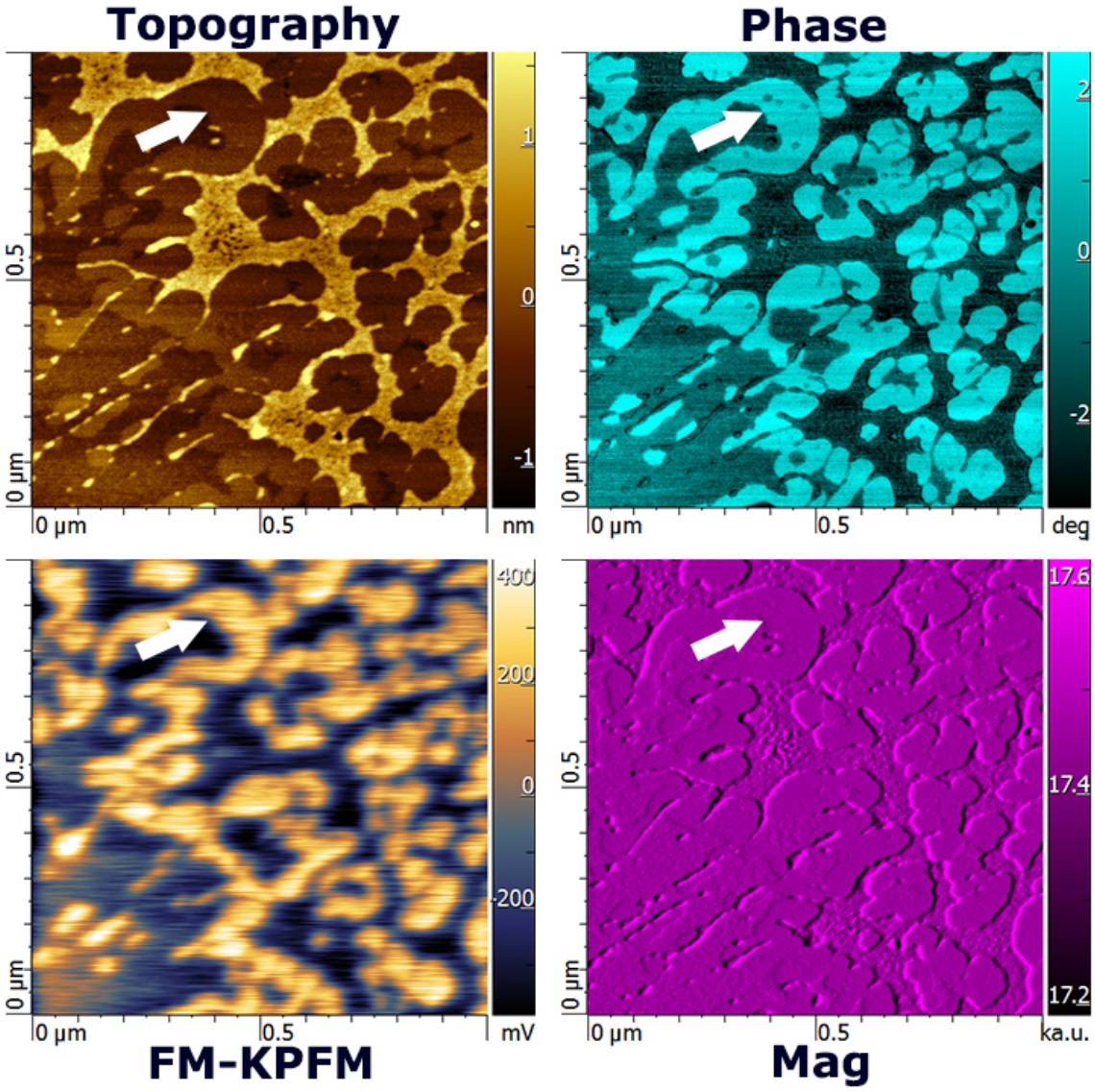

Figure 3.2: Images of size 1 μm x 1 μm of the DOPC-DPPC-GS monolayer formed in the presence of DNA: topography (top left), phase (top right), FM-KPFM (bottom left), and cantilever oscillation magnitude (bottom right). The white arrow points to a region of intermediate height, as described in the text, which corresponds to a region of higher surface potential and contrasting phase.

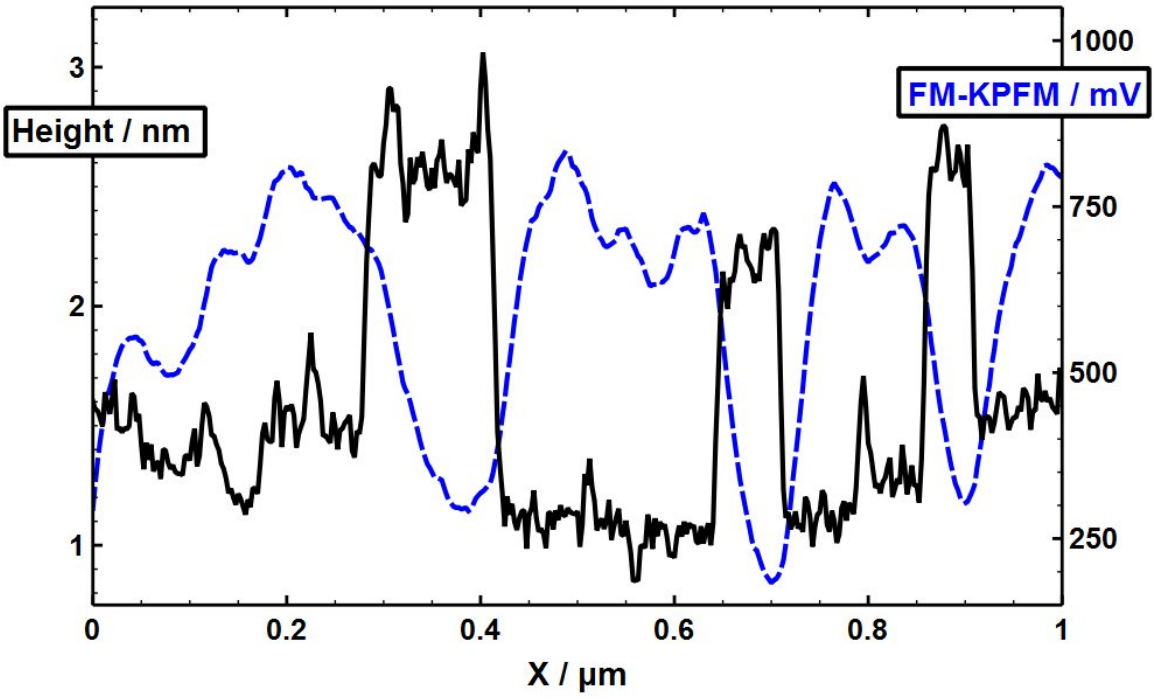

Figure 3.3: Horizontal cross-sections of the topography and FM-KPFM images in Fig. 3.2 at the 0.5 μm mark on the vertical axis. The areas of higher FM-KPFM signal correlate with topographical regions of height a few tenths of a nm above the baseline (e.g, at the 0.2 μm mark).

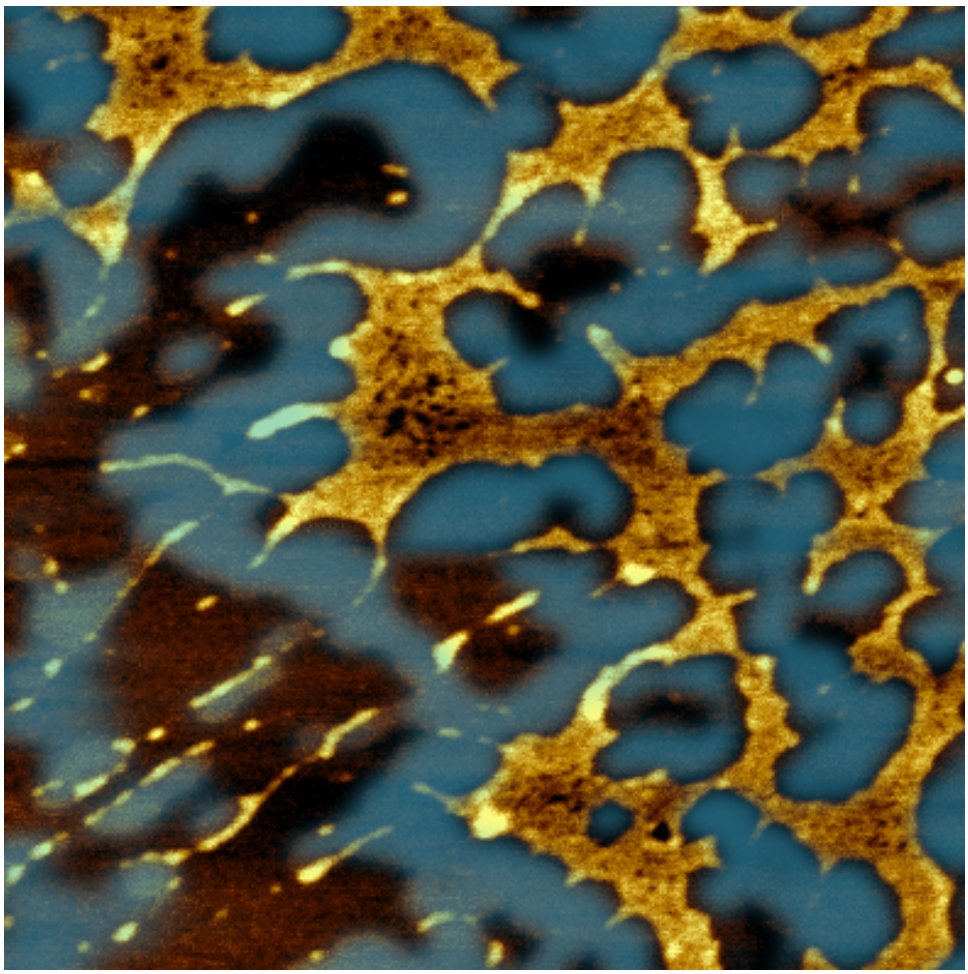

Figure 3.4: Overlay of the topography image in Fig. 3.2 with the FM-KPFM image. Only the bright (relatively high mV) regions of the FM-KPFM image were included here, with a small amount of Gaussian filtering applied, for clarity. The result shows the areas of higher surface potential correlating well with the areas surrounding those of the greater height.

Table 3.1: Image analysis results for height and surface potential differences between domains in lipid-gemini surfactant monolayers containing DNA (DOPC+DPPC+16-3-16 3:3:2). The control monolayer is identical to that which was presented in the previous chapter (but with surfactant), but is used here for comparison. The cross section method was used to calculate final result for the height and surface potential of the domains relative to the background. See the text for further details. Margins of error calculated at a 95% confidence level.

Region	Height / (nm)	FM-KPFM / (mV)
	Control Monolayer (no DNA)	
Domains[a] Δh	0.574 ± 0.001 nm	658 ± 17 mV
	With DNA	
Lower[b] Δh_l	0.446 ± 0.014 nm	561 ± 16 mV
Higher[c] Δh_u	1.197 ± 0.026 nm	–[d]

[a] Differences between the domains and background.

[b] Differences between the mid-region and background. See Fig. 3.6.

[c] Differences between the highest region and the mid-region. See Fig. 3.6.

[d] Only the mid-region showed a positive KPFM signal, so there is only one value to report relative to a 'background'.

gemini surfactants with sufficiently short tail lengths (generally below 16 carbon atoms) to reduce surface activity to zero suddenly become surface active when DNA is present in the subphase. This is due to charge neutralisation increasing the hydrophobicity of the gemini surfactant. Therefore, there is no doubt that DNA and gemini surfactant interact very strongly. Here, the gemini surfactant is already surface active, and the DNA must bind up to the gemini surfactant from the subphase. Chen et al. (2002) proposes an arrangement where the negatively charged phosphate groups of the DNA bind to the cationic ammonium head groups of the gemini surfactant in chains, with the spacer group lying flat against the water surface for smaller spacers. This would assist in explaining the web-like connections of the features we identify in the topography, especially considering the height difference between the lowest and highest regions being on the order of 2 nm.[1]

However, what is most interesting about this result is the KPFM signal failing to correlate directly with the topography. Here, we have a positive KPFM signal that envelops the web-like features. We propose that the majority of net positive charge likely resides in those regions of positive relative surface potential. Comparing these regions with the background, and considering that DPPC forms a thicker monolayer than DOPC (Coban et al., 2007), we infer that the lower background may be composed primarily of DOPC, with the positive regions the DPPC-GS mixture. While the height alone (~ 2 nm) of the web-like higher features would lead us to expect them to contain the DNA, it is not until we consider that these regions are of lower surface potential than the lipid-GS region that we can propose that they are DNA-GS complexes of nearly unit charge ratio. A schematic of what this might look like is presented in Fig. 3.5. In this figure we show what the monolayer might look like in a simplistic way at the air-water interface with DNA dissolved in the subphase, and how the topography would change upon deposition onto a solid substrate for imaging.

In addition, it is noteworthy that the surface roughness of the lower and middle height regions are similar, at around $0.11-0.12$ nm, while the higher, web-like regions have a much higher roughness at about 0.22 nm in this image. One can also visualise the roughness qualitatively by observing the 3D rendering provided in Fig. 3.6; despite smoothing, it is

[1] This value, about 2 nm, is accordant with the rough diameter of a DNA molecule.

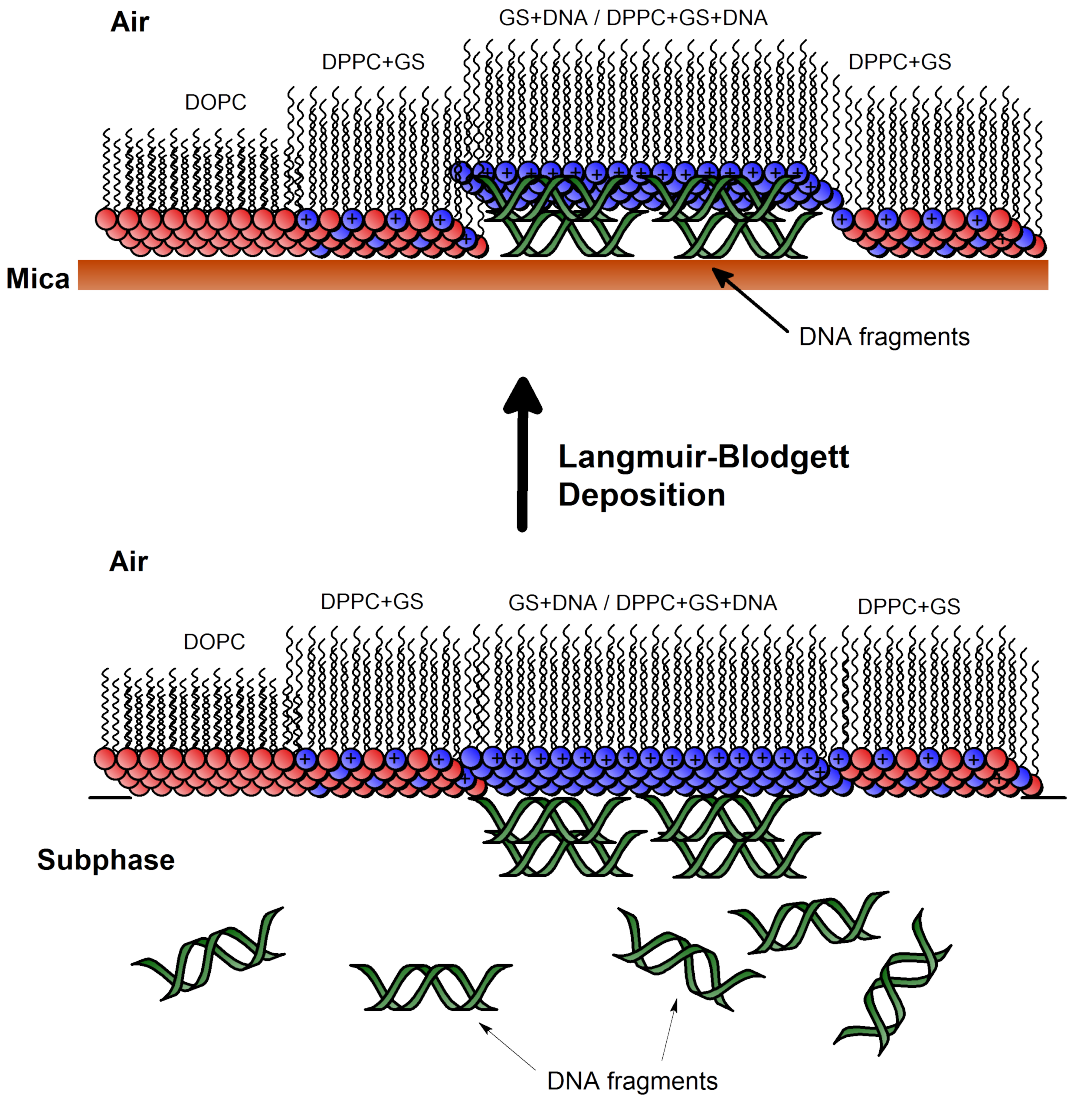

Figure 3.5: Schematic representation of proposed structure for DNA-lipid-GS monolayers. See also Fig. 3.6.

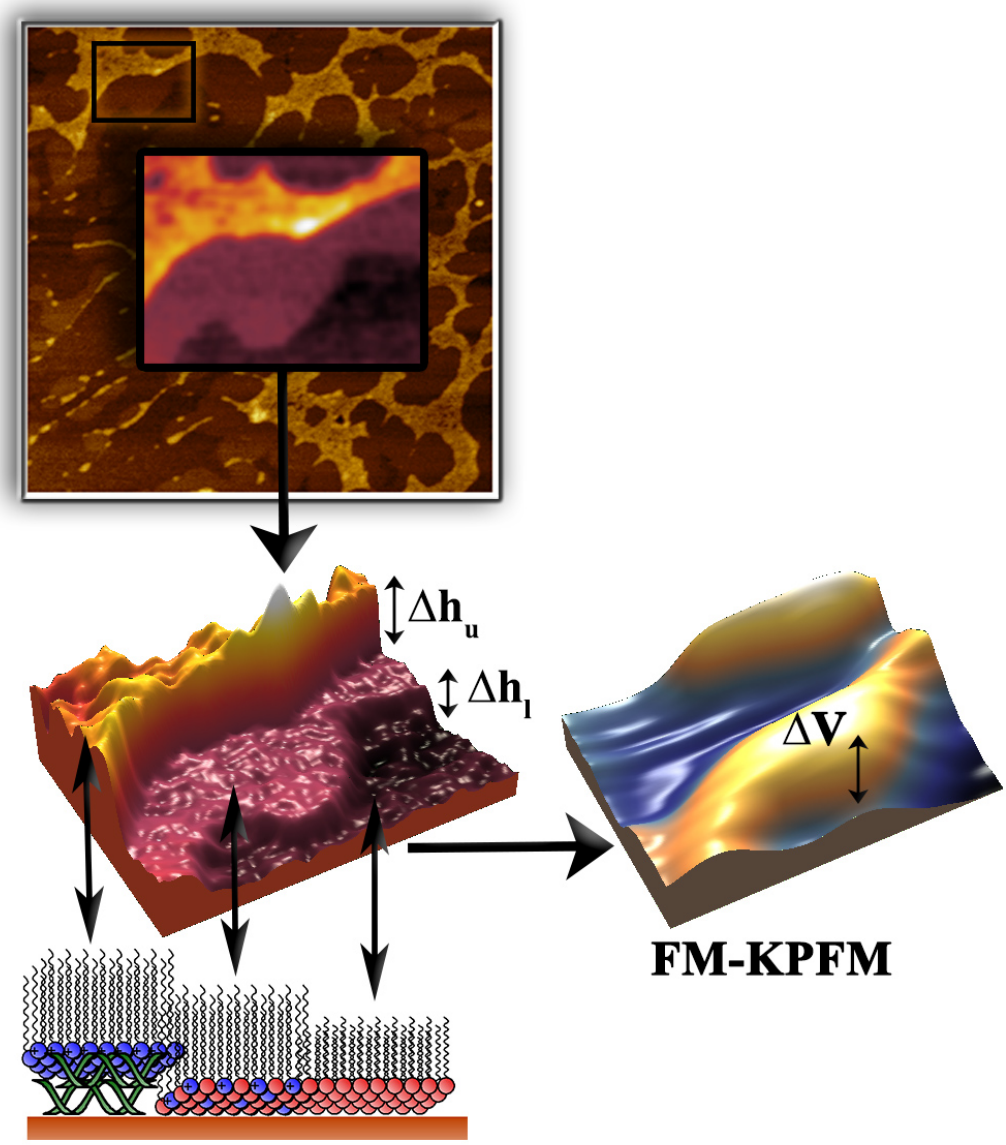

Figure 3.6: This 3D rendering from an inset of the topography image from Fig. 3.2 shows the three regions corresponding to values of Δh_l and Δh_u on a detail schematic from Fig. 3.5. To the right is a 3D rendering of the FM-KPFM signal of the same region, showing the signal ΔV that is generated by the mid-height region.

clear that the highest region is also the least uniform. This provides further evidence that the DNA is concentrated in these higher regions as the strands would naturally have more variation than a uniform monolayer component.

We have thus shown how KPFM can be used to qualitatively trace charges in complexes formed by DNA and GS, and provide key hints into the electrostatic interaction behaviour of these molecules. An understanding of the distribution of charges in these complexes cannot be revealed by topographical scanning alone, and in a biological context it is necessary to utilize KPFM imaging.

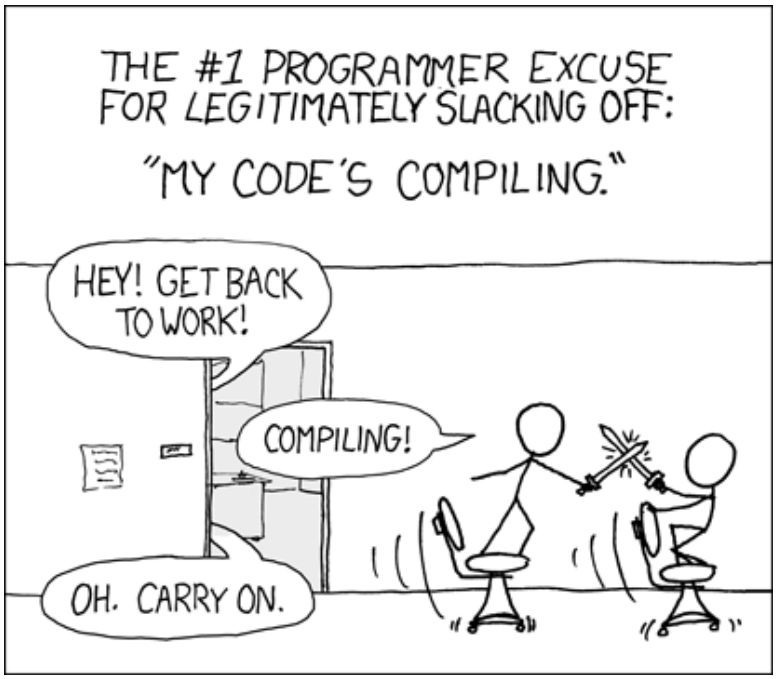

Reprinted from xkcd.com.

Have more than you show,
And speak less than you know.

William Shakespeare

Chapter 4

Monolayers of Gemini Surfactant-DOPE Transfection Complexes

4.1 Introduction

We have established in the previous chapter that DNA and gemini surfactants interact very strongly, as one naturally would expect, and visualised this via a monolayer study with AFM. Now we will turn to a similar study, but with direct application to gene delivery. By extending the experiments from the previous chapter to the construction of monolayers of materials that compose gene transfection complexes, we can visualise the nanoscale structure of such particles as if we were able to construct a macro version of one nanoparticle. By analogy, this is like peeling a basket of oranges and flattening out the rinds on a large surface. One would still be able to determine the structure of orange peel in this way, despite, say, an inability to do AFM on a single orange. In fact, monolayers have already been used to explore the properties of vesicle-forming surfactants (e.g. Barlow et al., 1997).

In the present case, the major shift from what we have shown in the previous chapter is replacing DOPC+DPPC with the helper lipid DOPE. As we have already discussed, DOPE has been found to greatly enhance transfection efficiency (Hirsch-Lerner et al., 2005). This is thought to arise from a conformational change induced by the DOPE molecules in which a normally lamellar phase is transformed to hexagonal (Wasungu & Hoekstra, 2006).

In such a system, the DNA would be coated by the cationic lipid-surfactant monolayers and arranged in a lattice (which we observed in the previous chapter). In addition, it is hypothesized that the addition of a neutral lipid like DOPE serves to add flexibility to the charge density introduced by the cationic surfactant, so that the lipid-surfactant mixture can have its charges diluted. The end result would then be that the charge density of the gene carrier vesicles may match that of the DNA it is carrying (Dabkowska et al., 2012). In any case, the positively charged surfactant molecules serve to compact the DNA (García et al., 2014).

Mixing behaviour of gemini surfactants with DOPE is therefore of considerable interest. Surfactants, when mixed, may cooperate and cause a decrease in their critical micelle concentrations (so-called synergistic behaviour) or they may do the opposite (antagonistic behaviour) and disrupt micelle formation, requiring a larger amount of surfactant to be present for micelles to form (Bergström & Eriksson, 2000). Interestingly, it turns out that DOPE and gemini surfactants of the 16-s-16 type mix antagonistically (Akbar et al., 2012). In contrast, mixing with phosphocholines is synergistic (Bakshi et al., 2006). The difference appears to lie in DOPE's structure, in that it tends toward negative curvatures owing to its smaller headgroup size compared to the phosphocholines (like DOPC). Akbar et al. (2012) found that shorter spacer groups (e.g., 16-3-16) mix more antagonistically with DOPE than with a gemini surfactant possessing a longer spacer (e.g., 16-7-16), while the introduction of a protonatable amine group in the longer spacer (16-7NH-16) put the surfactant somewhere in between. In all cases with DOPE, the mixing remained antagonistic.

Amine-substituted gemini surfactants are especially noteworthy. Recall our discussion in § 1.2, where we introduced these surfactants as structures that are responsive to the acidity of their environment. At moderately low pH, they become protonated and thus wield a 3+ charge, instead of the usual 2+. Such surfactants have been found to yield enhanced transfection efficiency compared to their non-substituted counterparts (Wettig et al., 2007; Yang et al., 2010; Donkuru et al., 2012).

To explore this phenomenon, we present in this chapter a study analogous to Chapter 3, but with monolayers of gemini surfactant and DOPE. We also examine the effects of lowering the pH of the subphase on the monolayer structure. With DNA present in the subphase at the time of monolayer formation, we can explore the structures induced when

DNA binds to the surfactant molecules. Such monolayers are directly analogous to the transfection complexes themselves, which we will explore in the following chapter.

4.2 Methods

4.2.1 DNA-Lipid-Surfactant Monolayer Construction

Sample preparation for AFM and KPFM imaging was performed using a similar method to that which was described in Chapter 2, but briefly: gemini surfactants of the *16-3-16*, *16-7-16*, and *16-7NH-16* type (the latter, for reference, being of type 1,1,9,9-tetramethyl-5-imino-1,9-alkanediammonium dibromide) were mixed with the lipid 1,2-dioleoyl-sn-glycero-3-phosphoethanolamine (DOPE), obtained from Avanti Polar Lipids. The three gemini surfactants used here were chosen to evaluate the effects of the spacer group (spacers of 3 and 7 carbon atoms), and also for the effect of an amine-substitution in the spacer group (7NH). In the latter case, a protonatable amine group is placed at the centre of the spacer group, which allows the charge on the surfactant to be modulated based on environmental pH. As discussed in § 1.5, the variation of pH is an important factor to be explored. For further details of these surfactants and their synthesis, see Wettig & Verrall (2001); Wettig et al. (2007) and references therein.

Lipids and surfactants were dissolved in chloroform at a concentration of 1 mg/mL and mixed at the appropriate molar ratio. Our monolayers were constructed on a clean Nima Langmuir trough (small) filled with approximately 50 mL of nanopure Milli-Q water. For cases in which DNA was present, we dissolved single-stranded salmon DNA, which was sheared into random lengths by sonication, into this subphase during its preparation. For the preparation of samples in an acidic environment, the trough was filled with acetate buffer (pH 4) prepared with nanopure Milli-Q water in cases as reported. The final DNA concentration we used was 10 μM in base pairs, comparable to other studies (Chen et al., 2002). Lipid-surfactant mixtures were deposited on the trough and compressed to a surface pressure of 35 mN/m. Clean mica slides were drawn up through the monolayer at constant pressure to deposit the film, which was dried afterwards with a gentle stream of nitrogen gas and then in a desiccator overnight.

4.2.2 Isothermal Pressure-Area Curves

Our isotherms were captured on a large Nima Langmuir film balance (having a surface area of 841 cm^2). With the trough clean and wide open, 20 μL of each mixture of amphiphile-chloroform solution was added, where the total concentration of solutes was kept at a constant 2.5 mM to ensure consistent depositions. After allowing the solvent to evaporate for 10 minutes, the barrier arms were compressed slowly at a rate of 15 mm/min until a maximum pressure was reached (75 mN/m, well beyond the collapse pressure of any of our mixtures). Each experiment was repeated to ensure reliability, and the data averaged. For our final pressure-area curves, the area was converted into area available per molecule, in $Å^2$.

4.2.3 Imaging

Imaging was performed on an AIST-NT Smart SPM using MikroMasch NSC-15-Pt cantilevers of resonant frequency approximately 325 kHz. Details of the methodology are largely described in § 1.3, and identical to § 3.2.2.

4.3 Results and Discussion

We begin by looking at the effects of adding DOPE and DNA to the gemini surfactant monolayers. In Figs. 4.1, 4.2 and 4.3 we show pressure-area isotherm curves for each of the surfactants in turn, and observe changes upon the addition of DOPE and DNA. In the case of 16-3-16, we present additional isotherms in which a gradual addition of DOPE has been added (a factor that we will explore in further detail in § 4.3.1).

As expected, the addition of DNA in all cases (surfactant only, or surfactant with DOPE) causes the isotherm curves to shift to the right, toward larger molecular areas. In other words, the pressure of monolayers with DNA bound is higher than it would be at a given molecular area had there been no DNA added. This suggests, not surprisingly, that DNA is incorporated into the monolayer, which is consistent with our earlier results. Interestingly, adding DNA has the largest effect on the monolayer containing only 16-3-16,

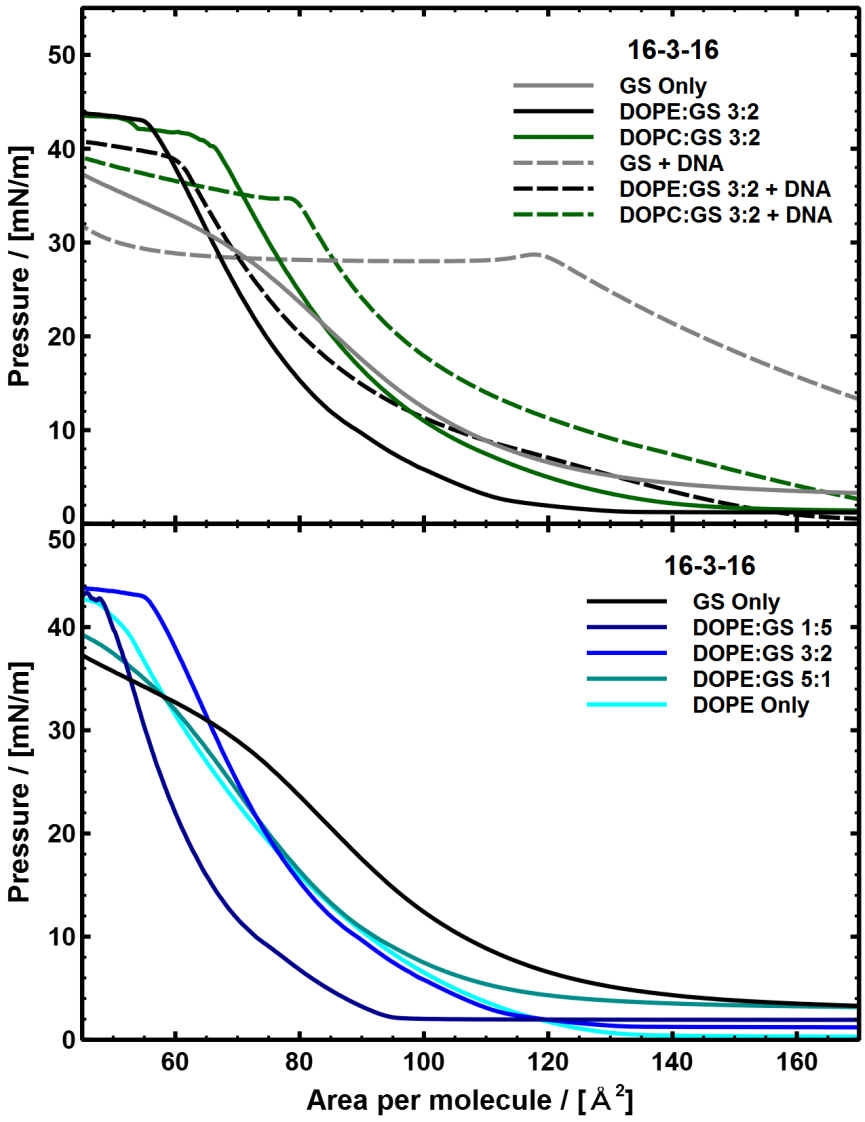

Figure 4.1: Isotherms of the surfactant 16-3-16, with lipids DOPC or DOPE (ratios given are molar), with or without DNA, as indicated. DNA in the subphase was at a concentration of 10 μM; these isotherms are indicated by dashed lines. The bottom panel shows the effects of varying the ratio of DOPE:GS.

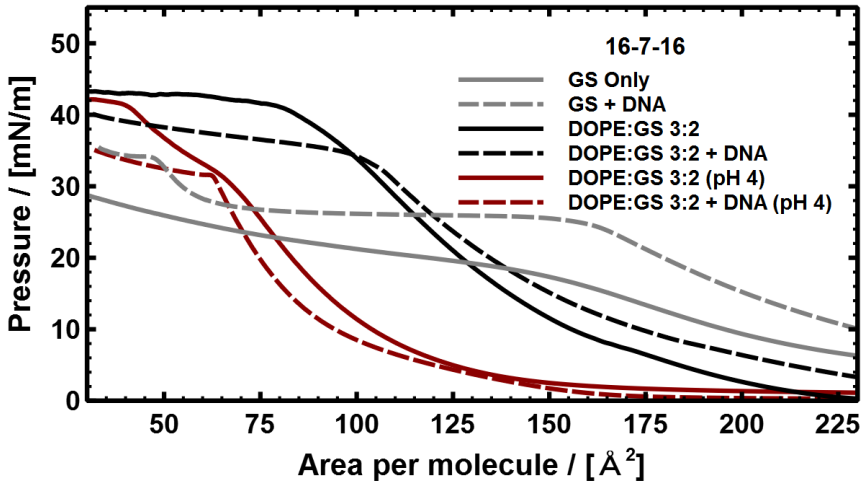

Figure 4.2: Isotherms of the surfactant 16-7-16, with DOPE and DNA as indicated. DNA in the subphase was at a concentration of 10 μM; these isotherms are indicated by dashed lines. The grey and black curves indicate isotherms over a pure water solvent subphase, while the dark red curves indicate isotherms over acetate buffer (pH= 4).

further suggesting that this gemini surfactant has a very large affinity for DNA binding. An expansion of the monolayer upon the addition of DNA is consistent with the work of Chen et al. (2002), which explored the effects of DNA on monolayers of gemini surfactant.

One of the other important considerations is the condensing effect of the helper lipid DOPE. As we have discussed previously, it has been shown that DOPE as a helper lipid yields greater transfection efficiency than the phosphocholines, like DOPC (Hirsch-Lerner et al., 2005; Wasungu & Hoekstra, 2006). For comparison, therefore, we show in Fig. 4.1 isotherms for 16-3-16 with DOPC (green curves). We see that the monolayers containing DOPC lie in between those of the gemini surfactant alone and those with DOPE. It is possible that DOPE induces a larger condensing effect on the DNA, and in fact, as will see later in the AFM results, these monolayers show some aggregate formation which was not observed in our DOPC+DPPC monolayers or those without helper lipid. Monolayers containing 16-7-16 and 16-7NH-16 show similar trends with the addition of DOPE and DNA as we observed with 16-3-16.

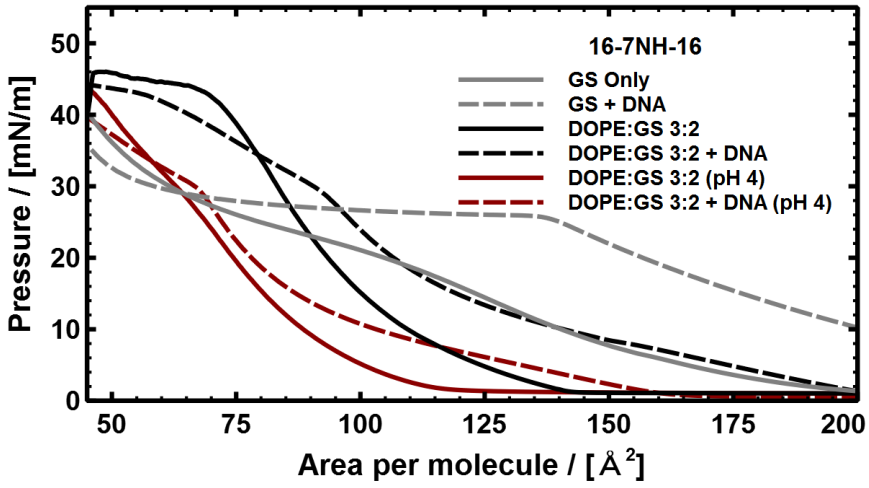

Figure 4.3: Isotherms of the surfactant 16-7NH-16, with DOPE and DNA as indicated. DNA in the subphase was at a concentration of 10 μM; these isotherms are indicated by dashed lines. The grey and black curves indicate isotherms over a pure water solvent subphase, while the dark red curves indicate isotherms over acetate buffer (pH= 4).

4.3.1 The Importance of the Spacer Group

Naturally, it is an important question to ask what effect the structure of the gemini surfactant has on the binding behaviour of DNA, and what sorts of properties these complexes have. In the present work, we are exploring three different gemini surfactants, each with different spacer groups but identical tails. In this section, we present AFM images of the monolayers formed by these three surfactants with DOPE and DNA, and compare their pressure-area curves in detail.

In Fig. 4.4 we show AFM and KPFM results for these three surfactants, with cross sections. The KPFM images are relatively unremarkable compared with our previous results in Chapter 3, but we do note some interesting signals. While the KPFM signal from the monolayer containing 16-3-16 is strong, we note that there are small aggregates present in this particular image, and that the remaining features are consistent with the other surfactants in that such aggregates exhibit a relatively negative KPFM signal. The web-like network of DNA-bound threads do show a slight negative signal as well, although it is quite weak. Interestingly, we do observe some spherical aggregates in some regions

which exhibit a positive KPFM signal (see Figs. C.7, C.8 and C.9 in the Supplementary Data of Appendix C).

A more quantitative comparison can be seen in the pressure-area curves we present in Fig. 4.5, in which we compile isotherms from each of the gemini surfactants with DOPE, with and without DNA. As we discussed previously, the addition of DNA causes an expansion of the monolayers in each case. However, the largest effect appears to be on the surfactant with the protonatable amine spacer, 16-7NH-16. This surfactant has the same number of atoms in its spacer group as 16-7-16, and yet gives rise to a more condensed monolayer (smaller molecular areas). We will explore the properties of this spacer group in more detail in § 4.3.2. In the present case, we observe the most condensed monolayer to be 16-3-16. While this is an interesting trend, we note that caution is in order; the effects of aggregation and multilayer formation are difficult to quantify, and much of the condensation may be due to nanoparticle formation. In addition, it is difficult to know exactly how much of the DNA has come up form the subphase and bound to the monolayer, so we must keep this in mind and make observations on a relative basis for the present work. We observe that the monolayers become more expanded in the order of 16-3-16, 16-7NH-16, 16-7-16; this is the same sequence as the order of decreasing antagonistic mixing behaviour observed by Akbar et al. (2012). It could be, therefore, that antagonistic mixing of gemini surfactants and DOPE leads to more condensed monolayers.

The Ratio of Gemini Surfactant to Helper Lipid

Yet another factor in the construction of surfactant delivery systems are the proportions of each component. In particular, the ratio of DOPE to gemini surfactant is important (Wang et al., 2007; Dabkowska et al., 2014), and so in this section we show the morphological differences in the monolayers formed using varying ratios of DOPE:GS. Recall that in Fig. 4.1 we compare pressure-area curves of the gemini surfactant 16-3-16 with DOPE at various ratios. The most expanded monolayer is the one containing only gemini surfactant (DOPE:GS ratio 0:1). Adding a little DOPE (1:5) causes the monolayer to condense to smaller molecular areas. However, further addition of DOPE results in an *expansion* of the monolayer, albeit to molecular areas that are still smaller than with gemini surfactant alone. It is interesting to note that the curve is relatively stable for the ratio 3:2 and above,

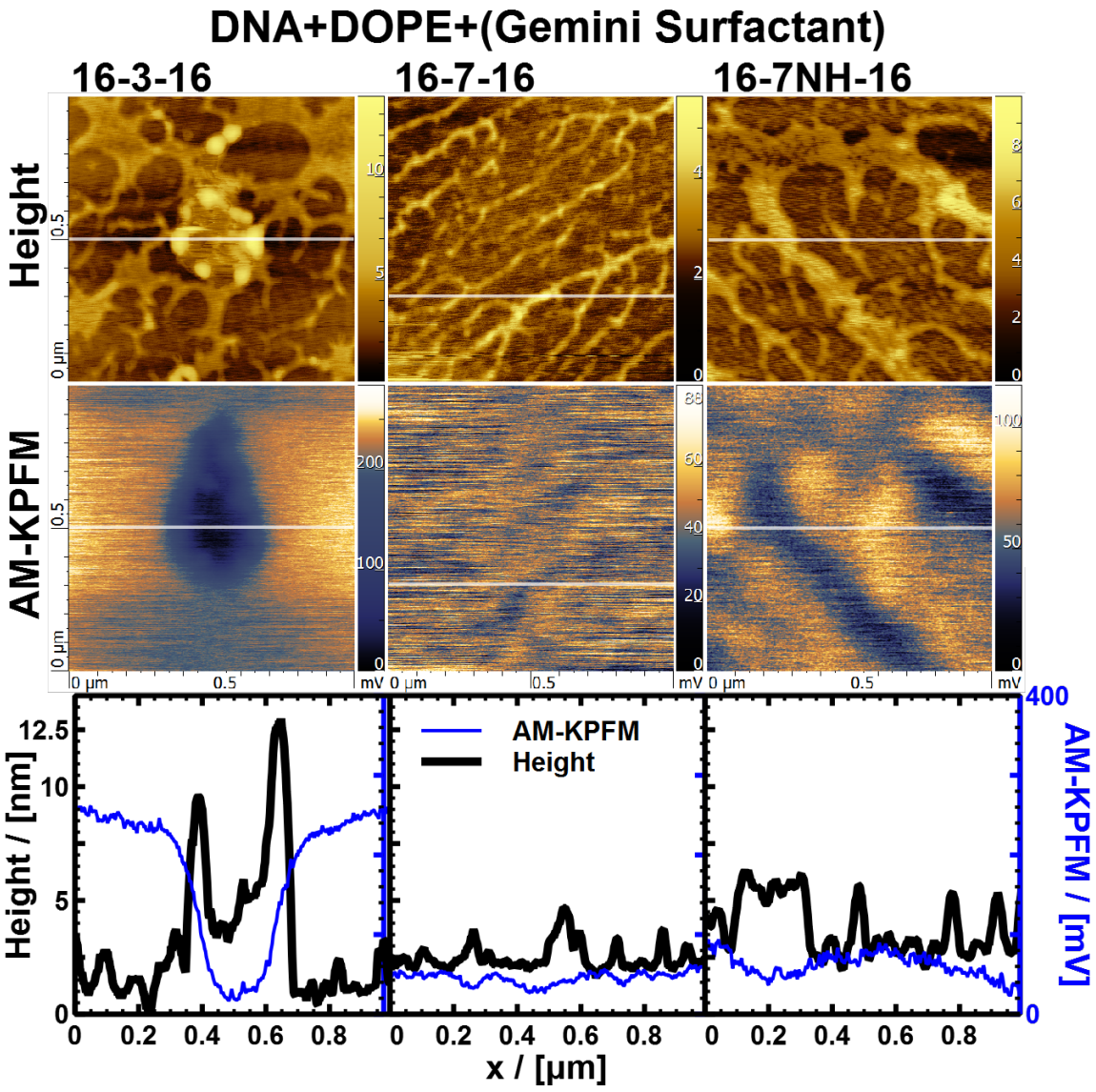

Figure 4.4: Small-scale AFM and KPFM images of DNA-DOPE-gemini surfactant monolayers, with cross sections. The thin blue line shows the AM-KPFM signal, and the thick black line shows the height in the plots; all scales are identical. In all cases, the deposition pressure was $\pi = 35\,\mathrm{mN/m}$, the ratio of DOPE:GS was 3:2, and the DNA concentration of the subphase was $10\,\mu\mathrm{M}$.

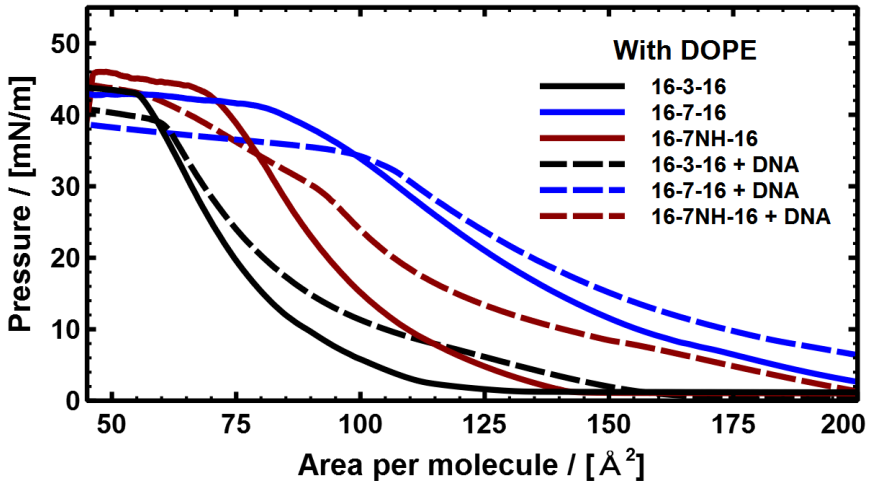

Figure 4.5: Isotherms of the surfactants 16-3-16, 16-7-16 and 16-7NH-16 with DOPE (molar ratio 3:2 DOPE:GS), with DNA in the subphase at a concentration of 10 μM as indicated. The solid lines indicate isotherms over a pure water subphase, while the dotted lines indicate isotherms over a subphase with DNA present.

suggesting that there is strong binding and incorporation of the DOPE into the monolayer as tightly bound complexes at small DOPE fractions, while at larger fractions the DOPE simply begins to incorporate into the monolayer as another natural component. Our pure DOPE monolayer is remarkably consistent with the others at larger DOPE fractions, and also consistent with prior studies (Rathman & Sun, 2005). The 'sweet spot' ratio of 3:2 (or slightly greater) also happens to be optimal for gene transfection (e.g. Wang et al., 2007, 2013), so perhaps there is a link between this observation and transfection efficiency.

Now we compare the observations in the pressure-area curves to the nanoscale morphologies shown in the AFM images of Fig. 4.6. While we see a tightly bound network of threads in the 16-3-16-only monolayer, we note the presence of aggregates in the 1:5 monolayer upon the addition of a small amount of DOPE. These aggregates could help to explain the observed condensation of the monolayer in the pressure-area curves. Further addition of DOPE produces larger threads of DNA-bound complexes. In addition, the larger DOPE fraction appears to induce more prominent electrostatic domains within the monolayer, as we can see from the cross sections. With the largest fraction of DOPE, 5:1,

we note that the threads become very thick, on the order of $\sim 500\,\text{nm}$ in some cases, which suggests that with a smaller fraction of cationic molecules with which to bind the DNA, these components form very tight complexes. However, these tight complexes appear to have little effect on the macro-properties of the monolayer (that is, the overall pressure-area relationship) compared to the other extreme (the 1:5 ratio).

4.3.2 Implications of Solution pH

Acidity is an environmental factor that varies with biological conditions, and thus presents an opportunity to be used as a trigger for the release of genes from their delivery systems (Wettig et al., 2007; Donkuru et al., 2012). Amine functional groups act as Lewis bases, and can be protonated under acidic conditions to attain an additional positive charge. Hence, the gemini surfactant 16-7NH-16 (or any other surfactant with an -NH group) will have a 3+ charge at low pH, versus the usual 2+ under neutral or basic conditions. To this end, in this section we present monolayers of the gemini surfactant 16-7NH-16 formed over acetate buffer (pH= 4), and compare them to those formed over nanopure water.

In Fig. 4.7 we show three monolayers of this pH-sensitive gemini surfactant, over nanopure water and over acetate buffer. In the latter case, we show two different pressures, $\pi = 15\,\text{mN/m}$ and $\pi = 35\,\text{mN/m}$ for comparison with a lower π. Once again, the KPFM signals from these monolayers are weak, although they do indicate a slight negative signal generated from the DNA-bound threads and aggregates. At higher pressure, we note the appearance of some aggregates which show up in the cross section a few nm higher than the threads. Perhaps the greater compression induces this formation of nanoparticles.

An examination of the pressure-area curves in Fig. 4.8 shows the dramatic effect of lowering the solution pH. These curves are all in the presence of DNA, and compare the surfactants 16-7-16 and 16-7NH-16 over pure water or over acetate buffer. Remarkably, the surfactant without the protonatable amine group shows the largest difference when the pH is lowered. This counterintuitive result can perhaps be explained by the larger charge density of the 16-7NH-16 molecules which might limit the space available for DNA binding. However, it should be noted that the buffer salts present in solution may have large effects on the monolayer properties that have yet to be fully explored (McLoughlin et al., 2005;

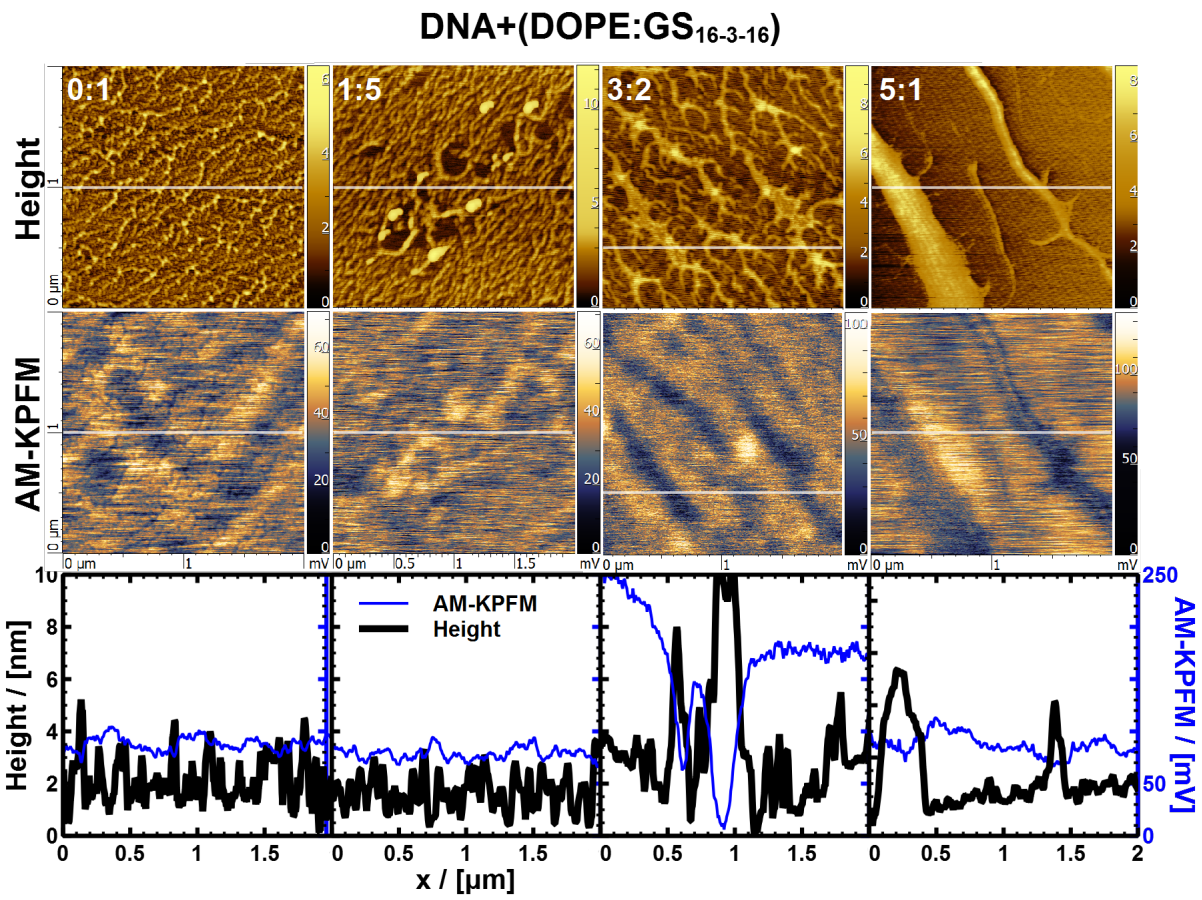

Figure 4.6: AFM and KPFM images of DNA-DOPE-16-3-16 monolayers, with cross sections. The thin blue line shows the AM-KPFM signal, and the thick black line shows the height in the plots; all scales are identical. The deposition pressure was $\pi = 35\,\mathrm{mN/m}$ for all but $0:1$, where $\pi = 15\,\mathrm{mN/m}$. This smaller pressure was required for the pure gemini monolayer due to the low collapse pressure in the absence of helper lipid. Ratios of DOPE:GS are indicated, and in all cases the DNA concentration of the subphase was $10\,\mu\mathrm{M}$ using a pure water solvent for the subphase.

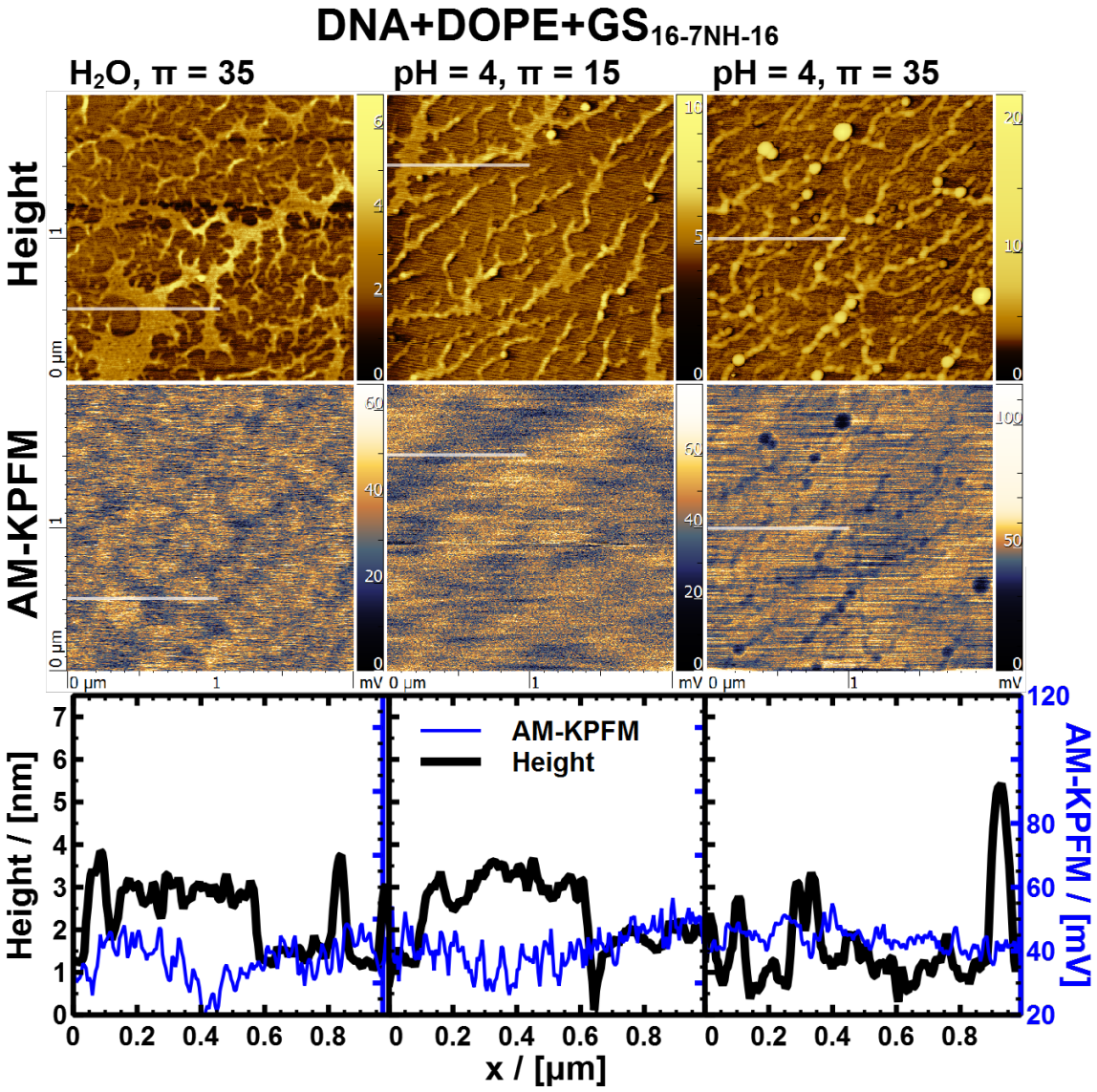

Figure 4.7: AFM and KPFM images of DNA-DOPE-16-7NH-16 monolayers, with cross sections. The thin blue line shows the AM-KPFM signal, and the thick black line shows the height in the plots; all scales are identical. The deposition pressure was as indicated above each height image, $\pi = 15$ or $35\,\mathrm{mN/m}$, the ratio of DOPE:GS was 3:2, and the DNA concentration of the subphase was $10\,\mu$M. Where we indicate H_2O or pH= 4, the latter was over acetate buffer, while the former used a pure water solvent for the subphase.

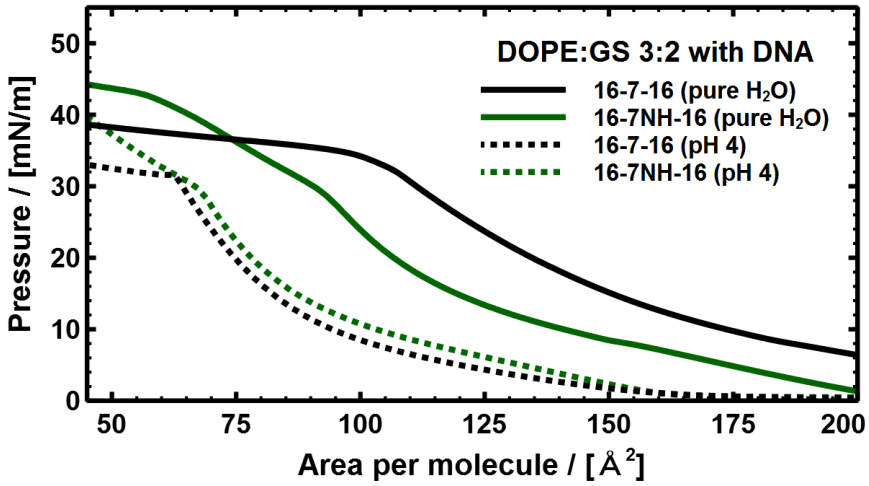

Figure 4.8: Isotherms of the surfactants 16-7-16 and 16-7NH-16 with DOPE (molar ratio 3:2 DOPE:GS), with DNA in the subphase at a concentration of 10 μM. The solid lines indicate isotherms over a pure water solvent subphase, while the dotted lines indicate isotherms over acetate buffer (pH= 4).

Cristofolini et al., 2007; Dabkowska et al., 2014).

4.3.3 Heights and Surface Potentials

As a comparison to our results from the previous chapter, we show in Table 4.1 a summary of height and surface potential differences between the DNA-laden domains and the background for a few of our monolayers. We note the higher heights (statistically significant given our confidence intervals) of the domains in the 16-3-16 monolayer containing DOPE (2.10 nm), compared with a mixture of DOPC+DPPC (total height 1.643 nm). Confirming our qualitative observations, the surface potential differences of the DNA domains are weakly negative, although the 16-3-16 monolayer is significantly more positive than the other two. While the monolayers of 16-7-16 and 16-7NH-16 are statistically the same in terms of surface potential and height, the domains within the monolayer formed over pH= 4 buffer are not only significantly higher, but are also lower in surface potential compared to a subphase of pure water. Interestingly, this is consistent with zeta potential measurements reported by Wettig et al. (2007), who observed a drop in the potential of analogous

Table 4.1: Image analysis results for height and surface potential differences between domains in lipid-gemini surfactant monolayers containing DOPE and DNA with gemini surfactants as indicated, corresponding to the results shown in Figs. 4.4 and 4.7, all at a surface pressure of $\pi = 35\,\mathrm{mN/m}$. The cross section method was used to calculate these results for the height and surface potential of the domains relative to the background. See the text for further details. Margins of error were calculated at a 95% confidence level.

Gemini Surfactant	Subphase	Δh / (nm)	ΔV / (mV)
16-3-16	H_2O	2.10 ±0.06	-20.8 ±1.0
16-7-16	H_2O	1.60 ±0.11	-14.5 ±1.0
16-7NH-16	H_2O	1.70 ±0.08	-13.1 ±0.8
16-7NH-16	pH= 4	2.20 ±0.13	-10.3 ±0.9

12-7NH-12-DOPE-DNA complexes at lower pH.

4.4 Conclusions

We have presented in this chapter a series of monolayer experiments exploring the effects of gemini surfactant spacer groups, the addition of DOPE helper lipid, pH, and monolayer pressure. Our results are broadly consistent with previous studies on gemini surfactant binding to DNA (e.g. Chen et al., 2002, 2005, 2012), although this is the first study of its kind to explore at the nanoscale the properties of such monolayers with DOPE for the purposes of connecting observations with gene therapy. Other studies, like those referenced above and for instance Dai et al. (2013) and Luque-Caballero et al. (2014) have also shown very clearly the affinity of DNA for monolayer binding (particularly cationic monolayers).

Clearly, the addition of DOPE moderates the morphology of the complexes formed from DNA binding, as we demonstrated in § 4.3.1. This signifies the importance of the fraction of each transfection component, particularly given the observation that the ratio of helper lipid to gemini surfactant affects transfection efficiency (e.g. Wang et al., 2007). Further, it is evident that acidity plays a large role in the binding behaviour of DNA to these monolayers, and therefore such aspects must be considered in the interpretation of any gene therapy experiments. For example, one must be mindful of preparing transfection

complexes in one solution environment for morphological study, and then testing the transfection efficiency of such complexes in another solution (e.g., see Radwan Almofti et al., 2003).

A noteworthy result is the appearance of nanoparticles in our monolayers, which may contribute to the condensing effect observed in the pressure-area isotherms. Nano-sized particles of the gene transfection complexes may spontaneously form at certain pressures without pre-forming structures such as DOPE vesicles. It appears, therefore, that DOPE (unlike, say, DOPC) facilitates the formation of spherical aggregates with gemini surfactant and DNA. These results lend further credence to the assertion that studying monolayers in this fashion can yield meaningful conclusions for comparison to purely nanoparticle studies, such as that which is presented in the next chapter.

While the parameter space we have explored in this chapter is relatively small, it does shed considerable light on the aspects which have great impact on the nanoscale properties of the components important for gemini surfactant gene therapy. Certainly, it would be desirable in future to expand upon this study to include a broader spectrum of parameters such as various concentrations of DNA, a broader range of spacer and tail lengths for gemini surfactants, additional buffer solutions at a number of pH values, monolayers deposited at pressures spanning the length of the pressure-area curves, and many ratios of DOPE:gemini surfactant. We cannot hope to explore all of these in one study, but we have attempted here to pick out some of the parameters of top importance so that we may point to aspects which may yield greater insight into, and plans for, future research.

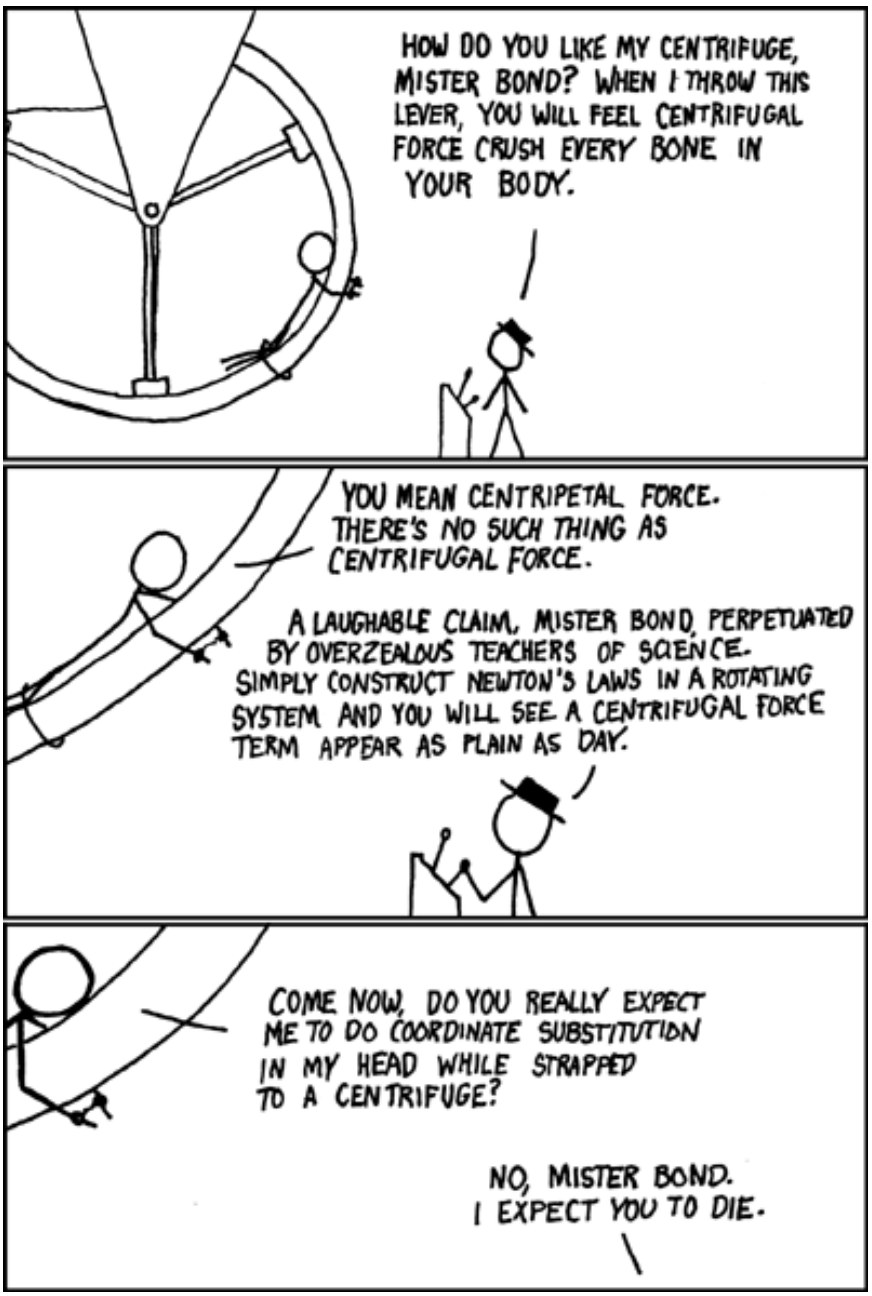

Reprinted from xkcd.com.

And as imagination bodies forth
The forms of things unknown, the poet's pen
Turns them to shapes and gives to airy nothing
A local habitation and a name.

William Shakespeare

Chapter 5

'Direct' Imaging of Gemini Surfactant Transfection Complexes

5.1 Introduction

In view of the monolayer studies presented in the preceding chapters, it is now time to explore the gene transfection complexes themselves. As we will see, analyses of the transfection nanoparticles by direct imaging is challenging for a number of reasons, but, in the end, it is these systems which are actually the therapeutic agents of interest. The nanoparticles are what the cells take up, and we would like to understand more fully the mechanism of this process. Characterisation of these nanoparticles is often done in terms of size or zeta potential, for example (e.g. Donkuru et al., 2010), and analyses by AFM vary from study to study. In an attempt to bring some consistency to this area of research, the present chapter aims to demonstrate how we can relate our previous monolayer studies to nanoparticles, and presents a methodical approach to AFM and KPFM characterisation of these complexes. As we have seen, monolayer methods can be applied in a very consistent and controlled manner, and allow a more detailed study of the interactions of each of the components of the complexes. Our goal is to understand how these effects manifest themselves when these systems are in nanoparticle form.

Characterisation of surfactant gene delivery systems has been done by way of some

direct imaging, most commonly by electron microscopy (e.g. Bajaj et al., 2007) and AFM (e.g. Kawaura et al., 1998; Sakurai et al., 2000; Nakanishi & Noguchi, 2001; Radwan Almofti et al., 2003; Wang et al., 2013). These studies have shown that complexes can, for instance, be prepared in solution and then deposited onto some flat substrate to be imaged by AFM (which is further explored here). Information can be gleaned from comparisons of the physical properties of the complexes on the nanoscale and their transfection efficiency. For example, Kawaura et al. (1998) found that complexes prepared with cholesterol as a helper lipid were most efficient at a size of 400 nm - 1400 nm; this size can be controlled to some extent with the ratio of the various components in the complex or by the specifications of the derivatives, for instance by using different kinds of helper lipds or surfactants (Bajaj et al., 2007). A higher proportion of cationic surfactant can lead to tighter compaction of the DNA, which may make it more difficult for release within the cell (Sakurai et al., 2000). Therefore, it is important to find an optimal ratio of DNA to surfactant, and any helper lipid. The existence of an optimal ratio of surfactant:lipid might therefore explain the need for a helper lipid to modulate the charge density of the monolayer which envelops and compacts the genetic material. This is likely to be a precarious balance between protecting the DNA and allowing it to be released at the right moment.

Gemini surfactants have been gathering interest as potential gene delivery vehicles for a few important reasons. Their ability to interact, compact and complex with DNA has been demonstrated in several studies (e.g. Wang et al., 2007; Wettig et al., 2008; Zhao et al., 2007; Wettig et al., 2008; Zhao et al., 2008; Donkuru et al., 2010; He et al., 2011; Wang et al., 2013). More significantly, not only have gemini surfactants been found to promote conformations that are favourable for transfection (e.g. Badea et al., 2007; Wettig et al., 2008; Yang et al., 2010), but they do so at lower concentration. While toxicity remains a concern for surfactant gene delivery, gemini surfactants have critical micelle concentrations that are one to two orders of magnitude lower than monomeric surfactants, and are thus able to compact DNA with less material; this serves to help mitigate potential toxicity effects and gives further motivation for their continued study (Pedroso de Lima et al., 2001; Wettig et al., 2008).

We present in this chapter a study of gemini surfactant gene transfection complexes with AFM and KPFM. Using the three gemini surfactants from our previous chapter, we

construct nanoparticles and deposit them directly onto mica for imaging and characterisation. These particles (complexes) can then be compared with other studies' results. Furthermore, we can examine the electrical properties of the nanoparticles. To-date, no applications of KPFM to these systems has been reported as far as we are aware, making this study the first of its kind.

5.2 Methods

5.2.1 Preparation of Transfection Complexes

Transfection complexes were prepared in solution and deposited onto freshly cleaved mica slides following closely the methodology presented in Wettig et al. (2007) and Wang et al. (2013). The transfection complexes are comprised of three parts: the gemini surfactant, a helper lipid, and DNA. These three components were prepared separately and then combined as follows.

To prepare the gemini surfactant solution, an appropriate amount of stock chloroform solution (1 mg/mL) of each gemini surfactant was placed in a small vial and the solvent allowed to evaporate over a gentle stream of nitrogen gas. The (precisely measured) dried surfactant was resuspended in nanopure (Milli-Q) water. The solution was then filtered through a 0.2 μm disc filter with a syringe.

Lipid vesicles of DOPE were prepared by first drying a film of the lipid in a glass vial by dissolving an appropriate amount of stock (25 mg/mL) chloroform-DOPE solution into 1 mL of HPLC grade ethanol, and evaporating over nitrogen gas. The film was resuspended in nanopure water and allowed to 'swell' for about one hour in a fridge. The solution was then subjected to sequential stirring (with a magnetic stir bar) and sonication until the solution was rendered clear. Often, this was achieved over a timescale of approximately 2 hours, with 15-minute intervals of stirring and sonication. As a final step, the vesicles were filtered through 0.45 μm disc filters.

Our DNA solution was prepared in the usual way, by first dissolving an appropriate amount of the sodium salt of salmon sperm DNA into nanopure water. All three solutions

were combined in the appropriate proportions to obtain a 3:2 molar ratio of DOPE:GS and a 5:1 charge ratio of GS:DNA. After 30 minutes of incubation at room temperature, small quantities (∼20-40 μL) of the transfection complex solution was placed onto freshly cleaved mica slides and allowed to adhere for 15 minutes. The solvent was then wicked away with a Kimwipe and the sample dried overnight in a desiccator. For more detail on this procedure, refer to § A.2.

5.2.2 Imaging

Imaging was performed on an AIST-NT Smart SPM using MikroMasch NSC-15-Pt cantilevers of resonant frequency approximately 325 kHz. Details of the methodology are largely described in § 1.3, and identical to § 3.2.2.

5.3 Results

In contrast to the previous chapter, where we studied monolayers of the components of transfection complexes, in this study we are directly observing the complexes themselves. While there may be implications of examining these structures after they have dried, and further imaging them in air, we would expect to first order that these effects would be fairly constant for each type of complex we observe, and therefore we may still make relative comparisons. We begin by showing an AFM image of DNA alone (without any gemini surfactant or lipid present) in Fig. 5.1. In a similar way as that which was observed in the DNA-GS-lipid monolayers, we see a web-like network of fibrils approximately 2 nm high. However, with DNA alone and deposited in this fashion, the network is much more complex, tangled and interwoven. As we will see in the following data, the addition of gemini surfactant and DOPE leads to a condensation effect which compacts the DNA into spherical aggregates.

As a summary of detail images of the transfection complexes, we show close-up AFM and KPFM results in Fig. 5.2, followed by individual survey images including magnitude and phase in Figs. 5.3, 5.4 and 5.5, which are of a 10x10 μm field of view. The complexes appear to be dispersed on the mica, in some cases in patches (16-3-16). There is a general

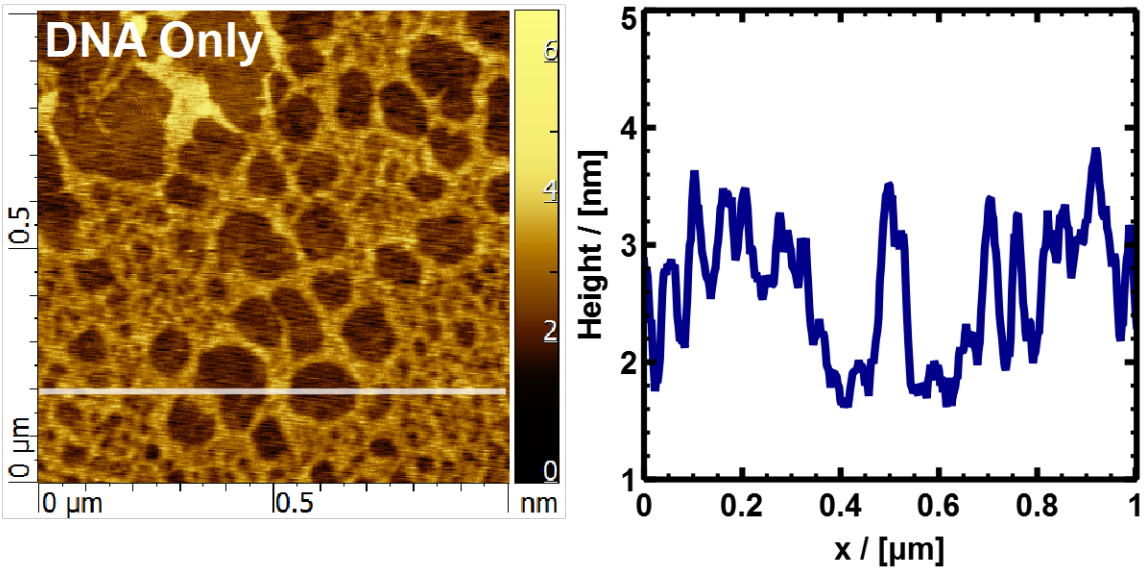

Figure 5.1: DNA deposited directly onto mica and imaged with our AFM. The cross section is taken from the white line at $y = 0.2\,\mu$m.

trend of small particles for 16-3-16, then larger ones for 16-7-16, with the largest being 16-7NH-16. This is also evident from the cross section data. KPFM results indicate that, with the exception of 16-3-16, the gemini surfactants exhibit a net positive surface potential relative to the background, but that the particles are surrounded by a layer of negative surface potential material. The 16-7-16 results are more difficult to interpret, as there appears to be a network of negatively charged DNA permeating the deposits with a few nanoparticles present which have a positive surface potential. Complexes of 16-7NH-16 are most remarkable, with many nanoparticles peppered throughout the deposits, all showing a relatively positive KPFM signal. We will discuss these features, and their potential implications, in the next section.

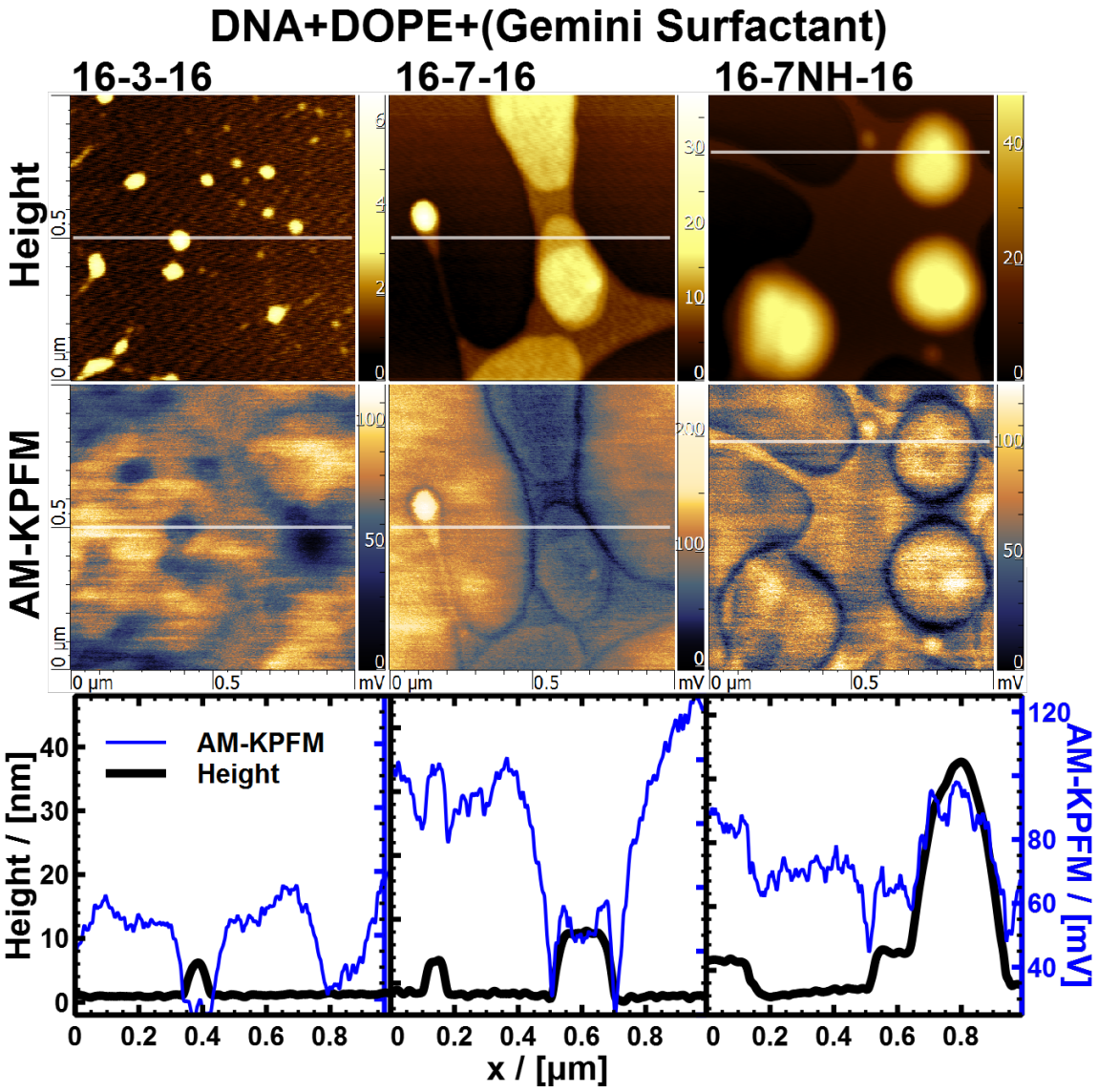

Figure 5.2: Small-scale (1 μm x 1 μm) AFM and KPFM images of gene transfection complexes, with cross sections. The thin blue line shows the AM-KPFM signal, and the thick black line shows the height in the plots; all scales are identical.

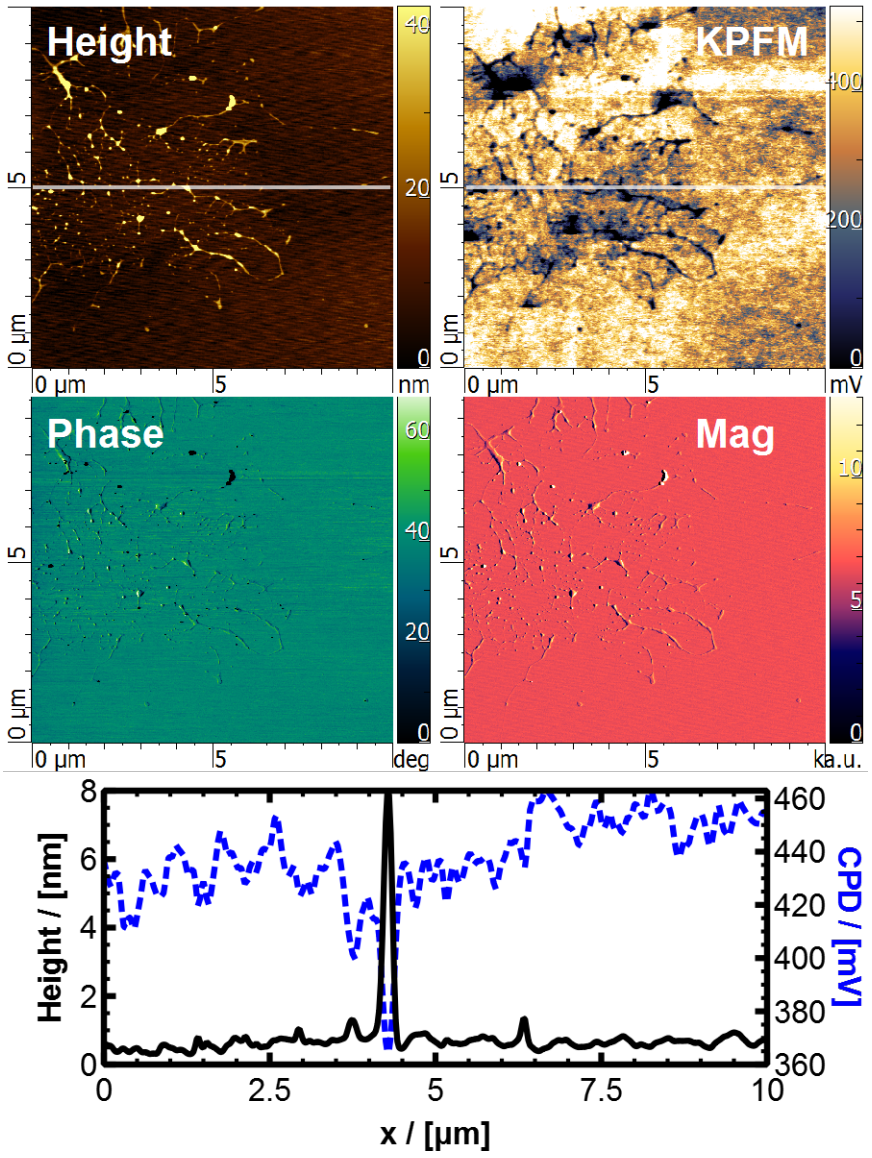

Figure 5.3: Large-scale (10 μm x 10 μm) AFM and KPFM images of gene transfection complexes of DNA, DOPE and gemini surfactant 16-3-16. The cross section was taken at $y = 5\,\mu$m.

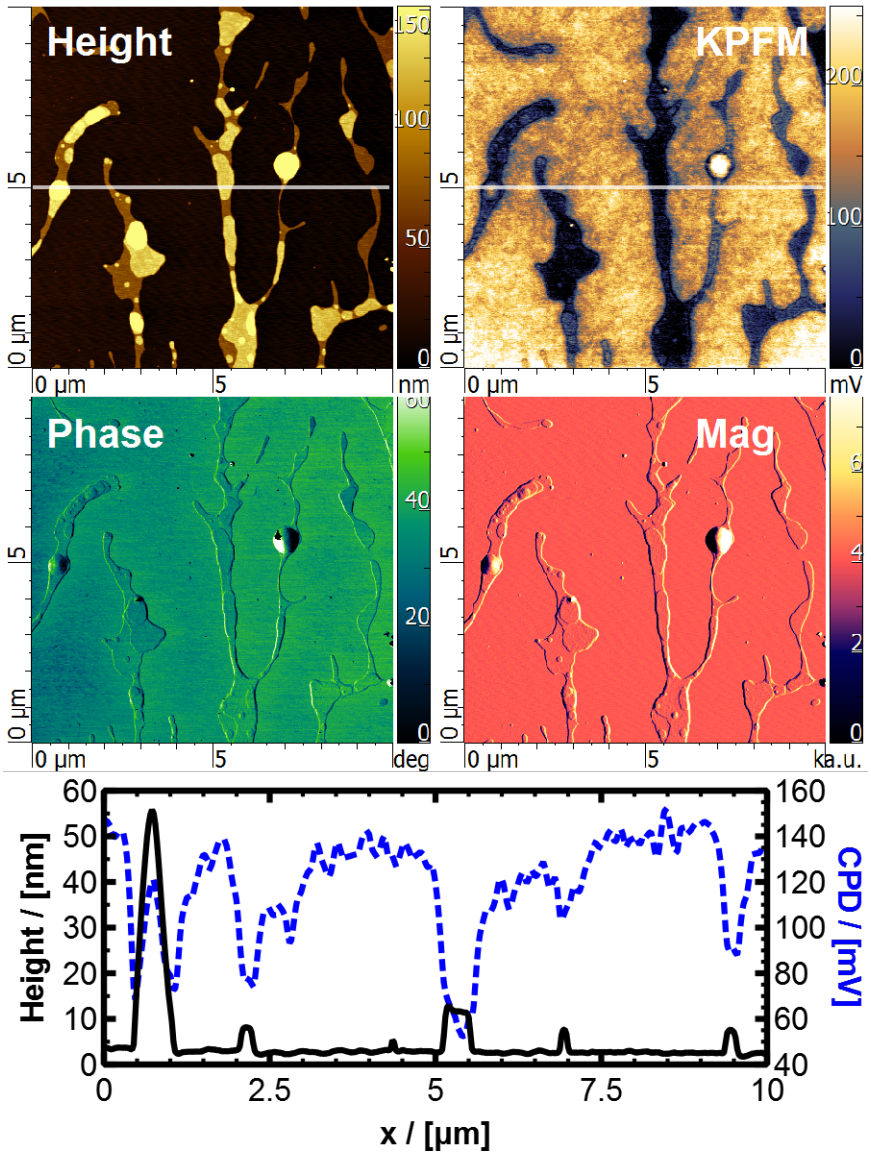

Figure 5.4: Large-scale (10 μm x 10 μm) AFM and KPFM images of gene transfection complexes of DNA, DOPE and gemini surfactant 16-7-16. The cross section was taken at $y = 5\,\mu$m.

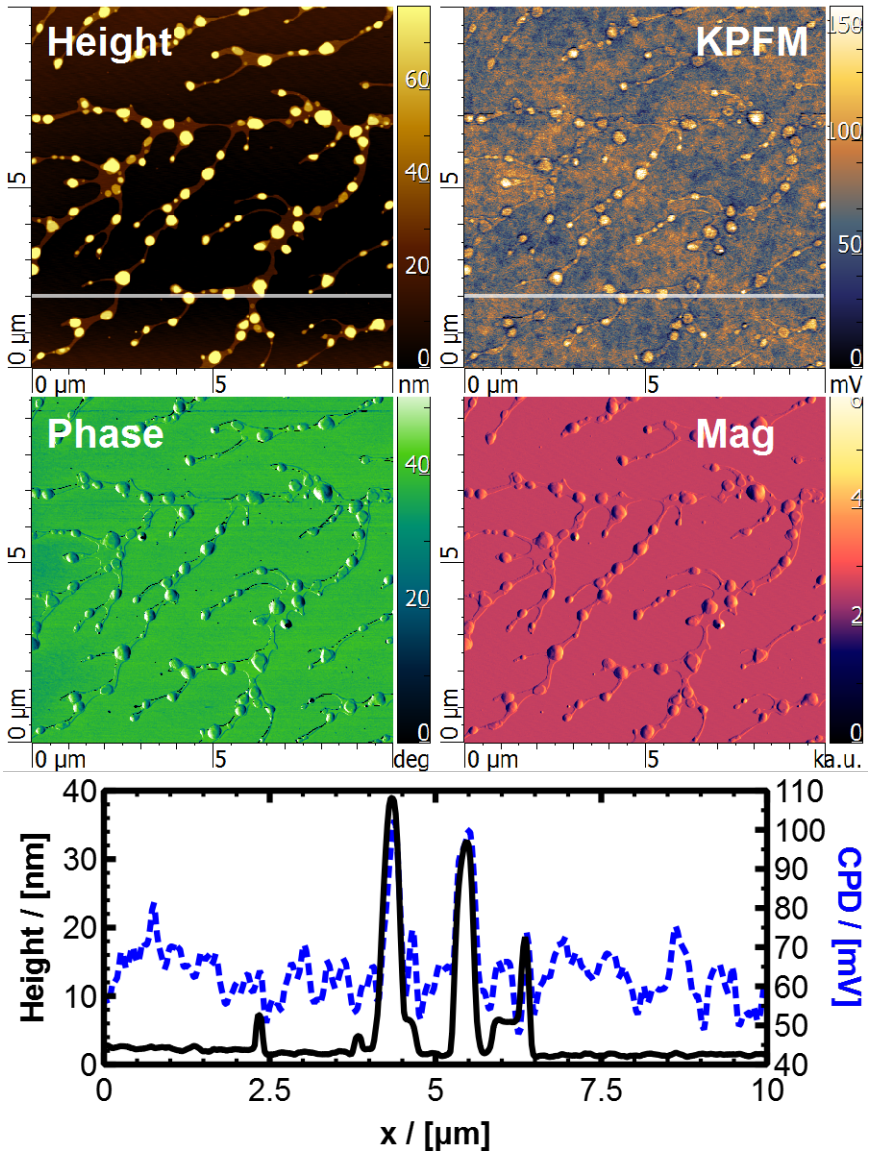

Figure 5.5: Large-scale (10 μm x 10 μm) AFM and KPFM images of gene transfection complexes of DNA, DOPE and gemini surfactant 16-7NH-16. The cross section was taken at $y = 2\,\mu$m.

5.4 Discussion

5.4.1 Quantitative Analysis of Nanoparticle Size Distributions

Analyses of the sizes of transfection complexes by AFM has largely been semi-quantitative to date (e.g. Donkuru et al., 2010), with descriptions limited to general observations which lead to 'classifications' of particle sizes. Indeed, the distribution of sizes of transfection complexes appears to be rather broad (e.g. Kawaura et al., 1998; Sakurai et al., 2000; Donkuru et al., 2010; Wang et al., 2013). A simple method by which particle sizes may be determined is from the use of dynamic light scattering (Berne & Pecora, 2000; Brar & Verma, 2011). Particles in solution are examined, giving rise to a distribution of sizes assuming they are spherical and fairly uniform in diameter. This technique is straightforward to implement and has been used to characterize the size of transfection particles(e.g. Wang & Wettig, 2011). However, this technique does have some disadvantages; for example, it is susceptible to uncertainties and bias introduced by contaminants that are difficult to detect and quantify, and is unreliable if there are multiple sizes of particles present in the solution (Bootz et al., 2004). The latter issue is of particular importance in the present case, since the transfection complexes are prepared by mixing three different components. Concerns arise, therefore, if these components are not completely condensed into nanoparticles.

In view of the above, we propose to use AFM image analysis in a more detailed quantitative manner to characterize transfection complexes, which also allows for meaningful comparisons between experiments. This method is direct, in that we can directly measure the sizes and morphologies of the nanoparticles and determine their distributions, and compare these distributions with other experiments (e.g., different gemini surfactant complexes). Although there is the notable issue of the effects of drying the complexes and convolution with the scanning probe tip, this method is not sensitive to the underlying particle distribution or any assumptions of conversion from light diffusion to particle size. In addition, it has the advantage over electron microscopy techniques in that it avoids artefacts or uncertainties introduced by sample preparation and fixation techniques (for instance, see Bootz et al., 2004). Fortunately, our nanoparticles are fairly widely dispersed, so such image analysis is more straightforward than for highly complex samples (Klapetek et al., 2011).

The technique begins with a calibrated AFM height image of the nanoparticles of interest. Using the program GWYDDION, one may select the individual nanoparticles by creating a mask via a thresholding approach. Since the nanoparticles are almost always much higher than any background materials, this typically gives excellent results. Properties of the individual nanoparticles can be extracted, such as their surface area, maximum, mean or median height within the particle boundaries, or their effective radii (the radius of a disc containing the same area as the particle). Any particles that are either extremely small (e.g., a pixel) or touching the edge of the image are filtered out.

Distributions of nanoparticle areas are shown, for each of our gemini surfactant complexes, in Fig. 5.6, plotted against their maximum height. One would expect, to first order, that particles with a larger area would be higher, and we do see this trend. We also see, from a quantitative view, that the 16-3-16 surfactant complexes have smaller areas than the others, and that the 16-7-16 surfactants are also small, but have somewhat larger maximum heights than 16-7NH-16. By far, the 16-7NH-16 surfactant complexes are more broadly distributed in size, and go up to areas of $0.1\,\mu\mathrm{m}^2$. In the top panel of this same figure we show normalised histograms of the area distributions for the complexes, which indicate that the 16-7NH-16 surfactant complexes have a higher fraction of their particles at larger areas than the other surfactants. The complexes from 16-3-16 are restricted to very small areas.

Next, we show in Fig. 5.7 the distributions of particle effective radii, plotted again against the particle maximum height, with histograms in the top panel. Once again we see that the 16-7NH-16 surfactant complexes are the largest, followed by 16-7-16, with 16-3-16 the smallest. We do note the presence of two pools of particles for the 16-3-16 surfactant complexes in terms of their maximum heights, where there are some which are clustered around 3.8 nm and others around 8 nm. No such separation is observed for the other surfactants. It's possible that these are simply the result of some particles 'sitting' on top of a layer of other uncomplexed molecules. In any case, our bottom-line analysis suggests that these transfection complexes are distributed over a range of diameters of a few tens to 200 nm for the 16-3-16 (peak near 50 nm) and 16-7-16 (peak near 100 nm) gemini surfactants, and over a larger range of diameters for 16-7NH-16 (a few tens to about 400 nm, peaking around 200 nm).

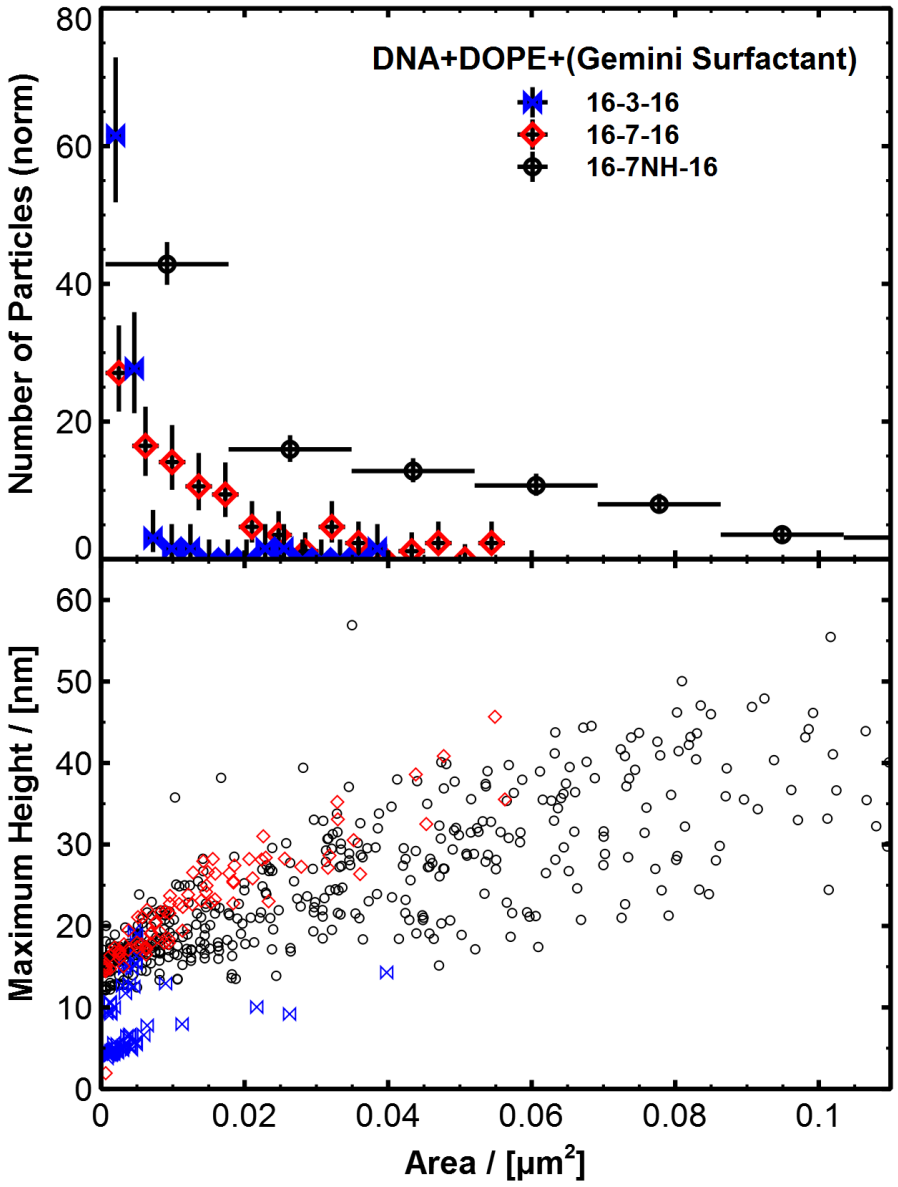

Figure 5.6: Distributions of areas for the gene transfection complexes as determined from an analysis of the AFM height images. Top panel: normalised histograms binning the number of nanoparticles found in the distributions in the bottom panel. Error bars were computed following Gehrels (1986). Bottom panel: plot of the maximum height of each nanoparticle versus particle area.

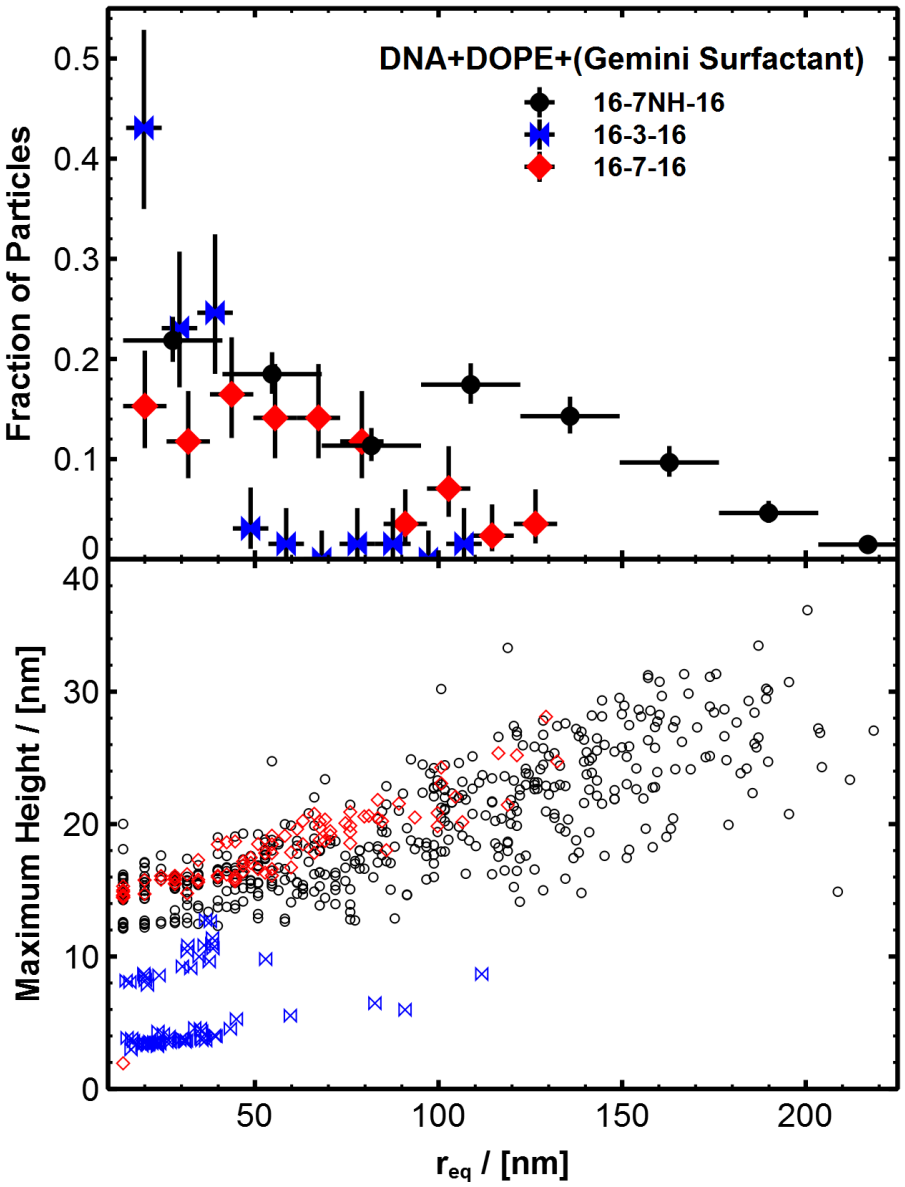

Figure 5.7: Distributions of equivalent radii for the gene transfection complexes as determined from an analysis of the AFM height images. Top panel: normalised histograms binning the number of nanoparticles found in the distributions in the bottom panel. Error bars were computed following Gehrels (1986). Bottom panel: plot of the average height of each nanoparticle versus particle equivalent radii. See the text for definitions.

5.4.2 Surface Potentials

An analysis of the surface potentials of our nanoparticles requires an analogous approach to what was done previously; namely, cross section measurements. We present these results in Table 5.1, where we show the surface potentials of the three types of nanoparticles computed from an averaging of results from many separate images. The confidence intervals on these results are somewhat larger than our monolayer calculations, owing to the larger variability in the properties of the particles. We find no difference between the 16-7-16 and 16-7NH-16 surface potentials. However, we do observe the curious result of a negative surface potential for the 16-3-16 particles. It is possible that these systems are achieving a conformation which is similar to a monolayer form (which has shown to give rise to a negative potential in the DNA-laden domains), or that the complexes are mixing such that the charge ratio (+/-) has become less than one, a situation which has been shown to produce a negative zeta potential (Wang et al., 2007). In any case, more extensive research on this system is needed to explore these issues. In addition, we note that while we do observe strong KPFM signals for these nanoparticles, direct comparisons with values obtained from our monolayers should not be made given the differences in the deposition procedures.

Table 5.1: Image analysis results for surface potential differences between gemini surfactant-DOPE-DNA nanoparticles and their background, using the cross section method. Margins of error were calculated at a 95% confidence level.

Gemini Surfactant	ΔV / (mV)
16-3-16	-35.2 $\pm$4.2
16-7-16	49.9 $\pm$2.1
16-7NH-16	51.5 $\pm$2.6

5.4.3 Implications of Nanoparticle Structure

The size range of our nanoparticles is broadly consistent with the general range of nanoparticle sizes on the order of a hundred nm (Donkuru et al., 2010), although our results for 16-3-16, suggesting they are of size less than 100 nm is somewhat inconsistent with the

light scattering results of Wang et al. (2013), which measured those complexes to be in the realm of 460 nm. However, that study did use a DOPE:GS ratio slightly larger than the present work. In any case, it is not surprising that we see a large range of nanoparticle sizes since we are using randomly sized fragments of DNA, and not strands of fixed size (plasmids). However, we can expect our results to be reliable on a relative basis so that we may compare gemini surfactants with each other.

All three of our gemini surfactants exhibit the characteristic 'beads on a string' morphology described in Sternberg et al. (1994), with diameters consistent with that study (a few hundred nm). The 'string' components in our images do suggest, as Pedroso de Lima et al. (2001) does, that the nanoparticles could be 'bathed' in sheets or tubules of lipid-gemini surfactant mixtures that lie in between the nanoparticles themselves. Such a model would not be inconsistent with our results.

5.5 Conclusions

We have demonstrated in this chapter how nanoparticle analyses might be done with AFM for gene transfection complexes using simple and freely-available software. Nanoparticles that were observed in our monolayer studies at higher surface pressure appear to manifest similarly to those we see in the direct depositions of the present chapter. Given the size distributions we found, studies in which gene transfection complexes are constructed with randomly sheared DNA fragments should take into account this variability. It has been suggested that transfection efficiency depends very much on the nanoparticle size, rather than the type of lipid or surfactant (Pedroso de Lima et al., 2001), and so perhaps an analysis such as that which we have presented in this chapter may be used in future research to draw correlations between the size *distributions* and transfection efficiency.

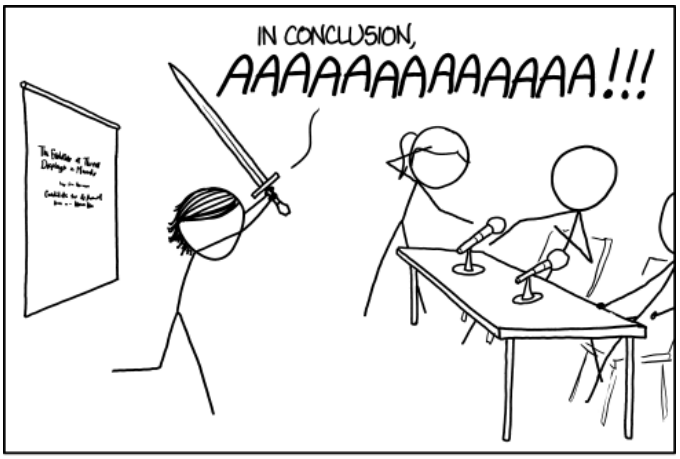

THE BEST THESIS DEFENSE IS A GOOD THESIS OFFENSE.

Reprinted from xkcd.com.

I have approximate answers and possible beliefs in different degrees of certainty about different things, but I'm not absolutely sure of anything, and of many things I don't know anything about, but I don't have to know an answer. I don't feel frightened by not knowing things, by being lost in the mysterious universe without having any purpose which is the way it really is as far as I can tell.

Richard Feynman

Chapter 6

Conclusions and Future Prospects

Recent advances in scanning probe microscopy technology have made the research presented in this thesis possible. We have presented a novel study of monolayers and gemini surfactant systems using state-of-the-art atomic force microscopy techniques which have led to new approaches for studies in gene therapy from a fundamental physics point of view. In particular, this thesis has discussed the following broad issues:

- Common cell membrane lipids have been studied for decades on the macro-scale both in terms of their dynamics (e.g., surface pressure) and electrostatics (overall surface potential). More recently, with the advent of AFM technology such monolayers have been studied *topographically* on the nanoscale, but *not* electrostatically before the present work.

- In their use as gene delivery vehicles, gemini surfactants must interact with cell membrane lipids. The nature of this interaction is not well understood, and this thesis presents some insight to their behaviour on the nanoscale when mixed with some common cell membrane lipids. In addition, the nanoscale electrostatic properties of such monolayers were explored.

- The binding behaviour of DNA to gemini surfactant is of considerable interest, given that this is the key interaction within gene delivery systems. Studies of this binding have been limited to macro-scale properties of monolayer dynamics and simple

AFM studies of the complexation process. In the present work we examined the electrostatic nature of these interactions but observing with KPFM these systems in monolayer and nanoparticle form.

- Physical characterisations of gene transfection complexes can benefit from the use of detailed quantitative measurements of the *distributions* of the sizes of such transfection complexes.

6.1 Nanoscale Electrical Properties of Lipid Monolayers

We have presented in Chapter 2 a study of lipid monolayers at the nanoscale using AFM and KPFM to probe not only topography, but also electrostatics. By constructing monolayers of different lipids we were able to show how morphological changes result from changes to the composition not only by varying the ratio of the lipids, but by adding gemini surfactant. The gemini surfactant was found to interact very strongly with the gel-phase lipid DPPC present in the monolayer, and also appeared to increase the height of the domain structures. In terms of electrostatics, the gemini surfactant, being positively charged, induced a stronger positive surface potential which we detected with KPFM. Thus, we were able to show how AFM can be used to observe molecular interactions (e.g., that the surfactant 'preferred' one lipid over another), and to trace these interactions by following the electrostatic signal. By combining our data with that which has been published from macro-scale observations of mono-lipid monolayers' surface potentials, we were able to compare our calculated difference in surface potential between the DOPC and DPPC domains with literature values to confirm a trend of greater differences of surface potential between the domains when the monolayer pressure is increased.

6.2 Morphology and Electrostatics of DNA-Surfactant Binding

Electrostatics has been implicated as the primary driver of the formation of gene transfection complexes, and yet most of the research reported to date has been on macro-scale

electric potentials, with the only features probed on the nanoscale being topographical. In this work, we have not only shown the effects of DNA binding on monolayer morphologies at the nanoscale, but have demonstrated the importance of probing the electrostatic potential at the same resolution. We revealed that maps of the electrical surface potential of monolayers containing cationic surfactant do not correlate entirely with their topographies, and thus KPFM imaging can give us information inaccessible by AFM alone. DNA binding to the gemini surfactant takes place within the gel-phase domains of lipid monolayers where the surfactant is present, and likely remains coated in residual surfactant molecules that are revealed in our KPFM images by a strongly positive signal. Given that the DNA is present in solution and may freely bind to the monolayer, it appears to prefer to bind in such a way that there is excess surfactant (giving rise to the positive KPFM signal); therefore, this may help to explain the greater transfection efficiency at relatively large $(+/-)$ charge ratios of $\sim 5-10$.

Extending this to monolayers containing gemini surfactant and the commonly used helper lipid DOPE, we showed that DNA strongly binds with these monolayers as well. The KPFM signal surrounding the DNA in this case is only weakly positive, but this is likely due to the fact that there is only one lipid present along with the gemini surfactant. Pressure-area isotherms of these monolayers analogous to gene transfection complexes showed the importance of DOPE in facilitating the condensation of DNA along with the surfactant. Without DOPE, these monolayers of DNA with gemini surfactant were much expanded, and with the addition of DOPE showed far smaller areas per molecule. Helper lipids give rise to far greater transfection efficiencies than surfactant and DNA alone, and the results in this thesis may help to explain why this is so.

6.3 Gene Transfection Nanoparticles Analysed by AFM and KPFM

Following from our monolayer studies on the materials composing gene transfection complexes, we investigated the morphologies and electrical properties of the complexes themselves with AFM and KPFM. We found that the nanoparticles that form have sizes dis-

tributed broadly from a few tens of nm to several hundred, and that it is difficult to pinpoint any narrow range of sizes at least for the form of DNA we use here. However, we were able to distinguish the particles based upon the spacer group of the gemini surfactants, and found that larger spacer groups form larger nanoparticles in the region of $\sim 200\,\text{nm}$, whereas the shorter spacers formed nanoparticles of a few tens of nm in diameter. This was consistent with the pressure-area isotherms, which showed that the shorter spacer group produced more condensed monolayers.

Importantly, we demonstrated the use of a simple particle analysis broadly employed in AFM but applied to these gene transfection systems. With this technique, many measurements can be made to produce quantitatively significant results that could then be compared with transfection efficiency data to drive future research.

6.4 Future Work

While this thesis is a compilation of years of research into the nanoscale structure and physical properties of monolayers and gene transfection nanoparticles, there is a great deal of parameter space that has been left relatively unexplored. Such a comprehensive study of all the possible experimental conditions that could lead to significant differences in the properties of the systems we have explored would take far too much time for even a several PhD theses, but here is an attempt to lay out some commentary on where future research in this respect might go.

In terms of the parameters themselves, which were explored to some degree in the present work, we have the following.

- Gemini surfactant type: spacer length, tail length.
- Gemini surfactant spacer or tail functional groups.
- Lipid type: e.g., DOPE, DOPC, DPPC and others.
- Ratio of lipid:GS.

- Ratio of GS:DNA, or concentration of DNA.
- DNA size or type: e.g., base pair length of strands, or plasmids (linear or circular).
- Solution pH: e.g., buffers at pH 4, 7, 9, or nanopure water.
- Monolayer pressure.

Clearly, we have had to narrow down considerably the choices presented in the above list. Each one of these parameters can answer different research questions, depending on the individual experiment or variable of interest. For example, the protonatable spacer group of 16-7NH-16 lends itself to an examination of the effects of pH. Data on transfection efficiencies of a series of gemini surfactants of progressively larger spacer groups or tail lengths could be correlated with nanoparticle size or monolayer pressure trends. It appears from our present work that the largest effects on our systems are the type of surfactant, the amount of lipid, and solution pH, and these may be useful to observe trends. While we have been using randomly sized DNA fragments in this thesis, a study using plasmids or single length DNA would be informative to determine which of the gemini surfactants may be appropriate or efficient for gene transfection, perhaps using their ability to compact DNA as a metric for this purpose. However, manufacturing DNA strands of a narrow range of sizes in the quantities required for these kinds of studies is extremely difficult. Plasmids are another option, but those which are therapeutically important are also expensive to replicate.

In addition to a broadening of parameter space, other types of instruments could be employed to examine different properties of the monolayers or particles we have studied. For example, individual bonds within the molecules of the monolayer may be probed using polarisation-modulated infrared reflection-absorption spectroscopy (PM-IRRAS); this technique has already been widely employed in general monolayer and interfacial studies (Blaudez et al., 1993; Dicko et al., 1998; Estrela-Lopis et al., 2001; Goto & Caseli, 2013), and there is huge potential for research on gemini surfactants and their interaction with DNA. In this case, bond stretching can be observed in real time as DNA binds with the monolayers on a Langmuir film balance.

While we have taken advantage of serious improvements in KPFM technology in order to conduct this research, one limitation that prevents us from examining the electrostatic properties of these biological samples is that our samples must be set in air, and not liquid. Liquid imaging for AFM has been around for quite some time, although it is a trickier technique. However, the unique requirements of KPFM prevent its operation in liquid due to spurious electromagnetic fields if any electrolytes are present in solution. While recent developments have employed KPFM in nonpolar solvents (Domanski et al., 2012), true KPFM in a liquid environment is still a long way away, although there is progress being made in this endeavour along with other advances in KPFM (Collins et al., 2015a,b).

In view of the above, it is clear that there are serious advantages to be had with multi- and interdisciplinary studies such as that which we have presented in this thesis. The combination of physics and nanotechnology with biology and pharmaceutics in the study of fundamental aspects of gene therapy can have real impact on clinical research, and signals the importance of continued work in these areas for the benefit of future healthcare.

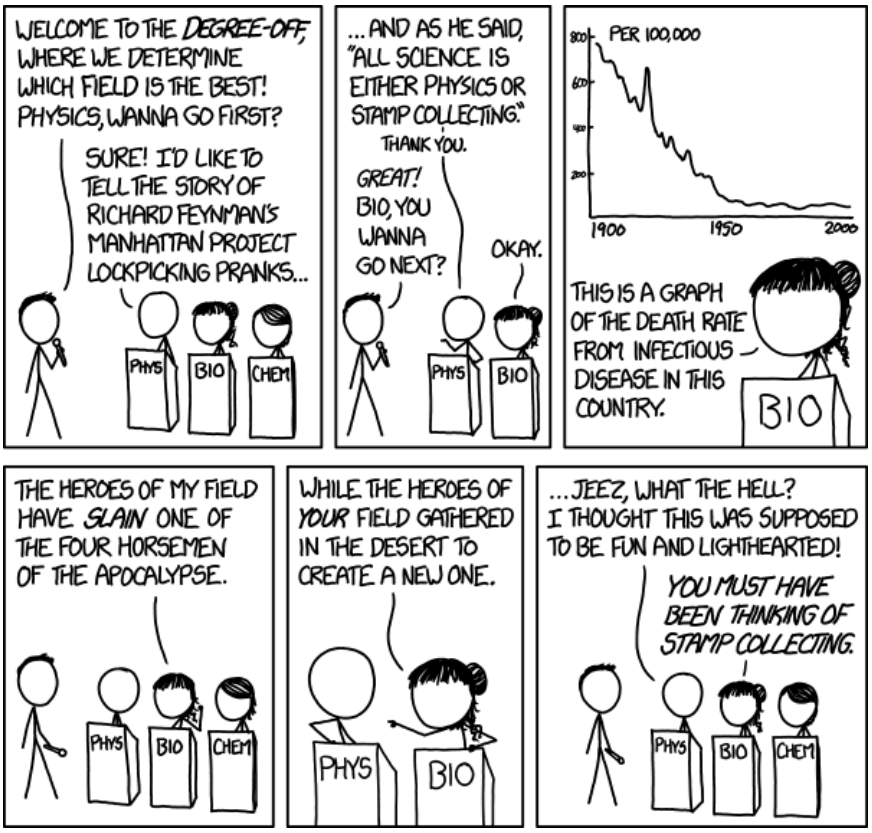

Reprinted from xkcd.com.

Bibliography

Ahmad, A., Evans, H. M., Ewert, K., George, C. X., Samuel, C. E., & Safinya, C. R. 2005, New multivalent cationic lipids reveal bell curve for transfection efficiency versus membrane charge density: lipid–DNA complexes for gene delivery, The journal of gene medicine, 7, 739

Akbar, J., Tavakoli, N., Gerrard Marangoni, D., & Wettig, S. D. 2012, Mixed aggregate formation in gemini surfactant/1, 2-dialkyl-sn-glycero-3-phosphoethanolamine systems, Journal of colloid and interface science, 377, 237

Alberts, B., Johnson, A., Lewis, J., Raff, M., Roberts, K., & Walter, P. 2002, Molecular Biology of the Cell, 4th edition (New York: Garland Science)

Allison, D. P., Mortensen, N. P., Sullivan, C. J., & Doktycz, M. J. 2010, Atomic force microscopy of biological samples, Wiley Interdisciplinary Reviews-Nanomedicine and Nanobiotechnology, 2, 618

Ashcroft, N. & Mermin, N. 1976, Solid State Physics (Philadelphia: Saunders College)

Badea, I., Wettig, S., Verrall, R., & Foldvari, M. 2007, Topical non-invasive gene delivery using gemini nanoparticles in interferon-γ-deficient mice, European journal of pharmaceutics and biopharmaceutics, 65, 414

Bajaj, A., Kondiah, P., & Bhattacharya, S. 2007, Design, synthesis, and in vitro gene

delivery efficacies of novel cholesterol-based gemini cationic lipids and their serum compatibility: a structure-activity investigation, Journal of medicinal chemistry, 50, 2432

Bakshi, M. S., Singh, K., & Singh, J. 2006, Characterization of mixed micelles of cationic twin tail surfactants with phospholipids using fluorescence spectroscopy, Journal of colloid and interface science, 297, 284

Barlow, D., Ma, G., Webster, J., Penfold, J., & Lawrence, M. 1997, Structure of the monolayer formed at an air-water interface by a novel nonionic (vesicle-forming) surfactant, Langmuir, 13, 3800

Barnes, G. & Gentle, I. 2011, Interfacial science: an introduction (Oxford University Press)

Beitinger, H., Vogel, V., Möbius, D., & Rahmann, H. 1989, Surface potentials and electric dipole moments of ganglioside and phospholipid monolayers: contribution of the polar headgroup at the water/lipid interface, Biochimica et Biophysica Acta (BBA)-Biomembranes, 984, 293

Bell, P. C., Bergsma, M., Dolbnya, I. P., Bras, W., Stuart, M. C., Rowan, A. E., Feiters, M. C., & Engberts, J. B. 2003, Transfection mediated by gemini surfactants: engineered escape from the endosomal compartment, Journal of the American Chemical Society, 125, 1551

Benvegnu, D. J. & McConnell, H. M. 1993, Surface dipole densities in lipid monolayers, The Journal of Physical Chemistry, 97, 6686

Berger, R., Butt, H.-J., Retschke, M. B., & Weber, S. A. 2009, Electrical modes in scanning probe microscopy, Macromolecular rapid communications, 30, 1167

Bergström, M. & Eriksson, J. C. 2000, A theoretical analysis of synergistic effects in mixed surfactant systems, Langmuir, 16, 7173

Berne, B. J. & Pecora, R. 2000, Dynamic light scattering: with applications to chemistry, biology, and physics (Courier Corporation)

Binks, B. 1991, Insoluble monolayers of weakly ionising low molar mass materials and their deposition to form Langmuir-Blodgett multilayers, Advances in Colloid and Interface Science, 34, 343

Blaudez, D., Buffeteau, T., Cornut, J., Desbat, B., Escafre, N., Pezolet, M., & Turlet, J. 1993, Polarization-modulated FT-IR spectroscopy of a spread monolayer at the air/water interface, Applied spectroscopy, 47, 869

Blodgett, K. B. 1935, Films built by depositing successive monomolecular layers on a solid surface, Journal of the American Chemical Society, 57, 1007

Bootz, A., Vogel, V., Schubert, D., & Kreuter, J. 2004, Comparison of scanning electron microscopy, dynamic light scattering and analytical ultracentrifugation for the sizing of poly (butyl cyanoacrylate) nanoparticles, European journal of pharmaceutics and biopharmaceutics, 57, 369

Brar, S. K. & Verma, M. 2011, Measurement of nanoparticles by light-scattering techniques, TrAC Trends in Analytical Chemistry, 30, 4

Brockman, H. 1994, Dipole potential of lipid membranes, Chemistry and physics of lipids, 73, 57

Camilleri, P., Kremer, A., Edwards, A. J., Jennings, K. H., Jenkins, O., Marshall, I., McGregor, C., Neville, W., Rice, S. Q., Smith, R. J., et al. 2000, A novel class of cationic gemini surfactants showing efficient in vitro gene transfection properties, Chemical Communications, 1253

Campen, R. K., Ngo, T. T., Sovago, M., Ruysschaert, J.-M., & Bonn, M. 2010, Molecular restructuring of water and lipids upon the interaction of DNA with lipid monolayers, Journal of the American Chemical Society, 132, 8037

Cárdenas, M., Nylander, T., Thomas, R., & Lindman, B. 2005, DNA compaction onto hydrophobic surfaces by different cationic surfactants, Langmuir, 21, 6495

Castano, S., Delord, B., Février, A., Lehn, J.-M., Lehn, P., & Desbat, B. 2008, Brewster angle microscopy and PMIRRAS study of DNA interactions with BGTC, a cationic lipid used for gene transfer, Langmuir, 24, 9598

Charrier, D. S., Kemerink, M., Smalbrugge, B. E., de Vries, T., & Janssen, R. A. 2008, Real versus measured surface potentials in scanning Kelvin probe microscopy, ACS nano, 2, 622

Chen, Q., Kang, X., Li, R., Du, X., Shang, Y., Liu, H., & Hu, Y. 2012, Structure of the complex monolayer of gemini surfactant and DNA at the air/water interface, Langmuir, 28, 3429

Chen, X., Wang, J., & Liu, M. 2005, Influence of surfactant molecular structure on two-dimensional surfactant–DNA complexes: Langmuir balance study, Journal of colloid and interface science, 287, 185

Chen, X., Wang, J., Shen, N., Luo, Y., Li, L., Liu, M., & Thomas, R. K. 2002, Gemini surfactant/DNA complex monolayers at the air-water interface: Effect of surfactant structure on the assembly, stability, and topography of monolayers, Langmuir, 18, 6222

Cheran, L.-E., McGovern, M. E., & Thompson, M. 2000, Surface immobilized biochemical macromolecules studied by scanning Kelvin microprobe, Faraday discussions, 116, 23

Chesnoy, S. & Huang, L. 2000, Structure and function of lipid-DNA complexes for gene delivery, Annual review of biophysics and biomolecular structure, 29, 27

Coban, O., Popov, J., Burger, M., Vobornik, D., & Johnston, L. J. 2007, Transition from nanodomains to microdomains induced by exposure of lipid monolayers to air, Biophysical journal, 92, 2842

Collins, L., Jesse, S., Kilpatrick, J. I., Tselev, A., Okatan, M. B., Kalinin, S. V., & Rodriguez, B. J. 2015a, Kelvin probe force microscopy in liquid using electrochemical force microscopy, Beilstein Journal of Nanotechnology, 6, 201

Collins, L., Okatan, M., Li, Q., Kravenchenko, I., Lavrik, N., Kalinin, S., Rodriguez, B., & Jesse, S. 2015b, Quantitative 3D-KPFM imaging with simultaneous electrostatic force and force gradient detection, Nanotechnology, 26, 175707

Cristofolini, L., Berzina, T., Erokhina, S., Konovalov, O., & Erokhin, V. 2007, Structural study of the DNA dipalmitoylphosphatidylcholine complex at the air-water interface, Biomacromolecules, 8, 2270

Dabkowska, A., Barlow, D., Hughes, A., Campbell, R., Quinn, P., & Lawrence, M. 2012, The effect of neutral helper lipids on the structure of cationic lipid monolayers, Journal of The Royal Society Interface, 9, 548

Dabkowska, A. P., Barlow, D. J., Clifton, L. A., Hughes, A. V., Webster, J. R., Green, R. J., Quinn, P. J., & Lawrence, M. J. 2014, Calcium-mediated binding of DNA to 1, 2-distearoyl-sn-glycero-3-phosphocholine-containing mixed lipid monolayers, Soft matter, 10, 1685

Dai, S., Zhang, X., Du, Z., & Dang, H. 2005, Fabrication of nanopatterned DNA films by Langmuir–Blodgett technique, Materials Letters, 59, 423

Dai, X., Wei, C., Li, Z., Sun, Z., Shen, R., & Zhang, Y. 2013, Self-assembly of DNA networks at the air–water interface over time, RSC Advances, 3, 16116

De Jonge, N., Peckys, D., Kremers, G., & Piston, D. 2009, Electron microscopy of whole cells in liquid with nanometer resolution, Proceedings of the National Academy of Sciences, 106, 2159

Demel, R., Van Kessel, W. G., Zwaal, R., Roelofsen, B., & Van Deenen, L. 1975, Relation between various phospholipase actions on human red cell membranes and the interfacial phospholipid pressure in monolayers, Biochimica et Biophysica Acta (BBA)-Biomembranes, 406, 97

Dicko, A., Bourque, H., & Pézolet, M. 1998, Study by infrared spectroscopy of the conformation of dipalmitoylphosphatidylglycerol monolayers at the air–water interface and transferred on solid substrates, Chemistry and physics of lipids, 96, 125

Dittrich, M., Böttcher, M., Oliveira, J. S., Dobner, B., Möhwald, H., & Brezesinski, G. 2011, Physical–chemical characterization of novel cationic transfection lipids and the binding of model DNA at the air–water interface, Soft Matter, 7, 10162

Domanski, A. L., Sengupta, E., Bley, K., Untch, M. B., Weber, S. A., Landfester, K., Weiss, C. K., Butt, H.-J., & Berger, R. 2012, Kelvin probe force microscopy in nonpolar liquids, Langmuir, 28, 13892

Donkuru, M., Badea, I., Wettig, S., Verrall, R., Elsabahy, M., & Foldvari, M. 2010, Advancing nonviral gene delivery: lipid-and surfactant-based nanoparticle design strategies, Nanomedicine, 5, 1103

Donkuru, M., Wettig, S. D., Verrall, R. E., Badea, I., & Foldvari, M. 2012, Designing pH-sensitive gemini nanoparticles for non-viral gene delivery into keratinocytes, Journal of Materials Chemistry, 22, 6232

Douglas, K. L. 2008, Toward Development of Artificial Viruses for Gene Therapy: A Comparative Evaluation of Viral and Non-viral Transfection, Biotechnology progress, 24, 871

Drolle, E., Gaikwad, R. M., & Leonenko, Z. 2012, Nanoscale electrostatic domains in cholesterol-laden lipid membranes create a target for amyloid binding, Biophysical journal, 103, L27

Dynarowicz-Łatka, P., Dhanabalan, A., & Oliveira Jr, O. N. 2001, Modern physicochemical research on Langmuir monolayers, Advances in colloid and interface science, 91, 221

Dynarowicz-Łatka, P. & Hac-Wydro, K. 2004, Interactions between phosphatidylcholines and cholesterol in monolayers at the air/water interface, Colloids and Surfaces B: Biointerfaces, 37, 21

Eftaiha, A. F. & Paige, M. F. 2012, Phase-separation of mixed surfactant monolayers: A comparison of film morphology at the solid–air and liquid–air interfaces, Journal of colloid and interface science, 380, 105

Elias, G., Glatzel, T., Meyer, E., Schwarzman, A., Boag, A., & Rosenwaks, Y. 2011, The role of the cantilever in Kelvin probe force microscopy measurements, Beilstein journal of nanotechnology, 2, 252

Erokhina, S., Berzina, T., Cristofolini, L., Konovalov, O., Erokhin, V., & Fontana, M. P. 2007, Interaction of DNA oligomers with cationic lipidic monolayers: Complexation and splitting, Langmuir, 23, 4414

Estrela-Lopis, I., Brezesinski, G., & Möhwald, H. 2001, Dipalmitoylphosphatidylcholine/phospholipase D interactions investigated with polarization-modulated infrared reflection absorption spectroscopy, Biophysical journal, 80, 749

Felgner, P. L., Gadek, T. R., Holm, M., Roman, R., Chan, H. W., Wenz, M., Northrop, J. P., Ringold, G. M., & Danielsen, M. 1987, Lipofection: a highly efficient, lipid-mediated DNA-transfection procedure, Proceedings of the National Academy of Sciences, 84, 7413

Feynman, R. P. 1965, The Feynman Lectures on Physics

Finot, E., Leonenko, Y., Moores, B., Eng, L., Amrein, M., & Leonenko, Z. 2010, Effect of Cholesterol on Electrostatics in Lipid- Protein Films of a Pulmonary Surfactant, Langmuir, 26, 1929

Franklin, B., Brownrigg, W., & Farish, M. 1774, Of the stilling of waves by means of oil. Extracted from Sundry Letters between Benjamin Franklin, LL. DFRS William Brownrigg, MDFRS and the Reverend Mr. Farish, Philosophical Transactions, 64, 445

Gaines Jr, G. 1966, Insoluble monolayers at gas-liquid interfaces (Interscience, New York)

Gao, P. & Cai, Y. 2009, Label-free detection of the aptamer binding on protein patterns using Kelvin probe force microscopy (KPFM), Analytical and bioanalytical chemistry, 394, 207

García, J., Marrón, E., Martín, V., Moyá, M., & Lopez-Cornejo, P. 2014, Conformational changes of DNA in the presence of 12-s-12 gemini surfactants ($s = 2$ and 10). Role of the spacer's length in the interaction surfactant-polynucleotide, Colloids and Surfaces B: Biointerfaces, 118, 90

Gehrels, N. 1986, Confidence limits for small numbers of events in astrophysical data, The Astrophysical Journal, 303, 336

Giessibl, F. J. 1997, Forces and frequency shifts in atomic-resolution dynamic-force microscopy, Physical Review B, 56, 16010

Giocondi, M.-C., Yamamoto, D., Lesniewska, E., Milhiet, P.-E., Ando, T., & Le Grimellec, C. 2010, Surface topography of membrane domains, Biochimica et Biophysica Acta (BBA)-Biomembranes, 1798, 703

Glatzel, T., Hoppe, H., Sariciftci, N. S., Lux-Steiner, M. C., & Komiyama, M. 2005, Kelvin probe force microscopy study of conjugated polymer/fullerene organic solar cells, Japanese journal of applied physics, 44, 5370

Glatzel, T., Sadewasser, S., & Lux-Steiner, M. C. 2003, Amplitude or frequency modulation-detection in Kelvin probe force microscopy, Applied Surface Science, 210, 84

Goddard, E. & Ackilli, J. 1963, Monolayer properties of fatty acids, Journal of Colloid Science, 18, 585

Goryl, M., Kolodziej, J., Krok, F., Piatkowski, P., Such, B., & Szymonski, M. 2005, Epitaxial nanostructures assembled on InSb (001) by submonolayer deposition of gold, Microelectronic engineering, 81, 394

Goto, T. E. & Caseli, L. 2013, Understanding the Collapse Mechanism in Langmuir Monolayers through Polarization Modulation-Infrared Reflection Absorption Spectroscopy, Langmuir, 29, 9063

Griffiths, D. J. 2013, Introduction to electrodynamics (Pearson)

Gromelski, S. & Brezesinski, G. 2004, Adsorption of DNA to zwitterionic DMPE monolayers mediated by magnesium ions, Physical Chemistry Chemical Physics, 6, 5551

Guzmán, E., Liggieri, L., Santini, E., Ferrari, M., & Ravera, F. 2012, DPPC–DOPC Langmuir monolayers modified by hydrophilic silica nanoparticles: Phase behaviour, structure and rheology, Colloids and Surfaces A: Physicochemical and Engineering Aspects, 413, 174

Hane, F., Moores, B., Amrein, M., & Leonenko, Z. 2009, Effect of SP-C on surface potential distribution in pulmonary surfactant: atomic force microscopy and Kelvin probe force microscopy study, Ultramicroscopy, 109, 968

Hansda, C., Hussain, S. A., Bhattacharjee, D., & Paul, P. K. 2013, Adsorption behavior of DNA onto a cationic surfactant monolayer at the air–water interface, Surface Science, 617, 124

Hao, C., Sun, R., & Zhang, J. 2013, Mixed monolayers of DOPC and palmitic acid at the liquid–air interface, Colloids and Surfaces B: Biointerfaces, 112, 441

Hayat, M. 2012, Fixation for electron microscopy (Elsevier)

He, Y., Shang, Y., Shao, S., Liu, H., & Hu, Y. 2011, Micellization of cationic gemini surfactant and its interaction with DNA in dilute brine, Journal of colloid and interface science, 358, 513

Hénon, S. & Meunier, J. 1991, Microscope at the Brewster angle: Direct observation of first-order phase transitions in monolayers, Review of Scientific Instruments, 62, 936

Hirsch-Lerner, D., Zhang, M., Eliyahu, H., Ferrari, M. E., Wheeler, C. J., & Barenholz, Y. 2005, Effect of 'helper lipid' on lipoplex electrostatics, Biochimica et Biophysica Acta (BBA)-Biomembranes, 1714, 71

Holthuis, J. C. & Levine, T. P. 2005, Lipid traffic: floppy drives and a superhighway, Nature reviews molecular cell biology, 6, 209

Hui, S. W., Langner, M., Zhao, Y.-L., Ross, P., Hurley, E., & Chan, K. 1996, The role of helper lipids in cationic liposome-mediated gene transfer, Biophysical journal, 71, 590

Ichii, T., Fukuma, T., Kobayashi, K., Yamada, H., & Matsushige, K. 2004, Surface potential measurements of phase-separated alkanethiol self-assembled monolayers by non-contact atomic force microscopy, Nanotechnology, 15, S30

Israelachvili, J. & Ruths, M. 2013, Brief History of Intermolecular and Intersurface Forces in Complex Fluid Systems, Langmuir, 29, 9605

Israelachvili, J. N. 2011, Intermolecular and surface forces: revised third edition (Academic press)

Israelachvili, J. N., Mitchell, D. J., & Ninham, B. W. 1977, Theory of self-assembly of lipid bilayers and vesicles, Biochimica et Biophysica Acta (BBA)-Biomembranes, 470, 185

Jackson, J. D. 1962, Classical electrodynamics (Wiley New York etc.)

Jacobs, H., Knapp, H., & Stemmer, A. 1999, Practical aspects of Kelvin probe force microscopy, Review of scientific instruments, 70, 1756

Jacobs, H., Leuchtmann, P., Homan, O., & Stemmer, A. 1998, Resolution and contrast in Kelvin probe force microscopy, Journal of Applied Physics, 84, 1168

Kaganer, V. M., Möhwald, H., & Dutta, P. 1999, Structure and phase transitions in Langmuir monolayers, Reviews of Modern Physics, 71, 779

Kalinin, S. V. & Gruverman, A. 2007, Scanning probe microscopy: electrical and electromechanical phenomena at the nanoscale, Vol. 1 (Springer)

Kalinin, S. V., Rodriguez, B. J., Jesse, S., Karapetian, E., Mirman, B., Eliseev, E. A., & Morozovska, A. N. 2007, Nanoscale electromechanics of ferroelectric and biological systems: a new dimension in scanning probe microscopy, Annu. Rev. Mater. Res., 37, 189

Kawaura, C., Noguchi, A., Furuno, T., & Nakanishi, M. 1998, Atomic force microscopy for studying gene transfection mediated by cationic liposomes with a cationic cholesterol derivative, FEBS letters, 421, 69

Kedrov, A., Janovjak, H., Sapra, K. T., & Müller, D. J. 2007, Deciphering molecular interactions of native membrane proteins by single-molecule force spectroscopy, Annu. Rev. Biophys. Biomol. Struct., 36, 233

Kirby, A. J., Camilleri, P., Engberts, J. B., Feiters, M. C., Nolte, R. J., Söderman, O., Bergsma, M., Bell, P. C., Fielden, M. L., García Rodríguez, C. L., et al. 2003, Gemini surfactants: new synthetic vectors for gene transfection, Angewandte Chemie International Edition, 42, 1448

Klapetek, P., Valtr, M., Nečas, D., Salyk, O., & Dzik, P. 2011, Atomic force microscopy analysis of nanoparticles in non-ideal conditions, Nanoscale research letters, 6, 1

Klein, D. R. 2013, Organic Chemistry, 2nd Edition (Wiley)

Koltover, I., Salditt, T., Rädler, J. O., & Safinya, C. R. 1998, An inverted hexagonal phase of cationic liposome-DNA complexes related to DNA release and delivery, Science, 281, 78

Koynova, R., Wang, L., & MacDonald, R. C. 2006, An intracellular lamellar–nonlamellar phase transition rationalizes the superior performance of some cationic lipid transfection agents, Proceedings of the National Academy of Sciences, 103, 14373

KSV Nima. 2015a, http://www.biolinscientific.com/technology/l-lb-ls-technique/, accessed 2015-01-04

—. 2015b, Biolin Scientific product brochure for KSV Nima Langmuir and Langmuir-Blodgett troughs, http://www.biolinscientific.com/product/langmuir-troughs-langmuir-blodgett-troughs/, accessed 2015-01-11

—. 2015c, Langmuir and Langmuir Blodgett Films, Application Note 107, http://www.lot-oriel.com/files/downloads/ksv/en/langmuirblodgett_en01.pdf, accessed 2015-01-04

Kubo, I., Adachi, S., Maeda, H., & Seki, A. 2001, Phosphatidylcholine monolayers observed with Brewster angle microscopy and π-A isotherms, Thin Solid Films, 393, 80

Kundu, S., Langevin, D., & Lee, L.-T. 2008, Neutron Reflectivity Study of the Complexation of DNA with Lipids and Surfactants at the Surface of Water, Langmuir, 24, 12347

Lancelot, E. & Grauby-Heywang, C. 2007, Comparison of the interaction of dihydrocholesterol and cholesterol with sphingolipid or phospholipid Langmuir monolayers, Colloids and Surfaces B: Biointerfaces, 59, 81

Langmuir, I. 1934, Mechanical properties of monomolecular films, Journal of the Franklin Institute, 218, 143

Laoudj, D., Guasch, C., Renault, E., Bennes, R., & Bonnet, J. 2005, Surface potential mapping of dispersed proteins, Analytical and bioanalytical chemistry, 381, 1476

Lawrence, M. J. 1994, Surfactant systems: their use in drug delivery, Chemical Society Reviews, 23, 417

Lee, G., Lee, W., Lee, H., Woo Lee, S., Sung Yoon, D., Eom, K., & Kwon, T. 2012, Mapping the surface charge distribution of amyloid fibril, Applied Physics Letters, 101,

Lee, J. & Chang, C.-H. 2014, The interaction between the outer layer of a mixed ion pair amphiphile/double-chained cationic surfactant vesicle and DNA: a Langmuir monolayer study, Soft matter, 10, 1831

Leonenko, Z., Rodenstein, M., Döhner, J., Eng, L. M., & Amrein, M. 2006, Electrical surface potential of pulmonary surfactant, Langmuir, 22, 10135

Leonenko, Z. V., Merkle, D., Lees-Miller, S. P., & Cramb, D. T. 2002, Lipid phase dependence of DNA-cationic phospholipid bilayer interactions examined using atomic force microscopy, Langmuir, 18, 4873

Leung, C., Kinns, H., Hoogenboom, B. W., Howorka, S., & Mesquida, P. 2009, Imaging surface charges of individual biomolecules, Nano letters, 9, 2769

Leung, C., Maradan, D., Kramer, A., Howorka, S., Mesquida, P., & Hoogenboom, B. W. 2010, Improved Kelvin probe force microscopy for imaging individual DNA molecules on insulating surfaces, Applied Physics Letters, 97, 203703

Li, R., Chen, Q., Liu, H., & Hu, Y. 2010, Influence of spacer of gemini on the interactions between cationic gemini surfactant and stearic acid in mixed monolayers, Langmuir, 26, 9342

Li, R., Chen, Q., Zhang, D., Liu, H., & Hu, Y. 2008, Mixed monolayers of Gemini surfactants and stearic acid at the air/water interface, Journal of colloid and interface science, 327, 162

Loppacher, C., Zerweck, U., Teich, S., Beyreuther, E., Otto, T., Grafström, S., & Eng, L. M. 2005, FM demodulated Kelvin probe force microscopy for surface photovoltage tracking, Nanotechnology, 16, S1

Lucas, T. R., Bauer, B. A., Davis, J. E., & Patel, S. 2012, Molecular dynamics simulation of hydrated DPPC monolayers using charge equilibration force fields, Journal of computational chemistry, 33, 141

Luque-Caballero, G., Martín-Molina, A., Sánchez-Treviño, A. Y., Rodríguez-Valverde, M. A., Cabrerizo-Vílchez, M. A., & Maldonado-Valderrama, J. 2014, Using AFM to probe the complexation of DNA with anionic lipids mediated by Ca 2+: the role of surface pressure, Soft matter, 10, 2805

Luzardo, M. d. C., Peltzer, G., & Disalvo, E. A. 1998, Surface Potential of Lipid Interfaces Formed by Mixtures of Phosphatidylcholine of Different Chain Lengths, Langmuir, 14, 5858

Lv, H., Zhang, S., Wang, B., Cui, S., & Yan, J. 2006, Toxicity of cationic lipids and cationic polymers in gene delivery, Journal of Controlled Release, 114, 100

Ma, B., Zhang, S., Jiang, H., Zhao, B., & Lv, H. 2007, Lipoplex morphologies and their influences on transfection efficiency in gene delivery, Journal of Controlled Release, 123, 184

MacDonald, R. C., Gorbonos, A., Momsen, M. M., & Brockman, H. L. 2006, Surface Properties of Dioleoyl-sn-glycerol-3-ethylphosphocholine, a Cationic Phosphatidylcholine Transfection Agent, Alone and in Combination with Lipids or DNA, Langmuir, 22, 2770

McConlogue, C. W. & Vanderlick, T. K. 1997, A close look at domain formation in DPPC monolayers, Langmuir, 13, 7158

McConnell, H. M. 1991, Structures and transitions in lipid monolayers at the air-water interface, Annual Review of Physical Chemistry, 42, 171

McGregor, C., Perrin, C., Monck, M., Camilleri, P., & Kirby, A. J. 2001, Rational approaches to the design of cationic gemini surfactants for gene delivery, Journal of the American Chemical Society, 123, 6215

McLoughlin, D., Dias, R., Lindman, B., Cardenas, M., Nylander, T., Dawson, K., Miguel, M., & Langevin, D. 2005, Surface complexation of DNA with insoluble monolayers. Influence of divalent counterions, Langmuir, 21, 1900

Melitz, W., Shen, J., Kummel, A. C., & Lee, S. 2011, Kelvin probe force microscopy and its application, Surface Science Reports, 66, 1

Menger, F. & Littau, C. 1993, Gemini surfactants: a new class of self-assembling molecules, Journal of the American Chemical Society, 115, 10083

Menger, F. M. & Littau, C. 1991, Gemini-surfactants: synthesis and properties, Journal of the American chemical society, 113, 1451

Mengistu, D. H., Bohinc, K., & May, S. 2009, Binding of DNA to zwitterionic lipid layers mediated by divalent cations, The Journal of Physical Chemistry B, 113, 12277

Michanek, A., Yanez, M., Wacklin, H., Hughes, A., Nylander, T., & Sparr, E. 2012, RNA and DNA association to zwitterionic and charged monolayers at the air–liquid interface, Langmuir, 28, 9621

Miñones Jr, J., Rodrıguez Patino, J., Conde, O., Carrera, C., & Seoane, R. 2002, The effect of polar groups on structural characteristics of phospholipid monolayers spread at the air–water interface, Colloids and Surfaces A: Physicochemical and Engineering Aspects, 203, 273

Mohn, F., Gross, L., Moll, N., & Meyer, G. 2012, Imaging the charge distribution within a single molecule, Nature nanotechnology, 7, 227

Moore, David S, M. G. P. & Craig, B. A. 2014, Introduction to the Practice of Statistics, 8ed (Macmillan)

Moores, B., Hane, F., Eng, L., & Leonenko, Z. 2010, Kelvin probe force microscopy in application to biomolecular films: frequency modulation, amplitude modulation, and lift mode, Ultramicroscopy, 110, 708

Moores, B. A. J. 2010, Scanning Probe Microscopy Methods to Study Electrostatic Properties within Biosystems, Master's thesis, University of Waterloo

Moraille, P. & Badia, A. 2002, Highly parallel, nanoscale stripe morphology in mixed phospholipid monolayers formed by Langmuir-Blodgett transfer, Langmuir, 18, 4414

Morris, V. J., Kirby, A. R., & Gunning, A. P. 1999, Atomic force microscopy for biologists, Vol. 57 (World Scientific)

Mozaffary, H. 1991, On the sign and origin of the surface potential of phospholipid monolayers, Chemistry and physics of lipids, 59, 39

Nakanishi, M. & Noguchi, A. 2001, Confocal and probe microscopy to study gene transfection mediated by cationic liposomes with a cationic cholesterol derivative, Advanced drug delivery reviews, 52, 197

Noguchi, A., Furuno, T., Kawaura, C., & Nakanishi, M. 1998, Membrane fusion plays an important role in gene transfection mediated by cationic liposomes, FEBS letters, 433, 169

Nonnenmacher, M., oï£¡Boyle, M., & Wickramasinghe, H. 1991, Kelvin probe force microscopy, Applied Physics Letters, 58, 2921

Nonnenmacher, M., O'Boyle, M., & Wickramasinghe, H. 1992, Surface investigations with a Kelvin probe force microscope, Ultramicroscopy, 42, 268

Paiva, D., Brezesinski, G., Pereira, M. d. C., & Rocha, S. 2013, Langmuir monolayers of monocationic lipid mixed with cholesterol or fluorocholesterol: DNA adsorption studies, Langmuir, 29, 1920

Pal, A., Mishra, B. K., Panigrahi, S., Nath, R. K., & Deb, S. 2012, Formation of Complex Langmuir and Langmuir-Blodgett Films of DNA with a Dichain Cationic Surfactant, Journal of Macromolecular Science, Part A, 49, 160

Palermo, V., Palma, M., & Samorì, P. 2006, Electronic characterization of organic thin films by Kelvin probe force microscopy, Advanced materials, 18, 145

Pedroso de Lima, M. C., Simões, S., Pires, P., Faneca, H., & Düzgüneş, N. 2001, Cationic lipid–DNA complexes in gene delivery: from biophysics to biological applications, Advanced drug delivery reviews, 47, 277

Petrucci, R. H., Herring, G. F., Madura, J. D., & Bissonnette, C. 2010, General chemistry: principles and modern applications (Pearson Education International)

Phillips, M. & Chapman, D. 1968, Monolayer characteristics of saturated 1, 2-diacyl phosphatidylcholines (lecithins) and phosphatidylethanolamines at the air-water interface, Biochimica et Biophysica Acta (BBA)-Biomembranes, 163, 301

Prenner, E., Honsek, G., Hönig, D., Möbius, D., & Lohner, K. 2007, Imaging of the domain organization in sphingomyelin and phosphatidylcholine monolayers, Chemistry and physics of lipids, 145, 106

Putman, C. A., Van der Werf, K. O., De Grooth, B. G., Van Hulst, N. F., & Greve, J. 1994, Tapping mode atomic force microscopy in liquid, Applied Physics Letters, 64, 2454

Qiao, L., Ge, A., Osawa, M., & Ye, S. 2013, Structure and stability studies of mixed monolayers of saturated and unsaturated phospholipids under low-level ozone, Physical Chemistry Chemical Physics, 15, 17775

Qibin, C., Xiaodong, L., Shaolei, W., Shouhong, X., Honglai, L., & Ying, H. 2007, Cationic Gemini surfactant at the air/water interface, Journal of colloid and interface science, 314, 651

Radwan Almofti, M., Harashima, H., Shinohara, Y., Almofti, A., Baba, Y., & Kiwada, H. 2003, Cationic liposome-mediated gene delivery: biophysical study and mechanism of internalization, Archives of biochemistry and biophysics, 410, 246

Rathman, J. F. & Sun, P. 2005, Biocomposite films synthesized at a fluid/fluid interface, Faraday discussions, 129, 193

Rullaud, V., Moridi, N., & Shahgaldian, P. 2014, Sequence-Specific DNA Interactions with Calixarene-Based Langmuir Monolayers, Langmuir, 30, 8675

Sadewasser, S. & Glatzel, T. 2012, Kelvin probe force microscopy (Springer)

Sakurai, F., Inoue, R., Nishino, Y., Okuda, A., Matsumoto, O., Taga, T., Yamashita, F., Takakura, Y., & Hashida, M. 2000, Effect of DNA/liposome mixing ratio on the physicochemical characteristics, cellular uptake and intracellular trafficking of plasmid DNA/cationic liposome complexes and subsequent gene expression, Journal of controlled release, 66, 255

Sanchez, J. & Badia, A. 2003, Atomic force microscopy studies of lateral phase separation in mixed monolayers of dipalmitoylphosphatidylcholine and dilauroylphosphatidylcholine, Thin Solid Films, 440, 223

Schmidt, M. L., Ziani, L., Boudreau, M., & Davis, J. H. 2009, Phase equilibria in DOPC/DPPC: Conversion from gel to subgel in two component mixtures, The Journal of chemical physics, 131, 175103

Seelig, A. 1987, Local anesthetics and pressure: a comparison of dibucaine binding to lipid monolayers and bilayers, Biochimica et Biophysica Acta (BBA)-Biomembranes, 899, 196

Sinensky, A. K. & Belcher, A. M. 2007, Label-free and high-resolution protein/DNA nanoarray analysis using Kelvin probe force microscopy, nature nanotechnology, 2, 653

Smaby, J. & Brockman, H. 1990, Surface dipole moments of lipids at the argon-water interface. Similarities among glycerol-ester-based lipids, Biophysical journal, 58, 195

Sternberg, B., Sorgi, F. L., & Huang, L. 1994, New structures in complex formation between DNA and cationic liposomes visualized by freeze-fracture electron microscopy, FEBS letters, 356, 361

Stottrup, B. L., Veatch, S. L., & Keller, S. L. 2004, Nonequilibrium behavior in supported lipid membranes containing cholesterol, Biophysical journal, 86, 2942

Sugimura, H., Hayashi, K., Saito, N., Nakagiri, N., & Takai, O. 2002, Surface potential microscopy for organized molecular systems, Applied surface science, 188, 403

Swalen, J. D., Allara, D., Andrade, J. D., Chandross, E., Garoff, S., Israelachvili, J., McCarthy, T., Murray, R., & Pease, R. 1987, Molecular monolayers and films. A panel report for the materials sciences division of the department of energy, Langmuir, 3, 932

Symietz, C., Schneider, M., Brezesinski, G., & Möhwald, H. 2004, DNA alignment at cationic lipid monolayers at the air/water interface, Macromolecules, 37, 3865

Thompson, M., Cheran, L.-E., Zhang, M., Chacko, M., Huo, H., & Sadeghi, S. 2005, Label-free detection of nucleic acid and protein microarrays by scanning Kelvin nanoprobe, Biosensors and Bioelectronics, 20, 1471

Tros de Ilarduya, C., Sun, Y., & Düzgüneş, N. 2010, Gene delivery by lipoplexes and polyplexes, European journal of pharmaceutical sciences, 40, 159

Van Meer, G., Voelker, D. R., & Feigenson, G. W. 2008, Membrane lipids: where they are and how they behave, Nature reviews molecular cell biology, 9, 112

Vie, V., Van Mau, N., Lesniewska, E., Goudonnet, J., Heitz, F., & Le Grimellec, C. 1998, Distribution of ganglioside GM1 between two-component, two-phase phosphatidylcholine monolayers, Langmuir, 14, 4574

Vogel, V. & Möbius, D. 1988a, Hydrated polar groups in lipid monolayers: effective local dipole moments and dielectric properties, Thin Solid Films, 159, 73

—. 1988b, Local surface potentials and electric dipole moments of lipid monolayers: contributions of the water/lipid and the lipid/air interfaces, Journal of colloid and interface science, 126, 408

Wang, C., Li, X., Wettig, S. D., Badea, I., Foldvari, M., & Verrall, R. E. 2007, Investigation of complexes formed by interaction of cationic gemini surfactants with deoxyribonucleic acid, Physical Chemistry Chemical Physics, 9, 1616

Wang, H., Kaur, T., Tavakoli, N., Joseph, J., & Wettig, S. 2013, Transfection and structural properties of phytanyl substituted gemini surfactant-based vectors for gene delivery, Physical Chemistry Chemical Physics, 15, 20510

Wang, H. & Wettig, S. D. 2011, Synthesis and aggregation properties of dissymmetric phytanyl-gemini surfactants for use as improved DNA transfection vectors, Physical Chemistry Chemical Physics, 13, 637

Wasungu, L. & Hoekstra, D. 2006, Cationic lipids, lipoplexes and intracellular delivery of genes, Journal of Controlled Release, 116, 255

Welti, R. & Glaser, M. 1994, Lipid domains in model and biological membranes, Chemistry and physics of lipids, 73, 121

Wettig, S. & Verrall, R. 2001, Thermodynamic Studies of Aqueous *m-s-m* Gemini Surfactant Systems, Journal of colloid and interface science, 235, 310

Wettig, S. D., Badea, I., Donkuru, M., Verrall, R. E., & Foldvari, M. 2007, Structural and transfection properties of amine-substituted gemini surfactant-based nanoparticles, The journal of gene medicine, 9, 649

Wettig, S. D., Verrall, R. E., & Foldvari, M. 2008, Gemini surfactants: a new family of building blocks for non-viral gene delivery systems, Current gene therapy, 8, 9

Williford, J.-M., Wu, J., Ren, Y., Archang, M. M., Leong, K., & Mao, H.-Q. 2014, Recent Advances on Nanoparticle-Mediated siRNA Delivery, Annual Review of Biomedical Engineering, 16

Wu, J.-C., Lin, T.-L., Jeng, U., & Torikai, N. 2006, Neutron reflectivity studies on the DNA adsorption on lipid monolayers at the air–liquid interface, Physica B: Condensed Matter, 385, 838

Yang, P., Singh, J., Wettig, S., Foldvari, M., Verrall, R. E., & Badea, I. 2010, Enhanced gene expression in epithelial cells transfected with amino acid-substituted gemini nanoparticles, European Journal of Pharmaceutics and Biopharmaceutics, 75, 311

Yasutake, M., Aoki, D., & Fujihira, M. 1996, Surface potential measurements using the Kelvin probe force microscope, Thin Solid Films, 273, 279

Zabner, J., Fasbender, A. J., Moninger, T., Poellinger, K. A., & Welsh, M. J. 1995, Cellular and molecular barriers to gene transfer by a cationic lipid, Journal of Biological Chemistry, 270, 18997

Zerweck, U., Loppacher, C., Otto, T., Grafström, S., & Eng, L. M. 2005, Accuracy and resolution limits of Kelvin probe force microscopy, Physical Review B, 71, 125424

Zhang, P. & Cantiello, H. F. 2009, Measurement of charge distribution in actin bundles by surface potential microscopy, Applied Physics Letters, 95, 033701

Zhang, S., Xu, Y., Wang, B., Qiao, W., Liu, D., & Li, Z. 2004, Cationic compounds used in lipoplexes and polyplexes for gene delivery, Journal of controlled release, 100, 165

Zhao, X., Shang, Y., Hu, J., Liu, H., & Hu, Y. 2008, Biophysical characterization of complexation of DNA with oppositely charged Gemini surfactant 12-3-12, Biophysical chemistry, 138, 144

Zhao, X., Shang, Y., Liu, H., & Hu, Y. 2007, Complexation of DNA with cationic gemini surfactant in aqueous solution, Journal of colloid and interface science, 314, 478

Zhou, T., Llizo, A., Wang, C., Xu, G., & Yang, Y. 2013, Nanostructure-induced DNA condensation, Nanoscale, 5, 8288

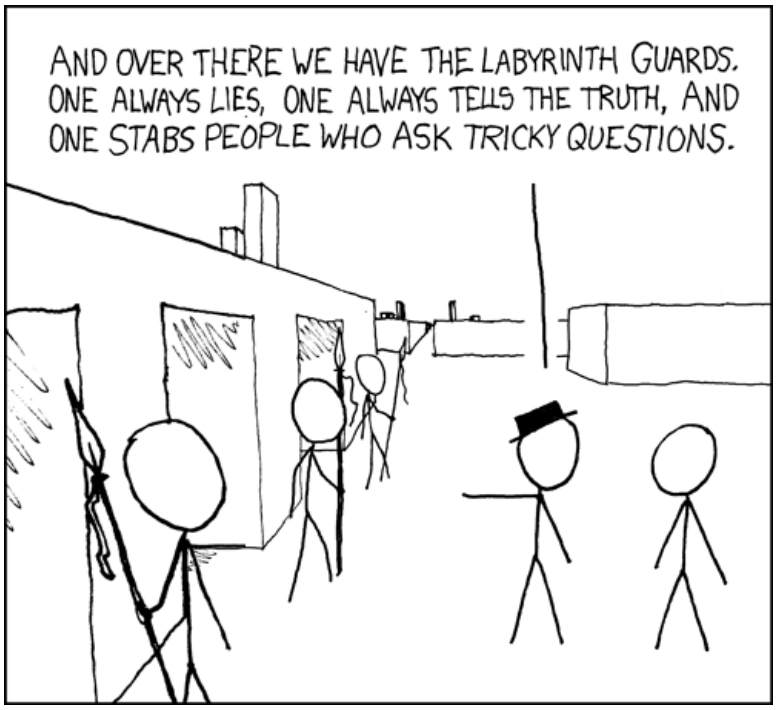

Reprinted from xkcd.com.

APPENDICES

It doesn't matter how beautiful your theory is, it doesn't matter how smart you are. If it doesn't agree with experiment, it's wrong.

Richard Feynman

Appendix A

Detailed Experimental Procedures

A.1 Langmuir-Blodgett Deposition

Following from our discussion in § 1.4.1, we provide here some detailed information on the experimental procedure for constructing Langmuir monolayers and then depositing them onto mica slides in preparation for imaging. It is assumed that the reader will be familiar with the general operating procedures for their trough apparatus, which can be learnt from the instrument operating manual and will not be repeated here.

The basic sequence of Langmuir-Blodgett deposition is solution and material preparation, cleaning, monolayer formation, monolayer compression, and finally deposition and drying.

Preparation

Lipids and surfactants should be prepared into solutions using chloroform as the solvent. In the present work, we used a final solute concentration of 1 mg/mL. This concentration has been found to be convenient for small troughs (requiring a minimal volume). To make solutions of multiple species, simply combine the appropriate volume of each stock solution to give the desired molar ratio. The final solution will then still have a concentration of

1 mg/mL. Solutions and stock solutions should be kept in the freezer until needed. When storing, it is desirable to top up the vials with nitrogen gas to avoid any possible oxidation.

An appropriate substrate onto which to deposit the monolayers is mica. Mica can be cleaved to atomci flatness, which is a critical advantage for AFM. The slides used in the present work were purchased as small cut squares 18 mm on a side, which fit nicely into the deposition well of the trough. It is necessary to clean and cleave the slides right before use, which can be accomplished using simple single-sided scotch tape, as follows: Take a section of tape and place it firmly over one side of the mica (with gloves). Carefully peel the tape back while applying pressure to the back of the slide, and take a layer of mica with the tape. This takes practise to get efficient, so it's best if someone can show you how this works. Ensure that an entire layer is removed, to leave a clean surface with no broken layers. Cleave two layers from each side, and secure it to the dipping arm. Lower the dipping arm to its lowest setting and manoeuvre the slide into the dipping well. The height will be adjusted later when the subphase is added.

Cleaning

Firstly, the trough must be cleaned, and filled with nanopure water. One may use chloroform or ethanol to clean the trough surface, although ethanol is considerably safer particularly in the absence of a fume hood. A Milli-Q system is a prime choice for nanopure water. In our trough, approximately 50-60 mL is used to fill the trough. If the experiment calls for buffer and not pure water, simply use nanopure water during the buffer preparation.

The pressure plate must also be cleaned. For filter paper plates, simply rinse with some ethanol and dry, twice, then submerge it into the subphase by its hook. It is only necessary to do this once before a series of experiments with the same monolayer and subphase composition.

It is also important to ensure that the aqueous surface is as clean as possible. Dust and other particles can land on the surface or escape initial cleaning. To clean it, vacuum small quantities of water from the surface, concentrating near the barrier arms. Close the arms to concentrate any contaminants, and vacuum again. Now open the arms, zero the

surface pressure, and close again. If the pressure increase is below 0.2 mN/m, then the surface may be considered clean.

Adding DNA Into the Subphase

If the experiment requires DNA or some other solute to be in the subphase, this can be prepared with the nanopure water. DNA can be difficult to dissolve, so it is advised to do the following: break up the solid DNA stock (scissors is fine) and swirl in a round bottom flask with some nanopure water. Gradually add the required volume of water to make a semi-concentrated stock solution (higher concentration that what is needed in the trough), and leave it in a fridge overnight. The next day, swirl again, and sonicate briefly to dissolve the rest and randomly cleave the fragments slightly. Use this stock to make the appropriate concentration and volume of subphase.

Monolayer Formation and Compression

With a clean and filled trough, adjust the mica slide so that the top of the slide is barely submerged into the subphase. Again ensure that the surface is clean with a pressure test, and vacuum slightly if necessary. Open the barrier arms completely. With a pipette, quickly deposit about 15 μL of lipid-surfactant chloroform solution onto the surface, placing drops in several widely separated regions of the surface. Ensure that the surface pressure does not climb above your desired deposition pressure. Allow the monolayer to rest and come to equilibrium for 10 minutes; this time period also ensures that all of the solvent has evaporated.

After these 10 minutes, set the instrument to *pressure control*, and compress to target pressure. In our case, we used 12-30 mm/min and in most cases a target pressure of 35 mN/m. The results do not vary with compression speed unless it is extremely high.

Isotherms

If deposition onto a solid substrate is not the goal, and instead a pressure-area isotherm is desired, simply omit the mica slide and use a *speed control* setting to compress the isotherm

at a constant speed until the barrier arms close to their minimum separation. In this case, a slower compression speed is desired so that the monolayer is minimally disturbed during the data collection.

Deposition

Once the monolayer has reached its target pressure, the mica slide can be slowly drawn up through the monolayer and into the air. With the constant pressure applied via a feedback loop by the instrument, as the monolayer is deposited the barrier arms will close just enough to maintain the target pressure. We use a slow deposition speed of 2-10 mm/min. Once the slide is out of the subphase, allow it to dry for a few minutes before removing it from the dipping arm. It should be placed in a desiccator immediately; drying gently with nitrogen gas is also an option, if desired, before storage. It is advisable to wait overnight before imaging, to draw out as much water as possible.

A.2 Preparation of Gemini Surfactant-DNA Nanoparticles

Transfection complexes were imaged in the present work by first preparing them in solution and then depositing them onto freshly cleaved mica (see previous section for the latter). The preparation followed closely the methodology in Wettig et al. (2007) and Wang et al. (2013) as examples of standard procedures. Here we provide details on our adapted procedure.

The final transfection complex solution requires three components: i) an aqueous solution of gemini surfactant, ii) an aqueous solution of DOPE vesicles, and iii) an aqueous solution of DNA fragments of random size. All of these are added in appropriate concentration ratios as determined by the individual experiment. The preparation of a DNA solution was described in the previous section and is not repeated here. The only difference being that, as a final step, the DNA solution should be filtered through a $0.2\,\mu$m disc filter to remove any large aggregates.

A.2. Preparation of Gemini Surfactant-DNA Nanoparticles

Gemini surfactants should be initially dissolved in chloroform at a concentration of 1 mg/mL (standard stock). To make an aqueous solution, an appropriate amount of the chloroform solution is placed in a small vial and the solvent allowed to evaporate off over a gentle stream of nitrogen gas. This allows a small and precise amount to be placed into the vial with a pipette, and the film left over is resuspended in nanopure (Milli-Q) water. Brief sonication helps to dissolve the surfactant at this point. Typically, we aim for a concentration near the CMC in the final product, and this serves as the benchmark for the calculations of volume of DNA and DOPE vesicle solutions to be added. The surfactant solutions are then filtered through 0.2 μm disc filters with a syringe.

Vesicles of DOPE can be prepared by repeated sonication and stirring of aqueous solutions of the lipid. The lipid typically comes in a concentrated stock solution of chloroform (e.g., 25 mg/mL). A desired amount of this stock solution is placed in a vial or round-bottom flask containing a small amount ($\sim$1 mL) of HPLC-grade ethanol. The solvent is then allowed to evaporate over a gentle stream of nitrogen gas to form a thin film. An appropriate amount of nanopure water is then added to re-suspend the DOPE, and the film allowed to rest ('swell') for about an hour. At this point the solution will appear cloudy with some visible particulate matter. Add a small magnetic stir bar and seal the vial/flask to prevent any contamination. Cycle with 15 minutes of sonication and 15 minutes of stirring until the solution appears clear. As a final step, the vesicles should be filtered through 0.45 μm disc filters.

To make the final transfection complexes, all three solutions are combined in appropriate ratios and allowed to stand for 30 minutes. Small quantities ($\sim$20-40 μL) are placed onto freshly cleaved mica slides and allowed to adhere for 15 minutes. The solvent is then wicked away by tilting the slide onto a Kimwipe, and the whole sample allowed to dry in a desiccator overnight before imaging.

A.3 AFM and KPFM Imaging with the AIST-NT Smart-SPM

Cantilevers

With this instrument, because the laser alignment is done by an infrared beam automatically, it is necessary to use cantilevers which have an appropriately reflective coating. The best cantilevers we have found to use with the AIST are from a company called MikroMasch, and for KPFM we have used the NSC-14-Cr/Au cantilever tips, which have a resonant frequency near 130 kHz, or NSC-15-Pt which have a resonant frequency near 325 kHz. Both work well.

Standard AFM

The AIST-NT Smart-SPM instrument is state-of-the-art for precise topographical and KPFM imaging. Setup is more straightforward than most instruments which allows more time to be spent on imaging. The operating manual presents clear directions and figures for the mechanics of the setup, but here we provide a few additional tips and a general overview of how to get started with AFM imaging on this instrument. In the next section we provide detail on imaging with the specialised KPFM modes that are available.

Installing the cantilever tip is straightforward, but requires a steady hand. For those who have not done this before, it is best to be shown. With practise, tip replacement takes under a minute. The next step is aligning the instrument's laser with the tip, which the engineers have made exceedingly simple. With the tip in the 'default' position, the instrument will automatically search for the cantilever and align the laser appropriately. This can even be visualised for confirmation within the software. Sometimes the software will search and fail to find the tip - this can often be diagnosed when the algorithm drags the location downward and/or if the visualisation fails to produce an obvious tip shape. In this case, it is often remedied by manually selecting a location higher up on the map and repeating the algorithm (thus starting at a location other than default). If this still fails, have a look at the tip under a standard microscope and see if it is broken (and if so,

replace it with a new tip). Tips are extremely sensitive, and will almost always break if they are dropped or struck.

Once the tip is aligned, the next step is to check the resonant frequency. For this, you should have already selected 'AC mode'. Again the frequency calibration is done automatically, and the user should confirm that the resonant peak is strong, clean, and where it should be. If all this checks out, imaging can begin once the sample is installed.

For standard topographical imaging, the mica slide can be placed on top of the sample stage without any adhesive. Simply place the circular stage into the instrument (see the manual for details) and place the mica slide on top (watch out to be wel clear of the tip; or better yet, install the sample before the tip).

Engaging the sample with the tip can also be done automatically by the software, or manually, depending on the user's preference or how much tweaking is necessary. A standard approach is often sufficient. Follow the process within the manual for this. Once the tip has approached and the landing is clean, switch to 'Q scan', and ensure that adaptive scanning is enabled. Adaptive scanning is useful for samples with a lot of irregular features, because it is more responsive and slows down the imaging for awkward structures to enhance image quality. A typical scan rate is 1 Hz for standard AFM topography imaging only. Ensure that height, mag, and phase signals are collected. As far as parameters go, the amplitude setting is the most influential. It is typically set to about 15 nm, but it can be used with reasonable success in the range of 10-20 nm. If image quality is suppressed on first try, a different amplitude setting can be attempted. Standard parameters for all other settings are generally sufficient for the purposes of the present work.

KPFM

Repeating what was described in § 2.2.3, for KPFM imaging of samples deposited onto mica, it is necessary to prepare the substrate in a manner that allows a bias voltage to be effectively applied. In our experiments, we have determined an optimal setup to be as follows. For square mica slides, we cut a square of aluminum foil several mm larger than the substrate, and adhere this to the bottom of the mica with conductive mesh double-sided tape. The edges are wrapped over onto the top surface to form a frame. Small pieces of

conductive tape are applied to the corners to ensure the foil adheres to the surface. The KPFM electrode (where the bias voltage is applied) is placed onto one of the pieces of conductive tape on the top surface. See Fig. 2.2.

In theory, our KPFM setup can produce the topography and surface potential difference images simultaneously, but in practise this does not yield optimal quality for topography. A superior method is to perform, line-by-line, a topography scan followed by a KPFM scan, and this is implemented automatically from the AIST-NT software. Occasionally, edge-effects were found at the point where the scans switched from AFM to KPFM, but this was usually resolved by allowing for a delay of 15ms between scans. Lateral KPFM resolution was further enhanced by choosing a closer scan height of several nm, and slightly reducing the amplitude of the second scan (to, say, 85%, but for FM mode only). A cantilever lift height of 8 nm suffices for most purposes. Lower lift heights can be used for fairly flat samples; samples with large variations in structure heights typically require 10 nm.

Practical Aspects of AM and FM-KPFM

There is a substantial difference between AM and FM modes within KPFM which should be mentioned. While this is discussed from a theoretical point of view in § 1.3.5, here we provide some commentary on the practical implications of this. It's true that FM-KPFM mode yields higher resolution that AM mode; this due to the origin of the signals used to compute the contact potential difference. In AM mode, as we have discussed, it is the electrostatic force which gives rise to the KPFM measurement. In FM mode, it is the electrostatic force *gradient*. In the latter, this is only large very near the surface, and thus the resolution is much higher due to less 'blurring' from nearby signals. In AM mode, the tip is also kept slightly higher, so it 'sees' more of the surface. These effects not only reduce spacial resolution, but they also reduce the KPFM signal resolution. In practical terms, this means that the typical signals from AM mode in our experiments are in the region of 10's of mV (< 100 mV), while in FM mode they are often in the 100's of mV. The differences between domains are less pronounced because of this blurring (Glatzel et al., 2003). Therefore, FM-KPFM images yield quantitative measurements that are closer to actual surface potential measurements. However, AM-KPFM is still perfectly acceptable for observing trends between samples. In any case, we can only measure differences at the

end of the day, because we are not operating at ultracold temperatures in an ultra high vacuum environment.

In view of the above, it would be desirable to use FM-KPFM in most cases, but the reality of its implementation is that it is tougher to get a high quality signal. This method appears to be far more sensitive to environmental conditions. Therefore, FM-KPFM is typically reserved for focussed studies, while AM-KPFM is preferred for higher output (i.e., in cases where a larger number of experiments are compared with each other). Since we typically only observe differences, AM-KPFM is sufficient for comparing sample-sample.

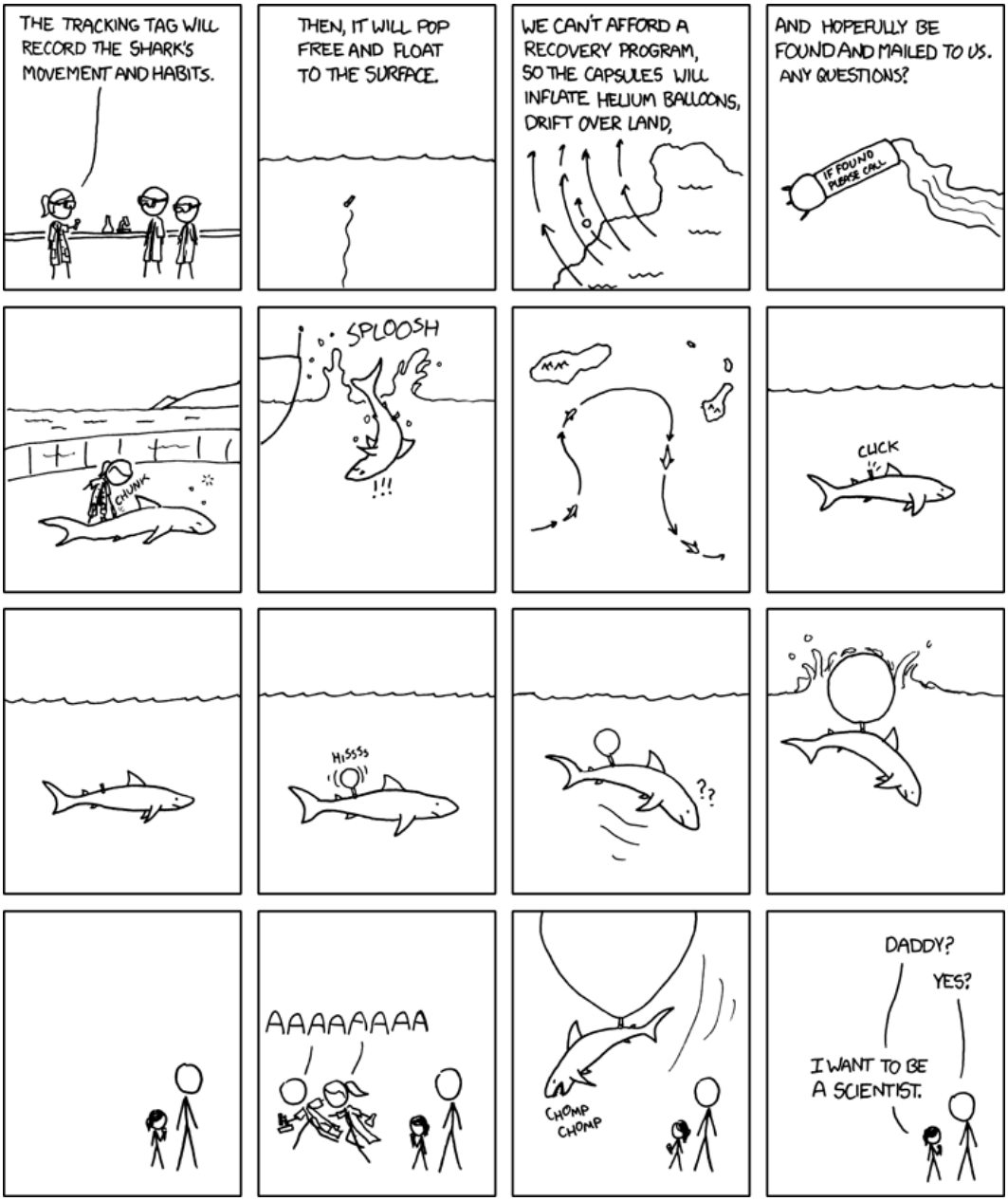

Reprinted from xkcd.com.

While the individual man is an insoluble puzzle, in the aggregate he becomes a mathematical certainty. You can, for example, never foretell what any one man will be up to, but you can say with precision what an average number will be up to. Individuals vary, but percentages remain constant. So says the statistician.

Arthur Conan Doyle

Appendix B

Image Processing and Statistical Methods for AFM and KPFM Analysis

B.1 Image Processing

When it comes to processing AFM images, it is certainly true that less is more. Minimal processing is critical to preserving the features from the original observations. However, it is necessary to apply a few critical calibrations in order to obtain reliable measurements. The raw data from the instrument is often completely uncalibrated. All AFM instruments will have accompanying image processing software which can perform basic calibration and analysis.

In almost all cases, a simple two-dimensional plane polynomial function fitted to the surface will suffice to calibrate ('flatten') the image, and produce a workable result. Similarly, a line-by-line fitting with a linear function will help to bring all of the scan lines into the same baseline. These two calibrations should be all that is necessary in a good quality image. In some cases, it may be desirable to interpolate over problem areas or artefacts, or to employ more sophisticated polynomial fits. However, if the final data are of sufficient quality, this should not be necessary (and thankfully it was not necessary in almost all of the final data presented in this thesis). For KPFM measurements, it is even more desirable to limit the use of fitting and calibrations to avoid biasing the measurements.

In preparation for cross section measurements, or to clean up the appearance of a rough image for publication when resolution is no longer a serious concern, a small amount of Gaussian smoothing works very well. Using a σ value of a pixel or less (in some cases up to 2) is normally sufficient, and does an excellent job of smoothing out the noise for presentations and calculations.

B.2 Statistical Analysis of Image Data

One of the most important calculations from AFM data is the difference in height (or contact potential difference, in the case of KPFM) between two domains within an image. This requires some careful analysis. While there are software packages out there which do a fairly good job of processing and extracting raw measurements, some more direct methods are occasionally necessary to obtain reliable results. Especially in the case of the AIST-NT data, which is fairly new, rather manual methods of measurement are necessary. However, the methodology presented in this section will of course work for any data, so long as one can extract the raw pixel values or cross sections of the images.

In § 2.3.4 we described three different methods for calculating the value of the difference of height or CPD within an image, and concluded that the cross section method was the most reliable. Therefore, we focus on that method alone from here on.

In this method, cross sections of the image are taken which show very clearly the two domains of interest. Often, the image processing software will automatically calculate the difference between two points, in both the x and y axes, for a user-selected set of points. Most of the effort in this method then goes into manually pinpointing locations and extracting values of the differences, say by selecting one point to be on the background and another to be at the top of the domain. It is recommended that as many as 50 cross section measurements be taken for each experiment in order to give reliable results, as there will be variability.

With the data in hand, one then calculates an average (mean) value for the difference, pooling all of the data. If, for example, there are two separate trials, the pooled mean can

be calculated from

$$\mu_{\mathrm{G}} = \frac{N_1\mu_1 + N_2\mu_2}{N_1 + N_2} \tag{B.1}$$

The pooled standard deviation for the two trials is

$$\sigma_{\mathrm{G}} = \sqrt{\frac{(N_1 - 1)\sigma_1^2 + (N_2 - 1)\sigma_2^2}{N_1 + N_2 - 2}} \tag{B.2}$$

Now, one may calculate the mean and associate uncertainty with the following formula:

$$\hat{\mu}_{\mathrm{G}} \pm z_{\alpha/2}\frac{\sigma_{\mathrm{G}}}{\sqrt{n}} \tag{B.3}$$

in which $z_{\alpha/2} = z_{0.025} = 1.96$ is the value of the 97.5^{th} percentile of the standard normal distribution. This gives a calculation of the mean difference, plus or minus an uncertainty holding true at a confidence level of 95%. This means, theoretically, that 95% of the time, the mean difference we obtain from any subsequent experiment will fall within this interval. See Moore & Craig (2014) for details.

Appendix C

Supplementary Data

Details that could throw doubt on your interpretation must be given, if you know them. You must do the best you can âĂŤ if you know anything at all wrong, or possibly wrong – to explain it. If you make a theory, for example, and advertise it, or put it out, then you must also put down all the facts that disagree with it, as well as those that agree with it. There is also a more subtle problem. When you have put a lot of ideas together to make an elaborate theory, you want to make sure, when explaining what it fits, that those things it fits are not just the things that gave you the idea for the theory; but that the finished theory makes something else come out right, in addition.

–

Richard Feynman

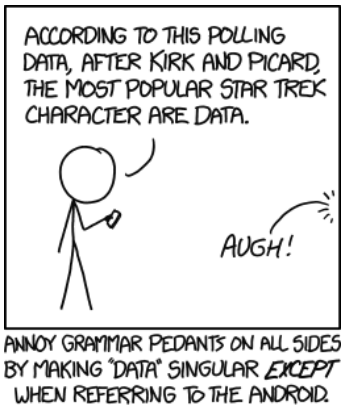

Reprinted from xkcd.com.

Supplementary Figures of DNA-Gemini Surfactant-Lipid Monolayers and Nanoparticles: AFM and KPFM

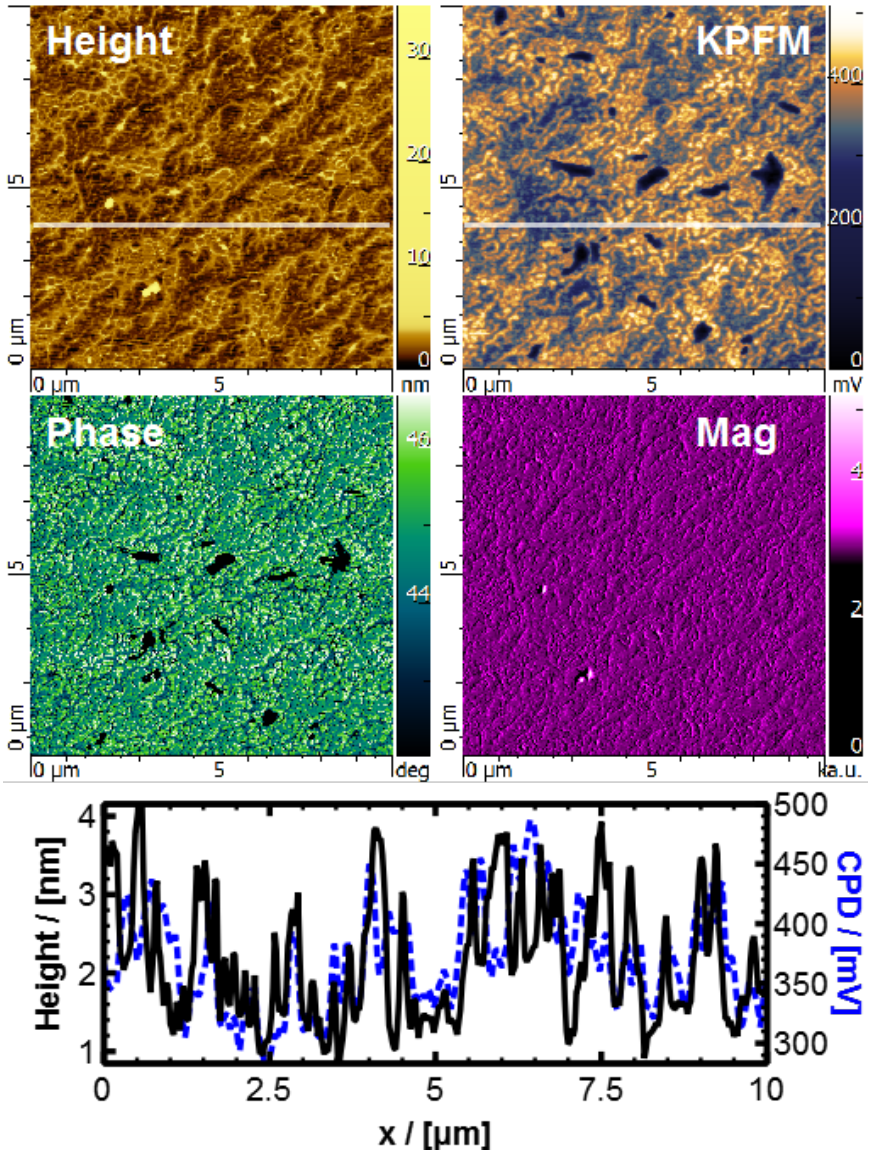

Figure C.1: Survey of AFM and KPFM results for monolayers ($\pi = 35\,\mathrm{mN/m}$) of 16-3-16:DOPC:DPPC in molar ratios of 2:3:3, with DNA present in the subphase at a concentration of $10\,\mu$M in base pairs. The field of view is 10 microns on one side. Cross sections are shown for the height and KPFM signals taken horizontally at $y = 4.0\mu$m, overlayed and scaled for ease of view.

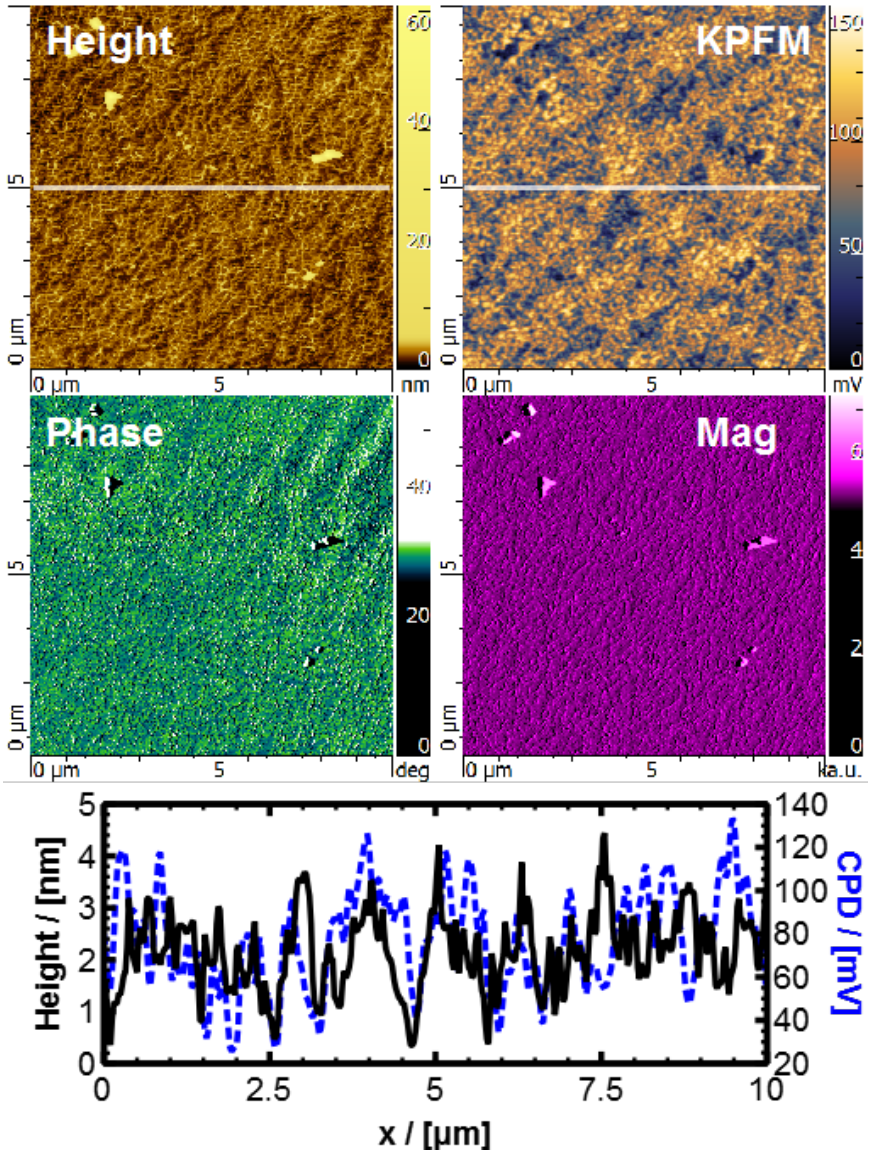

Figure C.2: Survey of AFM and KPFM results for monolayers ($\pi = 35\,\mathrm{mN/m}$) of 16-7-16:DOPC:DPPC in molar ratios of 2:3:3, with DNA present in the subphase at a concentration of $10\,\mu$M in base pairs. The field of view is 10 microns on one side. Cross sections are shown for the height and KPFM signals taken horizontally at $y = 5.0\mu$m, overlayed and scaled for ease of view.

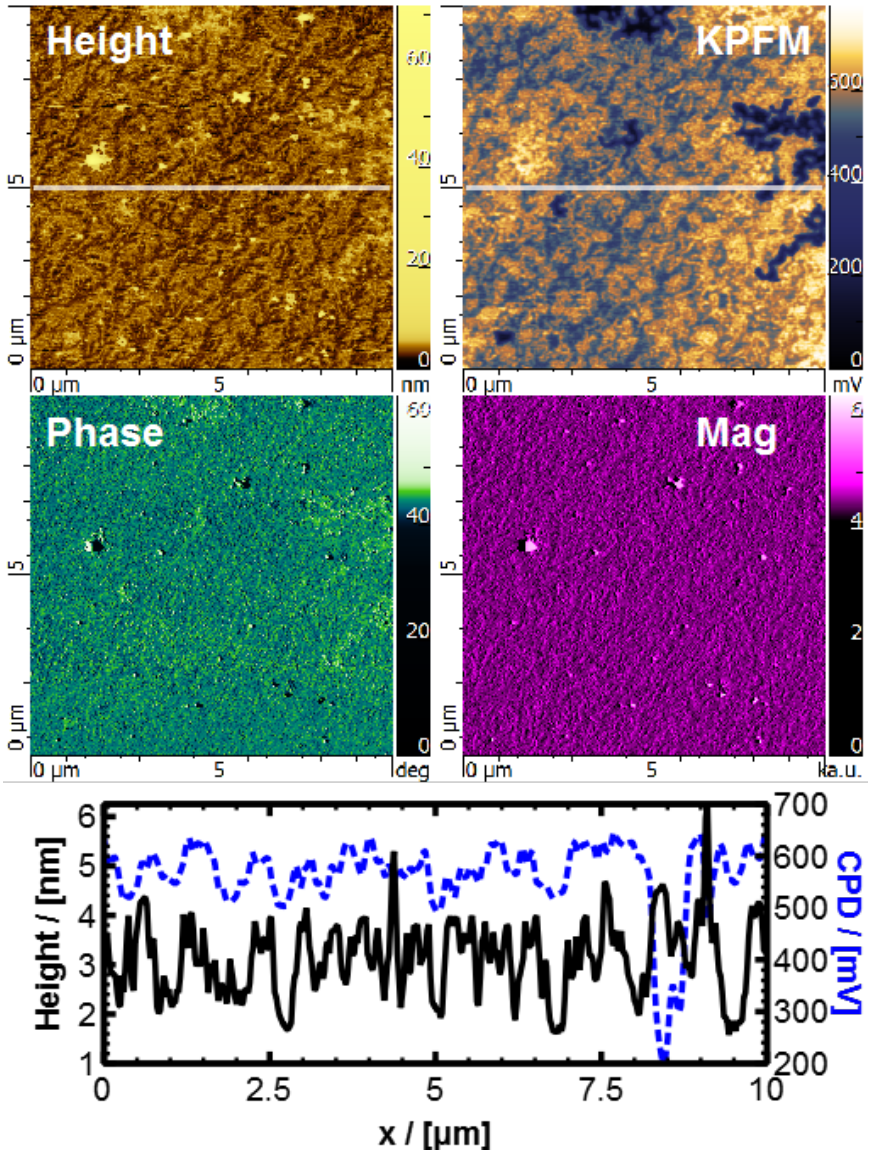

Figure C.3: Survey of AFM and KPFM results for monolayers ($\pi = 35\,\mathrm{mN/m}$) of 16-7NH-16:DOPC:DPPC in molar ratios of 2:3:3, with DNA present in the subphase at a concentration of $10\,\mu$M in base pairs. The field of view is 10 microns on one side. Cross sections are shown for the height and KPFM signals taken horizontally at $y = 5.0\mu$m, overlayed and scaled for ease of view.

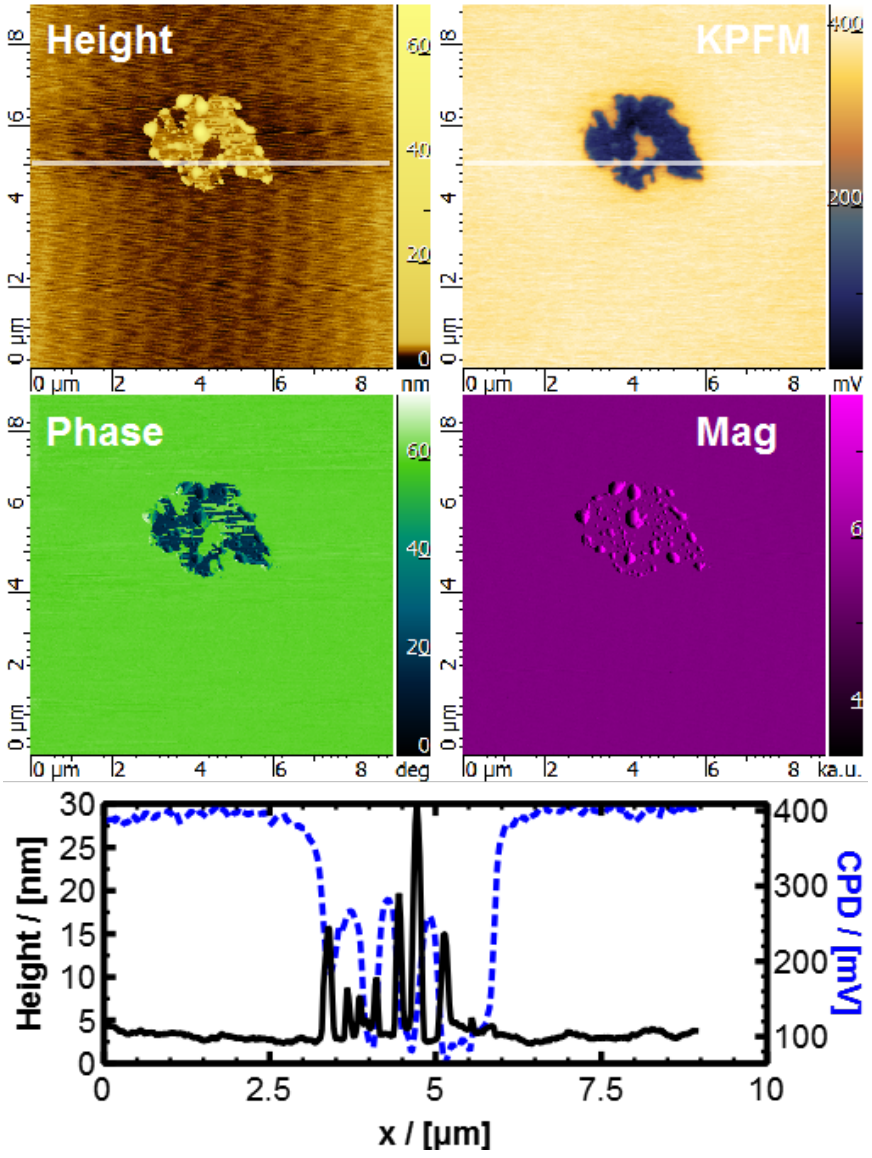

Figure C.4: Survey of AFM and KPFM results for a monolayer ($\pi = 35\,\mathrm{mN/m}$) of 16-3-16:DOPE in a molar ratio of 2:3, with a pure water subphase. The field of view is 10 microns on one side. Cross sections are shown for the height and KPFM signals taken horizontally at $y = 5.0\mu\mathrm{m}$, overlayed and scaled for ease of view.

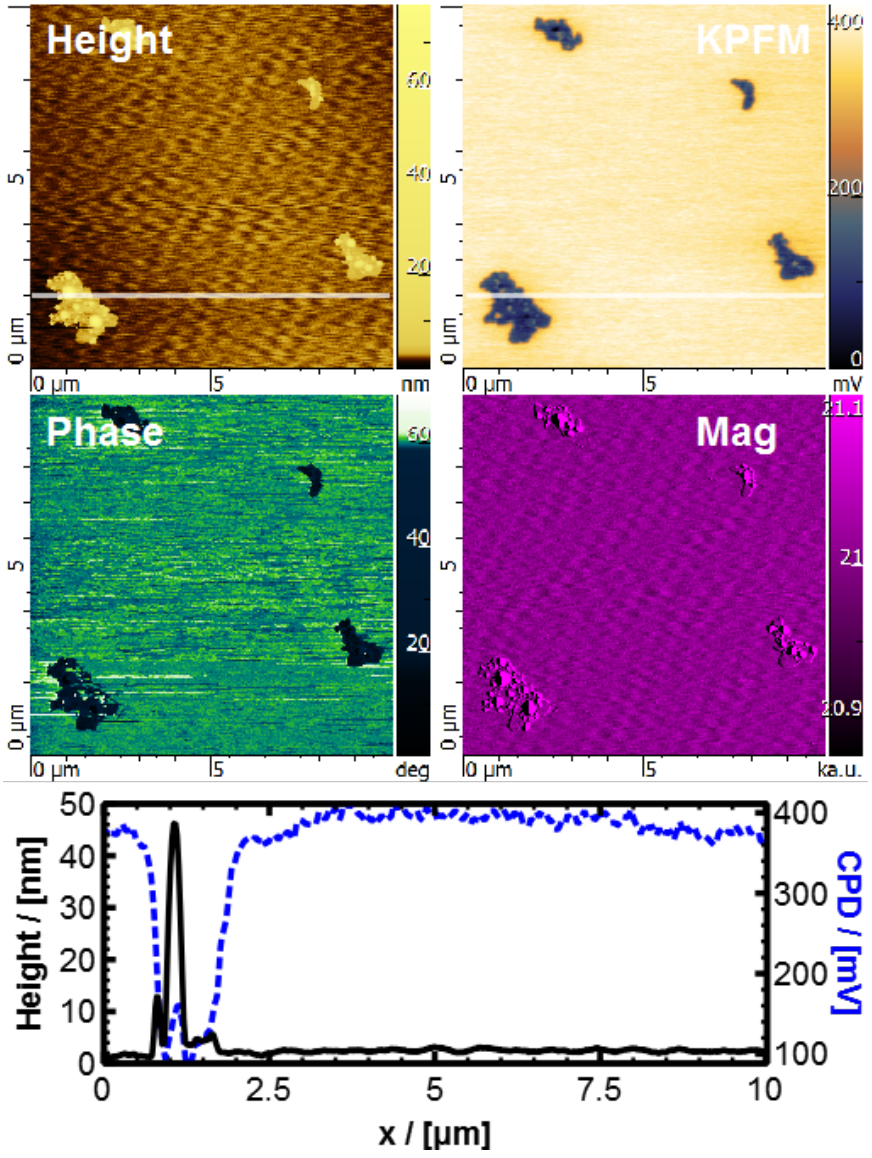

Figure C.5: Survey of AFM and KPFM results for a monolayer ($\pi = 35\,\mathrm{mN/m}$) of 16-7-16:DOPE in a molar ratio of 2:3, with a pure water subphase. The field of view is 10 microns on one side. Cross sections are shown for the height and KPFM signals taken horizontally at $y = 5.0\mu\mathrm{m}$, overlayed and scaled for ease of view.

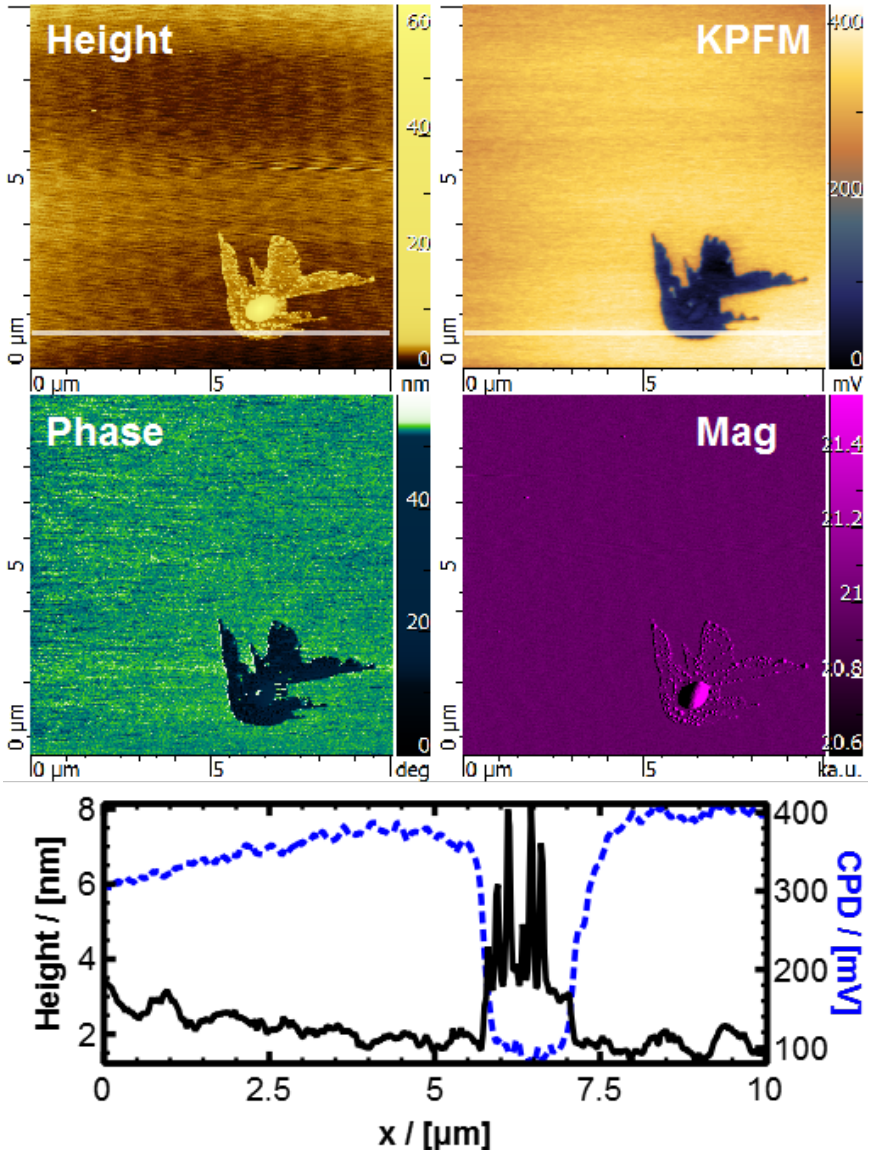

Figure C.6: Survey of AFM and KPFM results for a monolayer ($\pi = 35\,\mathrm{mN/m}$) of 16-7NH-16:DOPE in a molar ratio of 2:3, with a pure water subphase. The field of view is 10 microns on one side. Cross sections are shown for the height and KPFM signals taken horizontally at $y = 1.0\mu\mathrm{m}$, overlayed and scaled for ease of view.

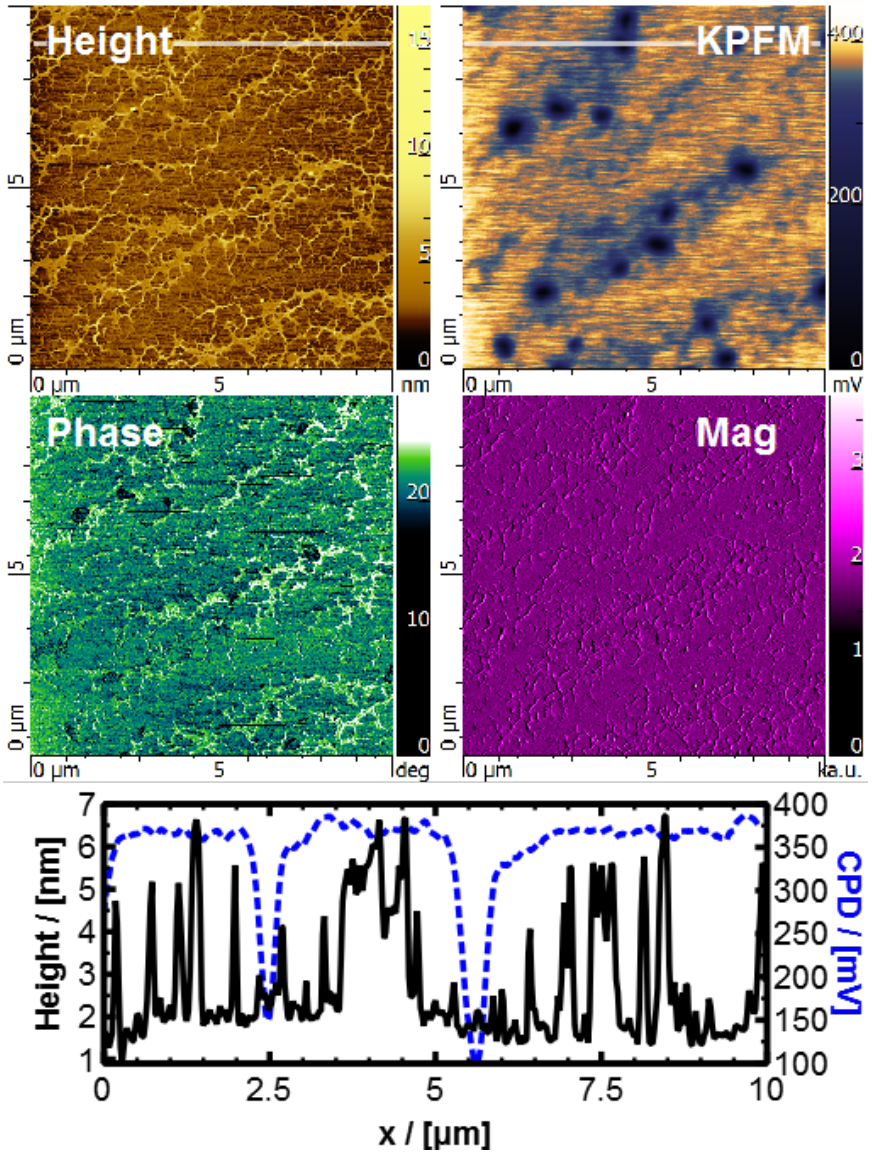

Figure C.7: Survey of AFM and KPFM results for a monolayer ($\pi = 35\,\mathrm{mN/m}$) of 16-3-16:DOPE in a molar ratio of 2:3, with DNA present in the subphase at a concentration of $10\,\mu$M in base pairs. The field of view is 10 microns on one side. Cross sections are shown for the height and KPFM signals taken horizontally at $y = 9.0\mu$m, overlayed and scaled for ease of view.

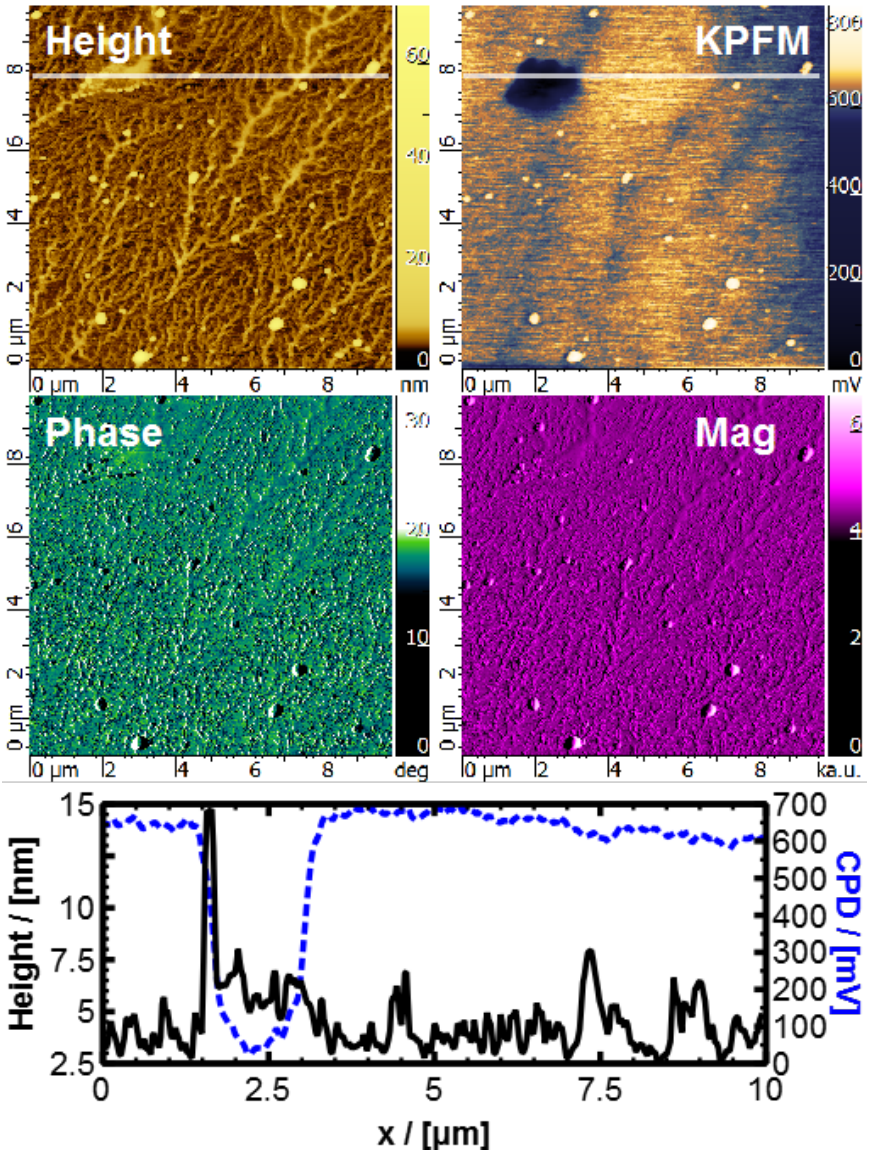

Figure C.8: Survey of AFM and KPFM results for a monolayer ($\pi = 35\,\mathrm{mN/m}$) of 16-7-16:DOPE in a molar ratio of 2:3, with DNA present in the subphase at a concentration of $10\,\mu$M in base pairs. The field of view is 10 microns on one side. Cross sections are shown for the height and KPFM signals taken horizontally at $y = 8.0\mu$m, overlayed and scaled for ease of view.

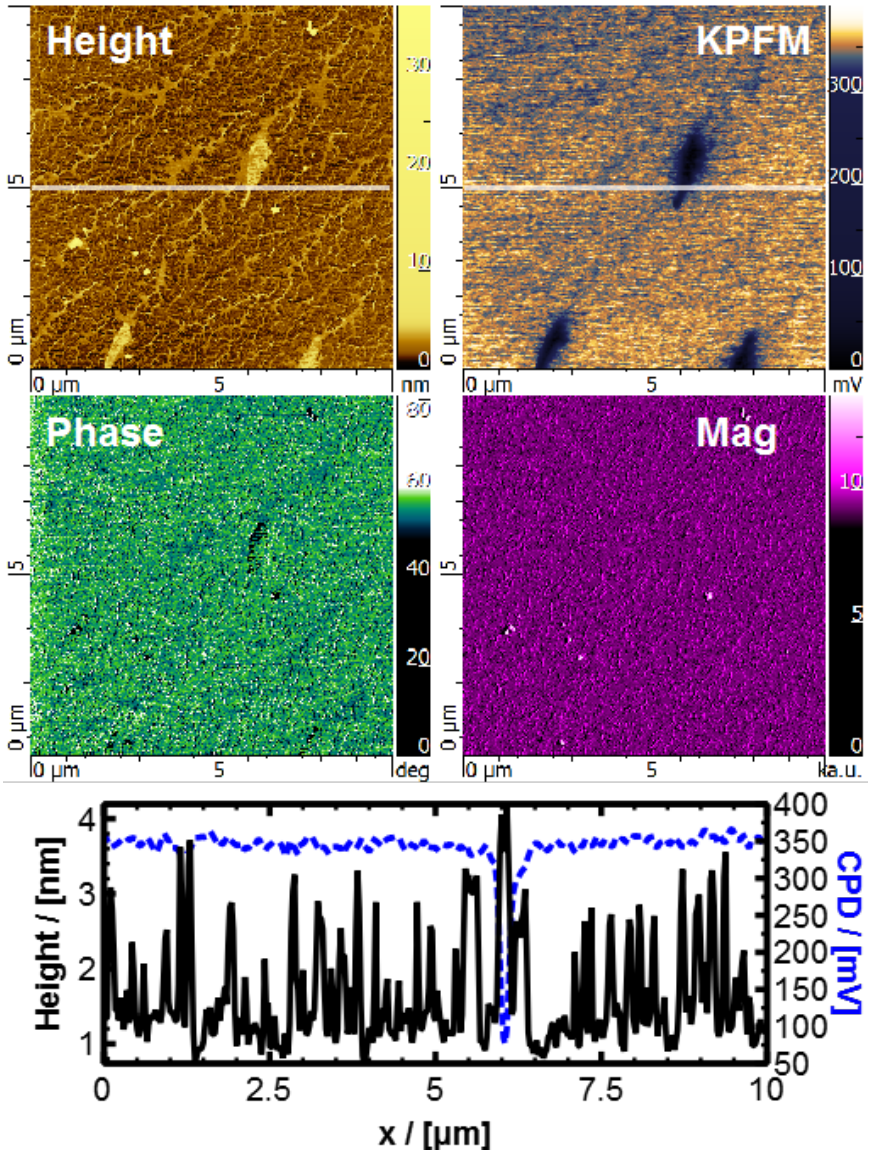

Figure C.9: Survey of AFM and KPFM results for a monolayer ($\pi = 35\,\mathrm{mN/m}$) of 16-7NH-16:DOPE in a molar ratio of 2:3, with DNA present in the subphase at a concentration of $10\,\mu$M in base pairs. The field of view is 10 microns on one side. Cross sections are shown for the height and KPFM signals taken horizontally at $y = 5.0\mu$m, overlayed and scaled for ease of view.

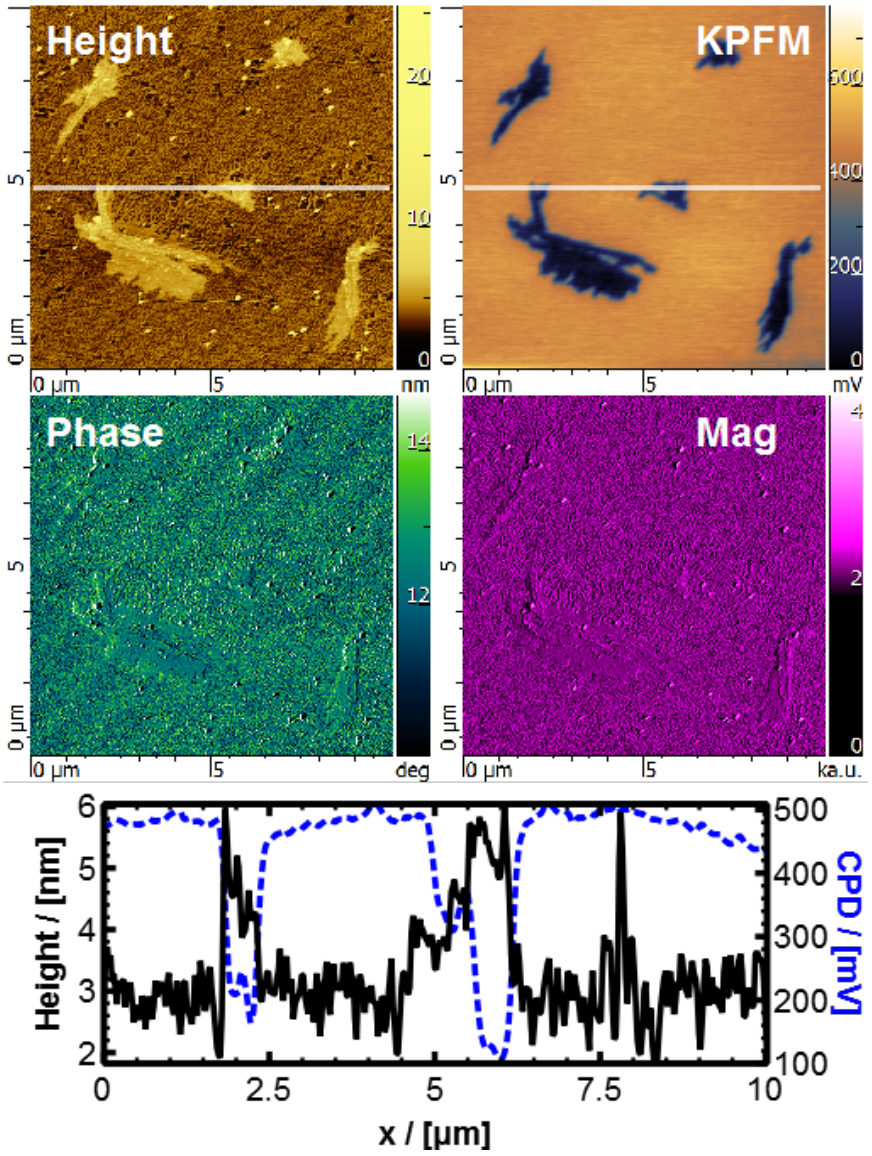

Figure C.10: Survey of AFM and KPFM results for a monolayer ($\pi = 35\,\mathrm{mN/m}$) of 16-3-16:DOPE in a molar ratio of 5:1, with DNA present in the subphase at a concentration of $10\,\mu$M in base pairs. The field of view is 10 microns on one side. Cross sections are shown for the height and KPFM signals taken horizontally at $y = 5.0\mu$m, overlayed and scaled for ease of view.

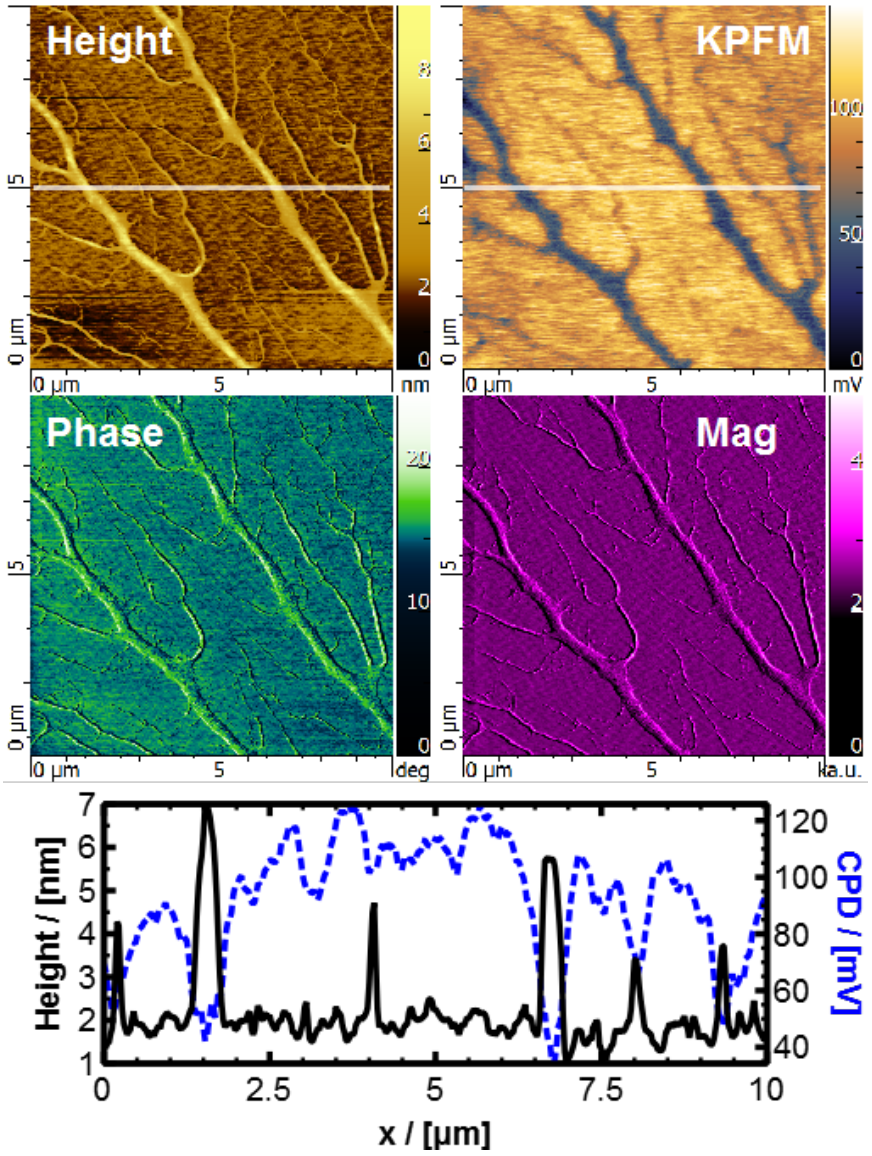

Figure C.11: Survey of AFM and KPFM results for a monolayer ($\pi = 35\,\mathrm{mN/m}$) of 16-3-16:DOPE in a molar ratio of 1:5, with DNA present in the subphase at a concentration of $10\,\mu$M in base pairs. The field of view is 10 microns on one side. Cross sections are shown for the height and KPFM signals taken horizontally at $y = 5.0\mu$m, overlayed and scaled for ease of view.

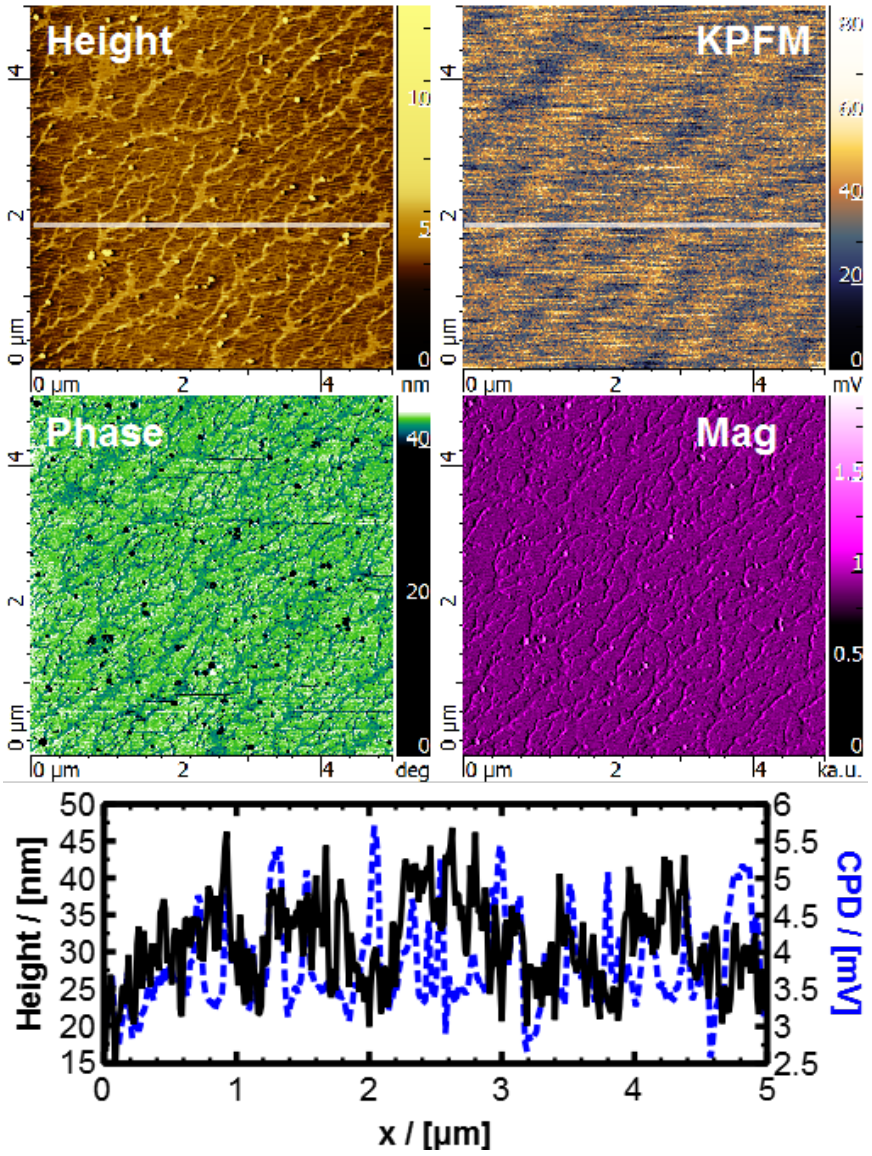

Figure C.12: Survey of AFM and KPFM results for a lower-pressure monolayer (π = 15 mN/m) of 16-7-16:DOPE in a molar ratio of 2:3, with DNA present in the subphase (acetate buffer, pH 4) at a concentration of 10 μM in base pairs. The field of view is 5 microns on one side. Cross sections are shown for the height and KPFM signals taken horizontally at $y = 2.0\mu$m, overlayed and scaled for ease of view.

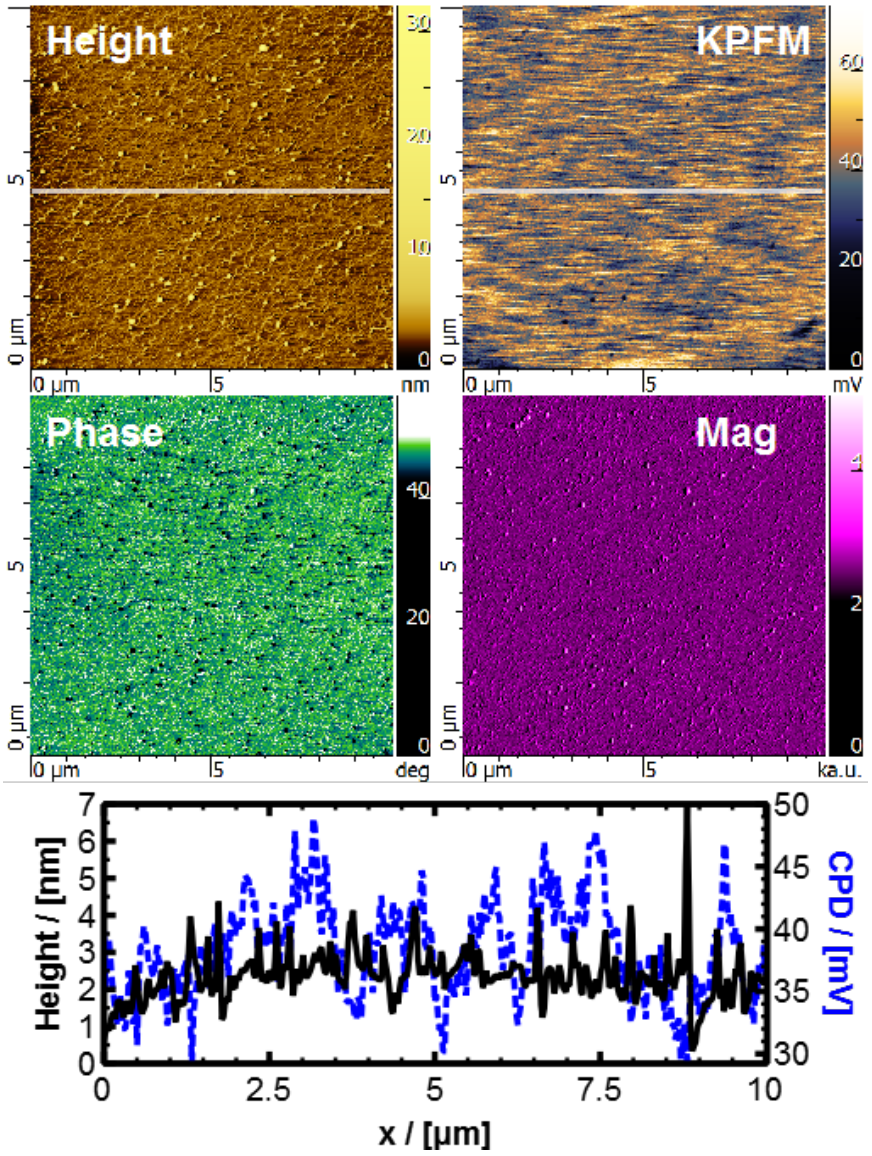

Figure C.13: Survey of AFM and KPFM results for a monolayer ($\pi = 35\,\mathrm{mN/m}$) of 16-7NH-16:DOPE in a molar ratio of 2:3, with DNA present in the subphase (acetate buffer, pH 4) at a concentration of $10\,\mu$M in base pairs. The field of view is 10 microns on one side. Cross sections are shown for the height and KPFM signals taken horizontally at $y = 5.0\mu$m, overlayed and scaled for ease of view.

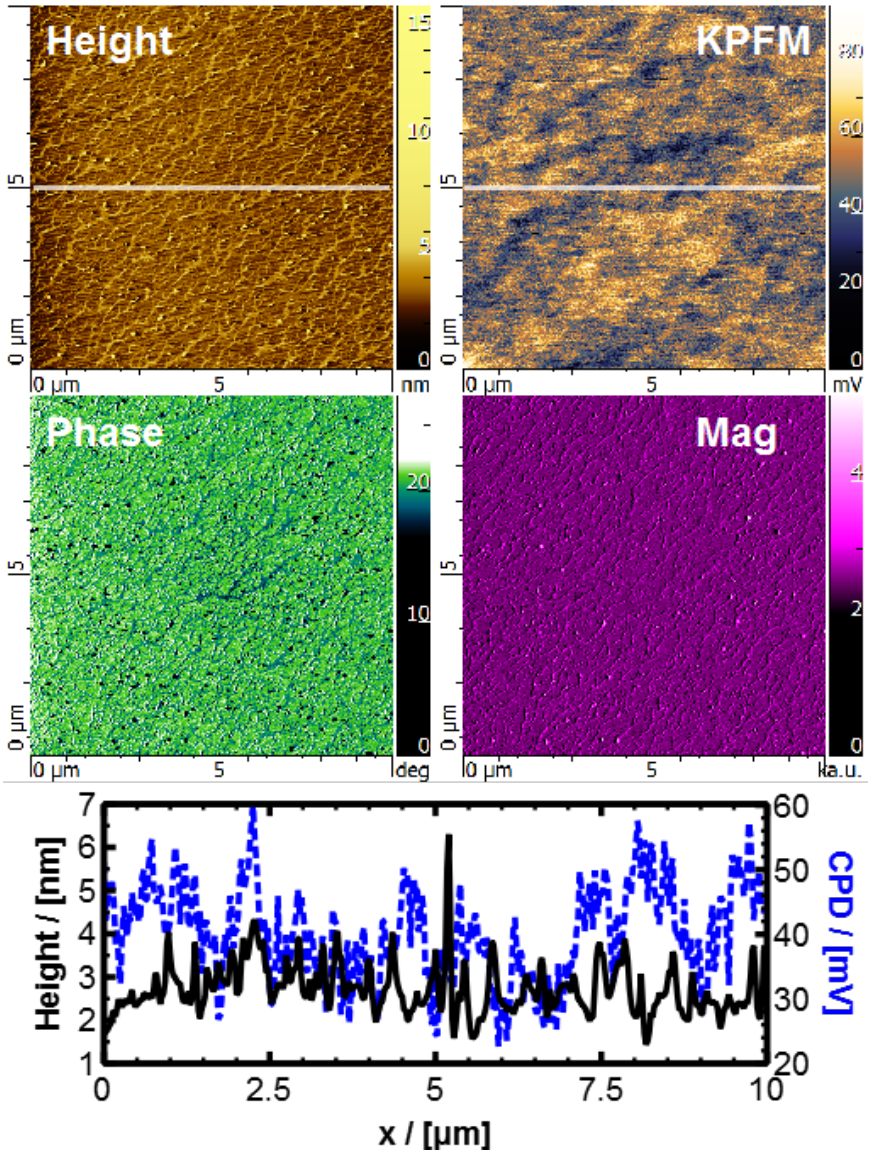

Figure C.14: Survey of AFM and KPFM results for a lower-pressure monolayer (π = 15 mN/m) of 16-7NH-16:DOPE in a molar ratio of 2:3, with DNA present in the subphase (acetate buffer, pH 4) at a concentration of 10 μM in base pairs. The field of view is 10 microns on one side. Cross sections are shown for the height and KPFM signals taken horizontally at $y = 5.0\mu$m, overlayed and scaled for ease of view.

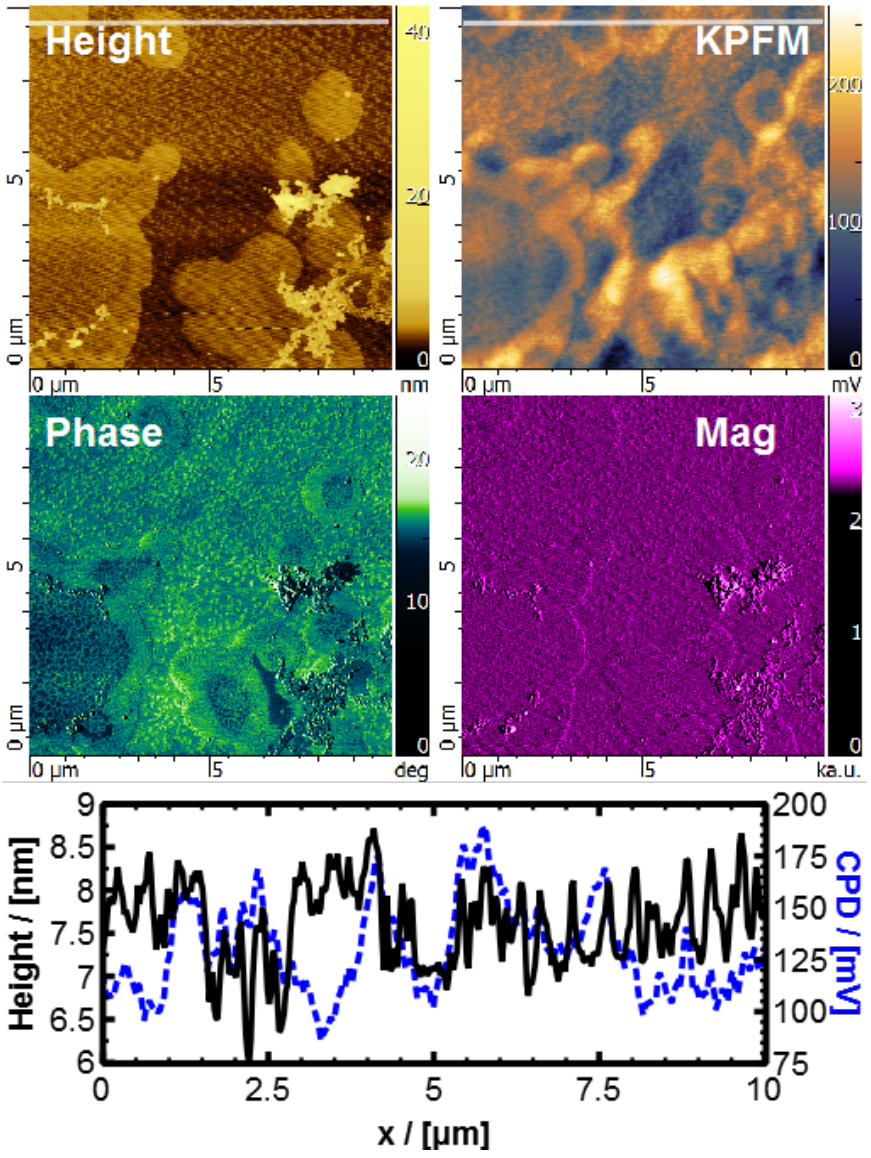

Figure C.15: Survey of AFM and KPFM results for a monolayer ($\pi = 35\,\mathrm{mN/m}$) of 16-7NH-16:DOPE in a molar ratio of 2:3, with a pure buffer (no DNA present) subphase (acetate buffer, pH 4). The field of view is 10 microns on one side. Cross sections are shown for the height and KPFM signals taken horizontally at $y = 9.5\mu$m, overlayed and scaled for ease of view.

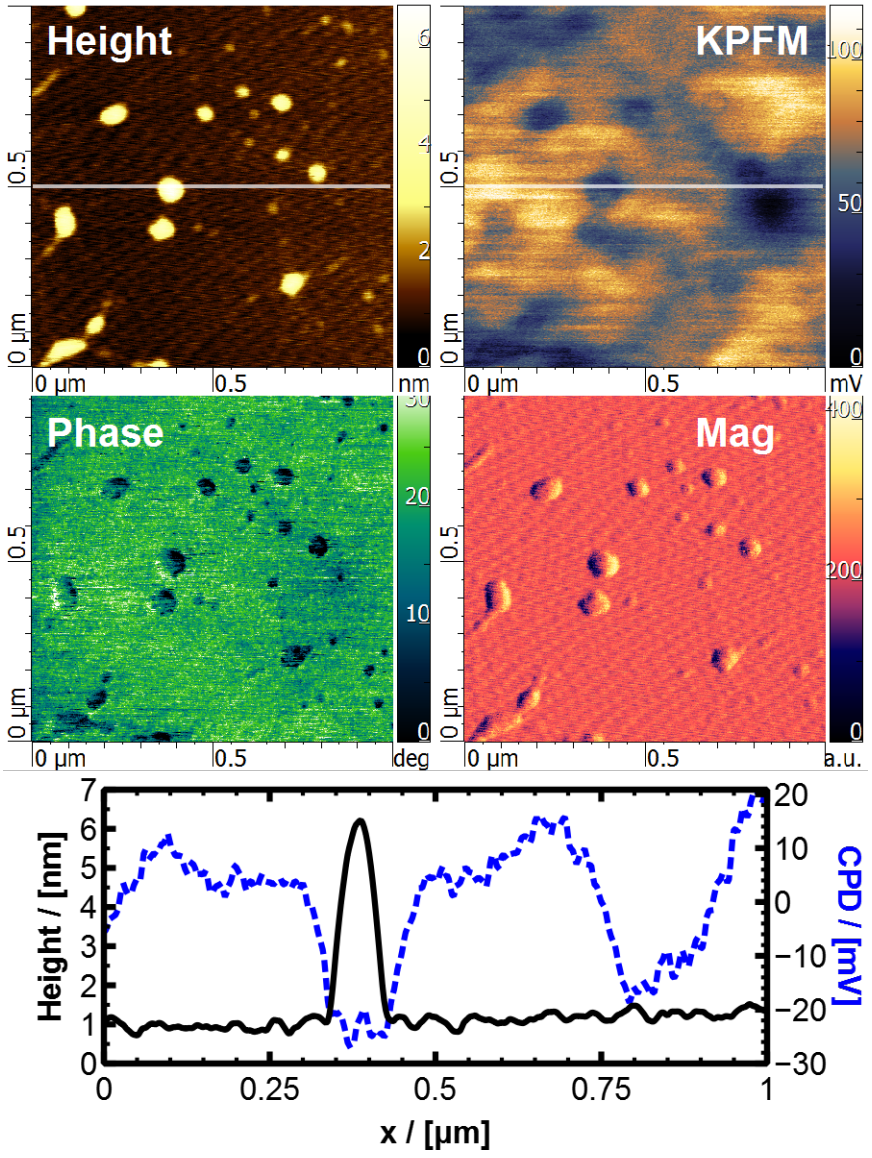

Figure C.16: Small-scale AFM and KPFM images of gene transfection complexes of DNA, DOPE and gemini surfactant 16-3-16. The cross section was taken at $y = 0.5\,\mu$m.

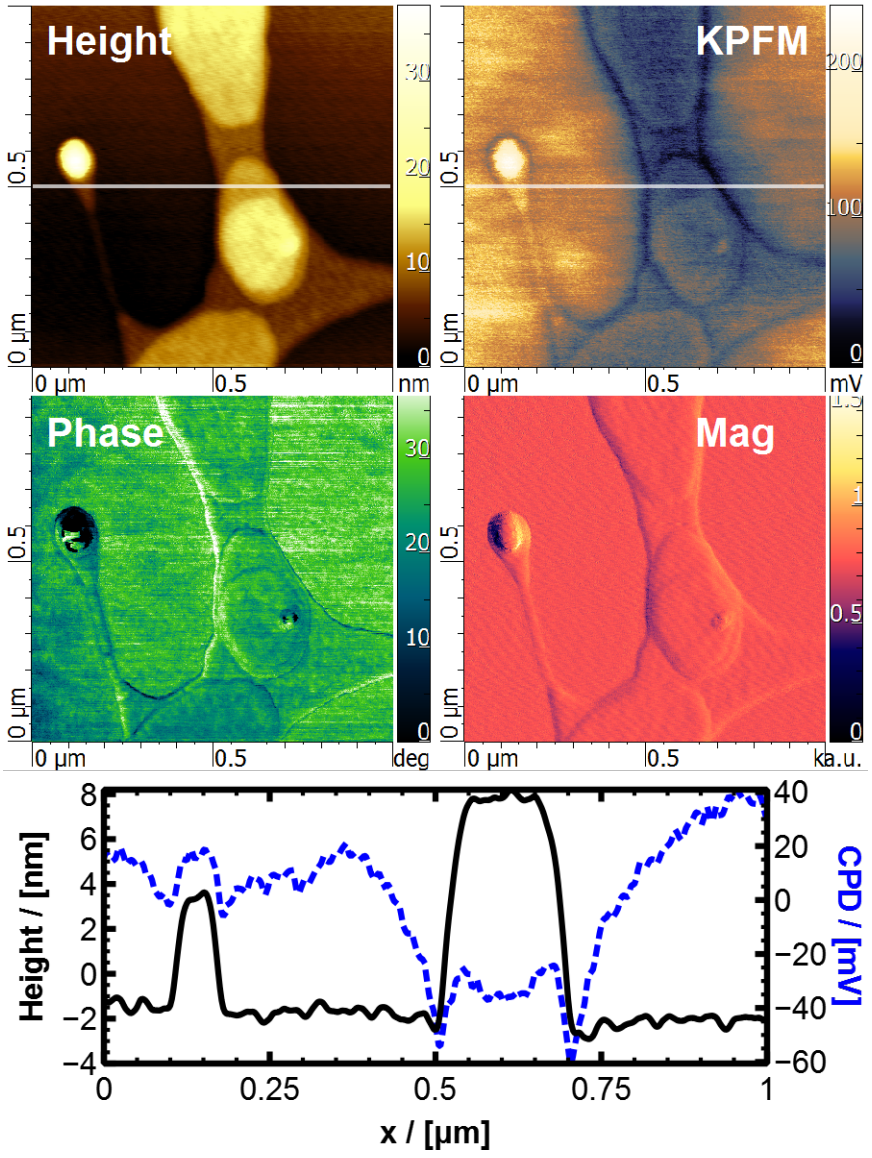

Figure C.17: Small-scale AFM and KPFM images of gene transfection complexes of DNA, DOPE and gemini surfactant 16-7-16. The cross section was taken at $y = 0.5\,\mu$m.

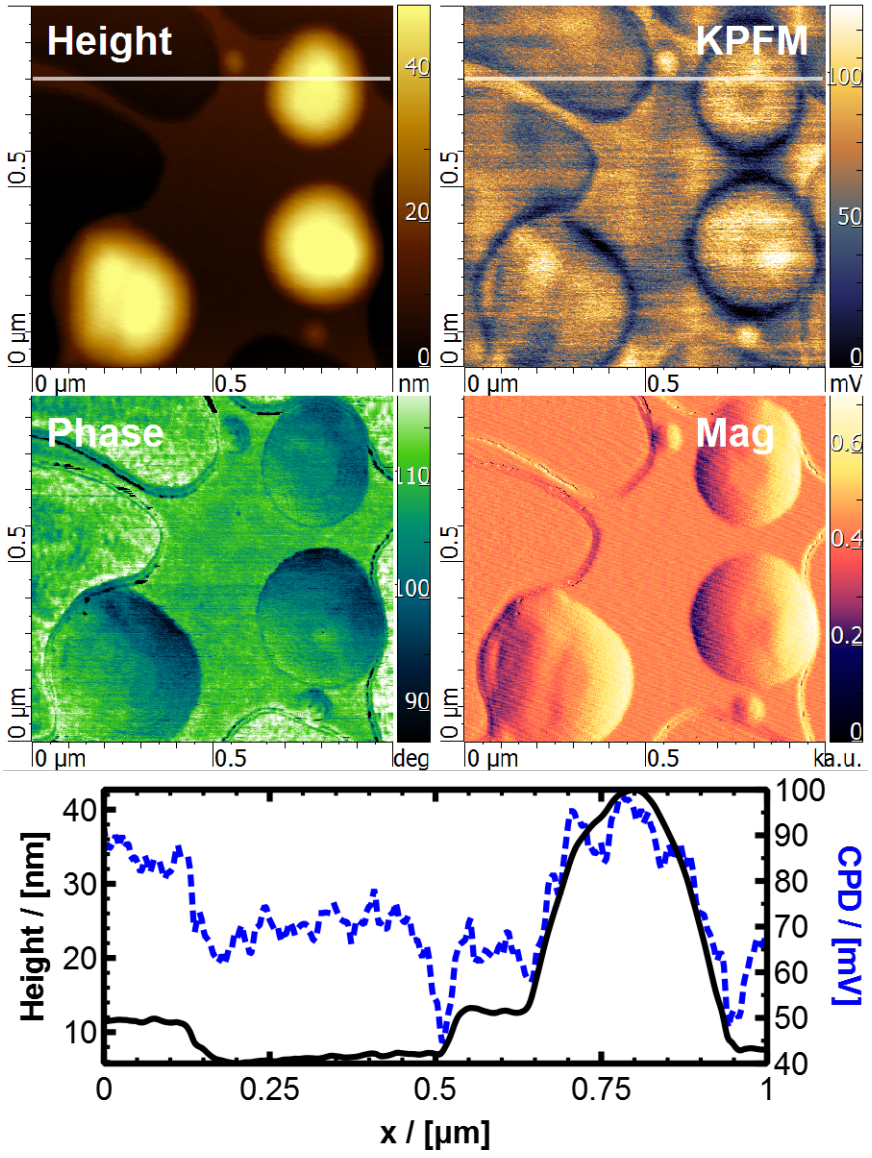

Figure C.18: Small-scale AFM and KPFM images of gene transfection complexes of DNA, DOPE and gemini surfactant 16-7NH-16. The cross section was taken at $y = 0.8\,\mu$m.

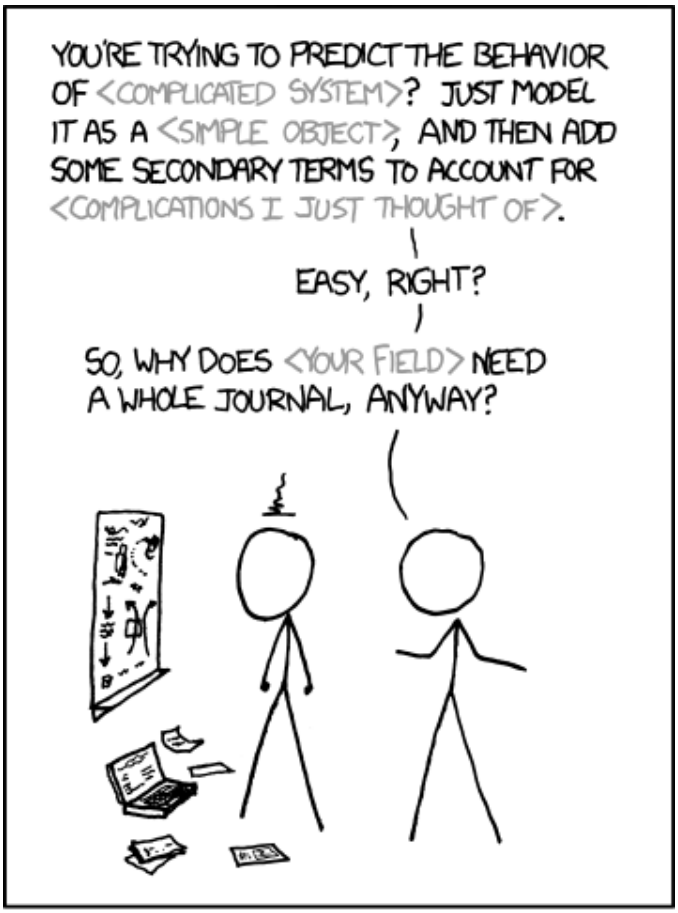

LIBERAL-ARTS MAJORS MAY BE ANNOYING SOMETIMES, BUT THERE'S *NOTHING* MORE OBNOXIOUS THAN A PHYSICIST FIRST ENCOUNTERING A NEW SUBJECT.

A Note to Student Readers

LONG after this thesis is accepted, I realise that graduate students and senior undergraduates will probably be the only group of people to read this through. Or at least I hope they will; I hope that this thesis is useful both as a reference and as a review of this rather interesting interdisciplinary field of study. It would be a shame if I put in all this work writing a dissertation, and after it served its noble purpose of admitting me to a doctoral degree, it were only used to take up space on a library shelf.

While I am a physicist by training, I somehow ended up in a mix that also included biology, chemistry, pharmacology, engineering, and of course nanotechnology (everybody wants to have *nano-* attached to their research these days). If you're like that - an interdisciplinary student of science - and want to learn about how you can mix physics and pharmacology on the nanoscale, you've opened the right book. Or maybe you want to know how to apply nanoscale imaging to biology. That's here, too, more or less. For those who would like to replicate or expand upon the research I have presented in this document, I've tried to make the appendices fairly comprehensive to walk you through the protocols and analyses.

However, this document is written (as it ought to be) as my dissertation, first and foremost, and therefore some assumptions of knowledge have been made. (If I had not, it could easily go on for thousands of pages, and I would still be a graduate student!) I assume that those who read this will have a basic grasp of physics, chemistry and biology equivalent to first or second year of university (at least by 2015 standards, which are considerably more lax than some few decades ago). Organic chemistry and thermodynamics would be helpful, too. Fundamental calculus and algebra would be nice, if not necessary, for without that, one cannot truly understand physics. Basic scientific research methods are a must.

If you have made it this far, thanks for reading, and I commend you; I have a few more tips. Along the road of graduate school, I have had to learn and re-learn almost everything to solidify my basic knowledge, and I'd like to recommend some great textbooks that have helped me along the way. I hope they will help you, too. Most of these are specific to the

research fields covered by this dissertation topic, but a few exceptional books I will mention for the basic sciences, for these I recommend for any Padawan interdisciplinary scientist. I've seen so many different textbooks, many of them downright awful, so hopefully this spares you some unnecessary effort. The list can be found immediately following this preface.

Feel free to e-mail me if you have any questions or comments. The address I provide below ought to be valid for as long as the *uwaterloo* server exits, which I expect will be a very long time.

Robert D. E. Henderson
Waterloo, June 2015
✉ rdehende@uwaterloo.ca

Reprinted from xkcd.com.

Recommended Books

Physics:

Feynman, R. P. 1965, The Feynman Lectures on Physics

This is perhaps the greatest reference for basic physics that has ever been written. Like most of Feynman's writing, a pleasure to read.

Biology:

Alberts, B., Johnson, A., Lewis, J., Raff, M., Roberts, K., & Walter, P. 2002, Molecular Biology of the Cell, 4th edition (New York: Garland Science)

For upper-year biology majors, this book covers most of cell biology and serves as a good overall resource for whatever you'd like to know on this topic.

Chemistry:

Petrucci, R. H., Herring, G. F., Madura, J. D., & Bissonnette, C. 2010, General chemistry: principles and modern applications (Pearson Education International)

Co-authored by one of Waterloo's best lecturers, this textbook is a great introduction to basic chemistry (although, if you're reading this, you probably don't need it, but that's no reason why it can't be on your shelf!).

Organic Chemistry:

Klein, D. R. 2013, Organic Chemistry, 2nd Edition (Wiley)

Organic chemistry books have come a long way in the past decade, and now offer a lot of creative presentation methods to teach the subject. This book, I have found, is rather clever and easy to learn from. But watch out - there are some typos, and some of the rigid faculty would disagree with some of Klein's definitions.

For technical background on some of the more specialised fields in this thesis, I recommend:

Electromagnetics:

Griffiths, D. J. 2013, Introduction to electrodynamics (Pearson)

It's extraordinarily rare to find textbooks that read like a novel. Every book that Griffiths writes is the best in the subject, and he has other texts for Quantum Mechanics and Particle Physics. Do yourself a favour and read them; he really teaches you how to *do* physics, and his writing is eloquent and smooth.

Surfactants and Interfacial Science:

Gaines Jr, G. 1966, Insoluble monolayers at gas-liquid interfaces (Interscience, New York)

This is a rather old book, but as old books generally do, it goes into a lot more detail on some of the physics and mathematics behind some of the derivations (particularly for the stuff on potentials). Don't be put off by its publication date. There's a lot of really good text in here which covers a lot of the historical research on lipids and their monolayers, and in useful detail.

Barnes, G. & Gentle, I. 2011, Interfacial science: an introduction (Oxford University Press)

For a more modern take on interfaces, without getting bogged down in derivations and too many technical details, this is a great book.

Israelachvili, J. N. 2011, Intermolecular and surface forces: revised third edition (Academic press)

Not for the faint at heart, Israelachvili presents a densely-packed compilation of just about everything you would need for a theoretical understanding of surface and interface science. But good luck - they call this a graduate level textbook, but really it's more of a resource for advanced researchers in the field. Think of it as the Jackson (1962) for interfaces.

Atomic and Kelvin Probe Force Microscopy

Morris, V. J., Kirby, A. R., & Gunning, A. P. 1999, Atomic force microscopy for biologists, Vol. 57 (World Scientific)

If you're new to AFM, particularly for biological applications, this is the first book you should read (as if you couldn't tell that from its title!). The basics of AFM are discussed here, along with many illustrative applications. Also see Allison et al. (2010).

Sadewasser, S. & Glatzel, T. 2012, Kelvin probe force microscopy (Springer)

Once you've got a solid understanding of the basics of AFM, and want to learn all about KPFM, this is a great general resource for it. However, take caution that KPFM is a relatively new technology (compared to a lot of others), and so you'll want to explore some of the key papers as well. Watch for these in this thesis. They include Nonnenmacher et al. (1991); Glatzel et al. (2003); Zerweck et al. (2005).

Of course, there are many more sub-topics presented in this thesis, and I've tried to point out some of the authoritative review articles and other key papers that will be of interest for background reading.